

AD-A126 990

LARGE AMPLITUDE ION WAVES(U) DARTMOUTH COLL HANOVER N H
DEPT OF PHYSICS AND ASTRONOMY J E WALSH 19 NOV 82
AFOSR-TR-83-0286 AFOSR-77-3410

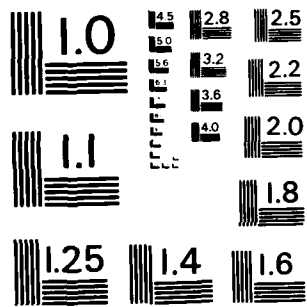
1/4

UNCLASSIFIED

F/G 20/7

NL





MICROCOPY RESOLUTION TEST CHART
NATIONAL BUREAU OF STANDARDS-1963-A

AD A126390

UNCLASSIFIED

SECURITY CLASSIFICATION OF THIS PAGE (When Data Entered)

REPORT DOCUMENTATION PAGE		READ INSTRUCTIONS BEFORE COMPLETING FORM
1. REPORT NUMBER AFOSR-TR- 83 - 0266	2. GOVT ACCESSION NO. A126990	3. RECIPIENT'S CATALOG NUMBER
4. TITLE (and Subtitle) LARGE AMPLITUDE ION WAVES		5. TYPE OF REPORT & PERIOD COVERED <i>Final</i>
		6. PERFORMING ORG. REPORT NUMBER
7. AUTHOR(s) John E. Walsh		8. CONTRACT OR GRANT NUMBER(s) <i>AFOSR-77-3410</i>
9. PERFORMING ORGANIZATION NAME AND ADDRESS Dartmouth College, Hanover, N.H. 03755		10. PROGRAM ELEMENT, PROJECT, TASK AREA & WORK UNIT NUMBERS 2301/A8 61102F
11. CONTROLLING OFFICE NAME AND ADDRESS AFOSR/NP Bolling AFB, Bldg. #410 Washington, D.C. 20332		12. REPORT DATE November 19, 1982
		13. NUMBER OF PAGES 248 292
14. MONITORING AGENCY NAME & ADDRESS (if different from Controlling Office)		15. SECURITY CLASS. (of this report) UNCLASSIFIED
		15a. DECLASSIFICATION DOWNGRADING SCHEDULE
16. DISTRIBUTION STATEMENT (of this Report) Approved for public release; distribution unlimited.		
17. DISTRIBUTION STATEMENT (of the abstract entered in Block 20, if different from Report) Approved for public release; distribution unlimited		
18. SUPPLEMENTARY NOTES		
19. KEY WORDS (Continue on reverse side if necessary and identify by block number) Millimeter Wavelength Radiation Sources, Cerenkov Radiation, Cerenkov Masers		
20. ABSTRACT (Continue on reverse side if necessary and identify by block number) Cerenkov Masers, which are mildly relativistic (100-200 KV), moderate-current, electron-beam (1-20A)-driven dielectric resonators, have been used to produce multihundred KW power levels in the middle part of the mm wavelength range. The devices make use of the fact that the evanescence scale length in the transverse direction of a slow wave is given by $\lambda_{BY} (\lambda - \text{wavelength}, \quad \beta - \text{velocity measured in units of the}$		

DD FORM 1473
1 JAN 73

UNCLASSIFIED

SECURITY CLASSIFICATION OF THIS PAGE (When Data Entered)

UNCLASSIFIED
 DIVISION OF THE SECRETARY OF DEFENSE

(Faint handwritten notes)

Accession For		<input checked="" type="checkbox"/>
NTIS GRA&I		<input type="checkbox"/>
DTIC TAB		<input type="checkbox"/>
Unannounced		<input type="checkbox"/>
Justification		
By _____		
Distribution/ _____		
Availability Codes		
Avail and/or		
Dist	Special	

~~UNCLASSIFIED~~

SECURITY CLASSIFICATION OF THIS PAGE(When Data Entered)

✓

FINAL REPORT: LARGE AMPLITUDE ION WAVES

USAF/OSR ** 77-3410

John E. Walsh
Department of Physics & Astronomy
Dartmouth College
Hanover, N.H. 03755

✓

AIR FORCE OFFICE OF SCIENTIFIC RESEARCH (AFSC)
NOTICE OF TRANSMITTAL TO DTIC
This technical report has been reviewed and is
approved for public release IAW AFR 190-12.
Distribution is unlimited.
MATTHEW J. KERPER
Chief, Technical Information Division

1/

✓

✓

CONTENTS

- I. Introduction
- II. Personnel
- III. Published Abstracts of Results Presented at Meetings
- IV. Publications

✓

Accession For	
NTIS GRA&I	<input checked="checked" type="checkbox"/>
DTIC TAB	<input type="checkbox"/>
Unannounced	<input type="checkbox"/>
Justification	
By	
Distribution/	
Availability Codes	
Dist	Avail and/or Special
A	

2

✓

✓

I. Introduction

This is a final report of work carried out under USAF/OSR Contract #77-3410 during the period June, 1977 through January, 1982. The research was originally devoted to problems associated with large amplitude ion waves and was under the direction of Professor Richard F. Ellis, who was at that time a member of the Department of Physics and Astronomy at Dartmouth College. When Professor Ellis left for the Lawrence Livermore Laboratory, the research was re-directed into the field of high power microwave generation. Research carried out under the earlier direction is listed but not discussed in detail in this document. This report deals largely with the high power microwave research.

✓

The principle result has been the attainment of multi-hundred KW levels of output power in the middle mm wavelength region of the spectrum. This has been accomplished with a mildly relativistic electron beam-dielectric resonator combination. All of the work contained in the remainder of this report is devoted to one or another aspect of these Cerenkov radiation sources. Recent experimental results are contained in the paper by S. Von Laven, et al., which has also appeared in Applied Physics Letters, (41(5), 408 (1982).

✓

Other papers contained herein address theoretical matters and variations of the basic device, which could prove important. Among these I might mention in particular the Cerenkov amplifier calculations of Capt. D. Wise. Experimental verification of some of the predictions contained in that section have now been completed.

3

✓

II. Personnel Supported in Part by USAF/OSR Contract 77-3410.

In addition to the Principal Investigator and the Senior Research Associate (Mr. Robert W. Layman), the following have received at least part of their support from this contract. Listed are the names, date of degree, and present affiliations.

Richard Majeski, Ph.D. 1979, University of Maryland.

Elizabeth Marden-Marshall, Ph.D. 1980, Wellesley College.

Scott Von Laven, Ph.D. 1982, KMS Fusion.

Kevin Felch, Ph.D. 1980, Varian Associates.

Douglas Wise, MA 1981, Department of Physics, USA West Point.

John E. Golub, AB 1981, Dept. of Physics, Harvard University.

William B. Case, Research Associate, Dept. of Physics, Grinnell College.

✓

III.

ABSTRACTS

1. Comparison of Local and Non-Local Models in Predicting Stability of Collisional Drift Waves, B.E. Marden, R.F. Ellis, and J.E. Walsh, Bull. Am. Phys. Soc. 23, 826 (1978).
2. Backscattering from Electron Beam-Dielectric Resonator Combinations, J.E. Walsh and G. Crew, Bull. Am. Phys. Soc. 23, 748 (1978).
3. A Cerenkov-Raman Radiation Source, K. Busby, K. Felch, R. Layman, and J. Walsh, IEEE International Conference Record 79 CH1410-0 -NPS, June 1979.
4. Stimulated Raman Scattering from Electron Beams in Dielectric Resonators, K. Busby, K. Felch, R. Layman, and J. Walsh, Bull. Am. Phys. Soc. 24, 607 (1979).
5. Raman Backscattering from Electron Beam-Dielectric Resonators, J. Walsh, D. Arion, K. Busby, and K. Felch, Bull. Am. Phys. Soc. 24, 1076 (1979).
6. Generation of Millimeter Microwaves Using the Cerenkov Interaction, K. Felch, K. Busby, J. Walsh, and R. Layman, Bull. Am. Phys. Soc. 24, 1076 (1979).
7. Growth of a Coherent Drift Instability in a Weakly Ionized Argon Plasma, B. Marden-Marshall, R. Ellis, and J. Walsh, Bull. Am. Phys. Soc. 24, 1048 (1979).
8. The Drift Instability in a Nonuniformly Rotating Plasma Cylinder, B. Marden-Marshall, R. Ellis, and J. Walsh, Bull. Am. Phys. Soc. 25, 866 (1980).
9. Cerenkov Amplifiers, D. Wise and J. Walsh, Bull. Am. Phys. Soc. 26, 936 (1981).
10. A High Power Cerenkov Microwave Source, S. Von Laven, J. Branscum, J. Golub, R. Layman, and J. Walsh, IEEE International Conference May 17-19, 1982.

*Work supported by US DoE Contract EY-76-C-02-3073.

W.W. Lee, Y.Y. Kuo, and R. Okuda, Phys. Fluids **21**, 617 (1978).

SR9 Numerical Study of Kinetic Tearing Modes. J. C. WHITSON, K. T. TSANG and JULIUS SMITH, ORNL. --Tearing modes are perturbations with even $B_z(x)$ and odd $B_\theta(x)$, where x is the distance measured from the rational magnetic flux surface concerned. Classical tearing mode eigenmode equations are derived from the fluid momentum balance equation and Ohm's law. Similar equations can be derived from the drift kinetic equation and Ampere's law taking into account diamagnetic drift, finite ion gyro-radius and kinetic dissipative effects. These equations are the same equations used in study of electromagnetic drift waves. However, the boundary conditions are different. Kinetic tearing eigenmodes must match to ideal MHD solutions outside the tearing layer instead of vanishing away from the rational surface. We study the stability of kinetic tearing modes numerically under various conditions: collisionless, collisional and with trapped electrons. Similar to the electromagnetic drift waves, there are two branches of tearing modes: the drift branch and the shear Alfvén branch. In the collisionless case, only the shear Alfvén branch can be destabilized by a finite ω .

*Operated by Union Carbide Corporation under contract W-7405-eng-26 with the U. S. Department of Energy.

SR10 Pitch Angle Scattering Model in Electromagnetic Drift Wave Calculation. JULIUS SMITH, K. T. TSANG and J. C. WHITSON, ORNL. --The simplest way to treat collision in drift wave calculations is by a number conserving Krook model with a constant collision frequency. It is now known that this model is always stable in electrostatic or electromagnetic calculations. It is then necessary to test the sensitivity of this result to the collision model used. Since the pitch angle scattering model is the next simple collisional model available, we develop a numerical procedure to provide the perturbed electron response subject to pitch angle scattering. This is then fed into the electromagnetic drift wave eigenmode solver to determine the stability.

*Operated by Union Carbide Corporation under contract W-7405-eng-25 with the U. S. Department of Energy.

SR11 Nonlocal Theory of Drift Waves. D. KELLY, Y. C. LEE, A. BUNOS, and B. D. FRID, UCLA. --Our earlier study of drift waves in shearless plasma sheaths having density gradient length, L , comparable to the ion cyclotron radius r_i , used a differential equation approximation to the integral-differential equation satisfied by the electrostatic potential. We have now examined the properties of the full equation, taking advantage of the fact that the integral operator involved has Hermite polynomials as eigenfunctions in the small frequency ($\omega \ll \omega_{ci}$) and small transverse wavenumber ($k_\perp r_i \ll 1$) regime. Expansion in Hermite polynomials and truncation of the resulting infinite set of equations yields the wavefunctions and associated growth rates of the ion acoustic type modes as functions of $v = (k_y/k_z) (m_e/m_i)^{1/2}$, T_i/T_e , $k_\parallel r_i$, and ϵ . As an example, we find for $\epsilon = 1$, $T_i/T_e = 0.1$, $k_\parallel r_i = 10$, and $\epsilon = 0.1$, that the eigenfrequency is given by $\omega = (0.71 + 10.23)(k_y/k_z)$, where $\epsilon = (T_e/m_i)^{1/2}$.

*Work supported by NSF and DOE.

¹Bull. APS **21**, 1121 (1976).

SR12 Time Evolution of the Linear Drift Wave Instability Obtained From an Integral Equation. G. Knorr, ORNL. --The Vlasov equations are written in a coordinate system tailored to the sheared magnetic field, linearized and integrated along the characteristics. The potential and the distributions are expanded into spatial modes to produce a set of coupled Vlasov integral equations. The off diagonal elements are due to magnetic shear and

finite Larmor radius, which may be large. The influence of increasing shear on convective and absolute instabilities and the eigenmode structure of the potential is discussed for different equilibrium density profiles.

*Research supported in part by the Department of Energy under contract EY-76-S-02-2059.

*Permanent address: Department of Physics, University of Iowa, Iowa City, Iowa 52242.

SR13 Comparison of Local and Non-Local Models in Predicting Stability of Collisional Drift Waves. B. E. MARDEN, W. F. ELLIS, and J. C. WHITSON, ORNL. --Theoretical density profiles are used in a comparison of the local slab model and both a local and a non-local cylindrical model for the collisional drift instability. We represent the density profiles by $n = \exp[-(r/r_0)^p]$ with $p \geq 2$. This choice allows not only a fit to a Gaussian profile but accounts for steeper and more localized gradients as well. We treat the profiles exactly in the non-local model and approximate them as Gaussians in the local model and demonstrate the failure of the Gaussian approximation for the steeper profiles. A discussion of stability, which includes the effects of zeroth order radial and axial electric fields, will be given. The slab model is found to differ significantly from both types of cylindrical models in predicting growth rate as a function of azimuthal mode number, m , and reasons for this will be presented.

*Work supported in part by Research Corporation and USAR/OSR Grant #77-3410.

**Present address: Y Division, Lawrence Livermore Laboratory, Livermore, CA 94550.

SR14 Phase Integral Calculation of DCLC Mode Instabilities. WILLIAM H. SHARP and HERBERT L. FISK, Lawrence Berkeley Laboratory. --Standard WKB methods for treating the effect of magnetic shear on the drift cyclotron loss cone (DCLC) mode are limited to weakly sheared plasmas. We discuss a more general phase integral technique for finding eigenfrequencies of a integral dispersion equation and use the method to analyze DCLC mode stability in a finite- B plasma slab with strong magnetic shear. * Research supported by the U. S. Department of Energy.

SR15 Effect of Lower Hybrid Waves to Drift Instabilities. S. C. CHIU, V. S. CHAN, and J. T. HSU, General Atomic Co. --We consider the possibility of drift-wave stabilization by lower-hybrid waves taking into account the effect of finite pump wavelength, ion Larmor radius, and a modified expression for the ponderomotive potential. These lead to different frequency shifts and growth or decay rates from previous works. Comparison with experiments and possible implications to drift turbulence are discussed.

*Supported by DOE Contract EY-76-C-01-0167, Project Agreement No. 15.

SESSION 5S: MULTIPOLES I AND SURMACS; TOPOLOTRON
Wednesday morning 1 November 1978
West Exhibit Hall at 9:30 A.M.

3S1 Comparison of a Hydrogen and a Deuterium Plasma in a Multidipole System. L. B. MARSHALL, K. N. LEE, and R. E. FRISBIE, James Madison University. --Hydrogen and deuterium plasmas are generated in a 40 liter multidipole device by 40 eV electrons emitted from tungsten filaments. The system is surrounded externally by ceramic magnets ($B_{max} = 1.7$ kG) arranged in a full-line cusp geometry. The radial ion saturation current profiles show that only a small amount of ions are lost in between the line cusps. By using a mass-spectrum analyzer, it is found that the percentage of atomic and molecular ions present in both plasmas are approximately the same. From the measured plasma densities and electron temperatures, a leakage current of the hydrogen or deuterium plasma from the line-cusps is estimated.

*Present address: Lawrence Berkeley Laboratory.

*Present address: Auburn University, Dept. of Physics.

✓

Abstract Submitted
For the Twentieth Annual Meeting
Division of Plasma Physics
American Physical Society
October 30 to November 3, 1978

Subject Category Number 4.8

Backscattering from Electron Beam-Dielectric Resonator Combinations. J.E. WALSH, G. CREW, Dartmouth College.*--A hybrid combination of stimulated Cerenkov and Raman Scattering processes can be used to produce coherent radiation. The relation between the frequency of an incident, ω_p , and a scattered, ω_s , photon is:

$$\omega_s/\omega_p = |(1 + \beta n)/(1 - \beta n)| \quad (1)$$

where $\beta = v/c$ and n is the index of refraction of a dielectric resonator. Equation (1) is valid both above and below the Cerenkov threshold. The apparent singularity at $\beta n = 1$ will be controlled either by electron recoil or dispersion of the medium. When an electron beam is used four parametric processes are possible. The gain for each is similar and is given by:

$$\Gamma = 2(n^2/\gamma^3)^{1/2} \beta_p \sqrt{\omega_s \Omega_b} / (\beta n + 1), \quad (2)$$

where β_p is the pump induced velocity modulation and Ω_b is the beam plasma frequency.

*Work supported in part by U.S. Army Grant #DAAG39-78-C-0032 and in part by AFOSR Grant #77-3410

() Prefer Poster Session

(x) Prefer Oral Session

() No preference

() Special Requests for placement
of this abstract:

Submitted by:


(signature of APS member)

John Walsh

(same name typewritten)

Dartmouth College

(address)

This abstract, in original form or a reasonable facsimile, plus two Xerox copies must be received NOT LATER THAN 11:00 AM, AUGUST 4, 1978 at the following address.

Burton D. Fried
P. O. Box F
Sherman Oaks, California 91413

7
✓

✓
Abstract submitted for the
1979 IEEE INTERNATIONAL CONFERENCE ON PLASMA SCIENCE
June 4-6, 1979

Please refer to "Last Call
for Papers" announcement for
instructions in preparing
your abstract.

A Cerenkov-Raman Radiation Source. K. BUSBY,
K. FELCH, R.W. LAYMAN, J.E. WALSH, Dartmouth College.*
--Stimulated Raman Scattering from an electron beam in
a dielectric medium shows a number of interesting and
potentially useful features¹. In a dielectric the
particle velocity can exceed the speed of light and
hence there are two possible dispersion curves along
which energy and momentum can be conserved. Further-
more, in the neighborhood of the Cerenkov velocity
threshold very large Doppler shifts can be obtained
and thus this interaction can be the basis of a short
wavelength radiation source.

In order to test the potential of such a
device an experiment which uses a mildly relativistic
electron beam, a dielectric resonator, and a rippled
magnetic field for a pump wave has been constructed.
The transverse component of the magnetic field is
approximately 300 G which implies an effective pump
wave intensity of 20 MW/cm².

With beam voltages between 100 and 200 KV and
beam currents in the 10A range, operation in the
lower and middle part of the mm wave length region of
the spectrum is anticipated. The performance of the
device will be discussed.

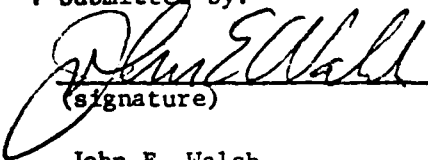
*Work supported in part by U.S. Army Grant #DAAG39-78-
-C0032 and in part by U.S.AFOSR Grant # 77-3410

1. J.E. Walsh, G. Crew, Bull. Am. Phys. Soc. 23, 748,
(1978)

. Subject category number:

- . () Prefer oral session
. () Prefer poster session
. (x) No preference
. () Special requests for
placement of this
abstract

. Submitted by:


(signature)

John E. Walsh

(same name typewritten)

Department of Physics

(full address)

Wilder Hall

Dartmouth College

Hanover, N.H. 03755

. I am member of the Committee
on Plasma Science and Appli-
cations:

() yes (x) no

Appendix III

Physics and Astronomy
Classification Scheme
Number

Abstract Submitted
for the Washington Meeting of the
American Physical Society

Suggested title of
session -
Electron Beams and
Free Electron Lasers

April 23-26, 1979

Stimulated Raman Scattering from Electron Beams
in Dielectric Resonators. K. BUSBY, K. FELCH, R.W.
LAYMAN, J.E. WALSH, Dartmouth College.*--The addition
of a dielectric resonator to an electron beam Raman
scattering experiment can dramatically shorten the wave-
length of the output radiation. Well above the guide
cutoff frequency the output wavelength λ_s is:

$$\lambda_s = \lambda_p (1 - \beta_0 n) / \beta_0$$

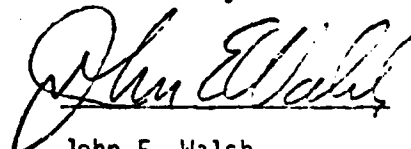
where λ_p is the pump ripple length and β_0 is average
electron beam velocity. A combination Cerenkov-Raman
scattering experiment has been designed to test this
reduction. We use a tubular dielectric resonator and a
rippled magnetic field as a pump field. The effective
intensity of the pump field is approximately 20 MW/cm².
This together with electron beam voltages and currents
of 100-200 KV and 10 A respectively will lead to stimu-
lated Cerenkov-Raman growth lengths of .2-.5 cm⁻¹. The
device performance will be discussed.

*Work supported in part by U.S. Army Grant #DAAG39-78-
C-0032 and in part by U.S.AFOSR Grant # 77-3410

Prefer Oral Session

Appendix II

Submitted by:



John E. Walsh
Dartmouth College
Hanover, N.H. 03755

✓
Abstract Submitted
For the Twenty-first Annual Meeting
Division of Plasma Physics
November 12 to 16, 1979

Subject Category Number 4.8

Raman Backscattering From Electron Beam-Dielectric Resonators. J.E. WALSH, D. ARION, K. BUSBY, and K. FELCH, Dartmouth College.*--It has been demonstrated experimentally and shown theoretically that the addition of a tubular dielectric resonator to a conventional electron beam-Raman backscattering experiment, results in a reduction of the energy required to produce radiation of a given wavelength.¹ The magnitude of the reduction will depend upon the filling factor and the relative dielectric constant of the loading material. It is therefore possible to use modest (100-200 KV) electron beams, a dielectric resonator, and a static magnetic field pump to achieve the kinematic conditions required for operation in the submillimeter region of the electromagnetic spectrum. Several problems associated with the goal of producing a relatively compact, coherent, tunable submillimeter source will be discussed, including beam quality requirements, beam to resonator coupling, and gain.
*Supported in part by US AFOSR Grant #77-3410.
¹K. Busby, K. Felch, R.W. Layman, and J.E. Walsh, 1979 IEEE COPS--Conf. Record, pg. 107.

✓
() Prefer Poster Session

(x) Prefer Oral Session

() No Preference

() Special Requests for placement
of this abstract:

() Special Facilities Requested
(e.g., movie projector)

Submitted by:

Kevin Lee Felch
(signature of APS member)

Kevin Lee Felch
(same name typewritten)

H.B. 6127, Dartmouth College,
(address) Hanover, N.H. 03755

This form, or a reasonable facsimile, plus Two Xerox Copies must be received NOT LATER THAN FRIDAY, AUGUST 17, 1979 at the following address:

Division of Plasma Physics Annual Meeting
Mrs. Marianne Weissenburger
Plasma Physics Laboratory
P.O. Box 451
Princeton, N.J. 08540

10

✓

Abstract Submitted
For the Twenty-first Annual Meeting
Division of Plasma Physics
November 12 to 16, 1979

Subject Category Number 4.8

Generation of Millimeter Microwaves
Using the Cerenkov Interaction. K. Felch, K. Busby, J.E. Walsh, and R.W. Layman, Dartmouth College. *--Earlier experiments involving the Cerenkov interaction between a relativistic electron beam and a dielectric loaded waveguide yielded 6 mm microwaves.¹ These experiments indicated that microwaves of significantly shorter wavelengths might be possible using the same procedures. The present experiments extend the previous attempts into the 3 mm range. Methods by which shorter wavelengths are achieved using the Cerenkov interaction and the short wavelength limit of such techniques will be discussed. Results of the latest experimental investigations will be presented.

*Work supported in part by U.S. Army Grant #DAAG39-78-C-0032 and in part by U.S. AFOSR Grant #77-3410.

¹K. Felch, K. Busby, J.E. Walsh, and R.W. Layman, Bull. Am. Phys. Soc. 23, 749 (1978).

✓

() Prefer Poster Session

(x) Prefer Oral Session

() No Preference

() Special Requests for placement
of this abstract:

() Special Facilities Requested
(e.g., movie projector)

Submitted by:

Kevin Lee Felch
(signature of APS member)

Kevin Lee Felch
(same name typewritten)

H.B. 6127, Dartmouth College,
(address) Hanover, N.H. 03755

This form, or a reasonable facsimile, plus Two Xerox Copies must be received NOT LATER THAN FRIDAY, AUGUST 17, 1979 at the following address:

Division of Plasma Physics Annual Meeting
Mrs. Marianne Weissenburger
Plasma Physics Laboratory
P.O. Box 451
Princeton, N.J. 08540

11

✓

✓

Abstract Submitted
For the Twenty-first Annual Meeting
Division of Plasma Physics
November 12 to 16, 1979

Subject Category Number 1.3 Waves in Nonuniform Plasmas

Growth of a Coherent Drift Instability in a Weakly Ionized Argon Plasma.* B.E. MARDEN-MARSHALL, R.F. ELLIS** and J.E. WALSH, Dartmouth College.-- A nonlocal cylindrical model, using arbitrary density profiles, is used to predict frequency, growth rate and radial shape of the collisional drift instability. The effects of an arbitrary radial electric field are included in both the electron and ion fluid equations and are found to be destabilizing. Comparison is made with a weakly ionized argon plasma for which $n \sim 10^{10} \text{ cm}^{-3}$ $B \sim 1 - 2 \text{ KG}$ $T_e \sim 2 \text{ eV}$ $p_0 \sim 1 \text{ mT}$ Experimentally, wave onset occurs when a positive DC bias is placed on a grid which separates the source region from the strong magnetic field region of the linear plasma device¹. This bias is believed to sever the stable source region from the inherently unstable strong field region, thereby allowing the waves to grow. By pulsing the grid we can trace the evolution of the wave shape, radial profiles, and system parameters as the instability grows.

¹W. Gekelman and R. Stenzel, R.S.I, 46, 1386 (1975).

*Work supported in part by Research Corporation and USAF/OSR Grant #77-3410.

**Present address: Department of Physics, University of Maryland, College Park, MD 20742.

✓
☒ (X) Prefer Poster Session

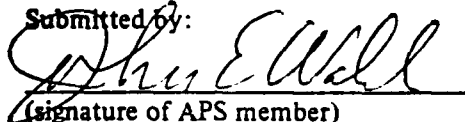
☐ () Prefer Oral Session

☐ () No Preference

☐ () Special Requests for placement of this abstract:

☐ () Special Facilities Requested (e.g., movie projector)

Submitted by:


(signature of APS member)

John E. Walsh

(same name typewritten)

Dartmouth College

(address)

This form, or a reasonable facsimile, plus *Two Xerox Copies* must be received NOT LATER THAN FRIDAY, AUGUST 17, 1979 at the following address:

Division of Plasma Physics Annual Meeting
Mrs. Marianne Weissenburger
Plasma Physics Laboratory
P.O. Box 451
Princeton, N.J. 08540

12
✓

integrated to study the anomalous transport. The resonant particle diffusion is investigated and is also compared with the results from the stochastic theory.

*Work supported by the U.S. Department of Energy Contract DE-AC04-76ET 53036.

¹W. Horton, Nucl. Fusion 20, 511(1980).

252 Triplet Interactions for the Toroidal Ion Pressure Gradient Drift Mode* Wendell Horton, University of Texas at Austin. --Interaction triplets $\omega_1, \omega_2, \omega_3$ with $\omega_1 + \omega_2 = \omega_3$ are analyzed for the ballooning ion pressure gradient mode¹ with growth rate $\gamma_k = k_z^2 \nu_{Ti} (1 + \eta_i)$ and phase velocity $U_k = 1 - (1 + \eta_i) k_z^2$ in which E×B convection produces a conservative mode coupling proportional to $A = k_z^2 \nu_{Ti} / 2$. Each triplet is equivalent to a 5D oscillator system with constant energy and a volume preserving flow. Coherent and stochastic solutions are found. Motivated by the small amplitude expansion solution, a symmetric triplet is found for which the system reduces to 4D. The maximum amplitudes are given by $|\phi_k| = \sqrt{4A} (1 + \eta_i) / k_y$ and $|\phi_{p_k}| = \sqrt{2} (1 + \eta_i) / k_y$. The 4D, volume conserving system is analyzed for regular and stochastic solutions in analogy with the Henon-Heiles problem.

¹W. Horton, D.I. Choi, W.M. Tang, "Toroidal Drift Modes Driven by Ion Pressure Gradients" submitted to Physics of Fluids.

*This work is supported by the U.S. Department of Energy Contract DE-AC05-76ET 53036.

253 Growth of a Drift Wave Due to an RF-Field in a Magnetized Plasma. A. J. ANASTASSIADES and C. L. XAPLANOERIS, Plasma Lab., Nuclear Research Center Demokritos, Athens, Greece. --We have studied a drift wave instability in a magnetized argon plasma due to an externally applied RF-field. The plasma is produced in a coaxial wave guide by RF-power. The magnetic field is applied in the direction of the coaxial waveguide axis. The radial gradient of the RF-field causes an azimuthal electron drift depending on the radial distance, the RF power and the electron neutral collisions. Our plasma parameters are $n_0 \sim 10^{18} \text{ cm}^{-3}$, $\omega \sim 2 \times 2.5 \text{ GHz}$, P varies from 10^{-3} to 10^{-1} torr , T_e varies from 30,000 °K to 90,000 °K, and RF-power varies from 20 to 120 watts. The drifting motion of electrons is coupled with the ion motion resulting to a drift wave instability. Our theoretical model predicts frequencies near the angular frequency Ω of the azimuthal drift motion of electrons and its harmonics, i.e., $\omega \approx \Omega, 2\Omega, 3\Omega, \dots$. A phase reversal of the wave is predicted too as the lower hybrid frequency varies from values lower than the RF-frequency to higher ones. Both dispersion relation and phase reversal for various electron drift velocities have been verified experimentally.

254 Experimental Investigation of Collisional and Collisionless Turbulence in a Tokamak* R. ALLEN and M. YAMADA, Plasma Physics Center, Princeton U. --The impurity driven drift waves in the tokamak have now been identified and more extensively investigated in both the collisional and collisionless regimes. The linear characteristics of the instability in both regimes are described by a local kinetic theory including collisions. In the collisionless case where several azimuthal modes are present, faster growing high- m modes are observed to couple with heavily damped low- m modes, transferring energy to a mode at the difference frequency. The collisional instability is observed to drive strong, radially outward anomalous diffusion as it saturates at an amplitude, $\delta n \sim 10\%$.

*This work supported by U.S. Department of Energy Contract No. DE-AC02-76-CN03073.

255 The Drift Instability in a Nonuniformly Rotating Plasma Cylinder.* E. MARDEN-MARSHALL¹, R.F. ELLIS² and J.E. WALSH, Dartmouth College. --The collisional drift instability, which is observed in a weakly ionized argon plasma with

$n \sim 10^{18} \text{ cm}^{-3}$, $T_e \sim 2 \text{ eV}$, $P_0 \sim 1 \text{ mTorr}$, $B \sim 2 \text{ kG}$ is compared to a cylindrical two-fluid model which allows for arbitrary density profiles and a sheared $\omega \times r$ rotation of the plasma. The drift waves are pulsed on and off, and the evolution of the radial wave and density profiles documented. The early stages of growth represent a linear regime; here experimental measurements of real frequency, growth rate and radial wave shape are made for comparison with the linear theory. Results indicate that both rigid body and sheared column rotation Doppler shift the real frequency, that both are destabilizing, but that neither has a noticeable effect on the shape or localization of the radial eigenmode.

*Work supported in part by Research Corporation and USAF/OSR GRANT #77-1-10.

¹Present address: Department of Physics, Wellesley College, Wellesley, MA 02181.

²Present address: Department of Physics, University of Maryland, College Park, MD 20742.

256 Integral Equation Solution of the Ion Temperature Drift Instability in a Tokamak* J. DENAVIT¹, J.E. MARMON², W.L. DAVIS, and W.L. VAN PEE³. Previous approximate solutions of the ion gyrokinetic equation concerning the drift instability relied on an ion temperature gradient were based on the invalid assumption that $k_y \rho_{Ti} \ll 1$. This permitted 1) the reduction of the integral equation to a differential equation, and 2) an analytic integration over v_{\parallel} of the gyrokinetic equation in slab geometry, thereby reducing its dimensionality and computation time. Although the possibility of performing this latter integration with an approximation is still under investigation, we have proceeded to recalculate these eigenmodes correctly by employing a gyrokinetic equation in v_{\parallel} , ω , x , and t and using an initial value approach.

¹Plasma Physics Laboratory, Princeton University, Princeton, NJ

²Northwestern University, Evanston, IL

³Mass. Inst. of Technol., Cambridge, MA

*Supported by the Union Carbide Corporation under contract A-7405-ENG-6 with the U.S. Department of Energy, Office of Fusion Energy.

257 Ion Temperature Gradient Modes in Toroidal Geometry.* C. Z. CHENG, Princeton U. and K. T. TANG, C. O. BRASLEY, JR., and W. VAN PEE, ORNL. --The linearized gyrokinetic equation describing the plasma dynamics in tokamak geometry is solved by an initial value approach employing high m ballooning mode formalism. The ion temperature gradient mode that is unstable in slab geometry is found to be further destabilized by the ion magnetic drifts. Real part of the mode frequency can be in resonance with the average ion magnetic drift frequency. For even very small toroidicity, this resonance can bring down the critical $n_i (\ln T_i / \ln N_e)$ to zero, in contrast with $n_i \geq 1$ in the slab case. Detailed results over a wide range of parameters will be presented.

*Supported by U.S. DOE Contract No. DE-AC02-76-CN03073.

258 A Linear Theory of the High S Universal and Drift Alfvén Modes. D. HASTINGS¹ and J.E. MARMON, MIT. --The linear high S behavior of two well known low frequency modes is examined in a slab geometry. For the universal drift mode with $n_i \ll 0$, $S \gg 1$ is found to be sufficient to stabilize the mode. In contrast to an understanding based on electrostatic theory, modes with $n_i = 0$, $w/k_{\parallel} v_{thi} \ll 0$ and $k_{\perp} \rho_{Ti} \ll 1$ are the hardest to stabilize. Stabilization is effected by the Doppler shift in the wave frequency ω due to the $\omega \times r$ rotation. This is because of inverse transit time damping which is

✓

Abstract Submitted
For the Twenty-third Annual Meeting
Division of Plasma Physics
October 12 to 16, 1981

Category Number and Subject Microwave Generation - 4.8

☒ Theory ☒ Experiment

Cerenkov Amplifiers*. D. WISE, J. WALSH,
Dartmouth College--A Cerenkov amplifier consists of
a tubular dielectric waveguide, a mildly relativistic
electron beam, and input/output coupling structures.
When the system is operated in the collective regime,
($\omega_p L / c\beta\gamma^{3/2}$) $\gg 1$, a criterion which is relatively
easy to satisfy in the mm and near mm region of the
spectrum, both wide band moderate gain, .5 - 1,
db/cm at about twenty-five percent band widths, and
much higher gain operation over narrower percentage
band-widths are possible. The beam parameters which
give the above performance are 200 KV and 1-20 A.
An analysis of the projected performance of this
system in operation as a reflection amplifier will
be presented.

*Work supported by AFOSR Contract # 77-3410D.

☒ Prefer Poster Session

☐ Prefer Oral Session

☐ No Preference

☐ Special Requests for placement
of this abstract:

☐ Special Facilities Requested
(e.g., movie projector)

Submitted by:

John Walsh

(signature of APS member)

Dartmouth College, Hanover

(same name typewritten)

NH 03755

(address)

This form, or a reasonable facsimile, plus Two Xerox Copies must be received NO LATER THAN
Thursday, July 9, 1981, at the following address:

Division of Plasma Physics Annual Meeting
c/o Ms. Joan M. Lavis
Grumman Aerospace Corporation
105 College Road East
Princeton, New Jersey 08540

17-19 May, 1982

A High Power Cerenkov Microwave Source.* S. Von Laven, J. Branscum, J. Golub, R. Layman and J. Walsh, Dartmouth College. An electron beam-driven dielectric-lined waveguide has produced 30-100 kilowatts of coherent radiation over an octave band on the TM01 mode of the waveguide. Operation on the TM02 mode has been realized as well. Impedance mismatches at the ends of the liner section provide a reflected signal, which undergoes amplification during successive passes.

This work employs a pulsed, 1-40 ampere beam of 100-250 keV electrons directed along the axis of a dielectric-lined circular waveguide¹.

The pulse duration is about four microseconds. Quartz ($\epsilon_p=3.78$), stycast ($\epsilon_p=5$), and boron nitride ($\epsilon_0=4.2$) liners of several thicknesses have been employed.

For most dielectric liners used, the fundamental output frequency is near the frequency at which the phase velocity of the TM01 mode is synchronous with the beam. Data will be presented for several liners in 12.5 mm diameter waveguide. A large systematic error is noted for the case of the 3 mm quartz liner. A surface charge build-up on the quartz is suspected of decelerating the beam to velocities synchronous with the observed output. The problem nearly disappears for 2 mm quartz. The longitudinal electric field associated with the 1 mm liner geometry is too weak to give good coupling for moderate beams.

The output power is found to increase as the square of the beam current in the 1-10 ampere range for the 2 mm quartz liner, again in 12.5 mm diameter waveguide. In a separate, absolute measurement with the same liner geometry, a 12-ampere, 115 kilovolt beam generated 30 kilowatts of radiation at 50 GHz. Powers up to 100 kilowatts were obtained at lower frequencies for 3 mm thick boron nitride in the 12.5 mm diameter waveguide. Power is often sufficient to cause atmospheric breakdown in X-band waveguide.

The range of frequencies obtainable on a single mode has reached nearly an octave. In some of the 12.5 mm diameter waveguide experiments and in a 9.5 mm waveguide experiment, it has been possible to suppress the TM01 mode and observe coupling to the TM02 mode. Frequencies between 100 and 120 GHz have been attained. The power is probably less than that obtainable on the TM01 mode, but still significant. Lower levels of output have been observed through a 200-GHz filter with the 2 mm quartz liner, 12.5 mm waveguide.

Discrete cavity modes are observed rather than a continuous waveguide spectrum. The Q of the liner section itself is an important parameter. Reduced reflectivity at either end raises the voltage threshold for output.

*Work supported by AFOSR Contract # 77-3410D.

¹K.L. Felch, K.O. Busby, R.W. Layman, D. Kapilow and J.E. Walsh, Appl. Phys. Lett. 38, 601 (1981).

✓

IV. PUBLICATIONS

1. Cerenkov and Cerenkov Raman Radiation Sources, John E. Walsh, in Physics of Quantum Electronics, edited by S. Jacobs and M. Scully, Vol. 7, p.255, (Addison-Wesley, Reading, MA 1980).
 2. Cerenkov and Cerenkov-Raman Masers: Experiments, K. Felch, K. Busby, R. Layman and J. Walsh, in Physics of Quantum Electronics, edited by S. Jacobs and M. Scully, Vol. 7, p.301, (Addison-Wesley, Reading, MA 1980).
 3. Cerenkov Free Electron Laser Gain and Superradiance, Ph.D. Thesis, Captain Douglas H. Wise, Dartmouth College, Hanover, N.H. 03755 (1981).
 4. The Cerenkov-Cyclotron Instability, Senior Honors Thesis, John E. Golub, Dartmouth College, Hanover, N.H. 03755 (1981).
 5. A High Power Cerenkov Maser Oscillator, S. Von Laven, J. Branscum, J. Golub, R. Layman and J. Walsh, submitted to Appl. Phys. Lett., May 1982.
- ✓

✓

CERENKOV AND CERENKOV-RAMAN RADIATION SOURCES

JOHN E. WALSH

INTRODUCTION

✓

Cerenkov radiation¹ takes its name from P.A. Cerenkov whose pioneering experimental research clearly established the nature of the electromagnetic radiation produced by a charged particle when it moves with superluminal velocity in a dielectric medium. The electron sources used by Cerenkov were weak and thus he studied the radiation produced by single particles (spontaneous emission). The analysis of Frank and Tamm² also applied to the single electron case. We will be concerned in this paper with a tutorial discussion of practical radiation sources which make use of the Cerenkov process and hence we will be interested in stimulated as well as spontaneous Cerenkov emission. The former one of these is like the latter a potential source of short wavelength radiation. Cerenkov's original experiments were in the visible range of

17

✓

✓

the spectrum and more recently it has been demonstrated that a highly relativistic electron beam-noble gas combination is a bright incoherent source of radiation in the vacuum ultraviolet region³. In other experiments mm wavelength Cerenkov radiation has been obtained^{4,5,6}. It is of interest therefore, to consider the possibility of constructing Cerenkov lasers over the entire range of the electromagnetic spectrum for which suitable dispersive materials can be found.

Cerenkov radiation can be thought of as a decay process in which an electron moving through a dielectric emits a photon and drops to a lower energy state. We will also be interested in a related process where an electron either scatters an incoming photon or emits two photons. Unlike Cerenkov radiation which has no vacuum counterpart the first of these is analogous to Compton scattering. The dynamics of the scattering are, however, both complicated and enriched by the presence of the dielectric. In a Cerenkov oscillator or amplifier the single electron is replaced by a beam whose intensity is sufficient to cause stimulated emission. A related device in which an electron beam in a dielectric interacts with an incident photon beam, can be imagined. If the electron beam is intense enough to support collective plasma oscillations the incident photons scatter off of these and the device would be called a Cerenkov-Raman laser or maser. As the wavelength of the scattered photon is decreased the electron beam loses its collective nature and the scattering becomes a single particle process. Stimulated scattering still occurs in this limit, however, and devices operating in this range are designated Cerenkov-Compton radiation sources. The

18

✓

✓

definition of the division between Cerenkov-Raman and Cerenkov-Compton devices adopted here is consistent with that used for devices⁷ operated without a dielectric.

As is the case with straight Cerenkov sources, Cerenkov-Raman or Compton devices are in principle capable of working at wavelengths as short as the visible or vuv regions of the spectrum. At the present time, however, practical devices have been operated in the mm range⁸. A primary purpose of these tutorial notes is to explore in some detail the criteria which must be met if short wavelength operation is to be achieved.

The notion that superluminal velocity charged particles could be used as a radiation source is quite old. Heaviside⁹ in 1889 and Sommerfield¹⁰ again in 1904 solved for the electromagnetic fields produced by a charged particle moving with greater than light velocity. Both of these analyses preceded special relativity and assumed that it was possible for a particle to have a velocity greater than that of light in a vacuum. If, however, the velocity of light c is replaced by c over the index of refraction n , their solutions are consistent with the work of Frank and Tamm². There are also some scattered observations of Cerenkov radiation. M. Curie¹¹ in 1911 deduced that one component of radiation produced in the walls of a glass container containing radioactive material was due to the presence of high speed electrons, and Mallett¹² in 1926 performed several related experiments. Taken as a whole, however, none of the early work was sufficiently complete or correct to jeopardize the position of Cerenkov and of Frank and Tamm as the founders of the subject of Cerenkov radiation.

19
✓

✓

Following this original^{1,2} work a very large number of papers devoted to the subject have been written. A review article by Bolotovskii¹³ contains over four hundred references. Much of the emphasis in this work was on the application of Cerenkov radiation to the production of useful radiation sources in the millimeter, the submillimeter and the far infrared regions of the electromagnetic spectrum. Almost every conceivable electron beam dielectric structure combination has been analyzed.

It is, of course, not practical to propagate an electron beam through a solid dielectric and hence particular importance is attached to the radiation produced by electrons moving along the axis of a channel in a dielectric. Ginzburg¹⁴, analyzed a number of these problems in detail. He found that in addition to the fact that spontaneous Cerenkov emission is relatively weak in all regions of the spectrum below the visible¹⁵, there is not surprisingly also a relation between the size of the channel and the wavelength of the radiation produced. One method of circumventing the relative weakness of the process at longer wavelengths is to bunch the electrons. If the scale¹⁶ length of the bunch is small compared to the wavelength the radiation intensity is increased by the square of the number of electrons in the bunch. A number of experiments using this technique were performed. Notable among these were the experiments of Coleman⁴ and of Lashinsky⁵. In all of the analyses and experiments mentioned the electron beam intensity and dielectric resonator designs were such that stimulated emission was not a factor.

Most, although not all of the early work was devoted to straight Cerenkov radiation. The problem of the

✓

radiation produced by an oscillator moving through a dielectric was, however, analyzed by Frank¹⁷ and a later analysis of this and similar problems with emphasis on its use as a radiation source was performed by Ginzburg¹⁸. In the latter work expressions for the power radiated by both sub and superluminal oscillators were given. More recently in a series of publications Schneider and Spitzer¹⁹ have analyzed the problem of photon-electron scattering in a dielectric medium. All of these analyses were devoted to single particle spontaneous emission processes.

The efficient production of stimulated Cerenkov or stimulated Cerenkov-Raman radiation requires electron beam densities and velocities which are in excess of those required by conventional microwave tubes. This is the primary reason why these mechanisms have not yet been used in practical radiation sources. However, the need for high power coherent sources in the shorter part of the millimeter range and for high or moderate power tuneable coherent sources in the submillimeter and far infrared regions of the spectrum has led to some acceptance of electron beams with parameters which are more than adequate for the production of stimulated Cerenkov radiation. An intense electron beam has been used to produce megawatt levels of radiation²⁰ and an electron beam generator similar to that used in high power klystrons has been used to produce both stimulated Cerenkov⁶ and stimulated Cerenkov-Raman³ radiation. The details of these experiments will be discussed elsewhere²². The remaining sections of these notes will be devoted to exploring the fundamental principles of device operation.

21

✓

KINEMATIC CONSTRAINTS ON CERENKOV AND CERENKOV-COMPTON SCATTERING

A number of useful conclusions can be drawn from an analysis of the constraints which energy and momentum

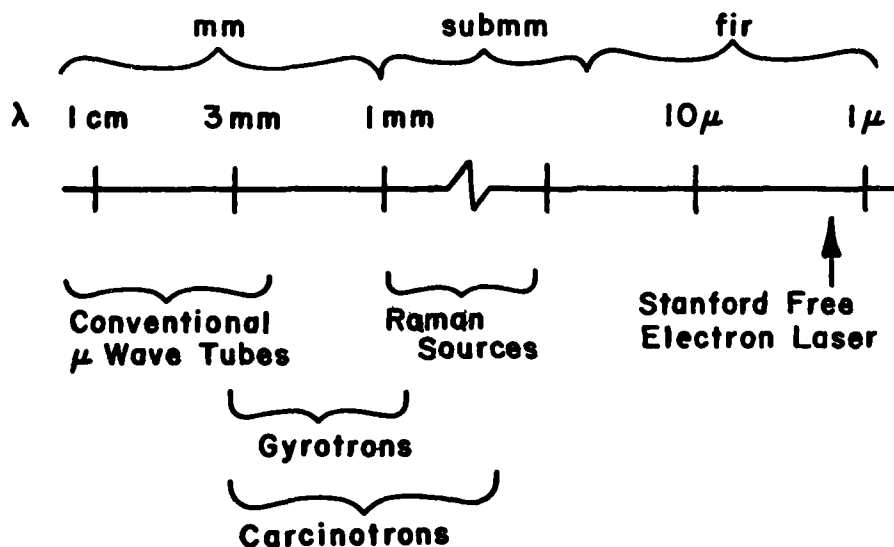


Fig. 1. Free electron radiation sources.

conservation impose on Cerenkov and Cerenkov-Compton scattering. In order to see why this is so we consider the diagrammatic representation of a section of the electromagnetic spectrum shown in Fig. 1. On the left we have conventional microwave tubes. These were developed during an earlier effort to overcome the difficulties encountered when attempts were made to develop radiation sources in the cm wavelength range. They are all characterized by the fact that at least one critical dimension, l , is of the order of the operating wavelength λ_0 .

✓

If an attempt is made to simply extend the successful microwave devices down in wavelength a number of fundamental difficulties^{23,24} become apparent. The quality factor, Q , of any (closed) resonator drops as $\lambda^{1/2}$ and furthermore as the resonator volume decreases power density increases and heat dissipation becomes a severe practical problem. Furthermore, if we choose $l \gg \lambda_0$ the resonator Q must rise at least as fast as $(l/\lambda_0)^3$ if the modes are to be resolved. In two and one dimensional resonators this restriction becomes $(l/\lambda_0)^2$ and (l/λ_0) respectively. Thus open resonators will be an advantage if we require $\lambda_0 \ll l$. Clearly however, something other than resonator geometry alone must determine the operating wavelength λ_0 for an electron beam device if it is to operate at λ_0 much less than say one mm.

✓

In a conventional laser λ_0 is, of course, set by atomic or molecular structure. For the short wavelength free electron sources mentioned on Fig. 1 several different techniques are used to fix the wavelength. The Stanford²⁵ free electron laser and the stimulated Raman scattering experiments performed at the Naval Research Laboratory²⁶ and at Columbia University²⁷ use the relativistic doppler shift. Hence λ_0 in those experiments is set by the wavelength of an incoming (pump) source (a static rippled or helical magnetic field with wavelength λ_p) and the beam energy. This is a good technique since it does not rely on resonator geometry but suffers from the disadvantage that λ_0 goes down approximately as the inverse of the electron beam energy squared and short λ_0 operation requires large beam energies. In the gyrotron, wavelength is determined by the cyclotron resonance. These are prime candidates for mm wavelength

✓

tubes but operation at wavelengths below one mm requires very large magnetic fields. The carcinotron is essentially a backward wave oscillator. The wavelength in these is set by geometry and because of this carcinotrons are probably the ultimate straightforward²⁸ extension of microwave tubes.

ENERGY-MOMENTUM CONSERVATION FOR CERENKOV SCATTERING. By considering the kinematics of Cerenkov radiation we will be able to determine the extent to which this mechanism can determine a value for λ_0 which is much less than λ . A quantum view of the radiation process is shown schematically in Fig. 2a. Applying the laws of conservation of energy and momentum and subsequently eliminating the momentum we obtain:

$$\hbar\omega [\hbar\omega(n^2-1) + E_0(\beta_0 n \cos \theta_c - 1)] = 0 \quad (1)$$

where,

$$\beta_0 = v_0/c$$

is the initial electron velocity measured in units of the light velocity and E_0 the electron energy is in the conventional notation:

$$E_0 = \gamma_0 mc^2 \quad (2a)$$

$$\gamma_0 = 1/(1-\beta_0^2)^{1/2} \quad (2b)$$

The index of refraction, $n(\omega)$, may depend upon frequency. If $\beta_0 n < 1$ the only solution of Eq. (1) is $\omega = 0$. When the beam velocity exceeds the Cerenkov threshold, $\beta_0 n = 1$, however, the Cerenkov decay process is allowed and we find:

$$\cos \theta_c = 1/\beta_0 n + f\omega(n^2-1)/E_0 \quad (3)$$

The second term on the right hand side of Eq. 3 is very small at any possible ω and hence in regions where n is frequency independent the emission threshold is also frequency independent. In the absence of dispersion we will

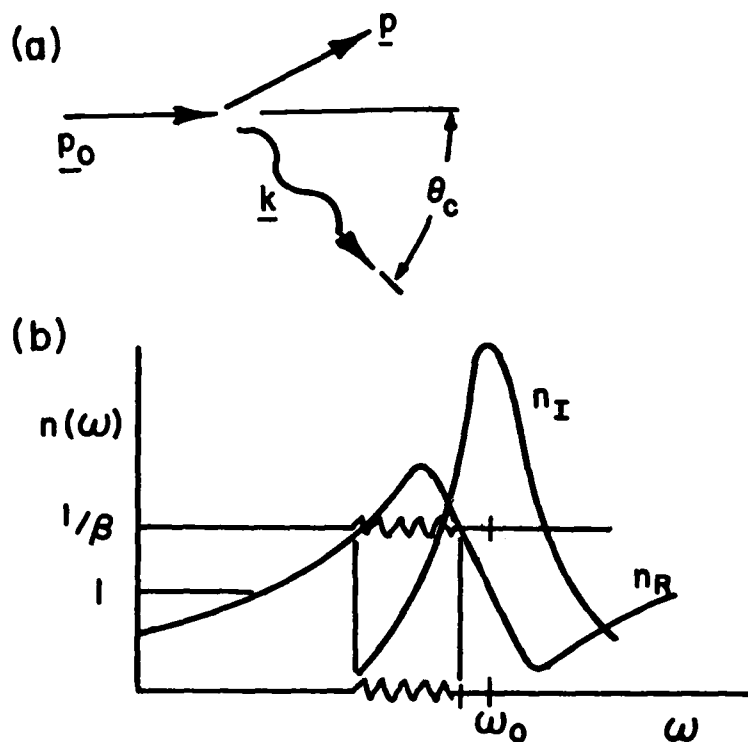


Fig. 2. a). Cerenkov scattering. b). Emission for $\beta n_R > 1$.

also find that the emission spectrum varies slowly with frequency. One method whereby the emission spectrum can be narrowed depends upon the rise in index of refraction near an absorption line. This is illustrated in Fig. 2b. The fact that the emission is near an absorption line means of

✓

course that a good deal of the emitted radiation can be reabsorbed. It is a technique which has been used in particle counting applications²⁹ and in producing bright incoherent vuv radiation³. Furthermore, elementary calculations indicate that strong stimulated emission can be obtained in the vuv from an electron beam noble gas combination³⁰. There is as yet no experimental verification of this latter prediction, a fact which is due in part to the great practical difficulties.

✓ CERENKOV SCATTERING IN BOUNDED MEDIA. There are highly transparent solid materials available over much of the spectrum shown in Fig. 1. These can be configured in a wide variety of electron beam dielectric resonator combinations. Some of these have been tested experimentally^{20,21} and found to work. Since they also show promise of working in the middle of the spectral range shown in Fig. 1 where moderate and high power sources are not now available, we will concentrate much of our discussion on this approach. Shown in Fig. 3 is a sketch of a dielectric tube waveguide and the dispersion curve for a TM guide mode. This mode is chosen in order to conform to the symmetry of the classical picture of Cerenkov radiation in an infinite dielectric which is that of a wake of radiation propagating at cone angle θ_c .

A detailed analysis of this problem is straightforward but quite complicated in detail. Fortunately, however, it is possible to deduce the most important conclusions with the aid of simple qualitative arguments. First we see that if $\beta n > 1$ there will be a coupling between an electron moving along the axis of the tube and the guide mode. Furthermore, due to the fact that

I
I
I

there is a unique relation between ω and k the Cerenkov emission will occur at a discrete frequency given by:

$$\omega = c k \beta \quad (4)$$

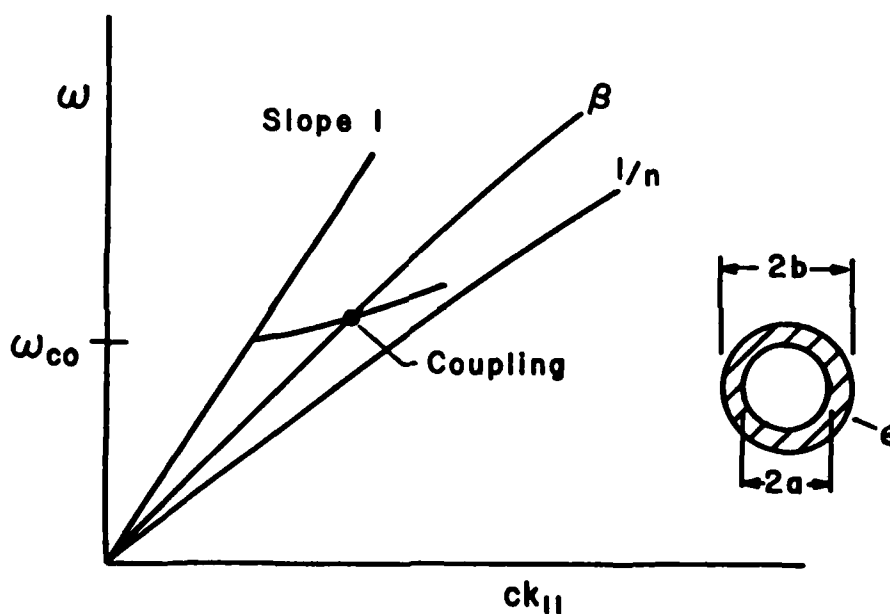


Fig. 3. Dispersion and coupling in a dielectric resonator.

Provided the guide modes are resolved with respect to transverse wave number, a series of lines, one for each mode, will be produced. As the emission occurs one can imagine the electron moving along the dispersion curve toward higher ω and k until the coupling is so reduced that emission no longer occurs. Treatment of the coupling is not

a purely kinematic process and hence it will be deferred until a later section.

Another important conclusion can be reached with the aid of Fig. 3. The cutoff frequency (ω_{co}) will depend inversely upon the wall thickness d and the square of the index of refraction of the material ($n^2 = \epsilon$). Hence:

$$\omega_{co} = 1/d(\epsilon-1)^{1/2} \quad (5)$$

and in general,

$$\omega \approx 1/d(\beta^2 \epsilon - 1)^{1/2} \quad (6)$$

The frequency at which the interaction occurs can be controlled both by d and by $\beta^2 \epsilon$. Thus insofar as kinematic constraints are concerned we have achieved conditions such that λ , the wavelength of the frequency produced can be much less than the characteristic dimension $2a$. Furthermore, by judiciously combining the use of d and $\beta^2 \epsilon$ some control over the separation of different transverse modes can be obtained. Before the choice of all parameters is made, however, the coupling must be investigated.

CERENKOV-COMPTON SCATTERING. Shown in Fig. 4 are sketches of two possible Cerenkov-Compton (electron photon scattering in a dielectric) scattering processes. In the first of these, Fig. 4a, $\beta_0 < 1/n$ and the event is analogous to ordinary Compton scattering in that an incident photon k_p (for pump) scatters off an electron which drops to a lower energy as it emits a photon k_s . There is, however, a very important difference. Application of the laws of energy

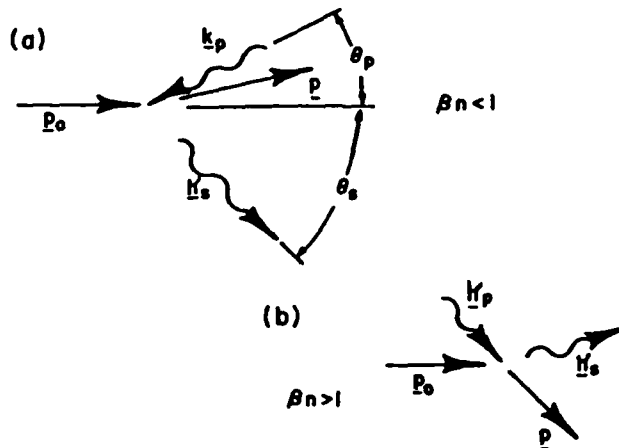


Fig. 4. Cerenkov-Compton scattering, $\beta n \gtrless 1$.

and momentum conservation lead to the conclusion that:

$$\frac{\omega_s}{\omega_p} = \frac{1 + \beta_o n(\omega_p) \cos \theta_p}{1 - \beta_o n(\omega_s) \cos \theta_s} \quad (7)$$

Hence ω_s becomes arbitrarily large as $\beta_o n(\omega_s) \rightarrow 1$. When electron recoil and or dispersion are included the frequency shift becomes finite but still very large in this same limit. Thus unlike similar stimulated scattering devices^{10,26,27} which operate without a dielectric, extremely high energies are not a prerequisite for large ω_s and hence this is a conclusion of some practical significance.

The presence of the medium makes possible $\beta n > 1$ and thus there are scattering processes which have no vacuum analog. These are shown in Fig. 4b. Application of the

conservation laws in this case leads to the relation:

$$\frac{\omega_s}{\omega_p} = \frac{\beta_o n(\omega_p) \cos \theta_p + 1}{\beta_o n(\omega_s) \cos \theta_s - 1} \quad (8)$$

for which comments similar to those made for Fig. 4a may be made in the limit $\beta_o n(\omega_s) \rightarrow 1$. There is, however, one difference, as $\beta_o n(\omega_s) \rightarrow 1$ from above unity the solution to the conservation equation moves into the complex plane and the process as expected, becomes forbidden.

If the effects of dispersion are included, multiple roots of Eqs. 7 and 8 can be obtained^{17,18,19}. These will be of some importance both in gasses when ω_s is near an absorption line and in the case where a dielectric waveguide is used to support the wave. Before analyzing the waveguide case, however, a very important practical modification to the scattering processes should be considered.

THE ZERO FREQUENCY PUMP. It might be anticipated that an intense source of incident, "pump", photons would be required if a useful level of stimulated radiation at ω_s is to be produced. This would be an important practical limitation if it were not for the fact that a rippled or helical static magnetic field with wavelength λ_p will serve³¹ as well. This so called zero frequency pump ($\omega_p = 0$, $k_p = 2\pi/\lambda_p$), which is also used in the vacuum version of stimulated scattering sources, is capable of providing enormous equivalent pump power in the rest frame of the electron.

Analysis of the kinematic relations which lead to Eqs. 7 and 8 with the assumption that ω_p is now zero leads

immediately to:

$$\omega_s = \frac{c\beta_o k_p \cos\theta_p}{1 - \beta_o n(\omega_s) \cos\theta_s} \quad (9a)$$

and,

$$\omega_s = \frac{c\beta_o k_p \cos\theta_p}{\beta_o n(\omega_s) \cos\theta_s - 1} \quad (9b)$$

for the subluminal and superluminal cases respectively. The advantages of a zero frequency pump thus apply to the Cerenkov-Compton processes. A further advantage not available in a vacuum is that now k_p can be chosen in order to get good depth of modulation. The frequency shift is controlled independently by $\beta_o n(\omega_s)$.

CERENKOV-COMPTON SCATTERING IN A WAVE GUIDE. The motion imparted to an electron by the pump is primarily transverse and hence this motion can couple to the TE modes of a guide. Shown in Fig. 5 is a sketch of the dispersion relation for a partially filled guide³² which is bounded by metal walls. Also shown are the beam line $ck\beta$ for the case $\beta n < 1$ and the zero frequency pump which is designated as a horizontal line segment of length k_p . It is clear from the diagram how the pump makes up the momentum difference between a beam mode and the scattered mode. Furthermore, it is also clear that there will in general be two solutions to the kinematic relations and a beam energy threshold below which the scattering process is forbidden. A sketch of the beam energy versus frequency curve is also shown on Fig. 5.

Comments made in a previous section regarding the role of d and ϵ in controlling the frequency of the fundamental mode generally apply to the Cerenkov mode as

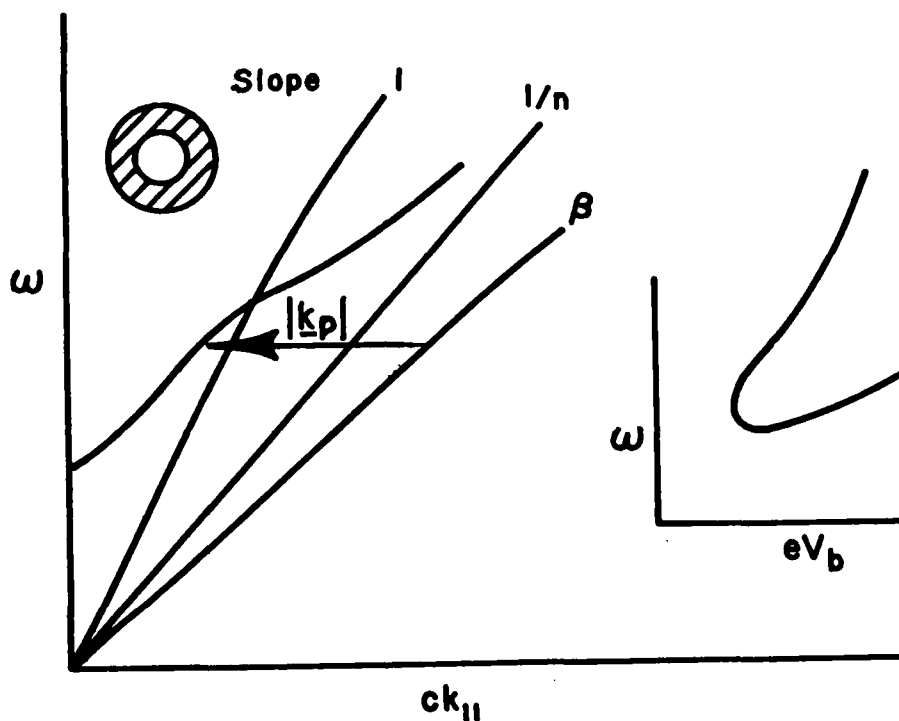


Fig. 5. Cerenkov-Compton scattering in a dielectric resonator.

well. There is one further significant difference. When $\omega/ck < 1$ the fields in the vacuum region must evanesce away from the dielectric (Fig. 6) and although some control over the decay length can be maintained by using large energy electron beams it will ultimately lead to weak coupling at large ω . When Cerenkov-Compton scattering is used, however, we can also couple to waves with $\omega/ck > 1$ and hence to fields which peak rather than evanesce in the region of the

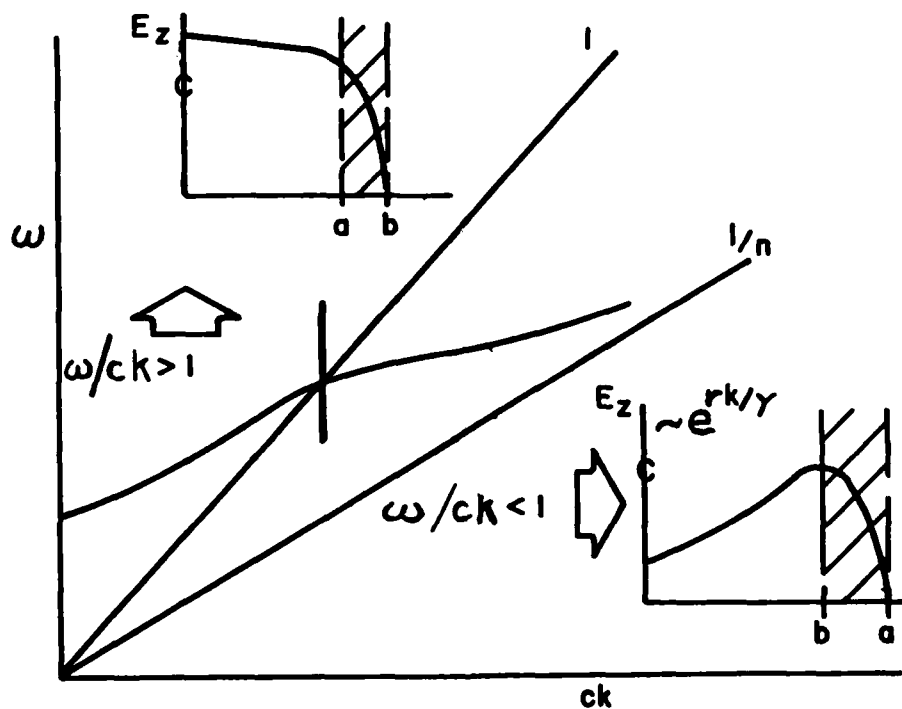


Fig. 6. Axial field strength $\omega/ck \approx 1$

electron. The advantage of the dielectric is not lost in this operating regime because the point where $\omega/ck = 1$ will still depend upon $(d^2(\epsilon - 1))^{-1/2}$ and the point near $\beta n = 1$ will still produce large frequency shifts at beam energies which are comparatively modest. The preceding discussion is primarily aimed at the regime $\beta_0 n < 1$ since there are practical advantages to operating with lower beam energies. Devices need not be restricted to this region, however,

✓

since the cross section for the process becomes large for both $\beta_0 n \lesssim 1$. Analysis of the related dynamical processes will show that gain can be achieved in both regimes.

CONCLUSIONS. We can conclude from the kinematic arguments presented in the preceding sections that one requirement for producing a high frequency free electron device, $l \gg \lambda_0$, can be met by Cerenkov and Cerenkov-Compton devices. Whether those possibilities are realized will depend also on the electron dynamics and the parameters of the electron beam used to drive the device. This will be taken up in the next sections.

CERENKOV EMISSION RATES

✓

The spontaneous and stimulated emission rates for Cerenkov radiation can be computed either classically or quantum mechanically. In the quantum calculation one would begin with the kinematic constraints discussed previously and use perturbation theory in the standard way to arrive at expressions for the emission rates. When the recoil terms ($\hbar \omega / E_0$) are small however, the resulting expressions are independent of \hbar . This is true in both the nonrelativistic and the extreme relativistic limit. It is a result of the fact that the electron is making transitions between continuum states and does not depend upon an assumption that there are a large number of photons present. Cerenkov radiation is thus an essentially classical process, and we will use classical formalism, Maxwell's equations and the relativistic Vlasov equation, in order to arrive at

expressions for the emission rates.

SPONTANEOUS CERENKOV EMISSION. The classical picture of Cerenkov emission is that of a wake produced when the particle velocity exceeds the speed of light in the medium. A sketch is shown in Fig. 7. The symmetry of the problem

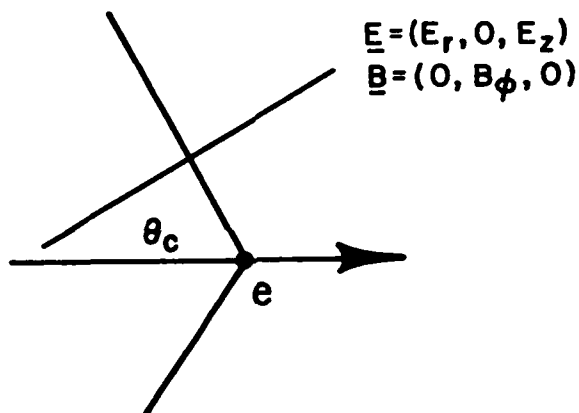


Fig. 7. Cerenkov wake and field components.

immediately dictates which electromagnetic field components, also stated on Fig. 7, are nonvanishing. Derivations of explicit expressions for these are readily available and need not be repeated. We will simply summarize the main conclusions.

If recoil and dispersion are neglected, closed form expressions for the fields as functions of r and z can be obtained. These diverge on the shock front defined by the Cerenkov cone however, and hence they are not the most useful form for further work. It is better to Fourier

transform the charge,

$$\rho = -e \frac{\delta(r)}{2\pi r} \delta(z-vt) \quad (10a)$$

and current,

$$\underline{J} = \underline{v} \rho \quad (10b)$$

which results in

$$\rho_{k,\omega} = -e \frac{\delta(r)}{r} \delta(\omega-kv) \quad (11a)$$

and

$$\underline{J}_{k,\omega} = \underline{v} \rho_{k,\omega} \quad (11b)$$

and use these as source terms in equations for the scalar and vector potentials. The equations governing the radial dependence are then Bessel equations. This in turn suggests that a Fourier-Bessel expansion is the best way to decompose the fields. In an infinite medium the Hankel transform is used, and an expression for the work done by the particle on each component of its own polarization field can be readily computed. The resulting expression is the well known formula for the intensity of radiation produced per unit path length per unit frequency interval:

$$\frac{dI(\omega)}{dz} = e^2 \omega (1 - 1/\beta^2 \epsilon(\omega)) / c^2 \quad (12)$$

Integration of Eq. 12 over all ω would result in the total power lost per unit path length. If dispersion is neglected however, this expression again diverges. This is a purely formal difficulty however, since $\epsilon(\omega) \rightarrow 1$ as $\omega \rightarrow \infty$ for any material and it is obvious that the integral is to be done only for regions where $\beta^2 \epsilon > 1$. As a measure of intensity per unit ω Eq. 12 is accurate even in regions when $\epsilon(\omega)$ is sensibly constant.

Evaluation of Eq. 12 also readily shows that very little radiation is produced until ω reaches the uv region of the spectrum. This conclusion is true even if a substantial beam of electrons is used in place of a single electron. If a beam of finite cross section is propagated in a dielectric the power produced per unit length of beam becomes

$$\frac{dP(\omega)}{dz} = \frac{eI}{c} \frac{\omega}{c} (1 - 1/\beta^2 \epsilon(\omega)) \quad (13)$$

where I is the beam current. If the current is expressed in amperes and the power density in watts we obtain:

$$\frac{dP(\omega)}{dz} = 10^{-8} I(A) \frac{\omega}{c} (1 - 1/\beta^2 \epsilon) \quad (14)$$

watts/cm for the power. Pure spontaneous Cerenkov radiation is therefore, a weak process throughout the wavelength range longer than a few tenths of a micron. We will find, however, that both radiation in a superadiant configuration and stimulated radiation are potentially strong processes.

Before leaving the topic of spontaneous Cerenkov

radiation it is useful to point out the differences which occur in the radiation formulas when a bounded medium is introduced. In the discussion of Fig. 3 we concluded that the emission in a dielectric tube was confined to a series of discrete frequencies, one for each mode. The discreteness would remain so long as the overall Q was such that the modes could be resolved. Straightforward extension of the techniques used in the infinite medium can be used to obtain

$$\frac{dI}{dz} = \frac{2e^2}{a^2} \frac{1}{J_1^2(x_{0l})} \quad (15)$$

for the power emitted into a mode whose field dependence is $J_0(x_{0l}r/a)$ where x_{0l} is a root of the Bessel function J_0 , and a is the guide radius. When a beam of current I is used, the expression analogous to Eq. 5 becomes:

$$\frac{dP}{dz} = \frac{2e}{a^2} \frac{I}{J_1^2(x_{0l})} \quad (16a)$$

$$= 2.88 \times 10^{-12} I(A)/a^2 J_1^2(x_{0l}) \quad (16b)$$

watts/ampere/cm. Again this is a very small amount of power but the comments pertaining to changes in the system which lead to either superradiant or stimulated emission lead to predictions of high available power output.

STIMULATED CERENKOV EMISSION RATES. The early theoretical and experimental attempts to turn Cerenkov radiation into a useful source made use of what could be termed pre-bunching.

✓

Clearly if a short (compared to the desired wavelength) bunch of electrons were used the intensity of the radiation would increase by the square of the number of electrons in the bunch. In principle the enhancement could be very large but in practice it is difficult to produce dense bunches with a scale length which is short enough to be interesting. It is better to use the process of stimulated emission. The scale length in this case is that of the stimulating radiation.

There are two basic regimes in which the stimulated process is important. In the first, which pertains to weak beams, spontaneously emitted photons are trapped in a resonator and these stimulate further emission. The energy build-up in this regime will be sensitive to resonator length and other cavity details and for this reason it will be defined as the interferential gain regime.³⁴ In order for subsequent electrons to add energy to the spontaneously emitted field left by earlier electrons, control of the overall phasing of beam and radiation must be maintained. The growth of radiation within the beam is not exponential and the reaction of the radiation back on the beam in this regime need not be treated self-consistently.

In the second regime the beam is strong enough to cause exponential amplification of the spontaneously created field within the beam itself, and the role of the cavity, if one is used, is somewhat different. Discussion of the details of the role played by resonators will be deferred until a later section. The gain in the exponential regime is subdivided according to whether the beam can be regarded as cold (negligible thermal spread) or warm (the thermal spread affects the gain). We can easily show that the

✓

decision about whether the beam can be regarded as warm or cold depends upon the beam density and the wavelength as well as the velocity spread. Consider a monoenergetic electron beam which is supporting a slow space charge wave propagating in the same direction as the beam. Assuming the fields are weak enough to allow the neglect of nonlinear effects, the dispersion relation of such a mode is easily derived with the aid of the equations of motion,

$$\frac{d(\gamma v_z)}{dt} = \frac{-e}{m} E_z \quad (17)$$

of continuity,

$$\frac{\partial n}{\partial t} + \nabla \cdot (n \underline{v}) = 0 \quad (18)$$

and Poisson's equation,

$$\underline{\nabla} \cdot \underline{E} = -4\pi e (n - n_0) \quad (19)$$

Fourier transforming we obtain for the slow space charge mode

$$\omega = kv_0 - \Omega_b / \gamma_0^{3/2} \quad (20a)$$

where

$$\Omega_b^2 = 4\pi n_0 e^2 / m \quad (20b)$$

is the beam plasma frequency and $\gamma_0 = (1 - \beta_0^2)^{-1/2}$ is related to the zero order energy of a beam electron.

The relation between the phase velocity of this mode and the beam velocity is shown in Fig. 8. Also shown in Fig. 8 are two typical velocity distributions. In one the beam and the modes are resolved in velocity and the beam is approximately "cold". In the other it is not and the beam

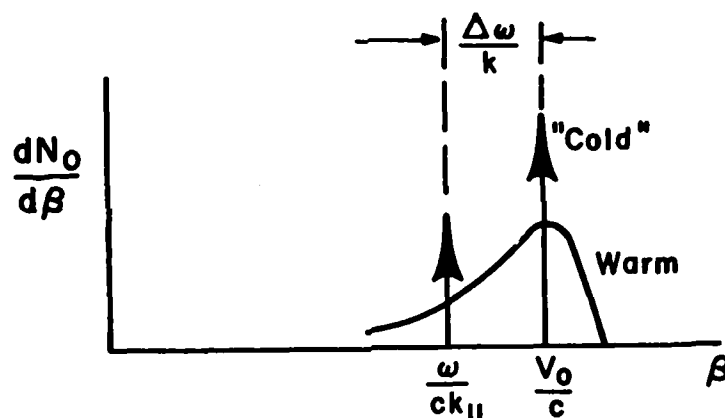


Fig. 8. Beam-space charge waves.

is "warm". Measured in the laboratory frame the velocity difference between the mode and the beam is

$$\Delta v = \Omega_b / \gamma_0^{3/2} k \quad (21)$$

If we now consider a beam whose velocity spread is equal to Δv we have a criterion for determining the wave length at which a beam can no longer be regarded as cold. It is convenient to express this in terms of energy spread:

$$\Delta v_b = c \Delta \gamma / \beta_o \gamma_o^3 \quad (22)$$

Equating (21) and (22) and using $k = 2\pi/\lambda$ we find a wavelength,

$$\lambda_c = 2\pi c \Delta \gamma / \beta_o \gamma_o^{3/2} \quad (23a)$$

which for $\lambda \gtrless \lambda_c$ defines a cold (warm) beam. If we rewrite the plasma frequency in terms of beam current we have an alternative expression

$$\lambda_c = 2\pi a \frac{\Delta \gamma}{\gamma} \left(\frac{I_o}{\beta_o \gamma_o I} \right)^{1/2} \quad (23b)$$

where a is the beam radius, I is the beam current, and

$$I_o = ec/r_o$$

is the "current" carried by an electron crossing a classical electron radius at velocity c and is equal to 17.5 KA. Discussion of the role of λ_c will be continued below.

Emission in the cold limit. The stimulated Cerenkov emission rate has been derived elsewhere. We will simply summarize the results of this calculation. The symmetry of the beam and the fields are the same as that of the spontaneous case and thus we will have for the equations of motion:

$$[\nabla_\perp^2 + (\frac{\omega^2 \epsilon}{c^2} - k^2)] \underline{A} = \frac{-4\pi}{c} \underline{J} \quad (24a)$$

and

$$[\nabla_A^2 + \frac{\omega^2 \epsilon}{c^2} - k^2] \phi = \frac{-4\pi}{c} \frac{c\rho}{\epsilon} \quad (24b)$$

In writing these we have already Fourier transformed in time and in z (the beam axis coordinate). We have also assumed that the beam is passing directly through the medium. This is not realistic for any case except perhaps a gas in the limit of extreme relativistic beam energy. In a practical configuration there will be one (or more) beam channels in a dielectric resonator. The boundary value problem is greatly complicated by this state of affairs and thus it is difficult to gain a grasp of the physical situation if all possible complications are put in at the beginning. We will assume, therefore, that the beam passes axially through a cylindrical resonator. The form factors which result when practical cases are considered will be discussed further in the concluding sections.

The charge and current in the cold beam limit may be computed either with fluid equations or the Vlasov equation. These depend upon \underline{A} and ϕ . Expanding the entire set of equations in a Fourier-Bessel expansion then yields a dispersion relation:

$$\omega^2 - \omega_k^2 = \frac{\Omega_b^2 (\omega^2 - c^2 k^2 / \epsilon)}{\epsilon \gamma^3 (\omega - ck\beta)^2} \quad (25a)$$

where

$$\omega_k^2 = c^2(p^2 + k^2)/\epsilon \quad (25b)$$

is the dispersion of the undriven guide, and p is the radial wavenumber. In deriving (25) we are also assuming that a strongly magnetized beam is used. The other quantities have been defined previously. The dispersion curves in the limit of zero coupling and finite coupling are shown in Figs. 9a

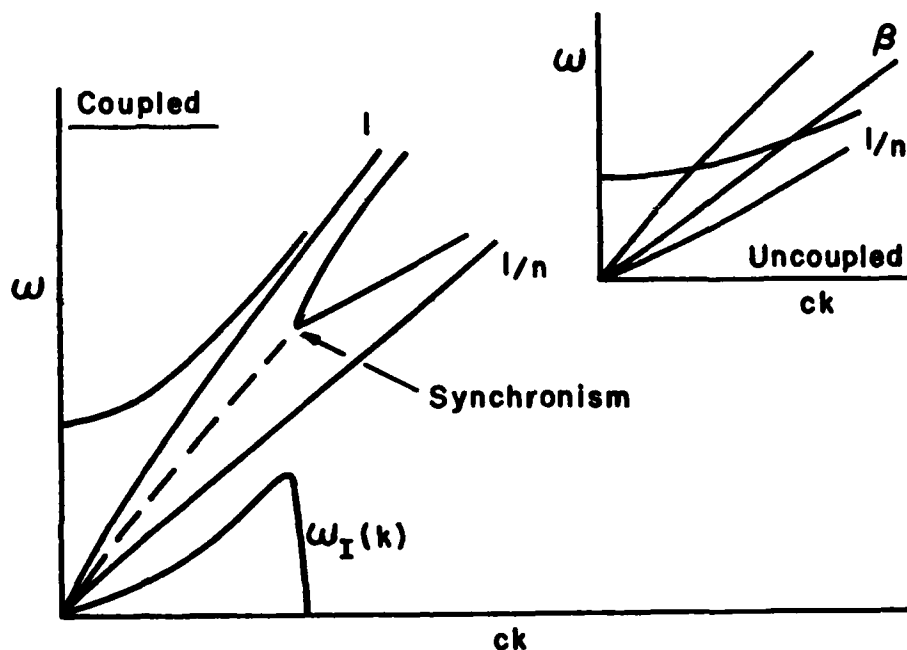


Fig. 9. Dispersion curves in the cold beam limit.

and 9b. There are four roots, two associated with the beam space charge modes and two with the unperturbed guide modes. When $\beta < 1/n$ all four roots are real while for $\beta > 1/n$ we have a complex conjugate pair of roots. The imaginary part

✓

of the frequency (the gain curve) for this limit is also shown in Fig. 9b. The gain not unexpectedly peaks near the region of strongest coupling:

$$\omega_k = ck\beta_o \quad (26)$$

Near this point the dispersion relation reduces approximately to a cubic and we have

$$(\omega - ck\beta_o)^3 - \Omega_b^2 ck\beta (1 - 1/\beta^2 \epsilon)/2\gamma^3 = 0 \quad (27)$$

Since we are on a root of the unperturbed guide mode we also have:

$$k = p/(\beta^2 \epsilon - 1)^{1/2} \quad (28)$$

✓

Rewriting Ω_b^2 in terms of the current and p in terms of the radius a , ($p = x_{0l}/a$), Eq. 27 can be expressed in terms of physically more intuitive variables:

$$(\omega - ck\beta)^3 - \frac{2I}{\beta I_o} \frac{(1 - 1/\beta^2 \epsilon)^{1/2}}{(\epsilon)^{1/2}} \left| \frac{c}{a\gamma} \right|^3 = 0 \quad (29)$$

Thus the gain and the frequency shift on resonance become

$$\omega_I = \frac{(3)^{1/2}}{2} \left(\frac{2Ix_{0l}}{(\epsilon)^{1/2} \beta_o I_o} \right)^{1/3} (1 - 1/\beta^2 \epsilon)^{1/6} \frac{c}{a\gamma} \quad (30a)$$

45

✓

✓

and

$$\Delta\omega_R = -\frac{\omega_I}{(3)^{1/2}} \quad (30b)$$

respectively. The gain and the frequency shift in spatial units are obtained by dividing Eqs. 30a and 30b by c . Relatively modest electron beam parameters result in substantial gains. A typical example is given in Table 1.

Table 1
Example of gains calculated for typical beam parameters.

ϵ	2.5	4
V_b (kv)	250	120
I_b (A)	17.5	17.5
$\alpha_I a$.138	.232

✓

Cerenkov emission rate in the warm beam limit. A discussion of the growth, or stimulated emission rate in the limit where the beam can no longer be regarded as monenergetic may also be found in the references.³³ Hence the discussion here will be brief. Assuming that a strong guide magnetic

✓

field coaxial with the beam direction renders the small signal motion one dimensional, the equations for the z components of the vector potential and the gradient of the scalar potential may with the aid of the equation of continuity be combined to give one equation for the axial component of the electric field:

$$[\nabla_{\perp}^2 + (\frac{\omega^2 \epsilon}{c^2} - k^2)] E_z = \frac{-4\pi i}{c^2} \frac{(\omega^2 - c^2 k^2 / \epsilon) \rho}{k} \quad (31)$$

In the preceding section the charge density ρ was computed using the fluid equations, now to account for thermal spread we will use the Vlasov equation:

$$\frac{\partial f}{\partial t} + v_z \frac{\partial f}{\partial z} + \dot{v}_z \frac{\partial f}{\partial v_z} = 0 \quad (32)$$

where in writing Eq. 32 we have used a velocity distribution and incorporated the assumption that the motion of the particles takes place primarily along the z direction.

Linearizing the Vlasov equation and Fourier transforming in t and z we obtain in the usual way an expression for ρ :

$$\rho = i n_0 e \int \frac{v_z (\partial f_0 / \partial v_z)}{\omega - k v_z} dv_z \quad (33)$$

If we substitute for \dot{v}_z from the equation of motion:

$$\frac{d(\gamma v_z)}{dt} = -\frac{e}{m} E_z \quad (34)$$

and substitute the resulting expression for ρ in the equation for E_z we then have

$$\left[\gamma^2 + \frac{\omega^2 \epsilon}{c^2} - k^2 \right] E_z = \frac{-\Omega_b^2}{c^2} \frac{(\omega^2 - c^2 k^2 / \epsilon)}{k} \times \int \frac{\partial f_0 / \partial v_z}{\omega - kv_z} dv_z E_z \quad (35)$$

If a delta function distribution in velocity is assumed the dispersion relation for the cold beam limit obtained in the preceding section is recovered. Restricting ourselves to the opposite limit we may use

$$\frac{1}{\omega - kv} = P \frac{1}{\omega - kv} - i\pi \delta(\omega - kv) \quad (36)$$

to obtain for the imaginary part of the frequency:

$$\omega_I = \frac{\pi \Omega_b^2}{2\omega_k} \frac{\beta^2 (1 - 1/\beta^2 \epsilon)}{\gamma^3} \frac{\partial f(\omega/k)}{\partial(\omega/k)} \quad (37)$$

In obtaining Eq. 37 we have also made use of the condition for phase synchronism

$$\omega = ck\beta \quad (38)$$

and we have ignored the small real part of the beam density dependent frequency shift.

The exact value of ω_I will depend to some extent on the detailed shape of $f(v_z)$. However if we assume that its width in velocity is Δv and that it varies smoothly around its peak the derivative may be replaced with Δv^{-2} . Making use of the relation between Δv and energy spread $\Delta \gamma$, the previous definition of ω_p^2 and dividing by c to obtain a spatial growth rate α we then have:

$$\alpha = \frac{1}{2} \left(\frac{\beta \gamma I}{I_0} \right) \frac{\lambda}{a} \frac{(1-1/\beta^2 \epsilon)}{a} \left(\frac{\gamma}{\Delta \gamma} \right)^2 \quad (39)$$

This result can be further reduced by evaluating it at the wavelength λ which represents the crossover between a warm and a cold beam and by making use of the relation between ω , the transverse wavenumber x_{0l}/a and the square of the sine of the Cerenkov angle $(1-1/\beta^2 \epsilon)$. The spatial growth measured in units of beam radius a then becomes:

$$\alpha a = \frac{\pi}{2} \left(\frac{x_{0l}}{2\pi} \right)^2 \left(\frac{\lambda}{a} \right)^2 \left(\frac{\gamma}{\Delta \gamma} \right) \left(\frac{\beta \gamma I}{I_0} \right)^{1/2} \quad (40)$$

Examination of Eqs. 39 and 40 shows that operation of a collective mode device in the submm-fir region of the spectrum is a realistic possibility. This point will be addressed further after the emission rate of the Cerenkov-Raman mode is computed.

CERENKOV-RAMAN EMISSION RATE

The procedure for calculation of the emission rate for the Cerenkov-Raman configuration is similar to that used in the preceding section. It is however slightly more involved since in addition to the beam oscillations, and radiation field we now also have a pump field. The discussion will be broken into two parts. In the first the interaction mechanism will be examined qualitatively and in the second the equations of motion will be developed in more detail.

CERENKOV-RAMAN COUPLING. The kinematics of Cerenkov-Compton scattering were explored in the second section. If the single electron is replaced by a beam and the photons by waves the Cerenkov-Raman instability can occur. This comes about in the following way. The electron beam supports space charge oscillations. If an electromagnetic wave propagates either along or counter to the electron beam the Lorentz force associated with the product of the transverse velocity imparted to the electrons by the electric field associated with the wave and the magnetic field of the wave will act along the direction of the beam propagation.

A synchronous or resonant coupling between three waves is possible. Imagine a beam on which there is a space charge oscillation with axial wave number k_b . If a wave with axial wave number k_p is propagating in the direction counter to the beam there is a beat force with wavenumber

$$k_s = k_b - k_p \quad (41)$$

✓

This implies that the interaction between a space charge oscillation and a counterstreaming "pump" wave generates a scattered wave. We will see that a large amplitude pump wave can induce growth of both the space charge and the scattered waves. Because the pump wave is scattered from a collective beam oscillation the designation of the process as Raman scattering is appropriate. The prefix Cerenkov is used because in the present case we are also examining the process when a dielectric resonator is used to support the scattered wave. It is meaningful to consider the scattering in regimes where the beam speed is either above or below the usual Cerenkov velocity and perhaps it would be proper to restrict the usage of the designation Cerenkov-Raman process to the former limit. However this would unduly clutter the notation. We will use the same designation for both limits and differentiate between subluminal, $\beta n < 1$, and superluminal $\beta n > 1$ where appropriate.

In order to extract a useful amount of gain from this interaction the pump field intensity must be very large. Hence in practice it is best to use a static rippled or helical magnetic field for the pump. In the rest frame of the electron this will result in a large transverse electric field while in the lab frame the pump will have zero frequency but non zero wavelength $\lambda_p = 2\pi/k_p$. Temporal synchronism will require:

$$\omega_s = \omega_b \quad (42)$$

The approximate dispersion relations for the space charge

and scattered modes are

$$\omega_b = ck_b \beta \quad (43a)$$

and

$$\omega_s = ck_s / n \quad (43b)$$

These together with the equation for spatial synchronism result in

$$\omega_s = \frac{c\beta k_p}{1 - \beta_o n} \quad (44)$$

the relation obtained from kinematic considerations in the second section. Reversal of the pump direction $k_p \rightarrow -k_p$ and the assumption $\beta n > 1$ immediately results in:

$$\omega_s = \frac{c\beta k_p}{\beta n - 1} \quad (45)$$

The kinematic arguments are thus equivalent to phase matching.

THE DISPERSION RELATION FOR CERENKOV RAMAN SCATTERING. In order to calculate the gain the dynamics of the interaction must be considered in more detail. There is now a transverse as well as a longitudinal current and hence the appropriate field equations are

$$\begin{aligned} & \left(\nabla^2 + \frac{\omega^2 \epsilon}{c^2} - k^2 \right) \begin{bmatrix} \underline{A}_\perp \\ E_z \end{bmatrix} \\ &= \frac{-4\pi}{c} \begin{bmatrix} \underline{J}_\perp \\ i(\omega^2 - c^2 k^2 / \epsilon) \rho / ck \end{bmatrix} \end{aligned} \quad (46)$$

Again we combine the z component of the vector and scalar potentials since this will simplify computation of ρ and \underline{J} . In order to exhibit the basic phenomena with a minimum of complication we will also assume that there are no transverse spatial variations.

Computation of the current is begun with the introduction of a Lagrangian:

$$L = -mc^2(1-\beta^2)^{1/2} - e\underline{\beta} \cdot \underline{A} + e\phi \quad (47)$$

The transverse canonical momentum

$$\underline{p}_\perp = \gamma mc \underline{\beta}_\perp - \frac{e}{c} \underline{A}_\perp \quad (48)$$

is a conserved quantity. If as is usually the case the beam enters the interaction region with no initial angular momentum $\underline{p}_\perp = 0$ and we have immediately:

$$c \underline{\beta}_\perp = \frac{e}{\gamma mc} \underline{A}_\perp \quad (49)$$

It is convenient to use the ordinary momentum

$$p_z = \gamma m v_z \quad (50)$$

✓

in the z direction and the equation of motion for this becomes

$$\dot{p}_z = -eE_z - \frac{m\gamma}{2} \left(\frac{e}{\gamma mc} \right)^2 \frac{\partial}{\partial z} A_\perp^2 \quad (51)$$

where in obtaining this result we have used the fact that p_\perp is conserved and the assumption that there is no spatial variation in the transverse direction.

If the transverse vector potential contains both pump and scattered components the second term on the right hand side of the equation of motion results in a force with wave number k_b and frequency $\omega_b = \omega_s$. This will drive the space charge oscillation.

Computation of ρ and J requires the introduction of the Vlasov equation. It is best in this equation to use the mixed set of coordinates p_\perp , v_z , z , and t . Linearizing we then have:

$$\rho = i n_0 e \int \frac{\dot{v}_z (\partial f_0 / \partial v_z) dv_z dp_\perp}{\omega - kv_z} \quad (52a)$$

and

$$J_\perp = i n_0 e \int \frac{v_\perp \dot{v}_z (\partial f_0 / \partial v_z) dv_z dp_\perp}{(\omega - kv_z)} \quad (52b)$$

The expression γ_\perp^2 equals $1/(1-\beta_\perp^2)^{1/2}$ and as we will see, the

54

✓

✓

wave number k is actually k_b .

The expression for ρ contains a term linear in E_z obtained earlier for the Cerenkov mode and a nonlinear drive term which depends upon the ponderomotive potential A_1^2 . The expression for \underline{J}_1 contains only nonlinear terms, the most important one of which is the one resulting from the product of E_z and \underline{v}_1 . This term drives the equation for \underline{A}_1 at the frequency ω_s .

Further progress requires evaluation of the integrals in Eqs. 52. In the wavelength limit where the beam may be regarded as cold we can assume:

$$f_0(v_z, p_1, z, t) = \delta(p_1) \delta(v_z - v_0) \quad (53)$$

and the integrals can be done immediately, yielding for the nonlinear contributions:

$$\rho^{NL} = \frac{in_0 e^2}{m} \frac{\gamma_1^2}{\gamma^3} \frac{k_b}{(\omega - k_b v_0)^2} \frac{e}{\gamma m c} \frac{\partial}{\partial z} A_1^2 \quad (54a)$$

and

$$\underline{J}^{NL} = \frac{in_0 e^2}{m} \frac{\gamma_1^2}{\gamma^3} \frac{k_b}{(\omega - k_b v_0)^2} \frac{e}{\gamma m c} \underline{A}_1 E_z \quad (54b)$$

The linear terms in ρ and \underline{J} simply are absorbed into the dispersion relation for the uncoupled waves.

The pump field is actually a spatial standing wave

✓

and hence it has components which vary as $\exp(\pm i k_p z)$. The component with the positive sign will combine with a term in the vector potential of the scattered wave with a similar sign to provide a resonant drive for the space charge mode. In the nonlinear current the pump term with the negative sign combines with a forward propagating component of the space charge wave to provide a resonant drive for the scattered wave.

Defining the magnitude of the relative velocity modulation provided by the pump as:

$$\beta_p = \frac{e}{\gamma m c^2} A_p \quad (55)$$

we arrive finally at a pair of coupled equations for the scattered and space charge waves:

$$D^T A_s = \frac{-i \Omega_b^2 k_b \beta_p \gamma^2}{\gamma^3 (\omega - k_b v_o)^2} E_z \quad (56a)$$

$$D^L E_z = \frac{-i \Omega_b^2 k_b \beta_p \gamma^2}{\gamma^3 (\omega - k_b v_o)^2} A_s \quad (56b)$$

The symbols D^T and D^L stand for the linear parts of the dispersion relations of the scattered (transverse) and space charge (longitudinal) waves respectively. The former one of these is:

$$D^T = \frac{\omega^2 \epsilon}{c^2} - k^2 - \frac{\Omega_b^2}{\gamma c^2} \quad (57)$$

and the latter is:

$$D^L = 1 - \frac{\Omega_b^2}{\gamma^3 (\omega - kv_0)^2} \quad (58)$$

A determinantal equation for the coupled modes could now be computed and its roots evaluated. However, in spite of the many simplifying assumptions made so far this remains a formidable task. The following procedure will be adopted.

Optimum coupling will occur near the region where the uncoupled waves are resonant modes, i.e. near where each satisfies its own linear dispersion relation. Near this frequency the coupled equations can be rewritten in the form:

$$\frac{\partial A_s}{\partial t} = -1 \left(\frac{\Gamma}{\partial D^T / \partial \omega} \right)_{\omega_s} E_z \quad (59a)$$

$$\frac{\partial E_z}{\partial t} = -1 \left(\frac{\Gamma}{\partial D^L / \partial \omega} \right)_{\omega_s} A_s \quad (59b)$$

where Γ denotes the factors which appear as coefficients on the right hand side of Eqs. (56). We are also now assuming the mode amplitudes A_s and E_z vary slowly as a result of the coupling although this is not the same as the original

definition which included the exponential factors and tacitly assumed that the amplitudes were constant.

A determinantal equation for Eqs. (59) can now be formed easily. We find for the imaginary part of the frequency

$$\omega_I = \gamma_1^2 (\Omega_b \omega_s)^{1/2} \beta_p / 2\gamma^{3/4} \quad (60)$$

It is also useful to state this in spatial units of the beam radius

$$\alpha a = \gamma_1^2 \beta_p (k_s a)^{1/2} \left(\frac{4I}{\beta \gamma^3 I_0} \right)^{1/2} \quad (61)$$

The growth rate increases as the square root of the scattered frequency and hence this is an intrinsically short wave length process provided the beam may be regarded as cold. As was the case with the pure Cerenkov mode the growth in the warm limit will decrease with decreasing wave length and hence the warm-cold transition wavelength discussed in the earlier sections although not an absolute limit for device operation is a useful figure of merit for estimating the high-low gain transition.

CONCLUSIONS

We have derived expressions for the frequency and the stimulated emission rate for Cerenkov and Cerenkov-Raman

✓

emission processes. In the limit where the driving electron beam can be regarded as monoenergetic the growth rate rises with frequency (as $\omega^{1/3}$ and $\omega^{1/2}$ respectively) for both processes and hence they are both intrinsically short wavelength interactions. Furthermore, by controlling the filling factor and the relative dielectric constant of the dielectric waveguide resonators, practical operation in a regime where the operating wavelength is much less than the characteristic transverse dimension of the resonator, has been achieved. The fundamental limitation to operation of these devices in the collective regime at short wavelengths would thus appear to be the electron beam quality. The dielectric resonator makes use of beams which although substantial, are nevertheless modest when compared to those used in other short wavelength free electron radiation sources. Operation in the lower part of the mm region of the spectrum has already been attained and operation in the submm regime appears very likely. The basic dielectric resonator-electron beam technique can most probably be made to work into the far infrared portion of the electromagnetic spectrum. The basic physical principles governing free electron radiation sources operation is very much the same for all devices. Hence we would expect that in general, devices such as we have discussed, would work at as short a wavelength as any other free electron laser.

ACKNOWLEDGEMENTS

The author would like to acknowledge innumerable enlightening discussions with Ken Busby, Kevin Felch, Geoff Crew, and Professor William Case of Hobart and William Smith

✓

Colleges. Support from Dartmouth College, the Department of the Army Grant DAAG39-78-C0032, the Air Force Office of Scientific Research Grant 77-3410, and the Office of Naval Research is also gratefully acknowledged.

REFERENCES

1. P.A. Cerenkov, Dokl. Akad. Nauk. SSSR 2, 451 (1934).
2. I.M. Frank, and Ig. Tamm, Dokl. Akad. Nauk. SSSR, 14, 109 (1937).
3. M.A. Piestrup, R.A. Powell, G.B. Rothbart, C.K. Chen, and R.H. Pantell, Appl. Phys. Lett. 28, 92 1976.
4. P. Coleman and C. Enderby, J. Appl. Phys. 31, 1695 (1960).
5. H. Lashinsky, J. Appl. Phys. 27, 631 (1956).
6. K. Felch, K. Busby, J. Walsh, and R. Layman, Bull. Am. Phys. Soc. 23, 749 (1978).
7. A. Hasegawa, Bell System Tech. Jour. 57, 3069, 1978.
8. K. Busby, K. Felch, R.W. Layman, J.E. Walsh, 1979 IEEE Conf. on Plasma Science---Conf. Record, 107.
9. O. Heaviside, Phil. Mag. 1888: Feb. p 130, Mar. p 202, May p 379, Oct. p 360, Nov. p 434, Dec. p 488.
10. A. Sommerfeld, Gotting, Nachricht. 99, 363 (1904).
11. E. Curie, Madame Curie (Heinemann, London 1941).
12. L. Mallett, C.R. Acad. Sci (Paris) 183, 274 187, 222 188, 445.
13. B.M. Bolotovskii, Usp. Fiz. Nauk. 75, 295 (1961); Soviet Physics Uspekhi 4, 781 (1962).
14. V.L. Ginzburg Dok. Akad. Nauk. SSSR 3, 253, 1947.
15. Cerenkov losses do not compete with other collisional radiation until the vuv region is reached.

- ✓
16. Prebunching will not necessarily be self-consistent.
 17. I.M. Frank, J. of Phys. 2, 49 (1943).
 18. V.L. Ginzburg Dok. Akad. Nauk. SSSR 56, 145, (1947).
 19. S. Schneider, and R. Spitzer, Nature 250, 643, (1974),
I.E.E.E. Trans MIT 25, 551 (1977).
 20. J.E. Walsh, T.C. Marshall and S.P. Schlesinger, Phys.
Fluids 20, 709 (1977).
 21. K. Busby, K. Felch, R.W. Layman, J.E. Walsh, Bull. Am.
Phys. Soc. 24, 607 (1979).
 22. Recent experimental results are discussed elsewhere in
this volume.
 23. J.R. Pierce, Phys. Today 3, 24 (1950).
 24. I. Kaufman, Proc. I.R.E. 47, 381 (1959).
 25. D.A.G. Deacon, L.R. Elias, J.M.J. Madey, G.J. Ramian,
H.A. Schwettmann, and T.I. Smith, Phys. Rev. Lett. 38,
892-894 (1977).
 26. P. Sprangle, R.A. Smith, and V.L. Granatstein, NRL
Memorandum Report 3888 (1978).
 27. R.M. Gilgenbach, T.C. Marshall, and S.P. Schlesinger,
Physics of Fluids, 22, 5, 971-977 (1979).
 28. Carcinotrons have been operated well into the
submillimeter regime.
 29. J.V. Jelley, Cerenkov Radiation and its Applications,
(Pergamon, London, 1958).
 30. M. Stockton, J. Walsh, J. Opt. Soc. Am. 68, 1629
(1978).
 31. R.M. Phillips, IRE Trans. Electron Devices, ED-7, 231
(1960).
 32. N. Marcuvitz, Waveguide Handbook (McGraw-Hill, New
York, 1951).

33. J.E. Walsh, "Stimulated Cerenkov Radiation," in Physics of Quantum Electronics, edited by S. Jacobs, M. Sargent, M. Scully (Addison-Wesley, Reading, Mass., 1978), Vol. 5.
34. A. Gover, A. Yariv, Applied Physics, 16, 121 (1978).

✓

CERENKOV AND CERENKOV-RAMAN MASERS: EXPERIMENTS

Kevin L. Felch, Kenneth O. Busby,
Robert W. Layman, and John E. Walsh

INTRODUCTION

✓

A recent series of experiments has shown the feasibility of producing mm microwaves by two different methods involving the interaction of a relativistic electron beam and a dielectrically lined waveguide. The Cerenkov maser produces coherent radiation by propagating a relativistic electron beam down a cylindrical waveguide, with an annular dielectric liner, at a velocity greater than the speed of light in the dielectric. The use of the Cerenkov interaction as a source of microwaves was first introduced by Ginzburg¹ in 1947, and since then several other authors have dealt with the problem.²⁻⁴ The first Cerenkov maser experiments to produce coherent microwaves were performed at Columbia University by Walsh, Marshall, and Schlesinger in 1975.⁵

63

✓

✓

The Cerenkov-Raman maser involves the interaction of a relativistic electron beam with a magnetic wiggler or "undulator," as it passes through a dielectrically lined waveguide. The earliest work^{6,7} involved the use of nonrelativistic electron beams for the amplification of microwaves. As relativistic field emission, high current sources became available, the use of undulators for the production of high frequency coherent microwaves became possible.⁸⁻¹¹ In addition, a series of tenuous electron beam experiments have been performed on the Stanford University superconducting linear accelerator.¹² All of such magnetic wiggler experiments fall into the broad category of free electron lasers. These initial magnetic wiggler experiments used cylindrical waveguides without dielectric liners as resonant structures.

Following the suggestions of Ginzburg¹³ and of Walsh and Crew¹⁴, we inserted a dielectric liner into the resonator structure to lower the beam energy required to obtain a given output microwave frequency. In the following we describe the Cerenkov radiation and Cerenkov-Raman scattering experiments as performed at Dartmouth College. Theoretical treatments of this specific work may be found in the references.¹⁵⁻¹⁷

THE CERENKOV EXPERIMENTS

The preliminary experiments performed at Columbia using the Cerenkov interaction to produce mm microwaves yielded microwave powers of 1 MW at frequencies between 30 and 60 GHz. These experiments employed a 1-10 KA, .5 MeV electron beam, produced by a field emission diode source.

The beam was directed down a cylindrical waveguide with an annular dielectric filler. For these experiments the beam pulse width was in the 50 nanosecond range and the repetition rate was on the order of minutes.¹⁸

The conversion efficiency of these experiments was around .1%. With this figure in mind it was felt that a cold, lower current beam, similar to those used in present day klystron technology, might give higher conversion efficiencies and become more of an actual mm microwave tube.

Using these ideas as a guideline, a relativistic electron beam accelerator was constructed at Dartmouth College, providing an electron beam capable of multi-microsecond pulses and high repetition rates. A schematic of the accelerator is shown in Figure 1. The cathode is either a dispenser or a barium oxide-coated cathode, which provides a solid, cylindrical electron beam of up to 30 A. Such thermionic cathodes produce electron beams with significantly less thermal spread than do those produced by field emission diodes. A pulse from a pulse-forming network is passed through a bifilar pulse transformer to the cathode and its heater transformer, lowering the potential from 0 to -200 kilovolts for 4 to 6 microseconds. The machine now runs at a repetition rate of 1 to 7 pps., but has the ability to operate at 200 pps. The electron beam is accelerated through a hole in a molybdenum anode which is held at ground potential. The beam then enters the partially filled cylindrical waveguide and continues down the tube until it is collected by a faraday cup.

The faraday cup is connected to ground through a 1 ohm resistor, enabling current measurements to be made. There is an axial magnetic guide field of 2 KG which

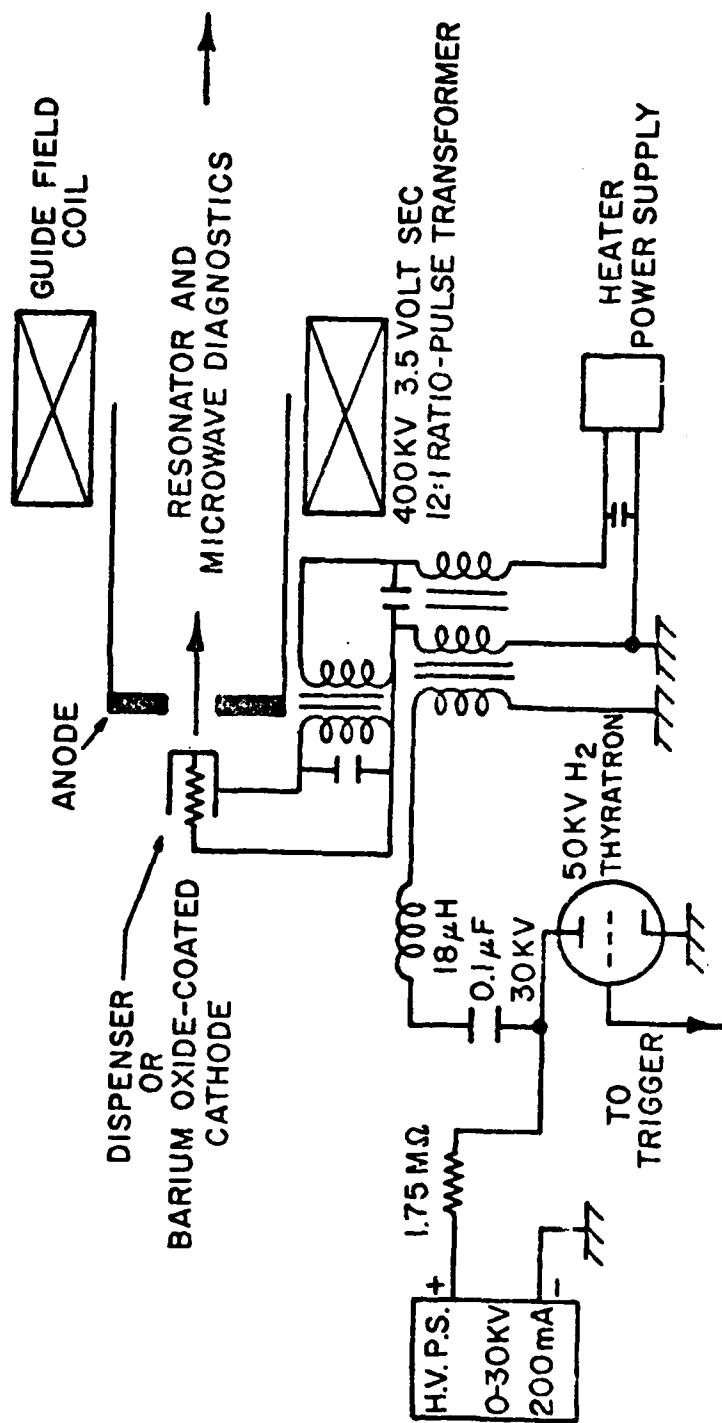


Figure 1. Schematic of 200 KV electron beam generator.

✓

confines the electron beam to the axis of the cylindrical waveguide.

The relative proximity of the cathode and anode with respect to the dielectrically filled waveguide is depicted in Figure 2. The actual magnetic field lines of the guiding field are mapped onto the resonator structure. The microwave diagnostics are coupled to the circular waveguide by means of a stub antenna which protrudes out of the rectangular waveguide and butts up against the quartz dielectric in the cylindrical guide. The antenna is constructed so as to couple to the radial electric fields of the TM_{01} circular waveguide mode, the mode which will be excited by the passage of an axial, relativistic electron beam in close proximity to the dielectric filler. The rectangular guide directs the microwaves out of the vacuum system to where measurements of power and frequency may be made.

✓ To detect the microwaves, ordinary crystal detectors of the 1N23 and 1N26 variety are situated in standard X band and K band mounts. Power measurements are then made using the power response of the detector crystals and measuring the coupling loss out of the cylindrical resonator. Both the crystal response and the cylindrical to rectangular guide coupling loss were tested and calibrated using known sources in the X, K, and Ka frequency bands.

Frequency measurements are made using a series of high pass microwave filters. Microwaves passing through a high pass filter have a frequency in excess of the cutoff frequency for that filter. A range of such filters will serve to pinpoint the operating frequency, and yield some information about the spectral distribution.

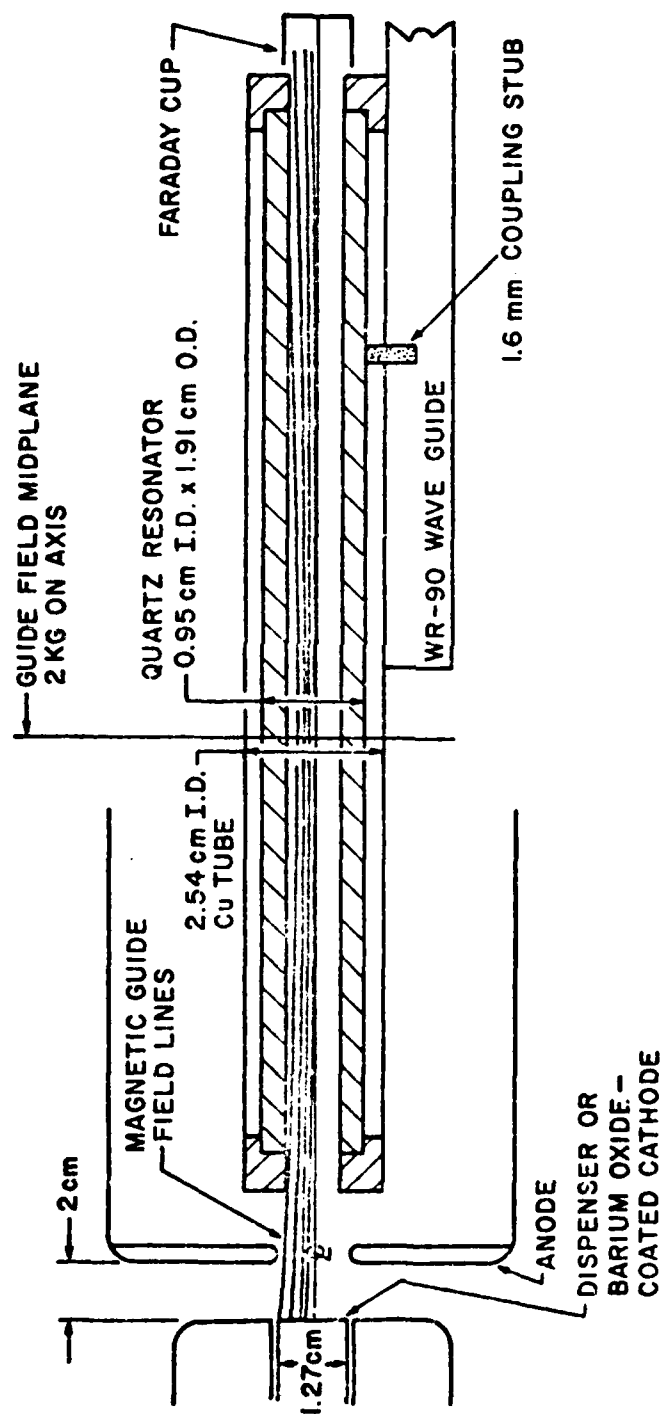


Figure 2. Schematic diagram of anode, cathode, and resonator structure for Cerenkov radiation experiments.

✓

Thus far, most experimental runs have employed quartz as a dielectric liner. For quartz, the dielectric constant at microwave frequencies is 3.78, so that the Cerenkov condition, $\beta^2 \epsilon > 1$, is satisfied for $\beta = .514$, $\gamma = 1.17$, giving an accelerating voltage of 87 KV as the Cerenkov "turn-on" voltage for the electron beam. The quartz filler shown in Figure 2 has an inner diameter of .95 cm and an outer diameter of 1.91 cm. The quartz tube is suspended in a concentric cylindrical copper tube of 2.54 cm in diameter.

RESULTS OF THE CERENKOV EXPERIMENTS

✓

Data for a typical shot are shown in Figure 3, including simultaneous traces of the microwave output and beam voltage and current. Microwave pulses of between 5mV and 2V in amplitude and 100 nanoseconds to 1.5 microseconds in width have been detected. The pulses occur on or near the peak of the voltage pulse in time. Pulses begin occurring at voltages between 90 and 110 KV as required by the Cerenkov condition and continue at voltages of up to 200 KV. Beam currents of between 100 and 500 mA are sufficient to initiate strong microwave production and higher currents of between 2 and 10 A result in an increase in microwave pulse height, up to the limits of the detector diodes. In addition, higher currents tend to broaden the pulse as well as render the microwave output more consistent and uniform.

It should be noted here that the detection system used in the above measurements was initially tested using an iris-loaded waveguide structure driven by the electron beam. Also, many null runs were carried out using no dielectric

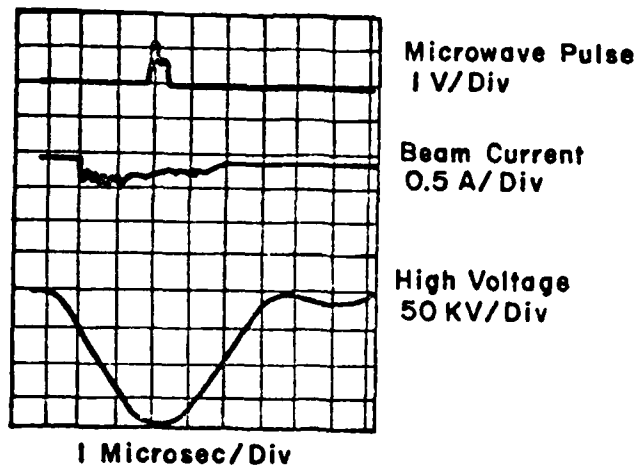


Figure 3. Typical Cerenkov microwave pulse with simultaneous beam voltage and current traces.

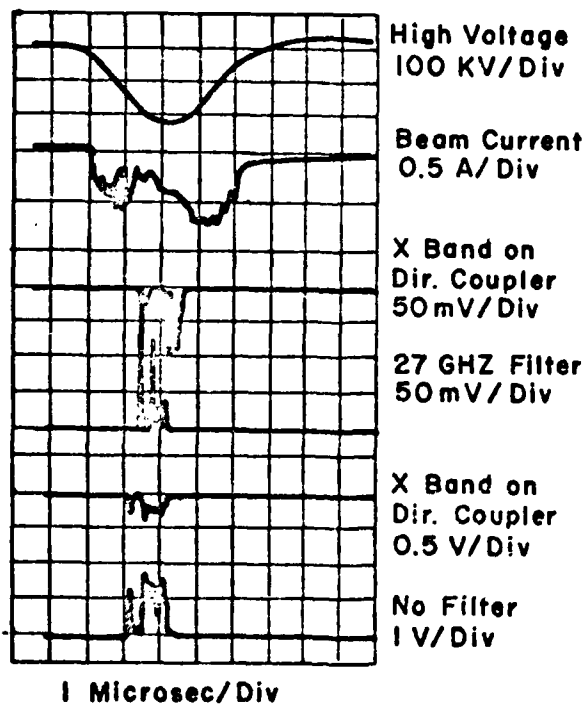


Figure 4. Cerenkov microwave pulses with and without filters and associated beam voltage and current traces.

filler in the waveguide, with the expected results that no microwave radiation was detected, whatsoever. Finally, recent runs using only the quartz filler and no outer metallic circular waveguide have yielded similar results to those observed with the waveguide in place. There are indications that this type of structure might be more efficient in converting electron beam energy into microwave power over a narrow bandwidth.

Frequency measurements on the microwave pulses indicate that the nominal operating frequency, using the present quartz filler and waveguide structure, is between 40 and 45 GHz.

There is also evidence that more than one frequency is obtained in a given microwave burst. Simultaneous observations of a single microwave pulse through a filter and an unfiltered parallel coupler is shown in the third and fourth oscilloscope traces of Figure 4. Note the way that peaks from the filtered pulse differ from those of the unfiltered pulse. Using the same set-up, except without a filter, the fifth and sixth pulses in Figure 4 were taken simultaneously a few shots later. Since the last two traces are quite similar, the differences in the third and fourth traces appear to be due to the presence of multiple frequencies.

Since the coupling out of the cavity is of a resonant nature the cavity tuning becomes important. For the present experiment this means that resonator tuning may be limiting the actual range of frequencies produced by the interaction of the beam and the loaded waveguide and that power detected outside may be significantly less due to the lack of optimal resonator tuning.

✓

Using the set of high pass filters mentioned previously, the spectral distribution of the microwaves seems quite sharply peaked around 40-45 GHz with perhaps several smaller peaks of lower frequency and virtually nothing at frequencies above 45 GHz.

With the power measuring considerations previously mentioned, microwave pulses of between 500 W and 1 KW in peak power have been detected, with 100 W serving as a very conservative lower peak power limit. These numbers include a 10-15 db coupling loss and a 10-15 db drop due to the detection system as shown by calibration with known sources near our operating frequencies. This 20-30 db figure when added to the 1 W signals detected outside gives the 100 W to 1 KW power measurements. Conversion efficiencies are from 1% to 10%. The higher value is due to the strong output that occurs with electron beam currents as low as 100 mA. Table 1 summarizes these results and the electron beam parameters.

Table 1
Summary of Results for Cerenkov Experiments

MICROWAVES:

Frequency - 40 to 45 GHz
Power - 500 W to 1 KW Peak
Pulse Width - 100 nS to 1.5 microseconds

ELECTRON BEAM:

Voltage - 100 to 200 KV
Current - .1 to 10 A
Repetition Rate - up to 7 Hz

By changing the diameter of the cylindrical waveguide and by experimenting with liners of different wall thicknesses and dielectric constant the frequency of the device may be readily tuned to higher or lower operating frequencies. Optimization of resonator tuning and microwave output coupling will serve to enhance the conversion efficiencies already detected. Experiments with these ideas in mind are now being performed at Dartmouth College.

THE CERENKOV-RAMAN SCATTERING EXPERIMENTS

A single particle picture for Cerenkov-Raman scattering is shown in the inset in Figure 5. A magnetic undulator serves as the pump photon in the scattering process and is represented by an excitation with wave number $k_p = 2\pi/\lambda_p$ (λ_p is the undulator period), and pump frequency zero. An electron moving along the axis of the undulator is scattered and emits photons. If the process takes place in a dielectric then we call the interaction Cerenkov-Raman scattering where the frequency, ω_s , of the emitted photon is:

$$\omega_s = \frac{ck_p \beta}{1 - \beta n} \quad (1)$$

The velocity of the electron is $v = \beta c$ and $n = (\epsilon)^{1/2}$ is the index of refraction of the surrounding medium. As βn approaches 1, the the upscattering becomes infinite in the approximation where dispersion and recoil are neglected.

In the experiment, the magnetostatic pump wave

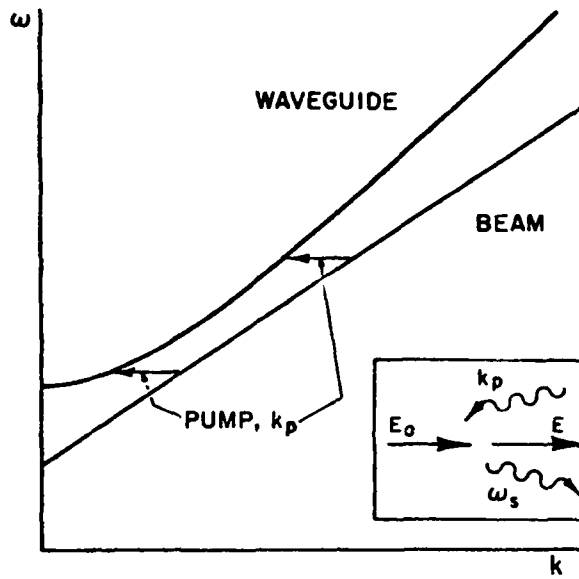


Figure 5. Dispersion relations for waveguide, electron beam, and undulator.

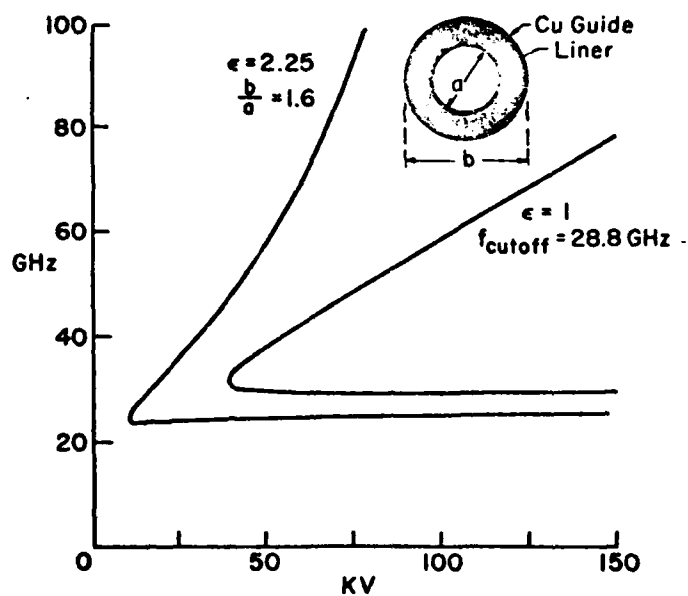


Figure 6. Plot of scattered frequency vs. electron beam voltage for empty and partially filled waveguides.

✓

couples the electron beam to a waveguide mode. The dispersion for the waveguide, the electron beam, and the undulator are shown in Figure 5. The electron beam, which can support either a plasma or a cyclotron mode, is assumed to be cold. The dispersion of the zero-frequency pump is a horizontal line segment with length $k_p = 2\pi/\lambda_p$.

The condition for interaction is that, at any given frequency, the difference in wavenumber between the waveguide and beam modes must be equal to k_p . As the beam velocity is increased from zero, there exists a minimum velocity for interaction at a single frequency. As the beam velocity is raised still further, the interaction splits into two branches. One branch tends toward higher frequency as the beam velocity increases, and the other branch tends toward the waveguide cut-off. Two examples with unfilled and partially filled waveguides are shown in Figure 6.

In comparison with the empty guide, the interaction with a partially filled waveguide turns on at a lower beam voltage and raises faster in frequency as a function of voltage. For all cases considered in the present paper, $\beta n \leq 1$, such that we are below the Cerenkov threshold.

The experimental apparatus is again shown in Figure 1. Beam currents range from 1 to 30 A, and are measured by a Pearson current transformer, since no faraday cup is used in these experiments. The electron beam is guided through a circular waveguide to the undulator by an external magnetic field. The undulator consists of alternating aluminum and iron washers of .5 cm in thickness, providing a 1 cm ripple period. A schematic of the undulator and resonator structure is shown in Figure 7. Inside the undulator, the magnetic field is the guide field plus an 8% ripple in the

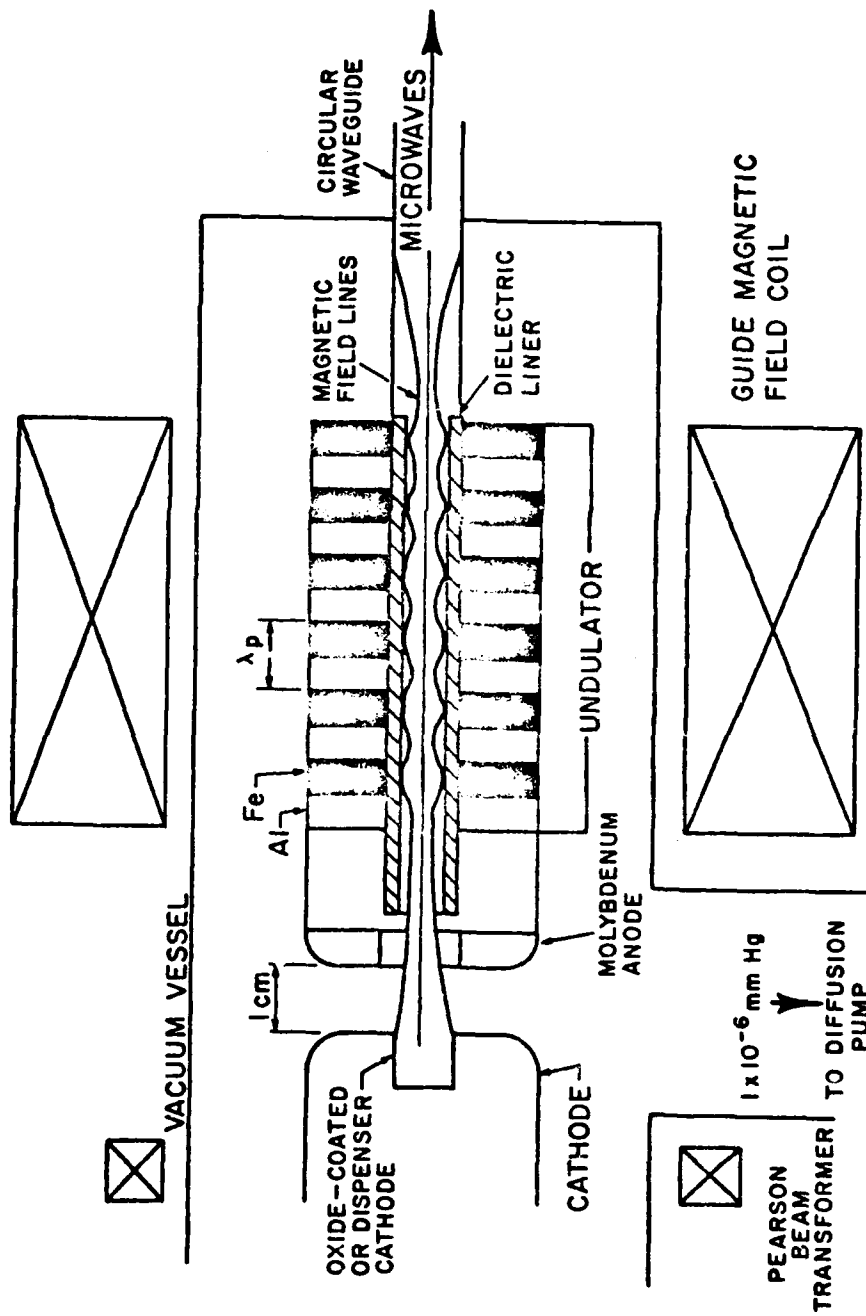


Figure 7. Schematic of anode, cathode, undulator, and resonator for Cerenkov-Raman experiment.

✓

z-component and a ripple in the radial direction determined by $\nabla \cdot \underline{B} = 0$. The interaction area is within the undulator, and is lined with an annular dielectric filler.

As the beam emerges from the undulator, it is guided by diverging magnetic field lines and deposited onto the inside surface of the waveguide instead of collected in a faraday cup as done in the Cerenkov radiation experiments. The microwaves travel from the interaction area down the waveguide through a circular to rectangular waveguide transition and into the diagnostics. Transitions are used to reduce reflections to insure that the machine works in a superradiant mode. A .030 inch thick teflon vacuum seal is placed behind the transition.

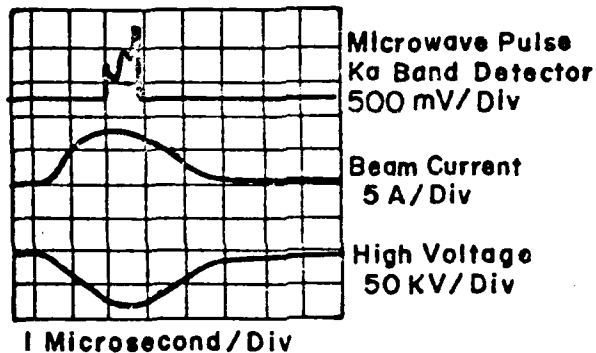
RESULTS OF THE CERENKOV-RAMAN SCATTERING EXPERIMENTS

✓

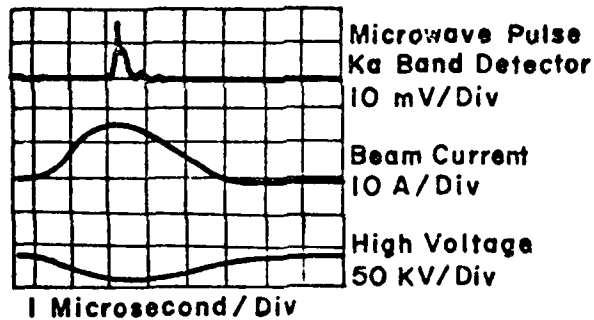
Simultaneous oscilloscope traces of beam voltage, beam current, and the resulting radiation pulses are shown in Figure 8. The top set of traces represents data for the vacuum Raman scattering case with no dielectric liner. The bottom set shows the results of inserting a polypropylene liner. As the beam voltage is increased from zero, a "turn-on" voltage is observed, corresponding to the lowest voltage at which radiation is detected. As the voltage is increased past this threshold voltage, the radiation pulse broadens out symmetrically about the high voltage pulse. As shown in Figure 8, and listed in Table 2, the threshold voltage for Cerenkov-Raman scattering is considerably less than the

✓

a. EMPTY WAVEGUIDE



b. DIELECTRIC-LINED WAVEGUIDE



✓

Figure 8. a). Microwave pulse and simultaneous beam voltage and current traces for Raman scattering in an empty waveguide.
b). Microwave pulse and simultaneous beam voltage and current traces for Cerenkov-Raman scattering in a dielectric-lined waveguide.

threshold voltage for vacuum Raman scattering. Using high pass frequency filters, initial characteristics of the frequency content of the microwave pulses may be investigated. As expected, the results of such frequency measurements show that higher frequency microwaves are associated with higher voltages and that for microwave pulses within a given frequency window of 60-70 GHz, the

✓

corresponding high voltage is much lower for the polypropylene-lined waveguide than for the empty waveguide. These two points reveal the nature of the frequency upshift in going from vacuum Raman scattering to Cerenkov-Raman scattering.

In addition to the voltage-dependent high frequency radiation, we have also detected the lower frequency radiation at about the cutoff frequency of the TE_{01} circular waveguide mode in the vacuum Raman scattering regime. This lower frequency branch also begins appearing at the threshold voltage, but the frequency remains nearly constant as the voltage is increased. Measurements of this lower frequency branch are made using interferometric techniques. The low frequency branch for the Cerenkov-Raman scattering case has yet to be observed. Power measurements indicate that the low frequency branch contains considerably more microwave power than the high frequency branch. For a typical 80 KV, 10 A electron beam, vacuum Raman scattering power conversion efficiencies of 0.1% to 1% and 0.01% to 0.1% are estimated for the lower and upper frequency branches, respectively. For the upper branch of the Cerenkov-Raman microwaves, power efficiencies of 0.001% to 0.01% are obtained.

It is found that by decreasing the strength of the magnetic field, a magnetic field threshold may be observed. Also, preliminary results indicate that the frequency of the upper branch may be raised by increasing the magnetic field strength, and hence the strength of the pump field, while the lower frequency branch is relatively unaffected by magnetic field strength in excess of the threshold magnetic field.

✓

The results of using circular waveguides of different diameters, with and without dielectric liners, are summarized in Table 2. The same basic tendencies concerning the existence of the two frequency branches and the frequency upshift in going from vacuum to Cerenkov-Raman scattering have been observed.

Numerous experimental runs have also been performed with a 3 cm period undulator and an empty waveguide. Using beam voltages of up to 200 KV, no microwaves at all were detected with this undulator spacing. Using the same techniques employed in producing Figure 6, we find that the threshold voltage for a 3 cm spacing is 290 KV, explaining why no radiation was detected using lower voltages. No Cerenkov-Raman scattering runs using the 3 cm undulator have been performed.

✓

If we use the experimental parameters used to obtain the above results and employ our simple model to predict the dependencies of frequency on beam voltage and magnetic field, we obtain the results listed in the second portion of Table 2. The cyclotron beam mode is used since the radiation does exhibit strong dependence on the magnetic field and better agreement is obtained using the cyclotron mode rather than the space charge mode. The theoretical magnetic field thresholds shown in Table 2 were calculated by finding the minimum magnetic field (and thus the minimum cyclotron frequency) required for interaction at an electron kinetic energy of 60 KeV. In comparing theoretical and experimental results, we note that the agreement is generally good. The only discrepancies crop up in comparing theoretical and experimental threshold voltages, but these values do show the correct tendencies for empty and

✓

dielectrically lined waveguides. The magnetic field thresholds agree reasonably well and the frequency of the lower branch is in excellent agreement. Since the frequency of the upper branch varies greatly with magnetic field and

Table 2
Summary of vacuum Raman and Cerenkov-Raman Results

Experimentally Observed Results	Vacuum		Cerenkov-Raman $\epsilon = 2.25$ (Polypropylene)	
	.5" Empty Guide	.375" Empty Guide	.5" Liner: b/a=1.6	.375" Liner: b/a=2.0
Voltage Threshold	60.0 KV	80.0 KV	30.0 KV	40.0 KV
Freq. of Low Branch	29.0 GHz	38.0 GHz	---	---
Freq. of High Branch	60.0 GHz	70.0 GHz	60.0 GHz	---
B Field Threshold at Voltage of 60 KV	5.5 KG	---	3.0 KG	3.0 KG
From Theory Waveguide: TE ₀₁ Mode Beam: Cyclotron Mode				
Voltage Threshold	40.0 KV	115.0 KV	10.0 KV	30.0 KV
Freq. of Low Branch	29.0 GHz	38.0 GHz	23.0 GHz	28.0 GHz
Freq. of High Branch	60.0 GHz	70.0 GHz	60.0 GHz	---
B Field Threshold at Voltage of 60 KV	5.0 KG	8.4 KG	2.4 KG	3.6 KG

✓

beam voltage, exact comparisons between theory and experiment are difficult. But using the voltage and magnetic field values from the experimental observations of the high frequency branch, we do see that the simple theory does predict the frequency of the upper branch quite well. Measurement of the frequency of the lower branch for the dielectrically lined waveguide runs has not been completed as there are coupling problems caused by the lower cutoff frequency of the partially filled waveguide compared to the empty waveguide.

CONCLUSIONS

✓ In summary, we emphasize the fact that the ability to produce high power mm microwaves using relativistic electron beams of modest voltages has been demonstrated using both the Cerenkov and Cerenkov-Raman scattering mechanisms. The Cerenkov microwave generator seems to have the advantage in terms of conversion efficiency, while the Cerenkov-Raman scattering scheme can operate at much lower beam voltages. Both mechanisms do appear to have the requisite capabilities to become viable high power mm microwave sources with correct optimization of the various experimental parameters.

ACKNOWLEDGEMENTS

The authors acknowledge the support of U.S. Army Grant #DAAG39-78-C-0032 and U.S. AFOSR Grant #77-3410, and the assistance of R. Duquette, P. Woods, C. LaTouche, T. Dobbins, and E. Perkins.

✓

REFERENCES

1. V.L. Ginzburg, Dok. Akad. Nauk. SSSR, 56, 3, 253-254 (1947).
2. M. Abele, Nuovo Cimento, 9, series 9, suppl.(3), 207 (1952).
3. J.V. Jelley, Cerenkov Radiation and its Applications, (Pergamon, London, 1958).
4. H. Lashinsky, "Cerenkov Radiation at Microwave Frequencies," in Advances in Electronics and Electron Physics, edited by L. Marton (Academic Press, New York, 1961), Vol. XIV, p. 265.
5. J.E. Walsh, T.C. Marshall, and S.P. Schlesinger, Physics of Fluids, 20, 4, 709 (1979).
6. H. Motz, Journal of Applied Physics, 22, 5, 527 (1951).
7. R.M. Phillips, IRE Trans. Electron Devices, ED-7, 231 (1960).
8. R.M. Gilgenbach, T.C. Marshall, and S.P. Schlesinger, Physics of Fluids, 22, 5, 971-977 (1979).
9. P. Sprangle, R.A. Smith, and V.L. Granatstein, NRL Memorandum Report 3888 (1978).
10. D.B. McDermott, T.C. Marshall, S.P. Schlesinger, R.K. Parker, and V.L. Granatstein, NRL Memorandum Report 3907 (1979).
11. A. Hasegawa, Bell System Technical Journal, 57, 8, 3069 (1978).
12. D.A.G. Deacon, L.R. Elias, J.M.J. Madey, G.J. Ramian, H.A. Schwettmann, and T.I. Smith, Phys. Rev. Lett. 38, 892-894 (1977).
13. V.L. Ginzburg, Dok. Akad. Nauk. SSSR, 56, 2, 145-148 (1947).

- ✓
14. J.E. Walsh, and G. Crew, Bull. Am. Phys. Soc. 23, 748 (1978).
 15. G. Crew, Honors Thesis (1978)---Available from the Dartmouth College Physics Department.
 16. J.A. Baggar, Honors Thesis (1977)---Available from the Dartmouth College Physics Department.
 17. J.E. Walsh, Elsewhere in this volume.
 18. J.E. Walsh, T.C. Marshall, and S.P. Schliesinger, op. cit.

✓

CERENKOV FREE ELECTRON LASER GAIN
AND SUPERRADIANCE

A Thesis
Submitted to the Faculty
in partial fulfillment of the requirements for the
degree of
Master of Arts

by
Captain Douglas H. Wise

DARTMOUTH COLLEGE
Hanover, New Hampshire

June 1981

Examining Committee:

Chairman

Dean of Graduate Studies

✓

ABSTRACT

The Cerenkov Free Electron LASER is proposed as the active medium for a Maser amplifier. The amplifier will function in the role of a reflection amplifier.

A geometry is proposed and the dispersion relation derived. A gain lineshape for the LASER is calculated and parametrically analyzed. The reflection amplifier is concurrently analyzed to compare amplifier performance to the active medium performance. Several methods for increasing gain are discussed.

An expression for power in the superradiant mode for the atomic LASER is compared with an analogous expression for the Free Electron LASER.

✓

ACKNOWLEDGEMENTS

Dr. John Walsh certainly deserves the bulk of the credit for the completion of this thesis. For it was he who introduced me to the topic, and with patience guided me through to its completion. This document symbolizes a unique two years for me at the Physics Department, and I would like to thank all who have helped me in my academic pursuits. Dave Speer, John Golub, and Scott Von Laven in particular have provided me with invaluable assistance and friendship.

I would also like to extend my sincere appreciation to the members of my family who have borne the discomfort and pain of many moves and many absences over the past years. And who always remained willing to sacrifice for me during my period of study.

This research was supported by AFOSR Grant#77-34109.

✓

TABLE OF CONTENTS

ABSTRACT	ii
ACKNOWLEDGEMENTS	iii
TABLE OF CONTENTS	iv
LIST OF ILLUSTRATIONS	v
CHAPTER 1: Introduction	6
CHAPTER 2: FEL Gain Analysis	10
Cold Beam Dispersion Relation	13
Gain Calculations	21
Parametric Analysis	22
Cold Beam Limit	36
Saturation	38
CHAPTER 3: Reflection Amplifier	40
Maser Operation	40
FEL Transmission Line Analysis	49
Gain Bandwidth Product	61
Artificial Q Variation	66
CHAPTER 4: Superradiance	70
CONCLUSION	76
APPENDIX 1: Fortran Computer Program	78
APPENDIX 2: Frequency Dependence of Peak Gain	85
REFERENCES	87

✓ LIST OF ILLUSTRATIONS

II-1	Sketch of FEL Geometry	12
II-2	No Beam Plot of $D(w,k)$	19
II-3	$D(w,k)$ Plot with Beam Line	20
II-4	Example of Gain Lineshape	23
II-5	Low Gain	25
II-6	High Gain	26
II-7	High Beta	27
II-8	Low Beta	28
II-9	Frequency as Function of Beta	30
II-10	Low Radius	31
II-11	High Radius	32
II-12	Frequency as Function of Radius	34
I.-13	110GHz Cooperation	35
III-1	MASER	41
III-2	MASER Equivalent Circuit	43
III-3	Transmission Line Circuit	45
III-4	Plot of Voltage gain	47
III-5	Line Model of the FEL	50
III-6	Lumped Circuit FEL	52
III-7	Power Gain	57
III-8	Power Gain	58
III-9	High Frequency Operation	60
III-10	Low Gain Axial Mode	64
III-11	High Gain Axial Mode	65
III-12	Normal Amplifier Gain	68
III-13	Increased r_{12}	69

CHAPTER 1
INTRODUCTION

Since the early days of RADAR in World War II considerable research effort has been expended in the development of short wavelength technology. The evolution of high power millimeter wave sources has been limited by the fact that conventional sources and amplifiers require resonant cavities of the same scale as that of the emitted radiation. Examples of these types of devices are the klystron and the Traveling Wave Tube. The main drawbacks of cavity devices lie in the high frequency regime in the areas of component manufacturing, energy loss, and heat dissipation. This "restriction" was soon to be abated when in 1953 Weber (WB) published an article which stated that amplification should be possible using a "population inversion" phenomena. The concept of inversion, defined mathematically as negative resistance, was used in the years immediately following Weber's article as the basis of a microwave amplifier called the MASER.

The need for an amplifier that produces short wavelength tunable, high power, coherent radiation has been well publicized by the defense and communications industries. To

the communications engineer the short wavelength sources/amplifiers provide a means to take advantage of an operational bandwidth behavior that narrows in response to increasing frequency. In addition higher frequency systems have less beam divergence for more efficient long distance communications links. For defense interests the shorter wavelengths provide a greater target acquisition capability and a reduction in the probability of intercept or jamming.

The MASER and a concurrently developed device, the parametric amplifier have been categorized as reflection type amplifiers. In its simplest form the reflection amplifier is a device which amplifies by reflecting radiation possessing a greater amplitude than that of the input signal. These two types of reflection amplifiers, the MASER and the parametric amplifier have assisted in this quest for higher frequency, tunable devices.

Recent advances in the development of the Free Electron LASER have permitted, with license, the suggestion of the possible existence of a Free Electron MASER. The Free Electron MASER would function in a manner similar in nature to the microwave MASER, with the primary difference being that the active MASER medium(ruby) would be supplanted by the beam driven resonant structure of the Free Electron

LASER. One of the disadvantages of the MASER is that its operating range is governed and restricted by the transverse dimensions of the cavity and more importantly by the energy level transitions of the enclosed medium. With the Free Electron LASER, on the other hand, we will have independence from the cavity dimensions and population inversion limitations.

The design of the Free Electron MASER is relatively straightforward. By using an appropriate coupling network, a low dielectric constant medium, and a mildly relativistic electron beam, an apparatus could be built. Subsequent analysis in this paper predicts such a device will operate well into the millimeter and submillimeter ranges.

Chapter 2 undertakes a brief description of the geometry of the beam driven dielectric Free Electron LASER. Through the use of classical fluid equations and Maxwell's equations we derive a dispersion relation which relates w to k for the beam waveguide system. This equation shows how the space charge waves of the beam couple to the electromagnetic wave in the presence of the dielectric. From this dispersion relation we can solve for the spatial gain and parametrically analyze for variations in beam current, beam energy, and resonator radius. Chapter 3 describes

✓

qualitatively MASER operation and shows how the Free Electron LASER can be used as the active medium in the reflection amplifier. The reflection process is modeled by deriving the reflection coefficient of a TM wave incident on an active dielectric cylinder; and shows that the reflection coefficient assumes a value greater than unity. The spectral distribution of the reflection coefficient is discussed along with the response of the peak gain resonant mode and its relation to the gain-bandwidth product for the Free Electron MASER amplifier.

✓

The final chapter discusses the Free Electron LASER analog of the optical LASER superradiance. In the optical(atomic) LASER, the power output in the superradiant mode is proportional to the square of the population inversion. The proportionality in the Free Electron LASER is shown to be the square of the beam current.

AD-A126 990

LARGE AMPLITUDE ION WAVES(U) DARTMOUTH COLL HANOVER N H
DEPT OF PHYSICS AND ASTRONOMY J E WALSH 19 NOV 82
AFOSR-TR-83-0286 AFOSR-77-3410

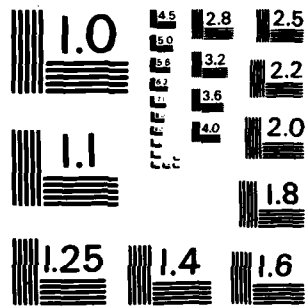
2/4

UNCLASSIFIED

F/G 20/7

NL





MICROCOPY RESOLUTION TEST CHART
NATIONAL BUREAU OF STANDARDS-1963-A

✓

CHAPTER 2

FREE ELECTRON LASER GAIN ANALYSIS

We shall be treating the Free Electron LASER only through its behavior as a separate element in a lumped circuit and as such need not attempt a microscopic description of the gain producing phenomenon. However, we need to analyze the system in close enough detail so as to adequately describe the system gain and to determine the effects on the gain lineshape resulting from modification of the system variables.

✓ The Free Electron LASER under consideration is a Cerenkov microwave generator(1,2) and may be represented as an infinite length of a cylindrical isotropic dielectric(of radius a) contained in a circular metallic waveguide. The walls of the waveguide are considered to have infinite conductivity. A relativistic electron beam is propagated axially through the dielectric with an electron velocity superluminal for the dielectric medium. We neglect the microscopic environment of each electron and confine our interest to the collective phenomena. We can thus use macroscopic plasma equations to describe the behavior. The electron motion is considered to be a cold plasma with no

thermal velocity dispersion. The electron motion is rendered unidirectional by the application of an external magnetic field, B_0 which maintains field lines parallel to the axis of the cylinder. A sketch of the geometry as described above is given in Fig.II-1.

We tacitly assumed, for convenience, that the beam propagates through the dielectric; but the problems associated with the beam propagation through the dielectric deserve some comment. By using a solid dielectric the beam would have difficulty propagating through the resonator. The electron beam would obviously lose much of its energy in collisional ionization of the dielectric. Two solutions to this problem are to provide for a channel for beam propagation or to use a less dense gaseous dielectric. The beam-channel concept is the most feasible and has been previously studied for use in the Free Electron LASER(3, 4,5). For conceptual purposes, however, our analytical assumption of the solid geometry is convenient. This geometry greatly simplifies the boundary conditions and the results from the solid dielectric geometry do not depart radically from the more difficult beam channel analysis.

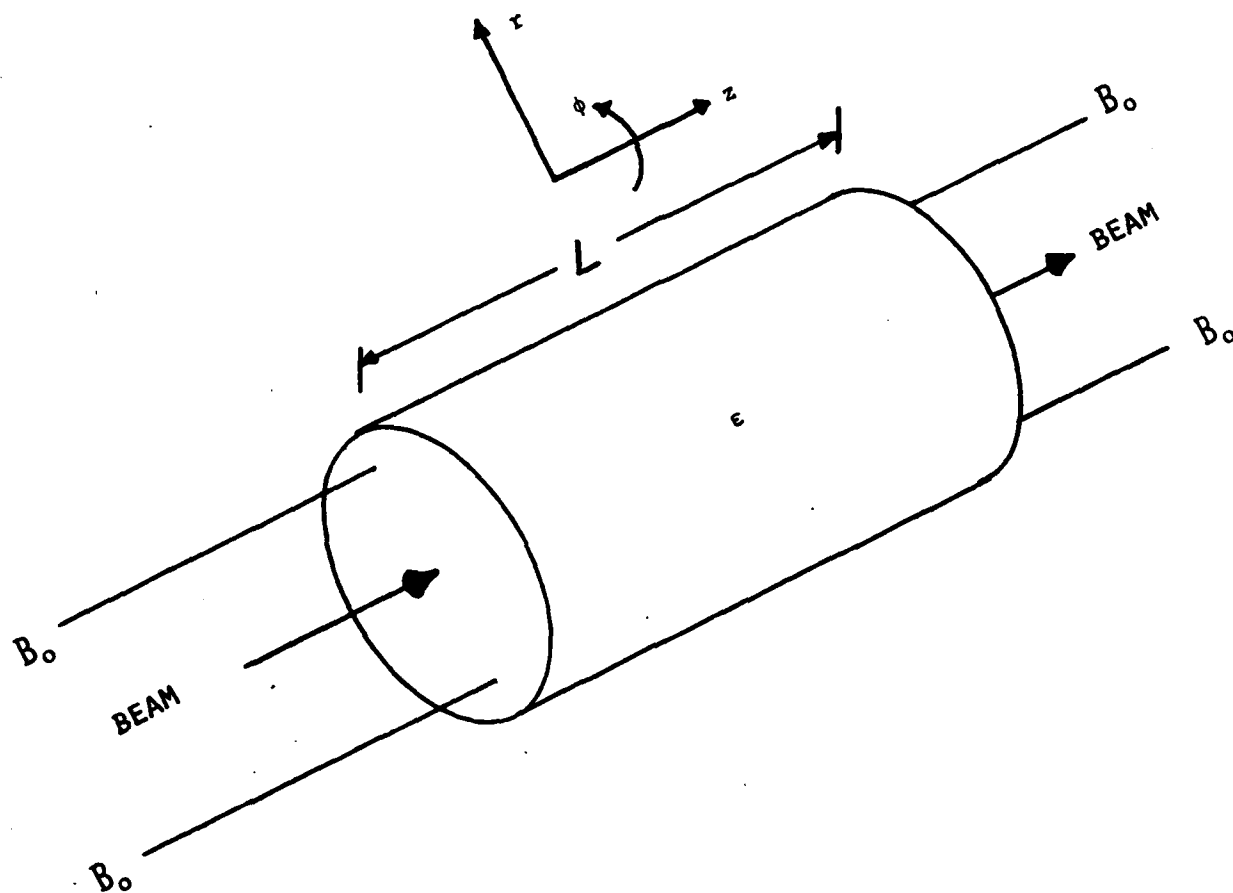


Fig. II-1, Free Electron Laser Geometry

It is instructive to discuss qualitatively the process that occurs in the amplifier. The pump radiation source produces an input wave which establishes normal modes of vibration appropriate for the geometry of the resonator. The electromagnetic fields of the incoming wave will interact with the electron beam to cause a redistribution or modulation of the electron velocities- thus causing bunching in the beam. If a greater number of electrons are caused to give up energy to the wave than absorb energy from the wave, a gain condition exists and the wave will grow until the gain saturates. The amplified radiation can then be coupled from the resonator through an appropriate network.

The cold beam dispersion relation

Our first step in a more rigorous analysis is to determine the modulated current density. With that in hand we can use the perturbed current density as the source term in Maxwell's equations in order to couple the beam to the wave in the dielectric and then write the wave equation. From the wave equation, the dispersion relation for the wave in the dielectric resonator may be determined. Once we have an appropriate analytical expression for the dispersion

relation we can solve for the spatial gain of the Free Electron LASER.

If the TM mode is assumed to be the mode in the guide, then the field components may be written:

$$\underline{E} = (E_r \hat{r} + E_z \hat{z})$$

$$\underline{B} = (B_\phi \hat{\phi})$$

We can couple the axial electric field the electron beam through Maxwell's Equations. As a starting point we to assume a macroscopic MHD description and use the equations of plasma physics. Thus we begin by applying small amplitude oscillations to Newton's second law:

$$\underline{F} = \frac{d\underline{p}}{dt} = \frac{d}{dt}(m\gamma \underline{v}) = -e(\underline{E} + \underline{v} \times \underline{B})$$

$$\underline{v} = \underline{v}_0 + \underline{v}_1$$

$$\underline{E} = \underline{E}_1$$

and after Fourier transforming the perturbed velocity may be expressed:

$$\underline{v}_1 = \frac{-ie \underline{E}_1}{m\gamma^3(\omega - kv_0)} \quad [1]$$

The linearized equation of continuity and Fourier transformation allows us to write the modulated particle number in terms of the unperturbed number and v_1 :

$$n_1 = \frac{-ikn_0 e v_1}{m\gamma^3(\omega - kv_0)} \quad [2]$$

Using equation 1, equation 2 may be rewritten:

$$J_1 = \frac{-ikn_0 e E_1}{m \gamma^3 (\omega - kV_0)^2} \quad [3]$$

If we linearize the Fourier transformed current density, and use equations 1 and 3, J_1 can be expressed:

$$J_1 = \frac{i\omega_b^2 \omega E_1}{4\pi \gamma^3 (\omega - kV_0)^2}; \quad \omega_b^2 = \frac{4\pi n_0 e^2}{m} \quad [4]$$

We now need to couple the perturbed current density to the waveguide modes through Maxwell's Equations. Writing the wave equation in cylindrical components and, recalling the field components of \underline{E} , E_r becomes:

$$E_r = \frac{-ik \frac{\partial E_z}{\partial r}}{k^2 - \omega^2 \epsilon / c^2} \quad [5]$$

Using the axial part of ∇ , the wave equation can be given as:

$$\nabla_1^2 E_z = \left(k^2 - \frac{\omega^2 \epsilon}{c^2} \right) \left(1 - \frac{\omega_b^2}{\epsilon \gamma^3 (\omega - kv_0)^2} \right) E_z \quad [6]$$

If we now impose the boundary condition that E_t must vanish on the walls of the guide and expand the radial component of E_1 in a Bessel series:

$$E_z = \left(\sum_l A(\omega, k) J_0(p_l r) \right)$$

We can then substitute the series definition into equation 6, and from that we may write:

$$D(\omega, k) = \omega^2 - \omega_{0k}^2 - \frac{\omega_b^2 \left(\omega^2 - \frac{c^2 k^2}{\epsilon} \right)}{\epsilon \gamma^3 (\omega - kv_0)^2} = 0 \quad [7]$$

$$\text{WHERE: } \omega_{0k} = \frac{c^2}{\epsilon} (p_l^2 + k^2)$$

This expression is defined to be the cold beam dispersion relation for any mode of the Free Electron LASER system(6).

To make this dispersion relation more responsive to real physical parameters, such as beam current, beam energy, and resonator geometry, it is only necessary to transform to an analytical expression containing these variables. From plasma physics we know that Ω_b^2 is defined to be:

$$\Omega_b^2 = \omega_b^2 = \frac{4\pi n_0 e^2}{m}$$

Assuming that the propagating beam is of a cylindrical geometry the current can be written:

$$I = -enAv$$

where: $A = \pi a^2$

and: $a = \text{radius of the beam cylinder}$

This implies that particle density can be expressed:

$$n = \frac{|I|}{eAv}$$

Now I_0 is defined to be:

$$I_0 = \frac{ec}{r_0}$$

where: $r_0 = e^2/mc^2$ which is the classical electron radius. Thus the original equation for the beam plasma frequency can be rewritten:

$$\omega_b^2 = \frac{4I_0 c^2}{I_0 \beta a^2}$$

Equation 7, in a simple way, relates k to w by way of the coefficients of an equation quartic in k and w . If the beam plasma frequency is initially set equal to zero, Fig. II-2, the resulting plot of the dispersion relation would describe the behavior of an electromagnetic wave propagating in a dielectric waveguide. The phase velocity of this wave at any point on the curve is the slope of the line connecting that point to the origin of the axes. The asymptote plotted is $w = ck/\sqrt{\epsilon}$ and the slope is defined as light speed in the dielectric medium. As we can see, the entire dispersion relation remains above the asymptotic limit, thus, each waveguide mode has a phase velocity greater than the light velocity in the medium. As a result, the coupling of an electron beam to any one of the cavity modes will permit a Cerenkov interaction to occur. The w versus k plot in Fig. II-3 contains the beam velocity line $w = ck\beta$ and assumes a small but finite value for the beam plasma frequency. As can be seen the beam velocity line will intersect the

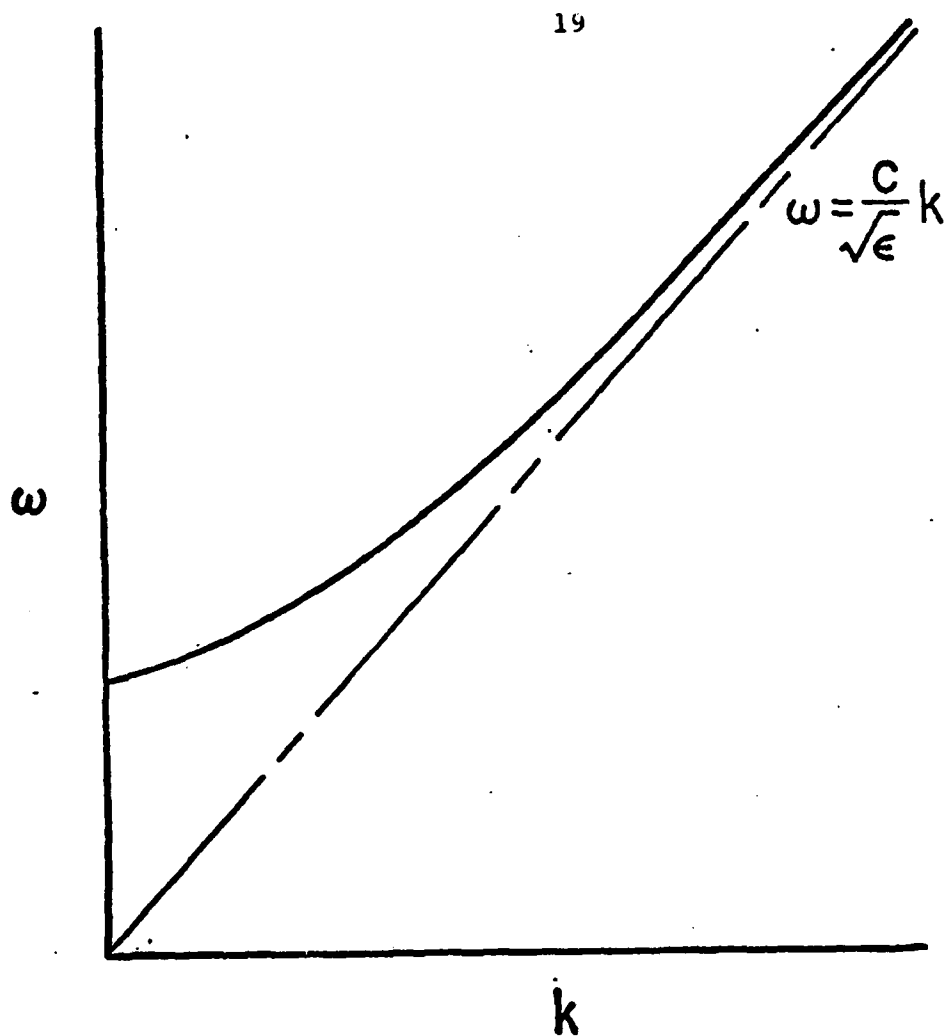


Fig.II-2. The no-beam dispersion relation. Since the entire hyperbola is above its asymptote of slope $c/\sqrt{\epsilon}$, all beam coupling modes fulfill the Cerenkov condition.

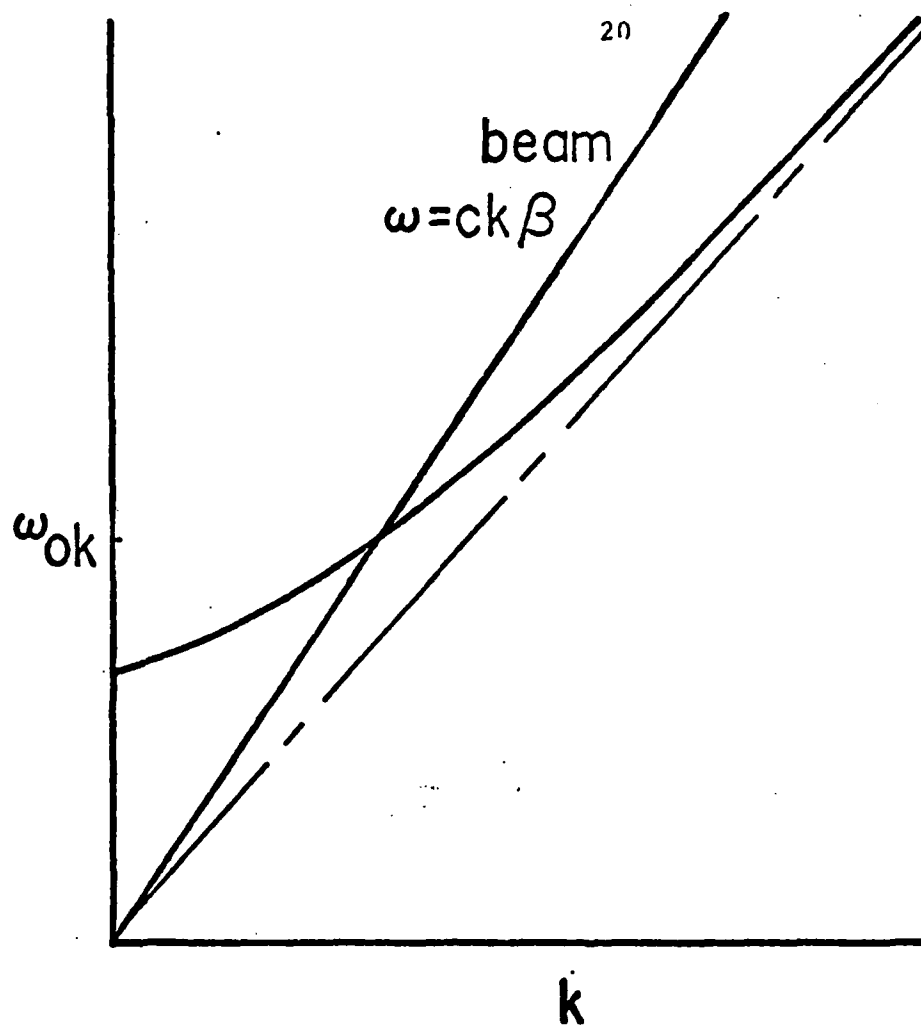


Fig.II-3. The beam is introduced into the system. ω_{0k} is the point of synchronism.

dispersion relation whenever the beam itself has a greater than light velocity.

The point of intersection of the two lines is where the greatest interaction of the electron beam and the guide should occur. This intercept, known as synchronism, shows the conditions where the phase velocity of the electromagnetic waves propagating in the dielectric is equal to the electron velocity. This coupling of the waves and beam permits an energy exchange to occur between the electrons and the modes of the axisymmetric resonator. We can thus infer from the strength of the interaction that the synchronous frequency is the frequency where maximum gain will be observed for our reflection amplifier.

Gain Calculations

Knowing equation 7, we can solve for the spatial gain of the Free Electron LASER by finding the imaginary roots of k in terms of w and other physical variables.

Equation 7 may be expanded and written in descending powers of k . The coefficients of each power of k clearly are a function of w , radius, beam velocity, and other variables. The solution for an analytical expression for the imaginary

✓

root of k is a time consuming task but is easily accomplished numerically. A computer program was written(Appendix 1) which solved for the imaginary roots of the dispersion relation. For a given beam velocity, resonator length, and radius a spectral line profile for the gain can be computed and plotted. An example of such a gain envelope is provided in Fig. II-4. In Fig. II-4 we have a plot of $\text{Im } k(\text{gain})$ versus w/c . This plot was done for a beam current of 10 Amps, beam velocity of $.614c$, and a resonator radius of 4mm. The important factor to observe is that there exists finite gain for the system up to the synchronous frequency; after which, the gain quickly drops to zero. Since we are interested in a device whose operating regime(synchronism) is in the millimeter wavelengths we will want the synchronous frequency to be as high as possible. In analyzing how the synchronous frequency and gain behaves, we shall find the wavelength of the output to depend on two areas of influence: electron beam characteristics, and the geometric parameters of the resonator. We shall investigate, in detail, the effects on the gain due to changes in the beam velocity, beam current, and the radial dimension of the resonator.

Parametric Analysis

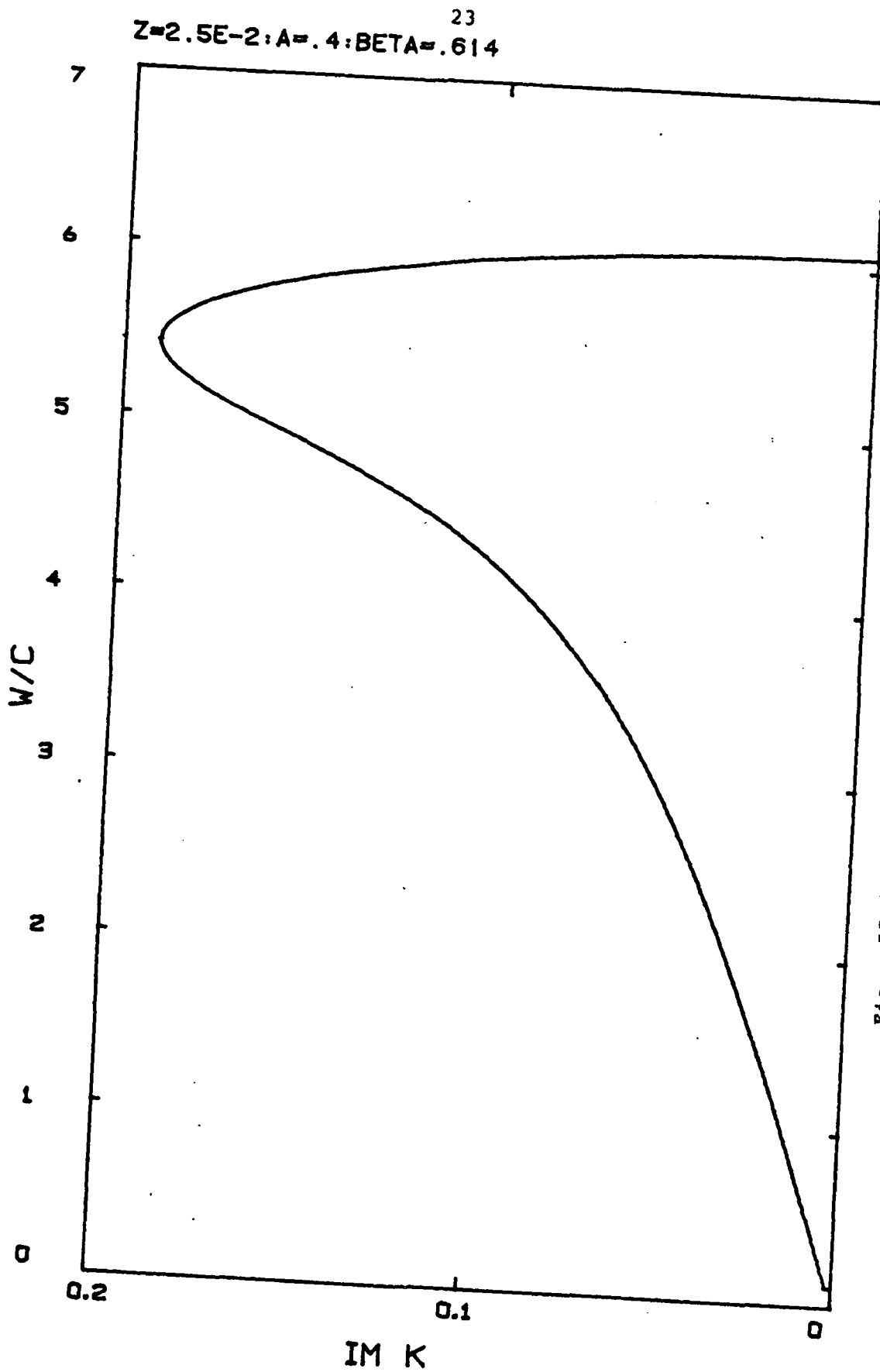
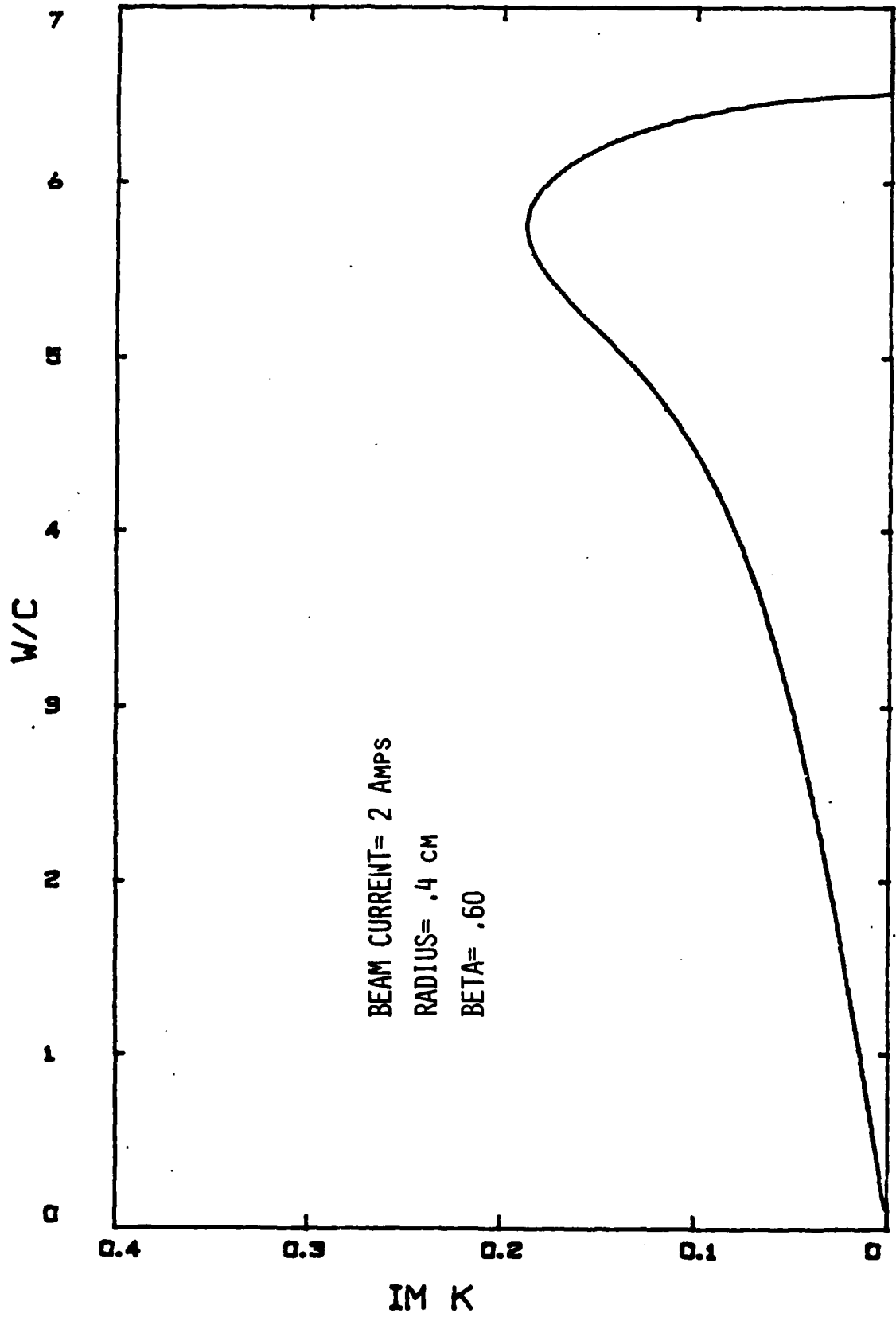


Fig. 11-4, Example Gain Lineshape

One of the key variables in the dispersion relation is the electron beam current. Figures II-5 and II-6 are representative of plots of gain, as a function of frequency, for two geometrically identical systems except for differing beam currents. They show how the lineshape responds when the beam current is 2 amperes and 11 amperes. With the lower beam current (Fig. II-5) the peak gain is less than that observed for the higher beam current. At the same time the monochromaticity of the lineshape also changes. A quick look at the two plots show the obvious lineshape broadening of the gain curve in the high gain regime as compared to the lower peak gain. Thus the higher peak gain is associated with a broader spectral gain. The change of the beam current does not effect the location of the gain peak, which is the point of the synchronous frequency. This is due to the fact that the synchronous point(intersection of the $D(w,k)$ curve and the beam energy line) remains stable during the beam current variations.

If beam current and resonator radius are maintained, variations in line shape from changes in beam velocity may be analyzed. In Figures II-7 and II-8, we can see the behavior as β is varied from .615 to .90. The shape of the curve(to include the half-width) remains invariant during the velocity shift with the only difference being a

$Z=2.5E-2; A=.4; BETA=.60$
Fig. II-5, Gain as Function of w/c

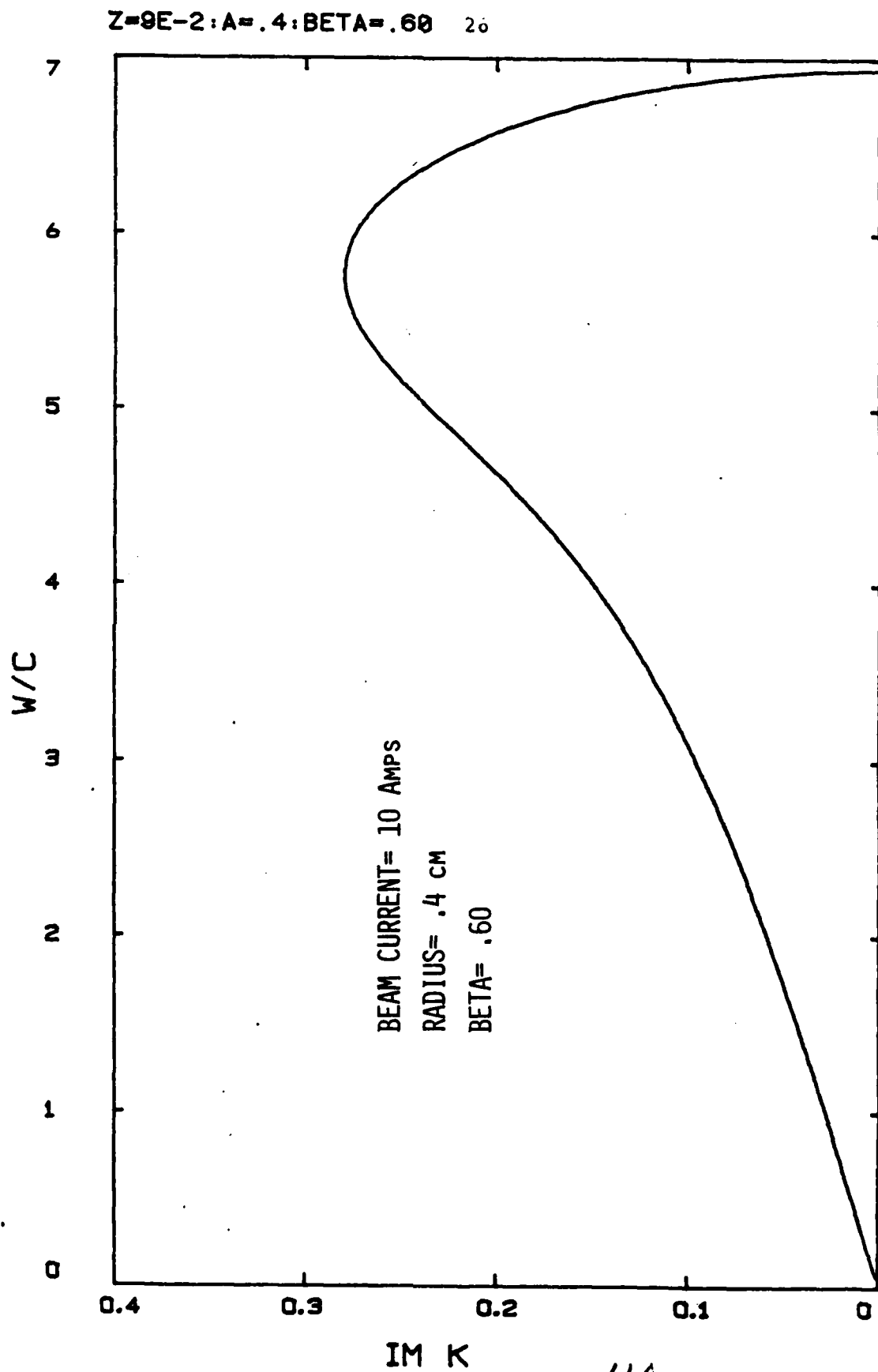


Fig. 11-6, Gain as Function of w/c

$Z=2.5E-2: A=.4: BETA=.9$ 27

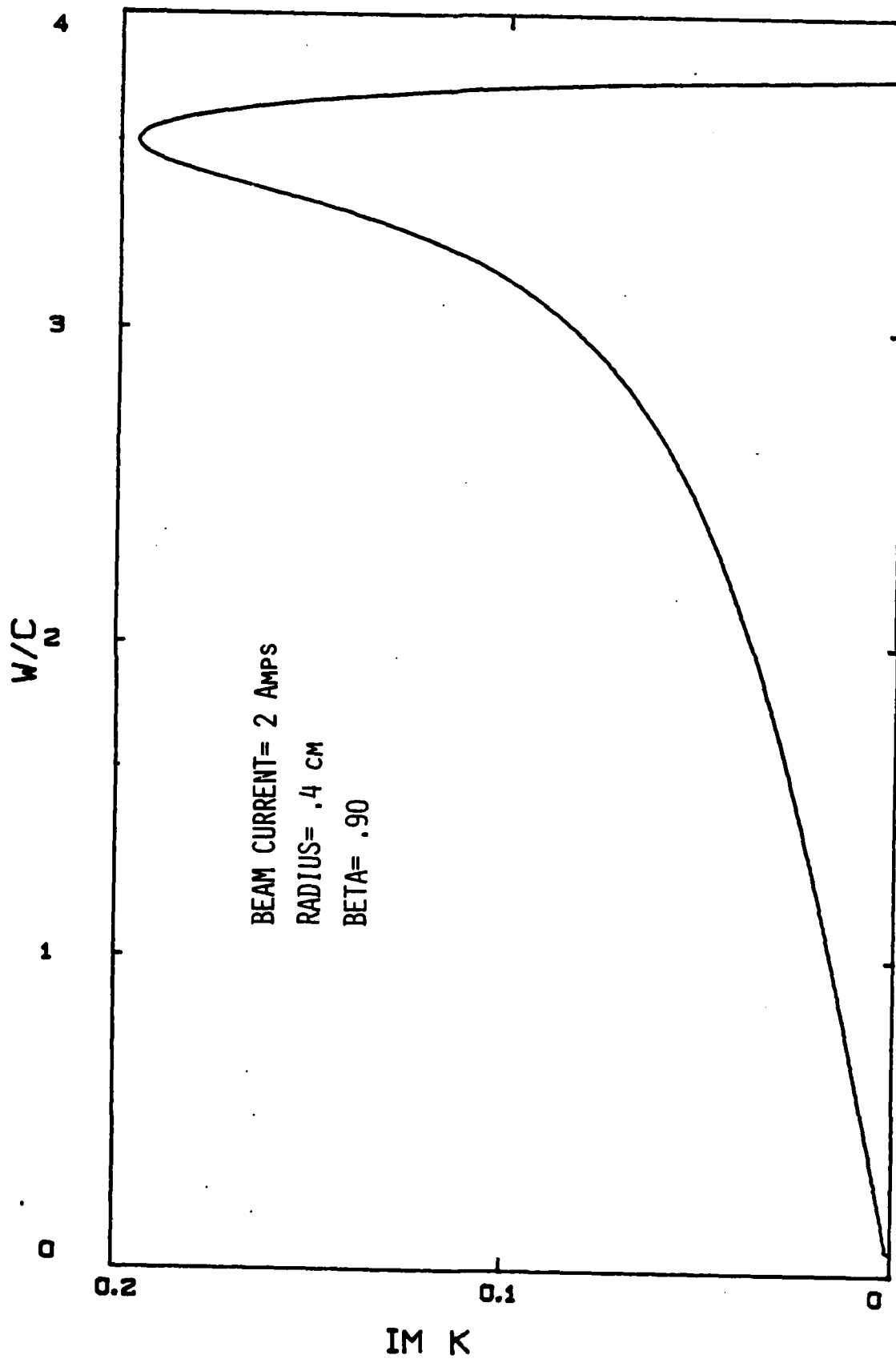


Fig. 11-7, Gain as Function of w/c for $Beta=.90$

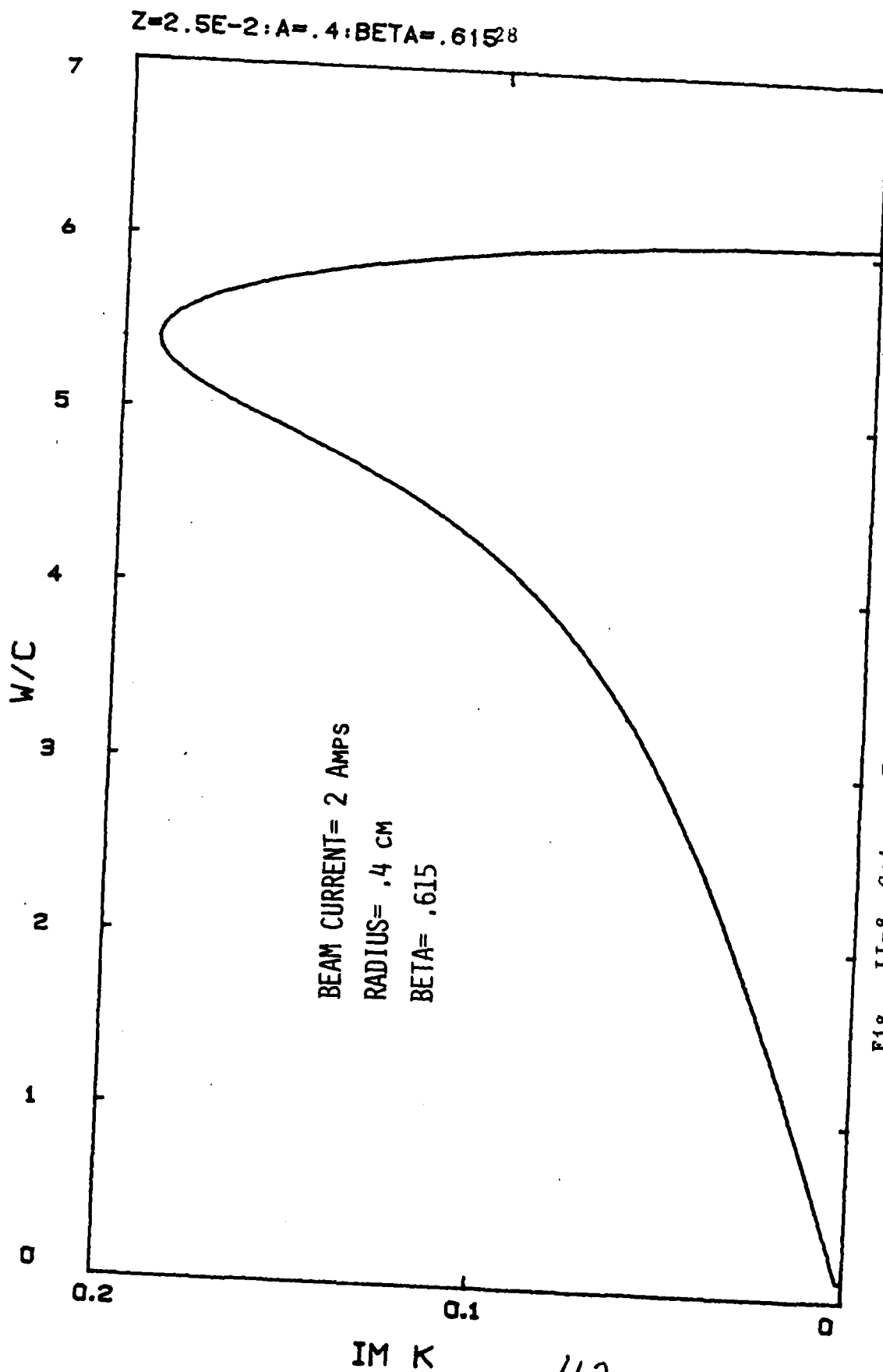


Fig. II-8, Gain as Function of w/c for $Beta=.615$

slightly higher peak gain exhibited at the upper end of the beam velocity spectrum (the peak gain actually increases by the one-third power of w , see Appendix 2). The important point to note is the significant change in the interaction frequency. Fig. II-9 shows the rapid increase in interaction frequency as the beam velocity is reduced from .90 to .60. The lower the value of β the higher we observe the frequency of the synchronous point. This is not unexpected. Referring back to Fig. II-3 we see that as we decrease the beam energy (decrease slope) the synchronous point shifts farther up the dispersion relation curve and has a higher interaction frequency. This shift of interaction frequency is noteworthy and the importance of this behavior should not be forgotten during our search for devices that function at the higher end of the microwave frequency spectrum.

We can show the effect on the gain and the synchronous frequency due to the introduction of changes in the longitudinal and radial dimensions of the resonator. If the length is changed, as in any resonant structure, only the longitudinal modes will be effected, and this is of little interest. Variations of the radial parameter does produce a relevant response. Figs. II-10 and II-11 give the gain

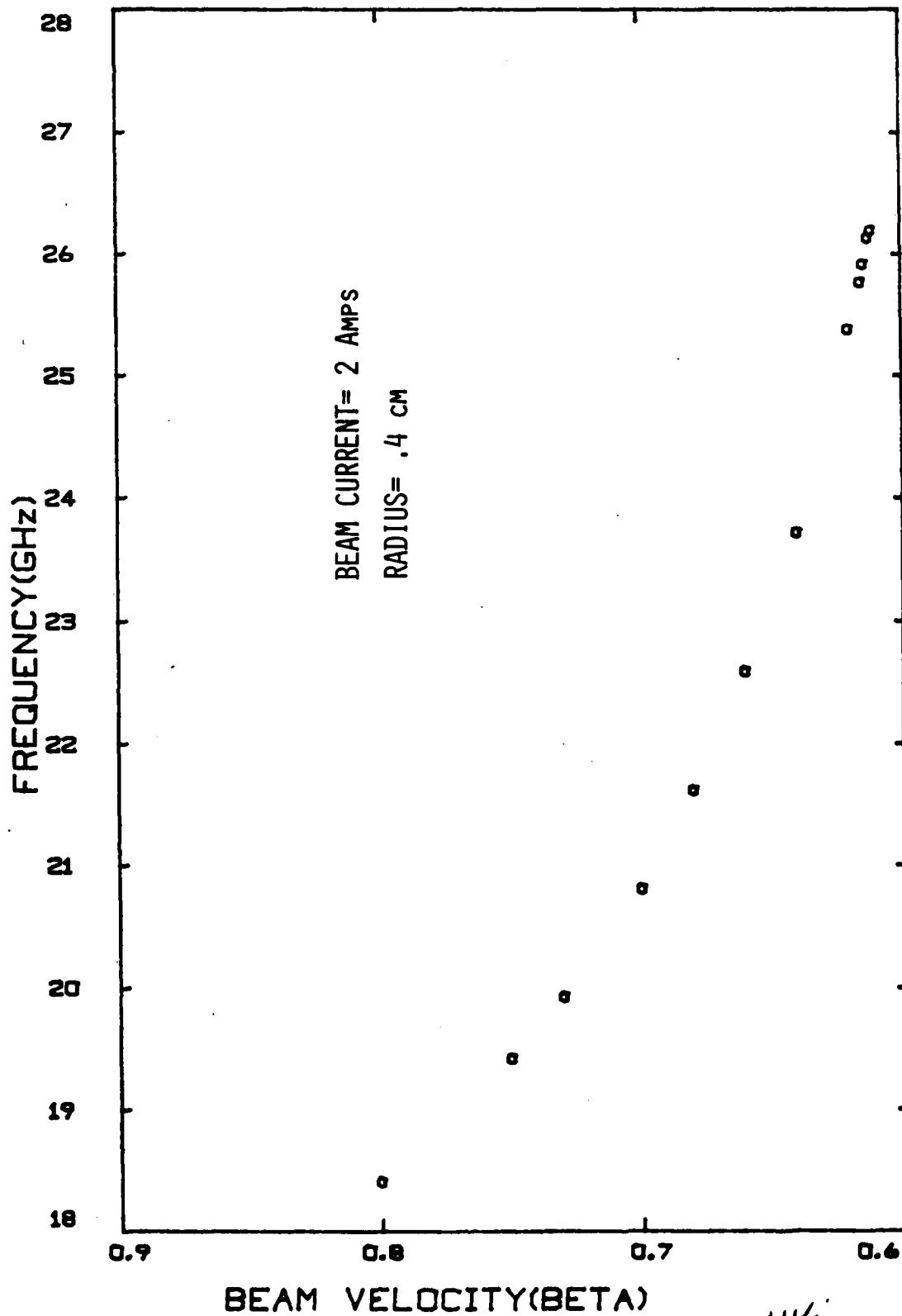
BETA VS FREQUENCY FOR $Z=2.5E-2$; $A=.4\text{cm}$ 

Fig. II-9, Plot of Operating Frequency vs Beta

$$Z=2.5E-2; \text{BETA}=.615; A=.27$$

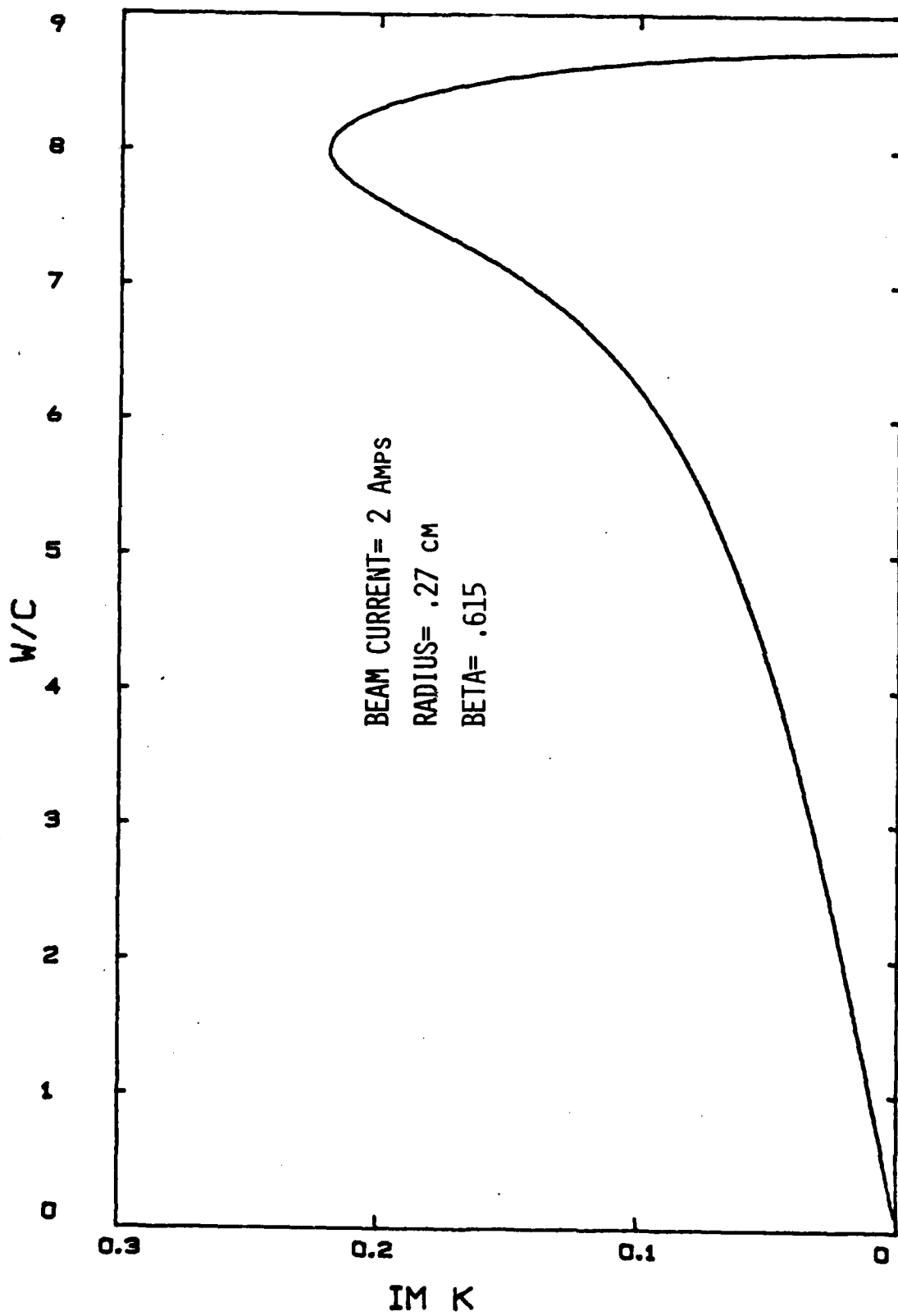


Fig. II-10, Gain Lineshape for Small Radius

115

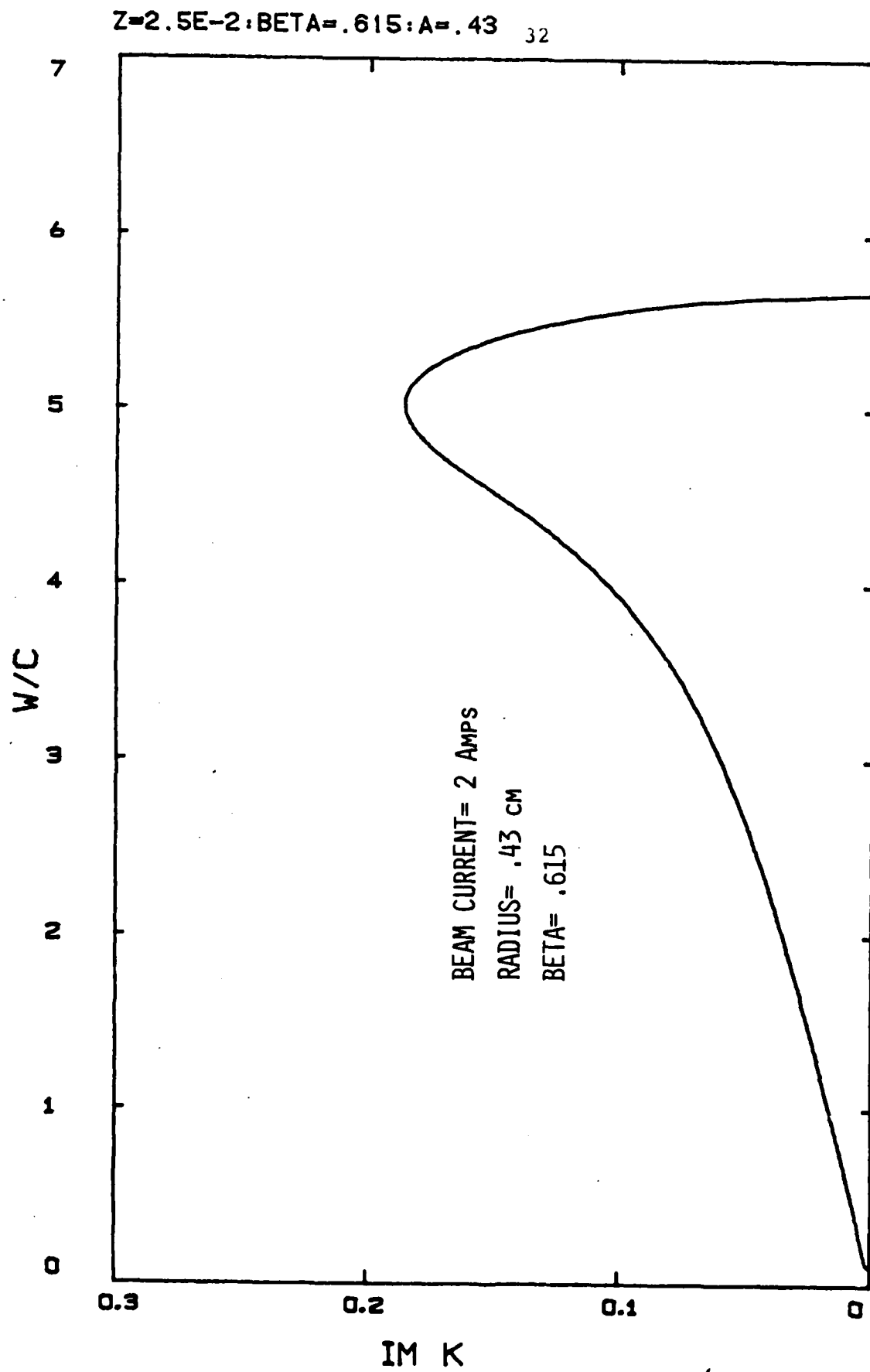


Fig. II-11, Gain Lineshape for Larger Radius

lineshape response for two identical systems with differing radii. In a comparison between the two curves we see no change in peak gain or spectral distribution. But for the smaller radius, however, the interaction frequency occurs at a higher frequency than that of the larger radius. This variation in coupling frequency in terms of radius may be seen more clearly in Fig. II-12 where interaction frequency, ω_k , is plotted as a function of the radial dimension. In the range of small radii the operating frequency shows a dramatic exponential "growth". We can see, therefore, that in the same manner as discussed previously this "tuning" effect could be used to design output performance at a specific frequency by the proper scaling of the resonator.

If the beam velocity and resonator radius are varied concurrently, some extremely high operating frequencies may be predicted. A realistic lower limit on the resonator radius can be established at 1.5mm. This 1.5mm limit is a high voltage engineering restriction derived primarily from the difficulty of focusing an electron beam any smaller than 1mm. With the radius established at 1.5mm, the beam velocity is reduced to .55c. Fig. II-13 shows that when the system is configured with the radius and beam velocity

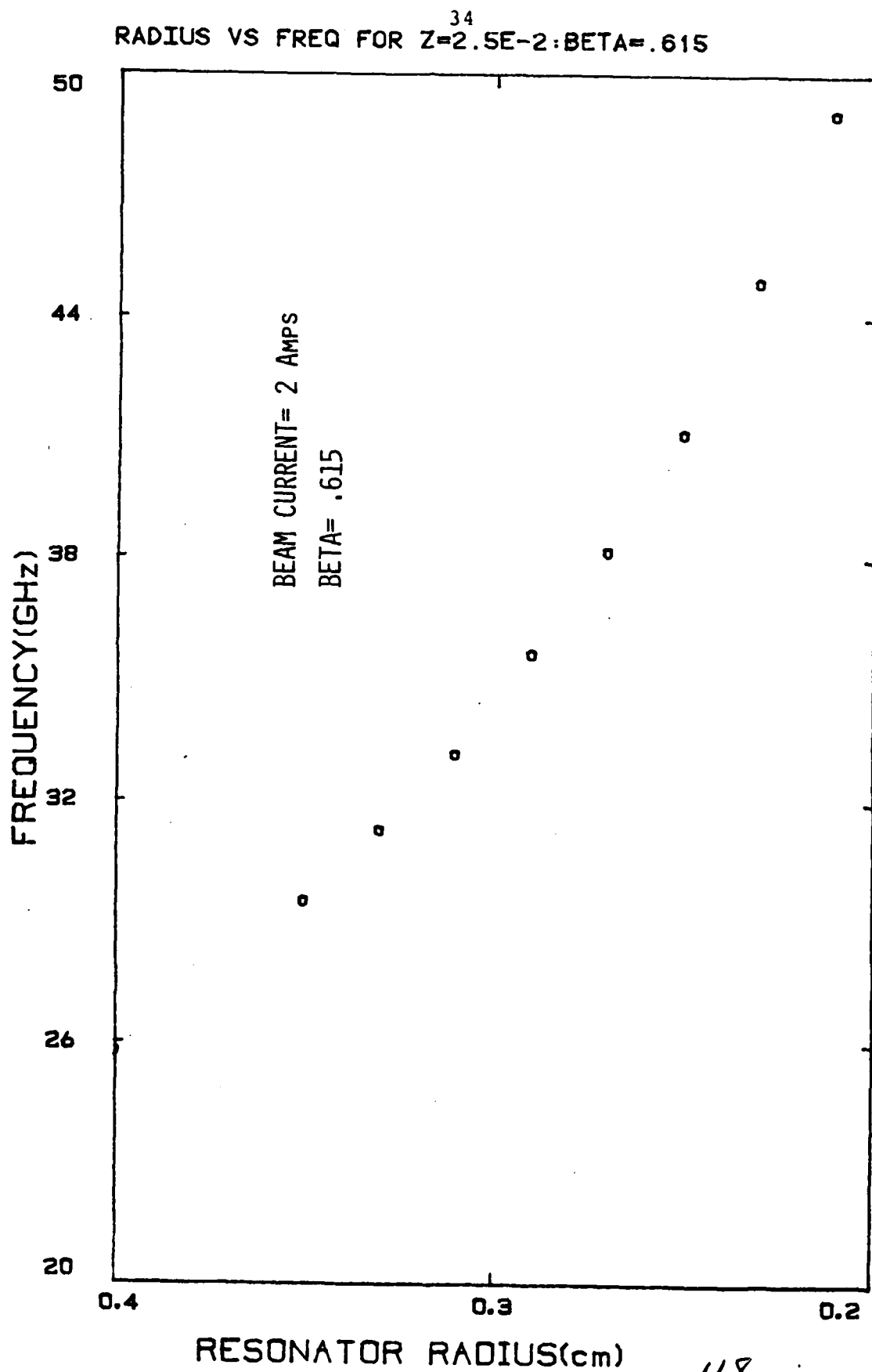


Fig. II-12, Plot of Operating Frequency vs Radius

$$Z=8E-2: A=.15: \text{BETA}=.55$$

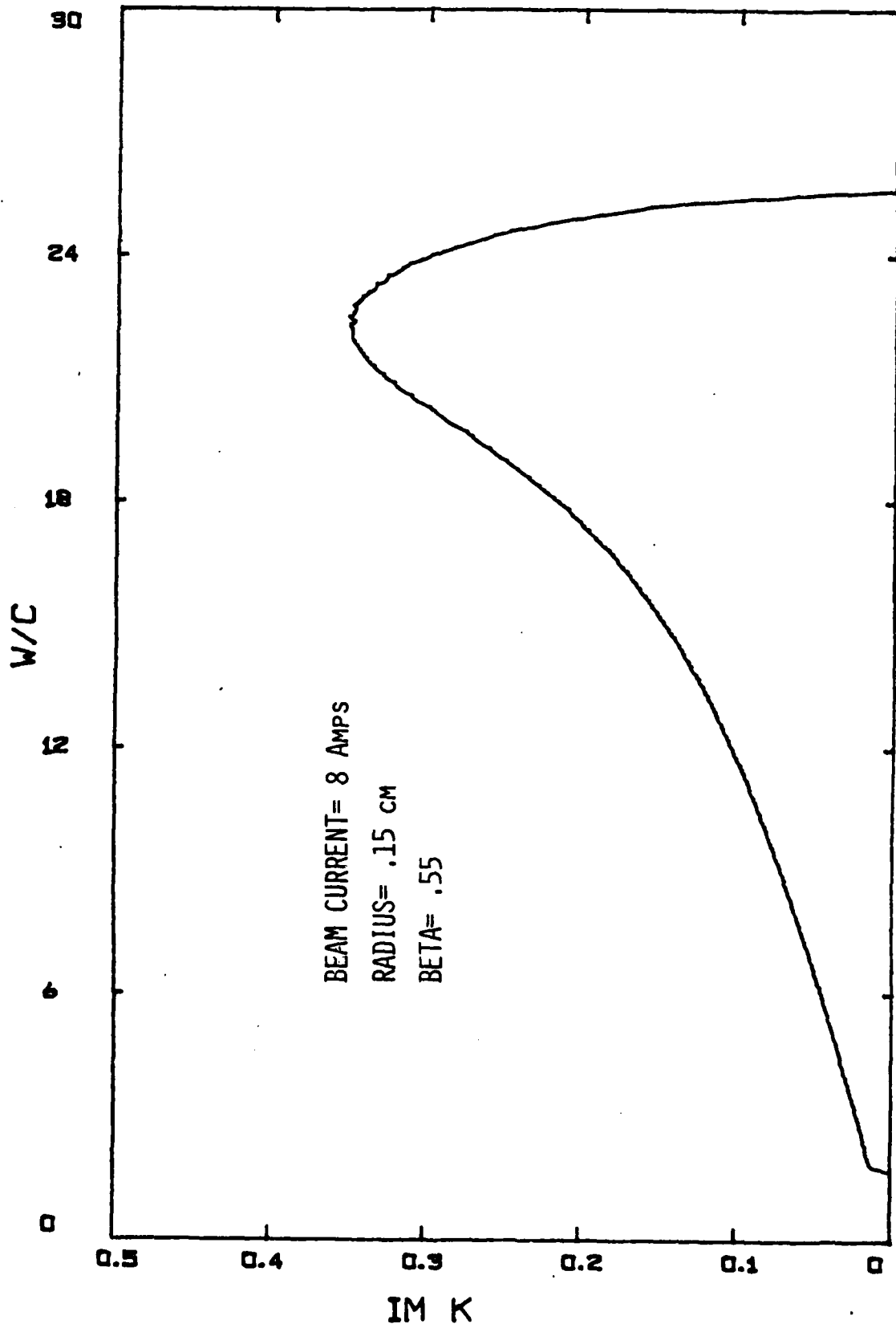


Fig. 11-13, Gain Lineshape for 110GHz

described, an operating frequency of 110GHz is predicted.

Cold Beam Limit

In the preceeding discussion of Free Electron LASER gain we have made the explicit assumption that the device will operate in the cold beam limit. This means that the electron beam is monoenergetic and is not affected by a velocity broadening. The cold beam criterion is primarily determined by observing the velocity distribution from the zero order beam velocity. If we look at the velocity of the slow and the fast space charge waves associated with the beam as compared to the zero order beam velocity the $\Delta(w/k)$ can be shown to be equal to:

$$\Delta V_b = V_0 - V_{scw} = \frac{\omega_b}{k \gamma_0^{3/2}}$$

Using this expression for ΔV_b we define "coldness" in the beam to imply that the beam velocity spread be much less than ΔV_b . From the same expression, we can define a warm beam as having a velocity spread, ΔV_b :

$$\Delta V_b \approx \frac{\omega_b}{\gamma_0^{3/2} k}$$

From these relations, a transitional wavelength between the warm beam and cold beam regions may be derived. Writing ω_b in terms of beam current, as before, and taking k to be $2\pi/\lambda_{trans}$, we can substitute into the expression for ΔV_b and show that:

$$\lambda_{trans} = \pi a \left(\frac{\delta \gamma}{\gamma} \right) \sqrt{\frac{I_0}{e \gamma I}}$$

Considering our present Free Electron LASER geometry, and a 1% energy spread from the thermionic electron gun, and with:

$$\gamma = 1.2$$

$$a = 4 \text{ mm}$$

$$I_0 = 17000 \text{ Amps}$$

$$I = 100 \text{ Amps}$$

a transition wavelength is determined to be 1.1mm. With the desired operating regime of the amplifier to be in the 90-100 GHz range, we are well above the cold beam limit.

In addition to being a convenient approximation, in order to insure that the device will perform optimally in the role as an amplifier, it will be necessary to operate in the cold beam limit. If a gain analysis, similar to the preceding gain analysis, is performed in the limit of a warm electron

beam, the following contrast to cold beam behavior may be drawn. The peak gain at synchronism for the cold beam approximation exhibits a growth proportional to the one-third power of the frequency. When the ω_{trans} is exceeded the gain curve for the warm beam device demonstrates a behavior and shape complementary to the cold beam response and the gain is proportional to the inverse power of ω_{int} . With the warm beam description, the gain is relatively low, and system losses equate to the gain from the wave-particle interaction. As a result, there is insufficient gain to permit amplification and the device will function as an oscillator. Therefore, for high gain operation we must operate in the cold beam region.

Saturation

The gain of the resonator is not unbounded. Saturation effects come into play to cap the maximum gain attainable with the amplifier. In our case, the major saturation mechanism is called electron trapping and occurs when the perturbing potential of the growing wave serves to trap the slower moving electrons. As a result the wave-particle energy exchange ceases, and the gain reaches a maximum value. The saturation calculations for the filled guide are quite

complex and lengthy and will not be addressed in this
tnesis(7).

✓

CHAPTER 3
REFLECTION AMPLIFIER

MASER Operation

✓ The MASER microwave amplifier discussed in the introduction is the most recent of the reflection type microwave amplifiers. The MASER is inherently a simple device and consists basically of three primary components: a circulator, an active medium, and a microwave cavity(Fig. III-1). The first component is the three port circulator. The three port circulator is a non-reciprocal microwave device composed of the symmetrical conjunction of three identical waveguides with an axially magnetized ferrite rod emplaced at the confluence of the guides. The major function of the circulator is to allow input signals and output signals in the coupling network to be isolated from perturbing reflections which might cause instability and produce unwanted oscillations in the amplifier. The second port of the circulator is matched to the second component which is a simple microwave cavity tuned to a specific operating frequency. The third component the active

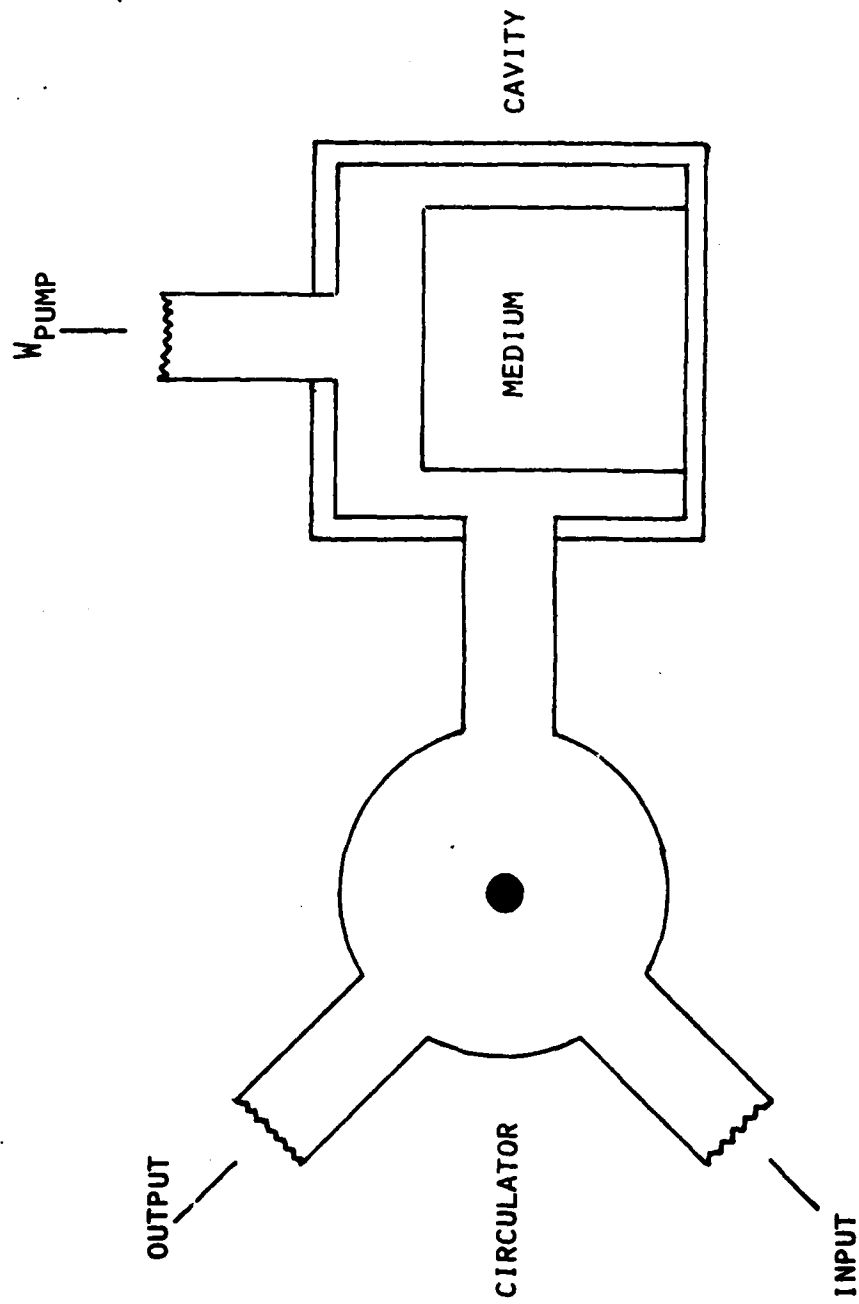


Fig. III-1, Sketch of Cavity MASER

medium, usually ruby, and a source of pump frequency, ω_p . The active medium and the ω_p use Weber's principle of the inverted population to produce a gain condition in the system. The applied signal, entering through the entrance port of the circulator and propagating into the resonant chamber causes many atomic transitions to occur. As a result, radiation of greater amplitude than the input signal is emitted from the MASER cavity at this applied frequency. We thus see that the medium exhibits a gain at the ω_{emit} and not a loss as would be expected if the medium was a normally absorbing dielectric.

The MASER, in the absence of the pump frequency, exhibits the characteristics of a common resonant cavity containing a dielectric filler. As such it can be represented by an equivalent circuit given by Fig. III-2. The energy storage capability of the cavity can be represented in terms of a characteristic inductance and capacitance, L_0 and C_0 . The gain of the inverted medium can be represented in terms of a quantity described as a negative load resistance, $-R_0$. A Q for the cavity can be calculated by the well known relation relation:

$$Q_m = \frac{\text{ANGULAR FREQ} \times \text{STORED ENERGY}}{\text{POWER DISSIPATED}}$$

176

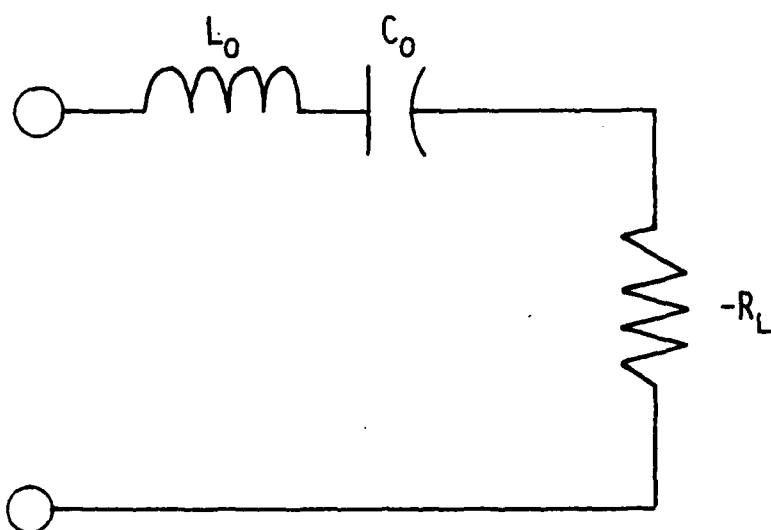


Fig. III-2, Cavity MASER Equivalent Circuit

As a consequence of the negative resistance quantity, the Q is obviously negative. This negative Q is defined to be a measure of the strength of the MASER action.

This negative character of the load resistance is the prime factor in the reflection amplification process.

Taken in its simplest form, the negative resistance amplifier can be modelled as a transmission line of characteristic impedance Z_0 terminated in a load impedance Z_L as given in Fig. III-3. From simple transmission line theory, a plane wave propagating down the line to the right will be reflected from the load impedance in proportion to the voltage reflection coefficient with a voltage gain of ρ :

$$\rho = \frac{Z_L - Z_0}{Z_L + Z_0} \quad [1]$$

The power gain of the amplifier then is defined to be $|\rho|^2$. If ρ is less than unity, power is absorbed. If ρ is greater than one, then power is emitted.

A better understanding of the reflection type amplifier can be gained by a detailed analysis of Equation 1. In our circuit model, at the point of the midband frequency, the impedances of the line and load assume purely resistive

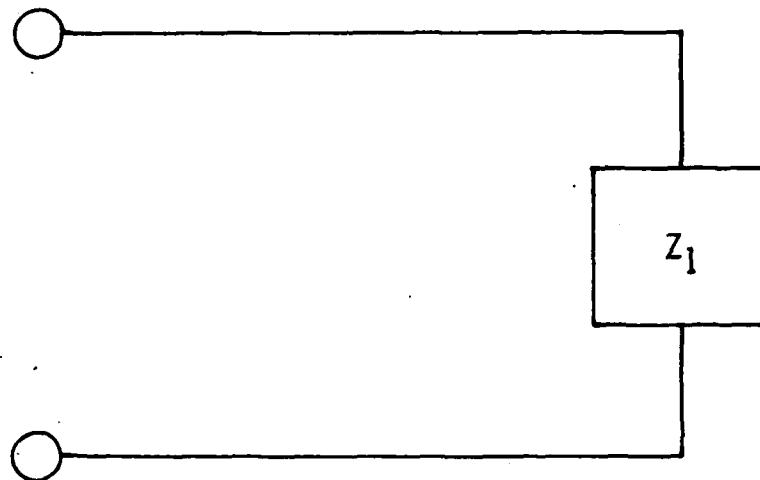


Fig. III-3, Transmission Line with Z_1

forms. The load resistance in this case (where we have the availability of negative R) can range over all real positive and negative values. Equation 1 thus becomes:

$$\rho = \frac{R_L/R_c - 1}{R_L/R_c + 1} \quad [2]$$

Fig III-4 is a plot of equation 2 with the reflection coefficient as a function of the resistance ratio. If R_L is varied over increasingly larger positive values, the reflection coefficient also increases and approaches 1 as a limit. This behavior is similar to that seen in the short circuited line. When the load resistance exactly equals the coupling resistance, the line is matched to the load, and, as expected, vanishes. If R_L assumes positive values smaller than R_c , but approaches zero, the reflection coefficient again approaches one. We can observe this in the $R_L=0$ or open circuited line. This value of unity for the reflection coefficient, unlike in the preceding analysis, is not a limiting value.

If we continue to vary R_L over small negative values (with respect to R_c), the reflection coefficient behaves by assuming values greater than unity, and thus a gain situation exists. The gain is possible because we have defined the negative resistance as giving power to the

✓

$$|P| = \frac{R_L/R_e - 1}{R_L/R_e + 1} \quad 47$$

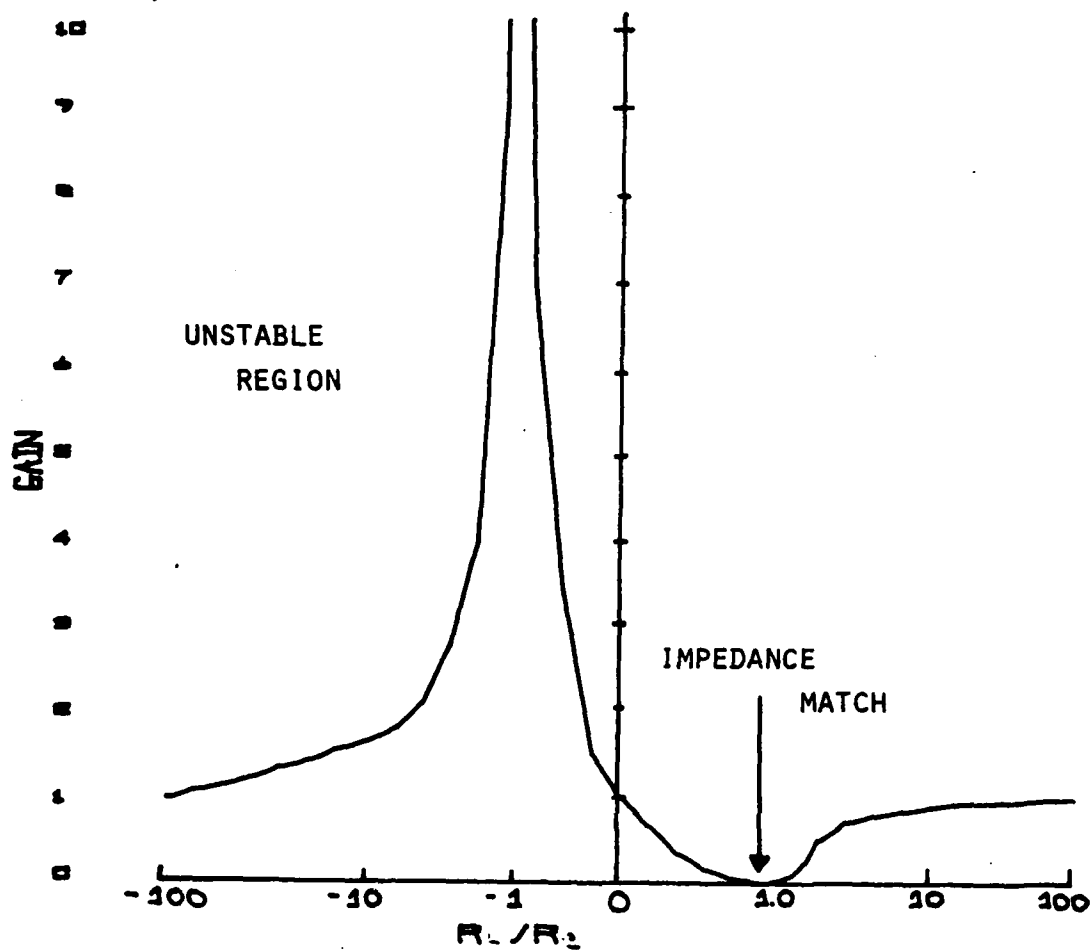


Fig.III-4GAIN BEHAVIOR OF THE NEGATIVE RESISTANCE AMPLIFIER

✓

circuit instead of absorbing it. As $R_l \rightarrow -R_e$, the reflection coefficient rapidly approaches infinity. When we reach the point where $R_l = -R_e$ we have an "anti-match" condition; and the value of the reflection coefficient equals infinity. At this point the circuit will jump into instability. If R_l becomes larger (in a negative sense), the reflection coefficient decreases from infinity and again approaches the finite value of unity, although the approach is from above 1 and not below. This condition defines a region of oscillation and not amplification.

✓

In order to have a large and finite value of gain, the anti-match condition must be approached carefully to avoid the problem of instability. We can reach that point by adjusting slightly the values of R_l or R_e . However, neither of the values can fluctuate to any great extent from their respective zero order values. If larger fluctuations are tolerated, the circuit can become overcoupled or undercoupled and the amplifier will operate in the unstable region and oscillate.

This behavior of the reflection coefficient is common to all reflection type amplifiers where we must be judicious in our adjustment of the external loading. We must establish it at a point where it barely exceeds the negative load

resistance. It is in this situation where we intend the circuit to remain under threshold and on the verge of oscillation.

Free Electron Laser Transmission Line Analysis

This latter transmission line analysis suggests a possible approach to the use of the Free Electron LASER as the circuit element which provides the negative resistance quantity present in our lumped circuit, Fig. II-2. With the Free Electron LASER the gain is a spatially distributed quantity, thus a distributed circuit analysis is needed. Fig. III-5 gives an equivalent circuit for such a device and consists of the Free Electron LASER modeled as an aperture coupled short circuited transmission line of length l . In this circuit the aperture coupling consists of a frequency dependent reactance and can be represented in the no loss condition by a reactance of jX . The short circuited line is a "lossy" line where we have normal wave attenuation in the forward propagation direction, but gain in the backward direction. This backward distributed gain is the spatial gain from the wave particle interaction in the Free Electron

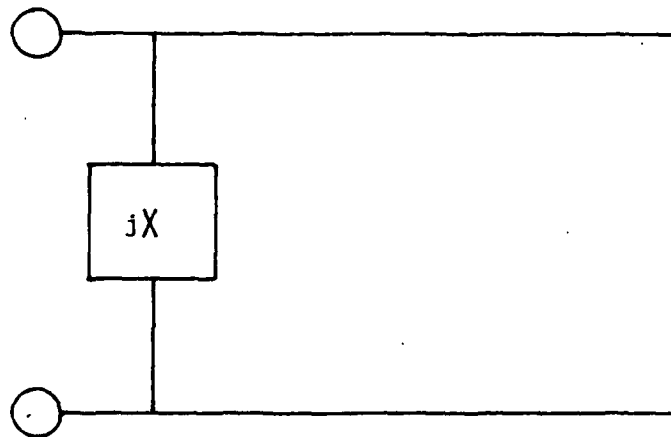


Fig. III-5, Free Electron Laser Microwave Amplifier Modeled as an Aperture Coupled Short Circuited Transmission Line

LASER discussed in Chapter 2. If the aperture coupled cavity itself is considered an element, Z_{in} , in another circuit, Fig. III-6; a reflection coefficient, ρ , as a function of frequency can be determined which relates gain per axial mode in the resonator structure. Z_{in} for this short circuit can be written from lossy line transmission line theory keeping the propagation constant in the forward direction (attenuation) separate from the propagation constant (gain) in the backward direction:

$$\frac{Z_{in}}{Z_c} = \frac{1 + e^{j(k_F + k_b)L}}{1 - e^{j(k_F + k_b)L}}; \quad k_{F,b} \equiv \alpha_{F,b} + j\beta_{F,b}$$

If the lossy line is considered in parallel with the aperture impedance (reactance) the Z_{in} for the entire cavity element is:

$$\bar{Z}_{in} = \frac{-\bar{X}_L \tan(\alpha L) e^{-(\beta_F + \beta_b)L}}{j\bar{X}_L + j \tan(\alpha L) e^{-(\beta_F + \beta_b)L}}$$

If the cavity is coupled to the external environment through a line of characteristic impedance Z_0 then the reflection

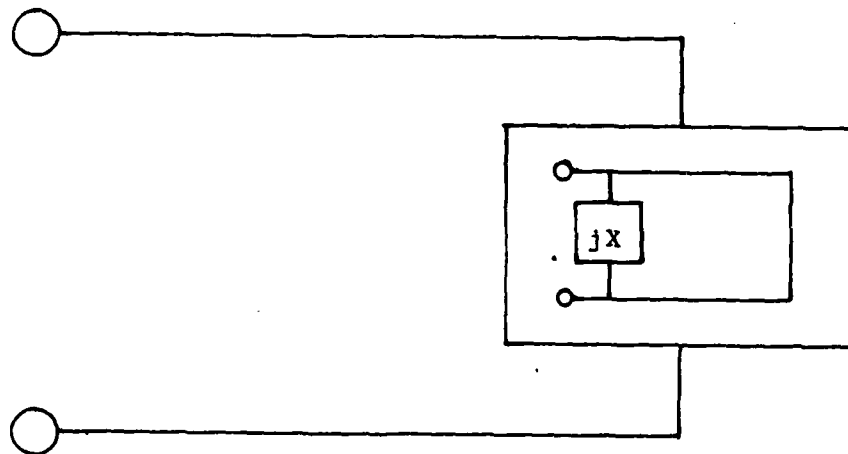


Fig. III-3, FEL Lumped Circuit Analysis

coefficient is a function of frequency and can be written:

$$\rho = \frac{\bar{Z}_{IN} - 1}{\bar{Z}_{IN} + 1} \quad [3]$$

The aperture impedance is determined by the geometry of the coupling circuit but can be considered to consist of a no loss series L-C circuit for simplicity.

The reflection coefficient in equation 3 is more easily determined and evaluated using radiation field quantities instead of transmission line analysis. Here, the reflection process can be modelled by a TN_{01} wave incident on a cylindrical slab of dielectric of length L. Applying the appropriate boundary conditions ρ for the cylinder can be expressed:

$$\rho = \frac{r_{12} + r_{23} e^{j(k_f + k_b)L}}{1 + r_{12} r_{23} e^{j(k_f + k_b)L}} \quad [4]$$

This cylindrical geometry for the reflection cavity was selected as it very closely resembles the Free Electron LASER geometry discussed in Chapter 2. r_{12} is the reflection coefficient from the first free space-dielectric

interface. r_{23} is the reflection coefficient from the dielectric-free space interface. Note that forward k is kept separate from backward k as in the transmission line model. Equation 4 can be simplified if r_{23} is set equal to one implying that we have total reflection from the end of the cylinder.

r_{12} , on the other hand, can be determined using the TM wave components and the boundary conditions for a wave incident on a slightly conducting medium. In the same manner the phase constants for both directions of propagation can be determined:

$$r_{12} = \frac{[\sqrt{\epsilon} - 1] + i \left[\frac{2\pi\sigma\epsilon'^{1/2}}{\epsilon\omega} \right]}{[\sqrt{\epsilon} + 1] + i \left[\frac{2\pi\sigma\epsilon'^{1/2}}{\epsilon\omega} \right]}$$

$$\alpha_{f,b} = \frac{\omega\sqrt{\epsilon}}{c} \left[1 + \frac{1}{2} \left(\frac{2\pi\sigma}{\omega\epsilon} \right)^2 \right]$$

Since the wave attenuates in the forward direction, the attenuation constant can be considered to be that due to a wave propagating in a normal dielectric medium:

$$\beta_f = \frac{2\pi\sigma}{c} \sqrt{1/\epsilon}$$

The expression for the power reflectivity can now be written in the form:

$$|R|^2 = \frac{E^2 + F^2}{G^2 + H^2}$$

$$\begin{aligned} \text{WHERE: } E &\equiv X + e^{-(\beta_F + \beta_b)L} \cos(2\alpha L) \\ F &\equiv Y + e^{-(\beta_F + \beta_b)L} \sin(2\alpha L) \\ G &\equiv 1 + X e^{-(\beta_F + \beta_b)L} \cos(2\alpha L) \\ &\quad - Y e^{-(\beta_F + \beta_b)L} \sin(2\alpha L) \\ H &\equiv X e^{-(\beta_F + \beta_b)L} \sin(2\alpha L) \\ &\quad + Y e^{-(\beta_F + \beta_b)L} \cos(2\alpha L) \end{aligned}$$

$$X \equiv \frac{AB + C^2}{B^2 + C^2} ; Y \equiv \frac{CB - AC}{B^2 + C^2}$$

$$A \equiv \sqrt{\epsilon} - 1 ; B \equiv \sqrt{\epsilon} + 1 ; C \equiv \frac{2\pi\sigma\sqrt{\epsilon}}{\epsilon\omega}$$

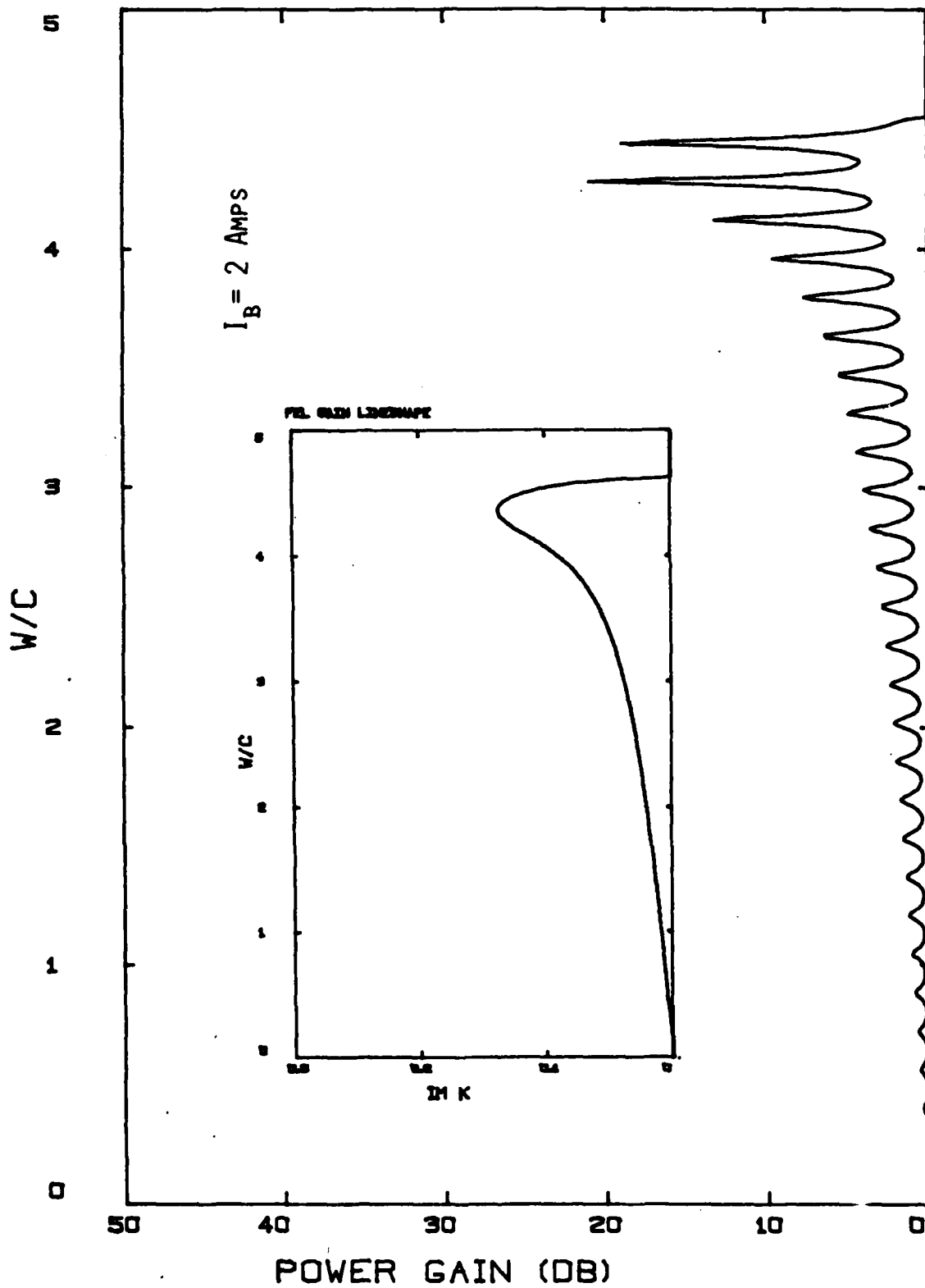
Since we intend to use the Free Electron LASER as the active medium in the reflection amplifier, the gain in the backward direction is the same gain envelope derived for the Free Electron LASER in Chapter 2. Recall from Chapter 2 that we analyzed the spatial spectral response of the Free Electron LASER. That same gain profile may be used to describe the gain in our cylindrical dielectric system above. A computer program was written which numerically computed the spatial gain, phase constants, and the attenuation constant; and then evaluated the reflection coefficient expression we

derived in equation 5.

By using the gain from the Free Electron LASER wave-particle interaction, we are able to operate the device in the region of finite and stable gain discussed in reference to Fig III-4. Because of the structure of the gain medium geometry as it relates to the reflection coefficient, we should see the reflection coefficient behave as a finite series of resonant responses each corresponding to a particular axial mode of the resonator. The amplitude of each resonance peak will be determined by the Free Electron LASER gain lineshape value for the particular resonance frequency. Since the Free Electron LASER gain bandwidth is finite and exhibits a cutoff immediately beyond synchronism, we should also see the amplifier, beyond synchronism, respond with a value for the reflection coefficient of less than unity. This will be manifested on the power gain curve by a zero value for the gain.

Figures III-7 and III-8 are two power gain curves where power gain is plotted as a function of w/c . An analysis of both figures show that the amplifier responds in the manner we predicted. The inset in each figure is the corresponding Free Electron LASER gain lineshape for the compatible frequency region. The Free Electron LASER system

REFLECTION AMPLIFIER POWER GAIN

Fig. III-7, Amplifier Gain as Function of w/c

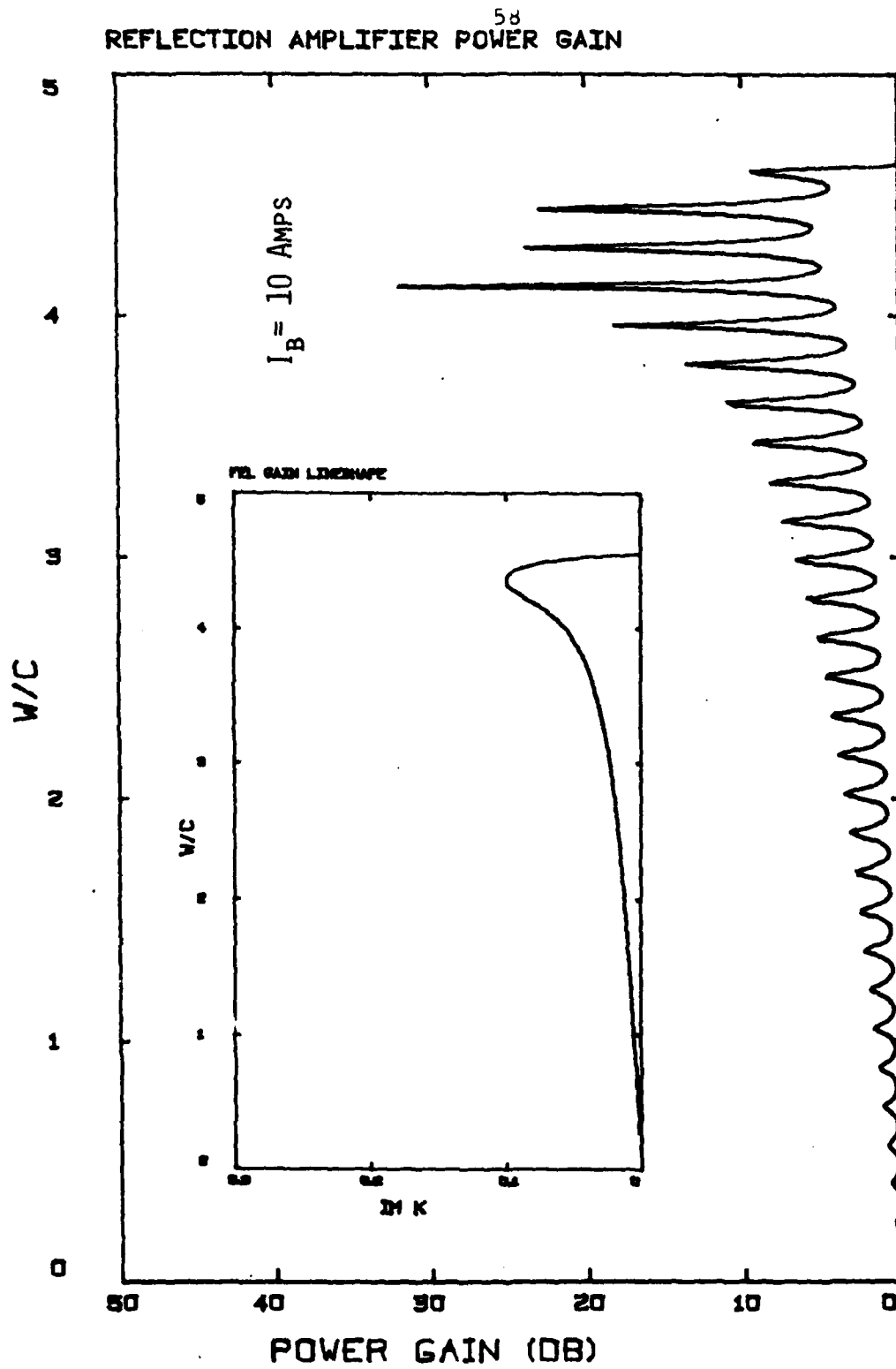


Fig. III-8, Amplifier Gain for Increased I_b

configuration for both plots is identical, with the exception of the beam current. We are driving a cylindrical quartz resonator of length 10cm and radius .4cm with a 2 Amp beam(Fig. 7) and a 10 Amp beam(Fig. 8) at a beam velocity of .7c. This Free Electron LASER geometry is consistent with a similar device which currently operates in the Dartmouth College Plasma Physics Laboratory.

Recall from our discussion in Chapter 2 that an increase in beam current results in an increase in the peak gain along the Free Electron LASER gain lineshape. In Fig. III-7 where we have the lower value for I_b we see a peak power gain from the amplifier of approximately 22dB. Comparing that to Fig III-8 where we have increased the value of I_b to 10 Amps, we see the amplifier peak gain respond with an increase of 11 db to 33dB. This response is what we predicted from the increase in gain from the gain medium.

The amplifier is also capable of responding, in kind, to changes in synchronous frequency. A comparison of the Free Electron LASER gain lineshape inset in Fig. III-9 to the similar inset in Fig. III-8 shows that synchronism occurs at a higher frequency for the system in Fig. III-9. This frequency shift resulted from a decrease in resonator radius, .4cm to .3cm. The power gain curve in Fig. II-9

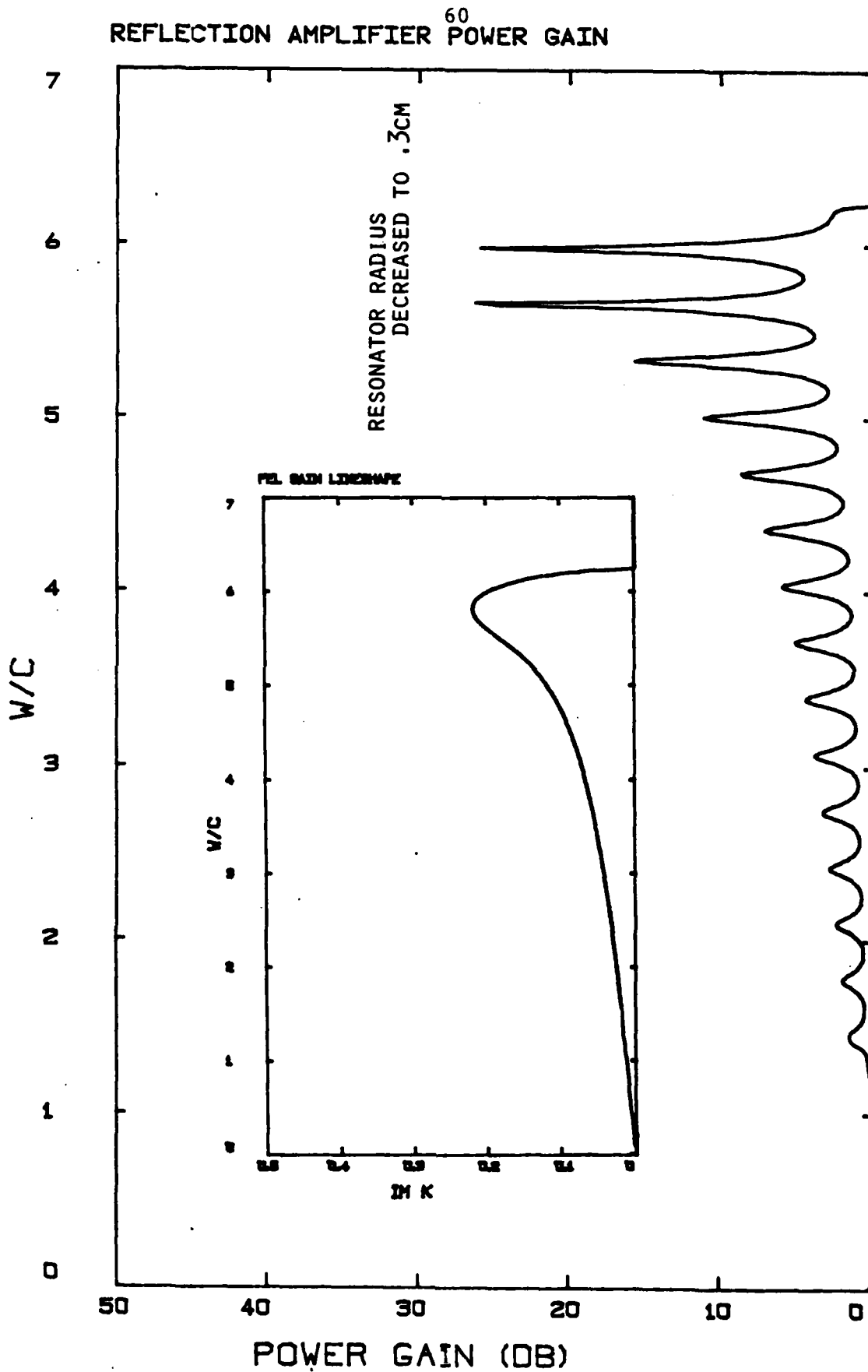


Fig. III-9, Amplifier Gain for Reduced Radius

shows that the amplifier peak gain also exhibits a corresponding shift in peak gain frequency. We can thus see that the amplifier geometry is completely compatible with the peak gain frequency flexibility exhibited by the gain medium. The device is capable of high frequency amplification.

Gain Bandwidth Product

This cavity amplifier is a multi-mode device that is capable of operating with an infinite number of axial modes. The amplifier gain profile clearly illustrates this property of the device. Referring to Fig. III-7 we can see a separate gain versus frequency curve for each axial mode of the amplifier. The axial mode gain curve we are most interested in is the peak gain response associated with the synchronous frequency.

The fixed gain-bandwidth product is characteristic of all singly resonant negative resistance amplifiers(8). Since, for the Free Electron MASER we are only interested in the performance of the device at the interaction frequencies, the peak gain axial mode lineshape we have isolated correlates to the singly resonant criterion. This

correspondence is valid providing the fractional difference between the interaction frequency and the operating frequency is very small.

We can rewrite Equation 2 in terms of two dimensionless quality factors: Q_e , and Q_m . Q_e corresponds to the external coupling network and Q_m to the active gain medium.

$$\rho \approx g_o = \frac{Q_m + Q_e}{Q_m - Q_e} \quad [6]$$

For our amplifier, Q_m is fixed by the nature of the beam driven system. Thus it becomes necessary only to vary Q_e in order to maintain control over the gain of the amplifier. The total Q for the system, Q_t , can be written as:

$$\frac{1}{Q_t} = \frac{1}{Q_e} + \frac{1}{Q_m} \quad [7]$$

Using equation 6 for the gain in terms of Q_e and Q_m ; and substituting in Equation 7 we can obtain:

$$Q_t = \frac{g_o}{2} Q_m \quad [8]$$

To relate Q_t to the half-width, recall Q_t can be defined as:

$$Q_t = \frac{f_o}{\Delta f}$$

Solving for and substituting our expression for Q_t , we arrive at the following:

$$(\Delta f) = \frac{1}{g_o} \left(\frac{2f_o}{Q_m} \right) \quad [9]$$

The right hand side of Equation is fixed by the beam driven medium and the operating frequency. This implies that as gain increases the bandwidth should decrease as $1/g_o$.

It is interesting to see that the Free Electron MASER behaves in the manner predicted by the fixed gain-bandwidth product. Several gain versus frequency curves are illustrated in Fig. III-10 and III-11. Recall that these lineshapes are the response curves for the isolated synchronous axial mode. Clearly for an increase in midband gain, the bandwidth narrows; and as the power decreases, the bandwidth widens. The computed gain-bandwidth product for a family of curves exhibits less than .5% variation and thus we see excellent agreement with the predicted fixed gain-bandwidth product response.

The preceding analysis indicates that high gain is possible from the amplifier by operating near the point of instability. The fixed product behavior shows that if we adjust the device for the highest gain possible we must

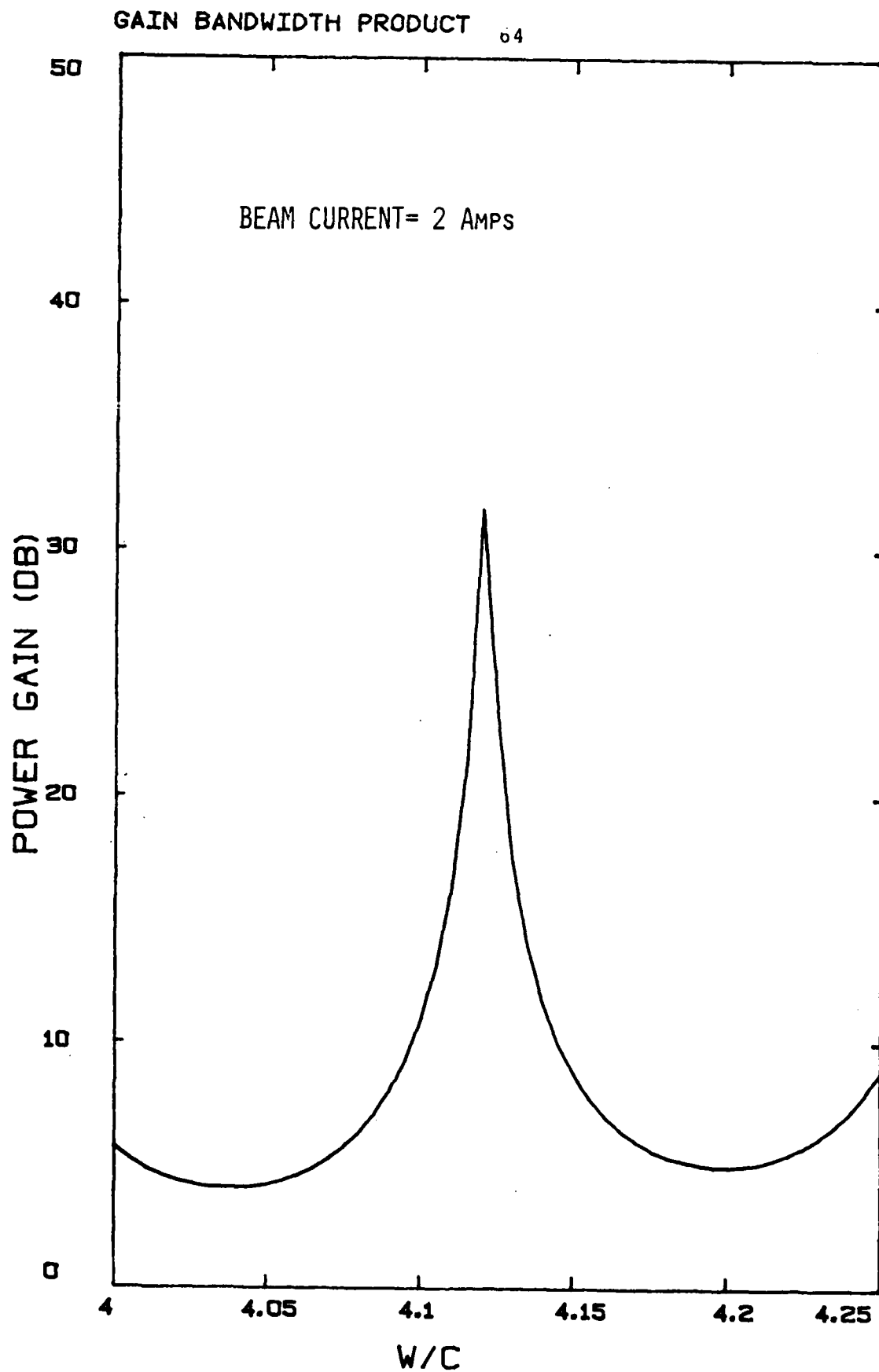


Fig. III-10, Isolated Peak Gain Axial Mode

148

GAIN BANDWIDTH PRODUCT 65

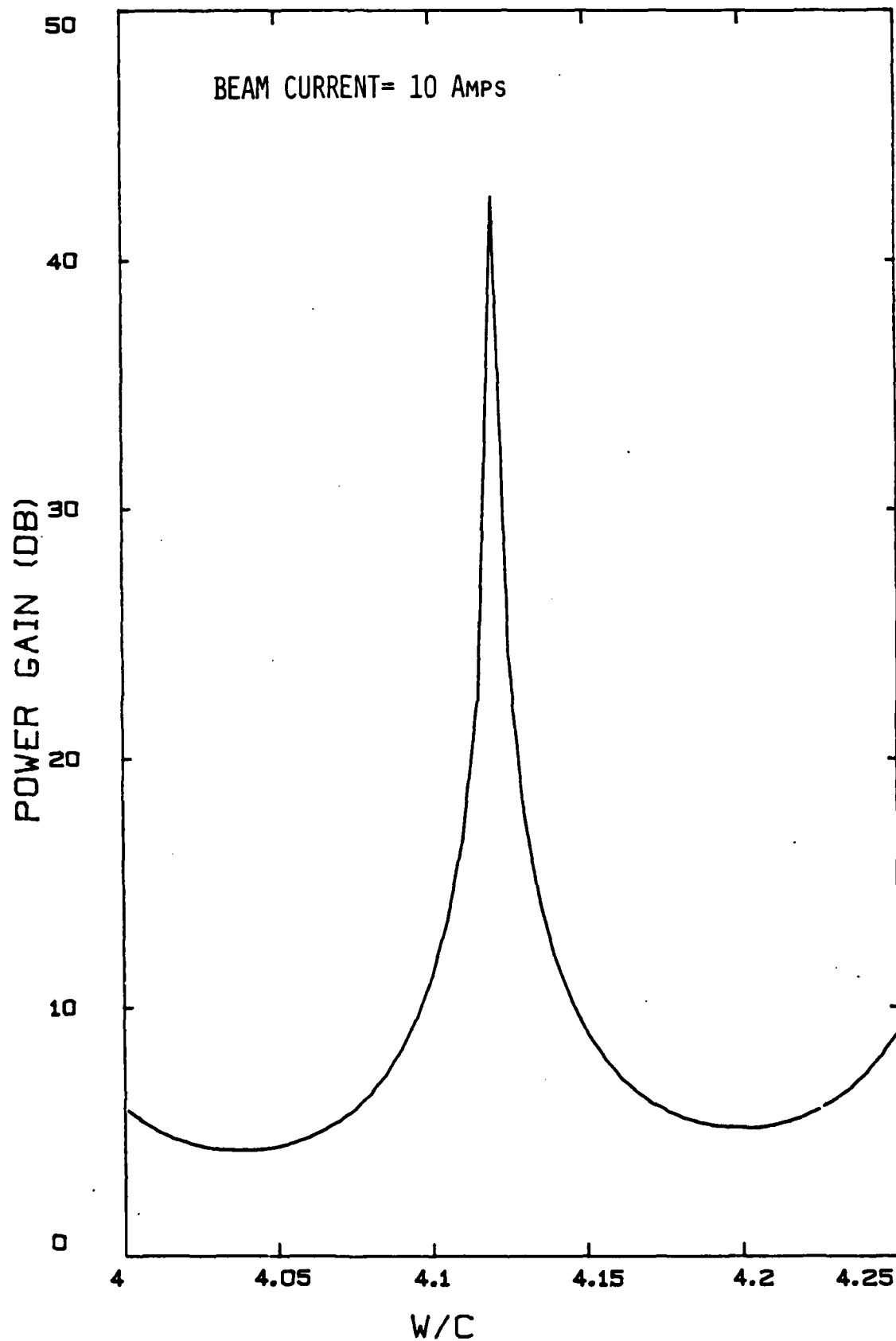


Fig. III-11, Isolated Peak Gain Axial Mode

149

suffer a tradeoff in the form of a reduced operational bandwidth. This forces us to optimize the design in terms of the ultimate use of the amplifier.

Artificial Q Variation

From Equation 8, we see that the gain is proportional to the total Q (recall that Q_m is fixed). If some means were available to increase Q_t then we expect to see an increase in the amplifier gain. A judicious management of Q_e will result in the desired increase of Q_t (reference Equation 7); but Q_e can not be increased without bound, for when $Q_e = Q_m$, the device passes into the region of instability, and the gain becomes infinite. For an excessive Q_e , the gain will assume a finite value, amplification will not occur, and oscillation will begin. Since Q_e is a function of the coupling network, variation of r_{12} will effect its value. In the foregoing analysis of the reflection amplifier, we have relied upon the flat dielectric face alone to give us the value for the coefficient, r_{12} , in Equation 4. If r_{12} is artificially varied (by changing the coupling characteristics), Q_t will vary in the same direction. These variations in the r_{12} value could possibly result from the partial silvering of the front dielectric plane, changing

the coupling aperture geometry, or through the utilization of a Fabry-Perot etalon to act as a variable reflectivity "mirror".

Fig. III-12 gives the amplifier gain response for a 2 Amp beam driven Free Electron LASER, where r_{12} is unaltered. We can make a comparison then with Fig. III-13, where r_{12} has been increased to a value 10% larger than that for Fig. III-12. The behavior of the altered r_{12} device is as predicted. We observe a peak gain increase of approximately 5dB.

UNCHANGED R12

63

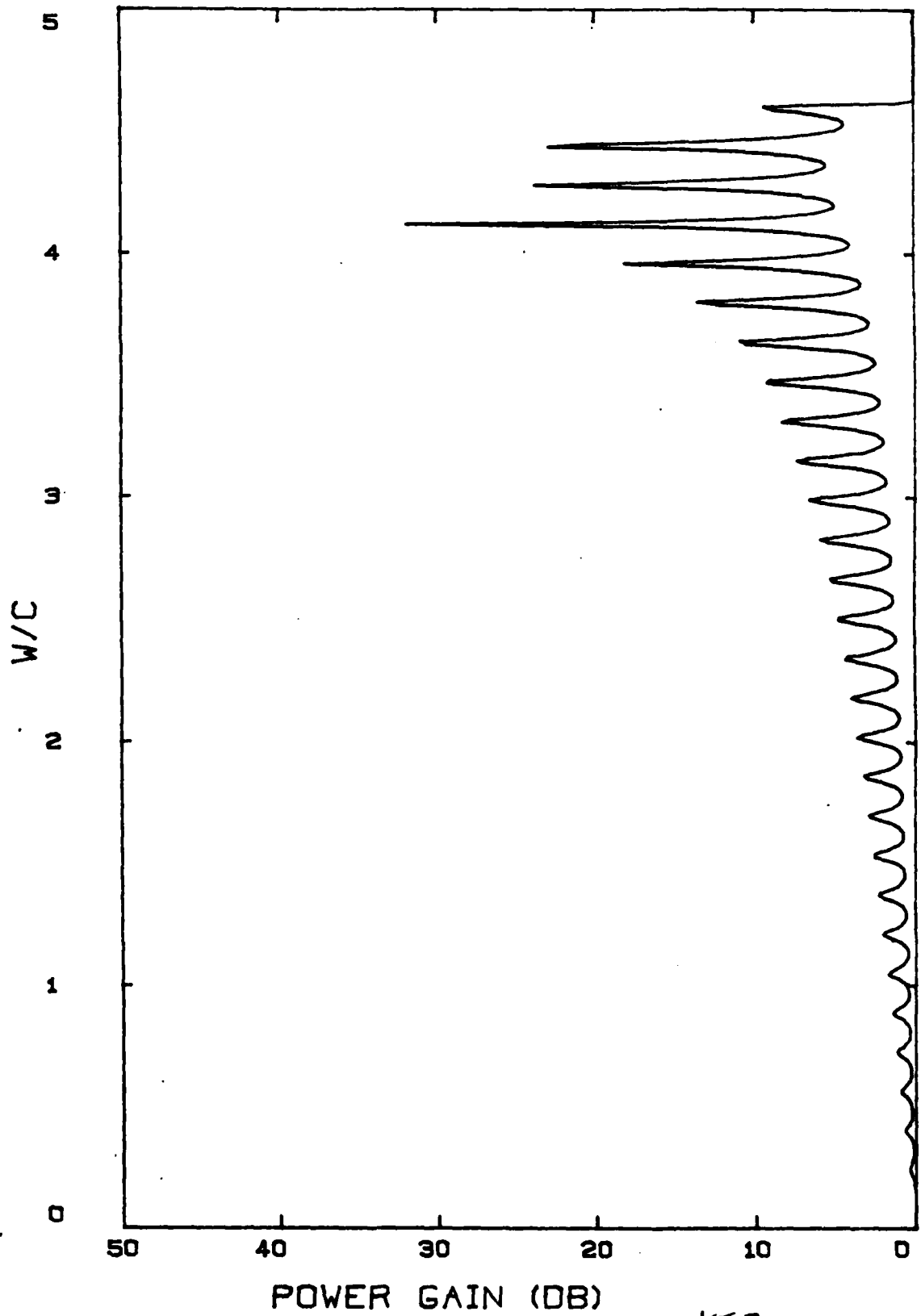


Fig. III-12, Gain Response for Normal r12

152

R12 INCREASED 10%

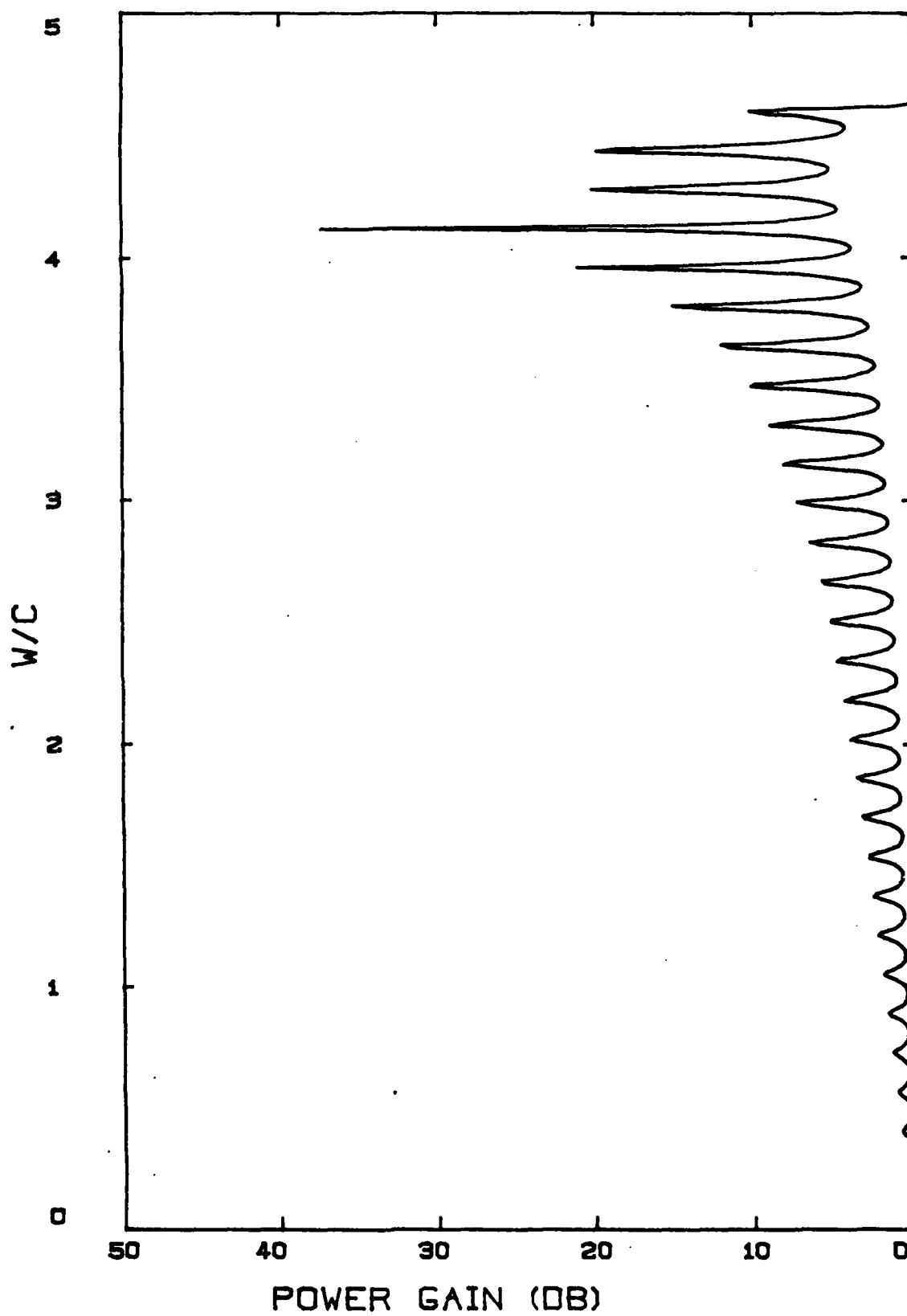


Fig. III-13, Gain Response for r12 Increased

153

CHAPTER 4

SUPERRADIANCE

Superradiance, in essence, is a transitional mode between the stimulated regime and the spontaneous regime. As such, it will allow us to derive an expression for the power emitted by the Free Electron LASER. In the optical MASER, the spontaneous emission rate or radiated power is linearly proportional to the population difference between the excited states and the ground state. The superradiant emission, however, is characterized by a proportionality where the power is a function of the square of the population difference. Qualitatively, the superradiant power is the power emitted from the LASER without the benefit of the multiple passage of the gain medium. It is observed in LASERS of high optical gain in the absence of a resonant cavity.(9).

In the LASER, the superradiant environment is generated when all the atoms in the medium contribute coherently to one dipole moment(10). The polarization can be shown to be proportional to the population inversion. If that polarization field oscillates in time, the power emitted is related to the product of the time derivative of the

polarization and the electric field. This electric field is not an applied field but the self field generated by the atoms themselves. If we relate the energy stored by the resonant enclosure to the power dissipated by the structure, the power radiated per unit volume can be expressed (Yariv):

$$P = \frac{\omega Q (N_b - N_A)^2 \nu^2 V_s^2}{\epsilon V_c}$$

This expression for the power per unit volume in the superradiant mode represents simple way for estimating power output of the device.

In a similar process, we should be able to generate an expression which provides a reliable estimate for the power out of the Free Electron LASER. The Free Electron LASER does not depend on the atomic process of population inversion, thus we will have to determine an appropriate analog. Recalling the geometry of Chapter 2, we can compute the power delivered to the radiant self field by taking the volume integral of beam current density dotted into the Electric field vector. Equating that quantity to the Q of the cylindrical cavity and the stored energy, we may solve for the electric field. If we then look at the power emitted by a resonant cavity, we can use the relation for the electric field previously derived, and with little effort

155

arrive at an expression for the power emitted by the Free Electron LASER in the superradiant mode.

Initially we want to determine the power supplied to the radiant field by the charged particles in the electron beam. We are working in the limit of an infinite external magnetic field so the motion of the electrons is restricted to the z-direction, only, so that $J = nev$. We again consider that only the TM modes in the waveguide satisfy the symmetry of the Cerenkov interaction in the axisymmetric resonator. Thus the field quantities have the form:

$$\begin{aligned} E_z &= E_r \hat{r} + E_z \hat{z} \\ B_z &= B_\phi \hat{\phi} \end{aligned}$$

By eliminating the explicit time dependence from the TM components using V and z , and keeping the z component of E , we can perform the integral of $J \cdot E$ and obtain:

$$S \int J \cdot E dv = J E_z \int_0^L \int_0^{P_0 r/a} \frac{e^{-j(\omega - kv)z/v}}{-j(\omega - kv)} \left| \frac{1}{v} \right| dz \quad [1]$$

$J = nev$
 $\eta = P_0 r/a$

For simplicity we define the result to be: χ . We can equate this expression for power to the power dissipated in a cavity of quality factor, Q .

Now considering on the left hand side all the field components and expressing B in terms of E_r and E_z , the left hand side becomes:

$$\frac{\omega \int \epsilon dv}{Q} = \frac{(E_z^0)^2 \omega}{4Q} \int_0^{R/a} \int_0^L \frac{a^2}{\rho_0^2} \eta \left\{ [J_0(\eta)]^2 + \frac{k^2}{[\frac{\omega^2 \epsilon}{c^2} - k^2]} [J_0'(\eta)]^2 \right\} d\eta dz \quad [2]$$

For convenience we define the integral on the right as ξ and equating to equation 1, we can solve for E_z^0 :

$$E_z^0 = \frac{J \xi Q}{\omega \chi} \quad [3]$$

The power radiated from a resonant structure can also be defined in terms of the Q and the stored energy:

$$P = \frac{\omega}{Q} \int \epsilon dv$$

Performing the integral of the energy density with E_z^0 and E_r as before, we obtain an expression for power in terms of (E_z^0) :

$$P = \frac{\omega}{Q} \frac{(E_z^0)^2 \chi}{4} \quad [4]$$

Using the result derived for E_z^2 in Equation 3, and substituting into Equation 4, we see that for the power emitted:

$$P = \frac{\omega}{4Q} \left(\frac{JSQ}{\omega\chi} \right)^2 \chi$$

$$= \left[\frac{Q|S|^2}{\omega\chi^4} \right] J^2$$

Re-expressing J in terms of beam current:

$$P = \left(\frac{Q|S|^2}{\omega\chi R^4 L^2 2\pi} \right) I_B^2 \propto I_B^2$$

As we can see, the power emitted is a function of the square of the beam current. Recalling the expression for the power from the atomic LASER as proportional to the square of the population inversion, we can infer that the Ib^2 term is analagous to the $(N_b - N_a)^2$.

CONCLUSION

we proposed in the introduction that the Free Electron LASER be used as the gain medium in a reflection microwave amplifier. The results obtained in this thesis support our proposal.

The Cerenkov Free Electron LASER has been modeled using a dielectric loaded waveguide with a relativistic electron beam propagating through the medium in the axial direction. A detailed gain analysis conducted for this geometry showed the Free Electron LASER gain to be capable of supporting amplification above oscillation. Parametric analysis of the gain response showed the performance of the amplifier to be related to beam dynamics and the resonator geometry. Our results indicate that useful amplifier characteristics should be available at frequencies in excess of 100GHz.

An expression was derived which showed that the superradiant power emitted for the Free Electron LASER is proportional to the square of the beam current. This is compared to the optical LASER superradiant output power which is proportional to the square of the population difference.

Continuation of research in this area is certainly possible. The solution of the annular cylinder geometry will be necessary for an accurate estimate of actual Free Electron LASER reflection amplifier performance.

APPENDIX 1

FORTRAN COMPUTER PROGRAM

```

100 *****
110 This program computes the value of the reflection coefficient
120 for an electromagnetic wave incident on an active dielectric
130 cylinder. The wave propagation in the forward direction is
140 determined by the relations for a wave travelling in a conducting
150 medium with the conductivity specified by the user. The wave
160 propagation in the backward direction is specified by a gain
170 in that direction and the phase constant from the original
180 conducting medium. The gain for the medium comes from
190 solving numerically the dispersion relation in Bagger
200 for the imaginary part of the propagation vector.
210 The forward direction is defined to be the direction the wave
220 is moving as it travels toward the origin of the electron beam.
230 The backward direction is defined to be in the sense of the
240 electrons in the electron beam.
250
260
270
280
290
300
310
320
330
340
350
360
370
375
380
390
400
410
420
430
440
450
*

```

This program computes the value of the reflection coefficient for an electromagnetic wave incident on an active dielectric cylinder. The wave propagation in the forward direction is determined by the relations for a wave travelling in a conducting medium with the conductivity specified by the user. The wave propagation in the backward direction is specified by a gain in that direction and the phase constant from the original conducting medium. The gain for the medium comes from solving numerically the dispersion relation in Bagger for the imaginary part of the propagation vector. The forward direction is defined to be the direction the wave is moving as it travels toward the origin of the electron beam. The backward direction is defined to be in the sense of the electrons in the electron beam.

```

*      Language:  FORTRAN
*
*      Written by D. H. Wise
*      *****
*
*      This call routine suppresses the underflow error messages
*      CALL UNDFL(j)
*
*      Opens the file for the storage of the reflection coefficient values
*      OPEN(1,"ZOFW1")
*      OPEN(2,"ZOFW2")
*
*      -----
*
*      Block of variable declarations
*      INTEGER N,NI
*      REAL EPS,DEN,X,Y
*

```

```

460 DIMENSION AR(5),AI(5),BR(5),BI(5),CR(5),CI(5)
470 REAL AR,AI,BR,BI,CR,CI
480 REAL A,Z,W,GAMMA,EPSILON
490 REAL P,SIGMA,LENGTH,IMK,ATTEN,PHASEC,C
500 REAL T1,U1,V1,X1,Y1,H,M
510 REAL J1,F1,G1,K1,P1,P2
520 REAL START,END,RADIUS,BETA,DELW
530 REAL B1,B2,B3,C1,C2,D1,D2,D3
540 INTEGER NDEG,IER
550
560
570
580
590

```

*

```

600 * Block of user supplied input data
610 PRINT, "INPUT CONDUCTIVITY"
620 INPUT, SIGMA
630 PRINT, "INPUT RESONATOR "
640 INPUT, LENGTH
650 PRINT, "RADIUS OF THE RESONATOR"
660 INPUT, RADIUS
670 PRINT, "VALUE FOR BEAM CURRENT"
680 PRINT, "ELECTRON VELOCITY"
690 INPUT, BETA
700 PRINT, "W FROM START TO END AND INTERVAL"
710 INPUT, START,END,DELW
720
730
740
750
760
770

```

*

```

780 * Computes initial constants for the program
790 NDEG=4
800 N=NDEG
810 N1=NDEG+1
820 EPS=1E-10
830 EPSILON=3.78
840 GAMMA=1.39
850
860
870
880
890
900
910
920
930
940
950
960
970
980
990

```

*

```

840      GAMMA=1.39
850      P=2.3/RADIUS
860      OMEGAP=3E-3
870      PI=3.141592
880      C=3E+10
890
900
910
920
930
940
950
960
970
980
990
1000
1010
1020
1030
1040
1050
1060
1070
1080
1090
1100
1110
1120
1130
1140
1150
1160
1170
1180
1190
1200
1210
1220
*
```

```

*      Assume a value for the roots of the interation process
*      X=0
*      Y=1
*
*      *****
*      This loop runs the entire program through the range of w/c
*      DO 88 W=START,END,DELW
*
*      This section of the program computes the values for the coefficients
*      of the quartic equation.
*
*      Coefficient of the 4th order term
*      AR(1)=- (BETA**2)/EPSILON
*
*      Coefficient of the 3rd order term
*      AR(2)=(2*W*BETA)/EPSILON
*      B1=(W**2)*(BETA**2)
*      B2=(W**2)/EPSILON
*      B3=(P**2)*(BETA**2)/EPSILON
*      B4=OMEGAP/((GAMMA**3)*(EPSILON**2))
*
*      Coefficient of the 2nd order term
*      AR(3)=B1-B2-B3+B4
*      C1=2*(W**3)*BETA
*      C2=((P**2)*2*W*BETA)/EPSILON
*
*      Coefficient of the linera term
*      AR(4)=-C1+C2
*
```

165

```

1220 AR(4)=-C1+C2
1230
1240 *      Computes the constant term
1250 D1=W**4
1260 D2=((W**2)*(P**2))/EPSILON
1270 D3=(W**2)*OMEGAP/((GAMMA**3)*(EPSILON))
1280
1290 AR(5)=D1-D2-D3
1300
1310
1320 -----
1330 *      Defines the values of any imaginary coefficients
1340 *
1350 AI(1)=0
1360 AI(2)=0
1370 AI(3)=0
1380 AI(4)=0
1390 AI(5)=0
1400
1410
1420 -----
1430 *      Newton-Raphson iteration process
1440 *
1450 BR(1)=AR(1)
1460 BI(1)=AI(1)
1470 CR(1)=AR(1)
1480 CI(1)=AI(1)
1490
1500 DO 100 I=2,N1
1510   BR(I)=AR(I)+BR(I-1)*X-BI(I-1)*Y
1520   BI(I)=AI(I)+BR(I-1)*Y+BI(I-1)*X
1530   CONTINUE
1540 DO 200 I=2,N
1550   CR(I)=BR(I)+CR(I-1)*X-CI(I-1)*Y
1560   CI(I)=BI(I)+CR(I-1)*Y+CI(I-1)*X
1570   CONTINUE
1580 DEN=CR(N)**2+CI(N)**2
1590 *

```

```

1580 DEN=CK(N)**2+CI(N)**2
1590 X=X-(BR(N1)*CR(N)+BI(N1)*CI(N))/DEN
1600 Y=Y+(BR(N1)*CI(N)-BI(N1)*CR(N))/DEN
1610
1620 IF ((BR(N1)**2+BI(N1)**2).GT.EPS) GO TO 10
1630
1640 *      Need to use the other root of the complex-conjugate pair
1645 WRITE(UNIT=2,FMT=800)W,Y
1646 800 FORMAT(1E16.8,"",1E16.8)
1650 IMK=-Y
1660
1670 *****
1680 *      Computes the attenuation constant for the forward direction
1690 *      and the phase constants for both directions
1700 *
1710 ATEN=(2*PI*SIGMA)/(C*(EPSILON**.5))
1720 PHASEC=(W*(EPSILON**.5))*(1+.5*((2*PI*SIGMA)/(C*EPSILON))**.2))
1730
1740 *      Computation of the reflection coefficient
1750
1760 *      The alphanumeric variables have no physical significance
1770 *      except for P1 and are used only to simplify the manipulations
1780 *      of the complex quantities.
1790
1800 T1=(EPSILON**.5)-1
1810 U1=(EPSILON**.5)+1
1820 V1=(2*PI*SIGMA*(EPSILON**.5))/(C*EPSILON*W)
1830
1840 X1=(T1*U1+V1**2)/(U1**2+V1**2)
1850 Y1=(V1*U1-T1*V1)/(U1**2+V1**2)
1860
1870 H=-LENGTH*(ATTEN+IMK)
1880 M=2*PHASEC*LENGTH
1890
1900 J1=X1+EXP(H)*COS(M)
1910 F1=Y1+EXP(H)*SIN(M)
1920 G1=1+X1*EXP(H)*COS(M)-Y1*EXP(H)*SIN(M)
1930 K1=X1*EXP(H)*SIN(M)+Y1*EXP(H)*COS(M)
1940 *

```

1940
1950
1960
1970
1980
1990
2000
2010
2020
2030
2040
2050
2060
2070
2080
2090
*

P1=(J1**2+F1**2)/(G1**2+K1**2)
P2=10*LOG10(P1)

*
WRITE(UNIT=1,FMT=900)W,P2
900 FORMAT(1E16.8,"",1E16.8)

88 CONTINUE

* *****

END

*

APPENDIX 2

FREQUENCY DEPENDENCE OF PEAK GAIN

In order to see how the peak gain behaves as a function of ω it is necessary to begin with the dispersion relation, equation 7, Chapter 2:

$$(\omega^2 - \omega_{0k}^2) - \frac{\omega_b^2 \left(\omega^2 - \frac{c^2 k^2}{\epsilon} \right)}{\epsilon \gamma^3 (\omega - kv_0)^2} = 0$$

The synchronous point becomes of interest because that is where the strongest wave-particle interaction occurs:

$$\omega \approx kv_0$$

If we look near the point $\omega = kv_0$, then we can expand the $\omega^2 - \omega_{0k}^2$ term to be:

$$(\omega + \omega_{0k})(\omega - \omega_{0k})$$

The dispersion relation can be rewritten using this expansion as:

$$(\omega + \omega_{0k})(\omega - \omega_{0k}) - \frac{\omega_b^2 \left(\omega^2 - \frac{c^2 k^2}{\epsilon} \right)}{\epsilon \gamma^3 (\omega - kv_0)^2} = 0$$

Working near synchronism we can use the approximation:

$$\omega - \omega_{0k} \approx \delta$$

which implies:

$$\omega + \omega_{0k} \approx 2\omega_k = kV_0$$

The substitution of these approximations for the expanded product term results in an approximate cubic form of the dispersion relation:

$$\frac{(\omega - \omega_k) 2\omega_k - \omega_b^2 \left(\omega^2 - \frac{c^2 k^2}{\epsilon} \right)}{\epsilon \gamma^3 (\omega - kV_0)^2} = 0$$

The roots may be solved for with the spatial gain=:

$$\beta_b \approx \frac{\sqrt{3}}{2ck} \left(\frac{\omega_b^2 \omega_k}{2\epsilon \gamma^3} \right)^{1/3} \left(1 - \frac{1}{\beta^2 \epsilon} \right)^{1/6}$$

This expression for the peak gain as a function of ω_{0k} shows a one third power dependence on the frequency.

REFERENCES

1. K. Busby, Ph.D Thesis, Dartmouth College
2. K. Felch, Ph.D Thesis, Dartmouth College
3. V. Ginzburg, Dok. Akad.Nauk SSSR, 56, 583 (1947)
4. Felch, op. cit.
5. J. Walsh, Physics of Quantum Electronics, Vol 5, 1978
6. J. Bagger, Honors Thesis, Department of Physics
Dartmouth College
7. J. Walsh, op. cit.
8. A. Siegman, Introduction to LASERS and MASERS,
Chapter 5, 1971
9. A. Yariv, Quantum Electronics, Chapter 15 (1975)
10. A. Yariv, op. cit.

THE CERENKOV-CYCLOTRON INSTABILITY

John E. Golub

June, 1981

Senior Honors Thesis
Dartmouth College,
Hanover, N.H. 03755

172

1/2

TABLE OF CONTENTS

Page:

Abstract	
Acknowledgments	
Contents	
Figures	
Chapter One	
I.1 Introduction	7
I.2 Posing the Problem	11
Chapter Two	
II.1 Cerenkov Theory	16
Chapter Three	
III.1 The Dispersion Function	26
III.2 Derivation of the Conductivity Tensor	29
III.3 Construction of the Dispersion Relation	37
III.4 Limit of Strong Magnetization	39
III.5 Limit of Weak Magnetization	42
III.6 Discussion	43
Chapter Four	
IV.1 Forward Propagation	52
IV.2 Analysis of the Dispersion Relations	56
IV.3 Solution of the Dispersion Relation	63
Chapter Five	
V.1 Solution of the General Dispersion Relation	70
V.2 Threshold	72

V.3 Validity of the Weak Beam Approximation	73
V.4 Analysis	74
Chapter Six	
VI.1 A Cerenkov-Cyclotron Free Electron Laser	80
Chapter Seven	
VII.1 Summary	89
VII.2 The Transition Wavelength	91
VII.3 Conclusions	94
References	96

✓

TABLE OF FIGURES

Figure I-1	Cerenkov radiation
Figure I-2	Electron beam normal modes
Figure II-1	Filled waveguide geometry
Figure III-1	The Model
Figure III-2	Synchronism with the slow cyclotron wave
Figure III-3	The unperturbed roots
Figure III-4	The perturbed roots
Figure IV-1	Root locus plot of the fast cyclotron mode; case 1
Figure IV-2	Root locus plot of the fast cyclotron mode; case 2
Figure IV-3	Root locus plot of the slow cyclotron mode; case 1
Figure IV-4	Root locus plot of the slow cyclotron mode; case 2
Figure IV-5	Gain vs. beam energy (forward propagation)
Figure IV-6	Gain vs. frequency (forward propagation)
Figure V-1	Gain vs. beam energy (general propagation)
Figure V-2	Gain vs. frequency (general propagation)
Figure V-3	Gain vs. applied magnetic field
Figure VI-1	Schematic of a Cerenkov-cyclotron free electron laser
Figure VI-2	Field strength vs. distance
Figure VI-3	Reciprocal Q vs. reciprocal beam energy
Figure VII-1	Distribution functions for cold and warm beams

ABSTRACT

We consider the excitation of an electromagnetic wave by a relativistic electron beam in the infinite medium. In the collective regime, instability can occur by coupling to either of the beam negative energy modes. The slow space charge interaction has been called the Cerenkov instability and detailed elsewhere. An investigation of the slow cyclotron interaction is presented here. The effect has been called the Cerenkov-cyclotron instability. It is a high frequency, high gain effect which has promise as a source of submillimeter radiation.

5 175

- ✓

ACKNOWLEDGEMENTS

It is a pleasure to acknowledge the support and guidance of professor John Walsh. Professor Walsh's insight and patience on so many occasions have made this work possible.

In addition, I thank Robert Layman, Scott Von Laven, Douglas Wise, David Speer, and John Branscum for many useful and enlightening discussions. Professors Agnar Pytte and Christine Celata are to be thanked for their support and encouragement. Also, I am grateful to Catherine LaTouche and to Teresa Dobbins for unending technical assistance.

Finally, I am indebted to the entire Dartmouth physics department for its support and enthusiasm over four years.

The work was supported in part by the Army Research Office, the Office of Naval Research, and the Air Force Office of Scientific Research.

Chapter One

I.1 Introduction

The advent of relativistic electron beam technology has renewed hopes for a powerful radiation source in the quasi-optical region of the electromagnetic spectrum. A number of devices currently employ such beams in an effort to reach high frequency, high power operation. Relativistic magnetrons and gyrotrons are examples.

Another such device is the free electron laser. Broadly, a free electron laser extracts kinetic energy from an electron beam and uses it to amplify a radiation field. In one version of this device, superluminal electrons stimulate Cerenkov radiation in a resonant cavity. Successive electrons do work on the laser field and give up energy to it. At only moderate beam energies, such radiation can fall into the millimeter and submillimeter regime. This device has been called the Cerenkov-type free electron laser.

Recall that Cerenkov radiation is produced when a charged particle moves through or near a dielectric medium with velocity

greater than the speed of light in the medium. The particle creates a "shock front" of electromagnetic waves. The angle at which the radiation propagates relative to the particle motion depends on the speed of the particle as well as the dielectric constant of the medium according to

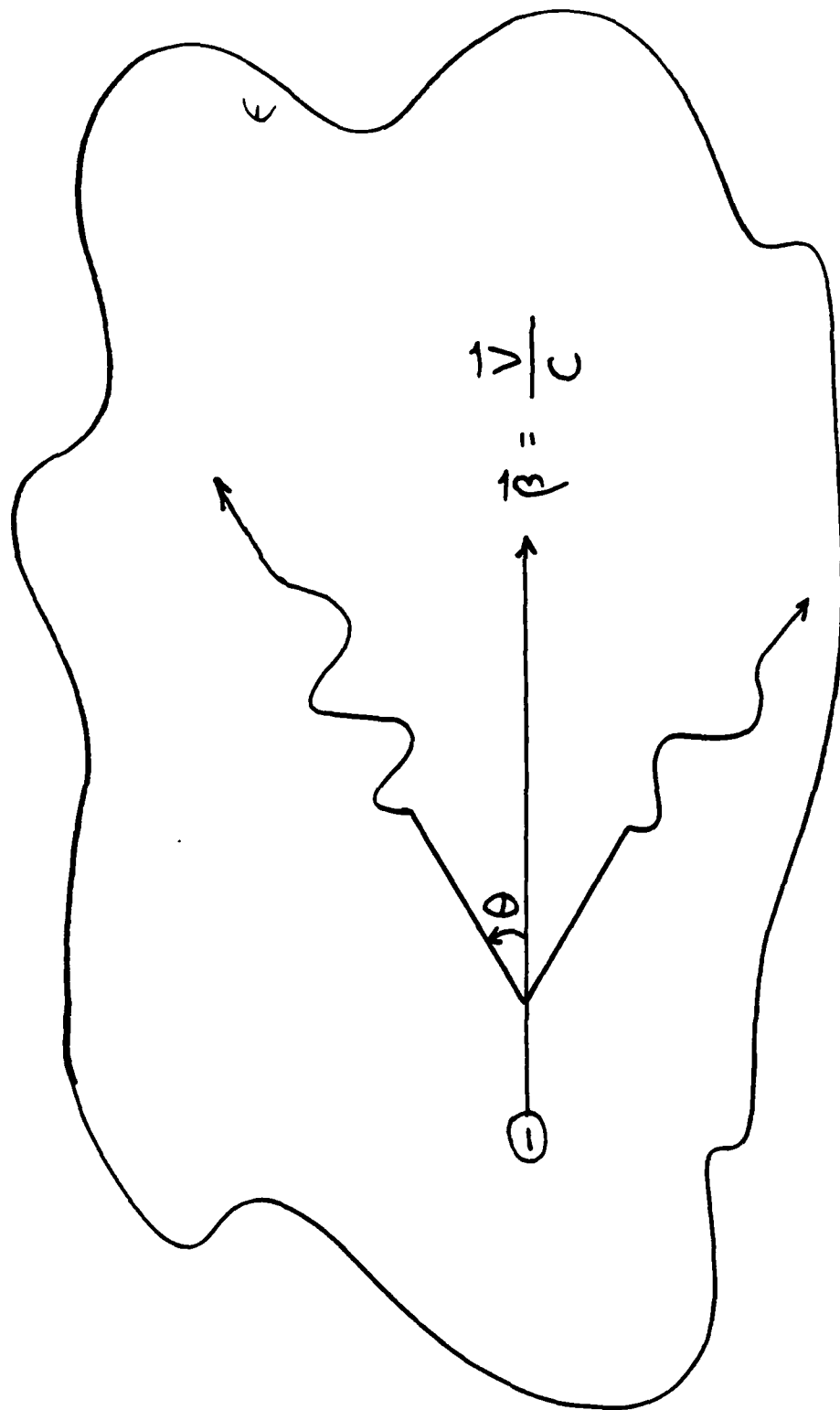
$$\cos \theta = \frac{1}{\beta \sqrt{\epsilon}}$$

The phenomenon is illustrated schematically in figure I-1.

Cerenkov type free electron lasers have several attractive features. First, they require only modest beam energies. Beams of five hundred KeV or less provide power levels and frequencies of interest. A Cerenkov type free electron laser can, therefore, be a relatively compact device.

Another nice feature of the concept relates directly to the wavelength of operation. In conventional travelling wave tubes, the interaction wavelength is related to some characteristic length of the system¹. High frequency operation of these devices is limited by the machinist's ability to accurately produce components whose dimensions may be less than one millimeter. This is not true of the free electron laser. The latter has already produced wavelengths smaller than the transverse dimension of the system².

Applications of a high power, high frequency radiation source are manifold. Fusion physics, spectroscopy, and communications provide examples of fields which would benefit.



$$\cos \theta = \frac{1}{\beta n}$$

Figure I-1 Cerenkov Radiation

The need for submillimeter waves in the fusion effort is particularly worthy of attention. A sketch of the primary fusion applications will also give information about the properties a useful source would have³.

Electron cyclotron resonance heating (ECRH) is the best known example. As a plasma is heated, resistivity falls and, so, limits joule heating. Attaining fusion parameters will require a heating scheme which is not self-limiting. While ECRH at the fundamental can be shielded in dense plasmas, heating at the second harmonic improves with increased temperature and density. In typical fusion devices where toroidal fields are in the range of tens of kilogauss, this implies the need for a source of high frequency waves. Frequencies in the tens of gigahertz will be necessary. In addition, power levels in excess of a megawatt may be required.

ECRH can be used to preferentially heat portions of the plasma. This is accomplished by tuning the rf to coincide with the local cyclotron frequency (or its harmonic). This permits preferential heating of the dense center of the plasma. Alternatively, it enables the experimenter to shape the current profile for improved stability. A radiation source for ECRH must be easily tunable.

I.2 Posing the Problem

A relativistic electron beam, propagated along a constant magnetic field, has four normal modes. Two of these are longitudinal oscillations and do not depend on the presence of an external field. These are the negative energy (or slow) and positive energy (or fast) space charge waves.

The terms "fast" and "slow" are easily understood. The phase velocity of the positive energy wave is greater than the electron beam velocity.

$$\left(\frac{\omega}{K}\right)_{\text{fast}} > V_0$$

We call this wave fast.

The phase velocity of the negative energy wave is less than the electron beam velocity.

$$\left(\frac{\omega}{K}\right)_{\text{slow}} < V_0$$

We call this wave slow.

The two remaining normal modes are transverse in character and do depend on the applied magnetic field. These are the negative energy (or slow) and positive energy (or fast) cyclotron waves. A plot of the dispersion relations is shown in figure I-2.

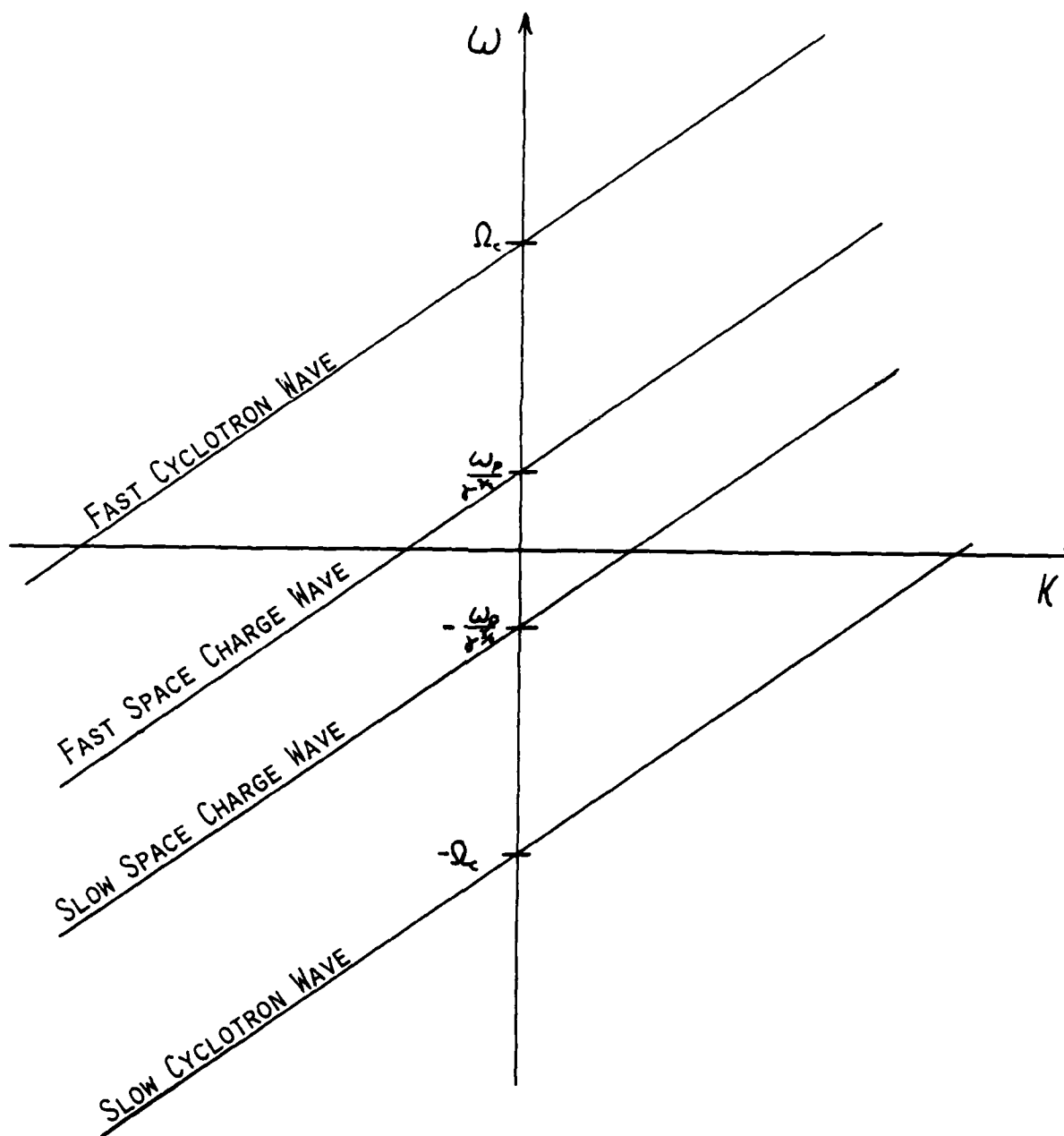


Figure I-2 Electron Beam Normal Modes

✓

As in the case of the beam space charge waves, we understand the terms "fast" and "slow" in terms of the phase velocities:

$$\left(\frac{\omega}{K}\right)_{\substack{\text{fast} \\ \text{slow}}} \gtrsim V_0$$

For propagation in the vacuum, all four waves are stable. If the magnetized electron beam is propagated through a dielectric medium, however, a negative energy wave can become unstable. Extensive theory has been developed to describe the exponential growth of the slow space charge wave⁴. Such growth occurs only for beam velocities greater than the speed of light in the dielectric medium and has therefore been called the Cerenkov instability.

Until now, the theory of the Cerenkov interaction has been limited. Only strongly magnetized beams and unmagnetized beams have been considered. In these limits, the electromagnetic wave couples to the slow cyclotron wave on the electron beam.

In the present work, we treat the general problem of finite magnetization. In this regime, the wave can couple to the slow cyclotron mode. Growth depends closely on the gyromotion of the electrons and has therefore been called the Cerenkov-cyclotron instability⁵.

In chapter two of this thesis, we will review the theory of the Cerenkov instability. This discussion serves three purposes. First, it broadly demonstrates the general method. Second, it

✓

introduces the important concept of "synchronism." Finally, it provides a background against which new results may be viewed.

In chapter three, we model the general problem. We use a linearized, cold fluid analysis to treat an electromagnetic wave propagating at an arbitrary angle through a magnetized electron beam in the infinite medium. The dispersion relation is derived. This, in turn, is manipulated to give a fairly compact algebraic relation. No approximation is made during this manipulation.

We go on to show that the Cerenkov dispersion relations for strong and weak magnetization are recoverable in the appropriate limits. This, together with a qualitative examination of the dispersion relation, supports the claim that we have correctly treated the general problem.

✓ In chapter four, we consider the case of a forward propagating electromagnetic wave. The dispersion relation is easily obtained as a limit of the general expression. The technique of root locus plotting is introduced and used to analyze the stability of the system. The dispersion relation is then solved in the neighborhood of the slow cyclotron solution to give expressions for the growth rate of the wave and the threshold of instability. These are, in turn, analyzed graphically.

In chapter five, we solve the general dispersion relation near the slow cyclotron root with the aid of a "weak beam"

✓

approximation. This approximation is evaluated and seen to be excellent. Expressions for the gain and threshold of the system are derived and discussed. The gain is found to be much greater than the chapter four results and comparable to the gain for the Cerenkov interaction on a strongly magnetized beam.

In chapter six, we give a brief discussion of the feasibility of a Cerenkov-cyclotron free electron laser. The coupling problem is discussed and the reciprocal quality of the system is introduced to account for frequency dependent losses in the laser cavity. This Q is compared to the figure dictated by theory.

Finally, we conclude in chapter seven. A summary of the work is presented and its most important approximation, beam coldness, evaluated.

✓

Chapter Two

II.1 Cerenkov Theory

Let us review the theory of the Cerenkov instability⁶. We will consider an electron beam propagating through a circular waveguide. The waveguide is filled with a homogeneous, isotropic dielectric of dielectric constant epsilon. The applied magnetic field is along the axis of the waveguide and is strong enough to confine the electrons to motion along this axis. This "infinite B₀" assumption is necessary in order to restrict ourselves to the study of longitudinal beam oscillations-- the space charge wave. Instability in the finite B₀ regime is the main focus of this thesis and will be discussed in detail in a later chapter. The geometry is shown in figure II-1.

Electric and magnetic fields in the dielectric satisfy Maxwell's equations in the absence of sources.

$$\nabla \times \mathbf{E} = -\frac{1}{c} \frac{\partial \mathbf{B}}{\partial t}$$

$$\nabla \times \mathbf{B} = \frac{1}{c} \frac{\partial \mathbf{D}}{\partial t}$$

An electromagnetic wave is introduced as a perturbation to the system. The resulting perturbed current density is used as a

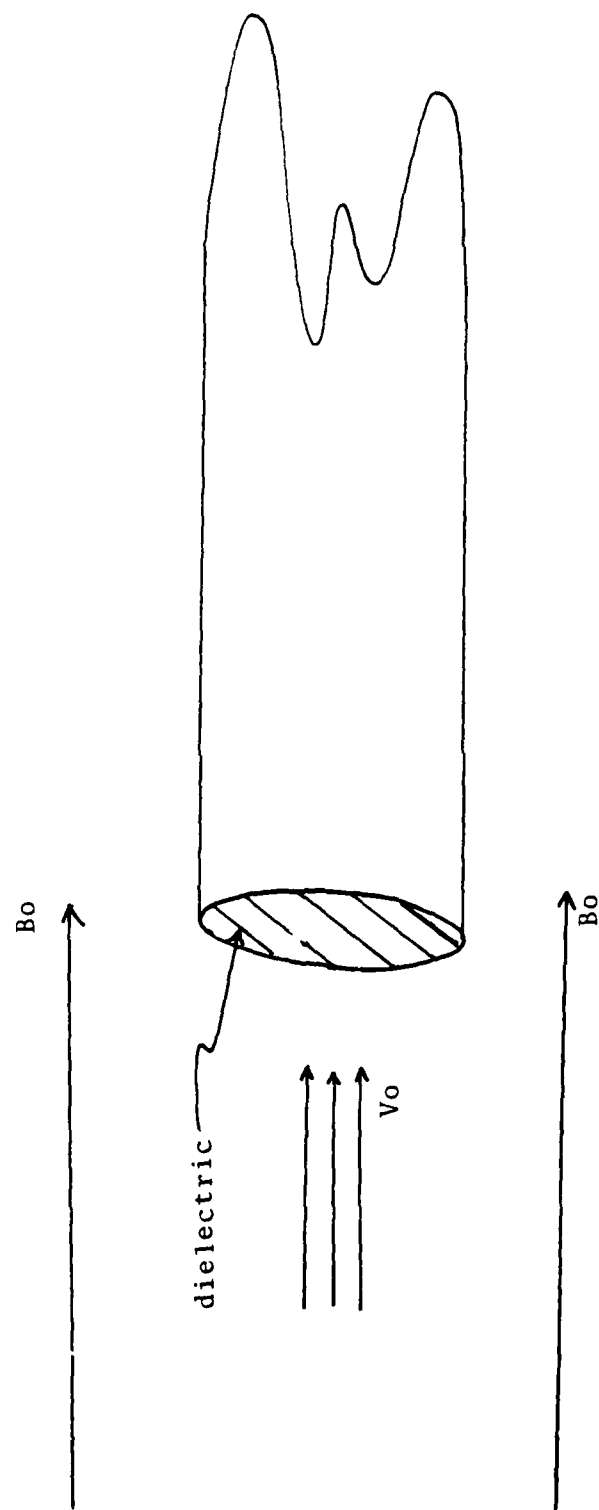


Figure II-1 Filled Waveguide Geometry

source term in Maxwell's equations to give

$$\nabla \times \nabla \times \underline{E} = -\frac{4\pi}{c^2} \frac{\partial \underline{J}}{\partial t} - \frac{1}{c^2} \frac{\partial^2 \underline{D}}{\partial t^2}$$

Next, we can split the $\nabla \times \nabla \times$ operator into transverse and parallel components. In the limit of infinite magnetic field, \underline{J} has no transverse component and the resulting (transverse) wave equation is homogeneous.

$$\left(\left[\nabla \cdot \nabla - \nabla^2 + \frac{\epsilon}{c^2} \frac{\partial^2}{\partial t^2} \right] \underline{E} \right)_{\perp} = 0$$

Assuming plane wave solutions of the form

$$\underline{E} \sim e^{i(\underline{k} \cdot \underline{r} - \omega t)}$$

we can rewrite the perpendicular wave equation

$$\left[\nabla_{\perp}^2 + \left(\frac{\omega^2 \epsilon}{c^2} - k^2 \right) \right] \underline{E}_{\perp} = 0$$

Next, we assume that the electric field vector is an eigenfunction of the ∇_{\perp}^2 operator. Then

$$\nabla_{\perp}^2 \underline{E}_{\perp} = -p^2 \underline{E}_{\perp}$$

where p , the transverse wave number, is dictated by the transverse boundary value problem. In our cylindrical geometry, the eigenfunction expansion is in terms of Bessel functions and so

$$p = \frac{x_{01}}{a}$$

where "x₀₁" is the 1-th root of the zero-th order Bessel function and "a" is the waveguide radius.

AD-A126 990

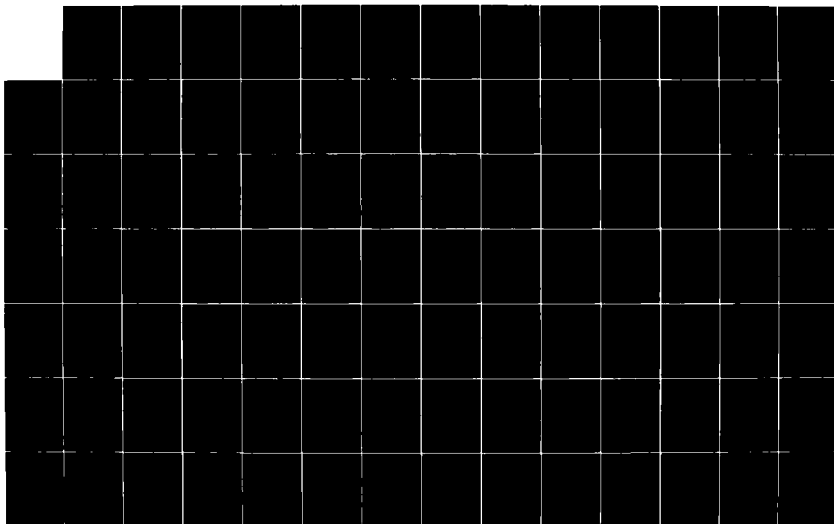
LARGE AMPLITUDE ION WAVES(U) DARTMOUTH COLL HANOVER N H
DEPT OF PHYSICS AND ASTRONOMY J E WALSH 19 NOV 82
AFOSR-TR-83-0266 AFOSR-77-3410

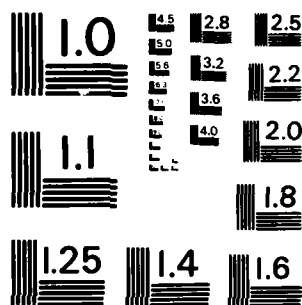
3/4

UNCLASSIFIED

F/G 20/7

NL





MICROCOPY RESOLUTION TEST CHART
NATIONAL BUREAU OF STANDARDS-1963-A

✓

Substituting into our transverse wave equation, we obtain

$$\left[-P^2 + \frac{\omega^2 \epsilon}{c^2} - k^2 \right] E_{\perp} = 0$$

Choosing the non trivial solution ($E \neq 0$), we arrive at the free wave dispersion relation.

This is a relation between ω and k governing the propagation of an electromagnetic wave through a dielectric-loaded waveguide. A plot is shown in figure II-2.

At this point it is instructive to plot the free wave dispersion relation and the slow space charge dispersion relation on the same axes. For beam velocities exceeding the speed of light in the dielectric, these curves will cross. At the point of intersection, the electron beam is moving with velocity equal to the phase velocity of the free wave. We call this intersection "synchronism." The electron beam is said to be synchronous with the electromagnetic wave.

The coupling between the electron beam and the electromagnetic wave is strongest at synchronism. We can use this fact to determine the direction of propagation for strongest coupling. We invoke the two synchronism conditions:

$$\omega \approx k V_0$$

$$\omega \approx c \sqrt{\frac{k^2 + P^2}{\epsilon}}$$

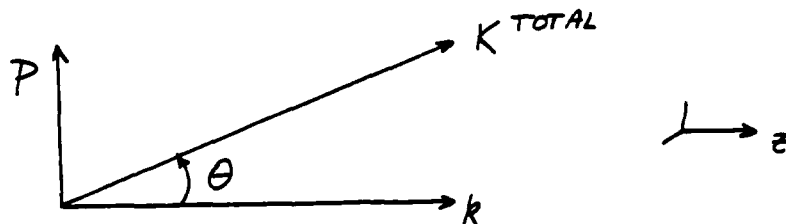
Solving simultaneously, we find

$$\beta^2 \epsilon = 1 + \frac{P^2}{k^2}$$

19

I-a

where $\beta = \frac{v}{c}$ is the beam velocity in units of the vacuum speed of light. Resolving the effective propagation vector into parallel and perpendicular components k and p ,



we can define the angle theta by

$$\tan \theta = \frac{p}{k}$$

Theta is, then, the angle formed by the propagation vector of the electromagnetic wave and the z-axis.

Substituting this expression into 1-a we find,

$$\beta^2 \epsilon = 1 + \tan^2 \theta$$

or

$$\cos \theta = \frac{1}{\beta \sqrt{\epsilon}}$$

But this is just the Cerenkov angle. We see then, that the strongest coupling between an electromagnetic wave and the slow space charge wave occurs when the radiation propagates at an angle equal to the Cerenkov angle to the electron beam.

We will extract one final piece of information from figure II-2 before moving on. It is clear that the two dispersion curves can only intersect if the slope of the slow space charge

line exceeds the slope of the free wave asymptote. Symbolically,

$$V_0 > \frac{c}{\sqrt{\epsilon}}$$

This relation defines a threshold condition for the onset of instability and is called the Cerenkov threshold. Below the Cerenkov threshold, the electron beam is stable. Only when the beam exceeds the Cerenkov threshold does the system destabilize.

To gain information about the coupled system we must return to the inhomogeneous wave equation and consider now its axial component.

$$\left(\left[\nabla_{\perp}^2 - \nabla^2 + \frac{\epsilon}{c^2} \frac{\partial^2}{\partial t^2} \right] \underline{E} = -\frac{4\pi}{c^2} \frac{\partial j}{\partial t} \right)_{||}$$

Again, we assume plane wave solutions and so Fourier transform to give

$$\left[\nabla_{\perp}^2 + \left(\frac{\omega^2 \epsilon}{c^2} - k^2 \right) \right] \underline{E}_{||} = \left(\frac{\omega^2 \epsilon}{c^2} - k^2 \right) \left(\frac{\epsilon_{||} - 1}{\epsilon} \right) \underline{E}_{||}$$

Here $\epsilon_{||} = 1 - \frac{\omega_p^2}{\gamma^3 (\omega - k V_0)}$ is the z-z element of the beam dielectric tensor. While the dielectric tensor has not been derived, it is sufficient to realize that the quantity $\frac{\epsilon_{||} - 1}{\epsilon}$ relates the perturbed current density to the electric field.

Once again assuming $E_{||}$ to be an eigenfunction of the ∇_{\perp}^2 operator, we arrive at

$$\left[\frac{\omega^2 \epsilon}{c^2} - k^2 - p^2 - \frac{\omega_p^2 (\frac{\omega^2 \epsilon}{c^2} - k^2)}{\epsilon \gamma^3 (\omega - k V_0)^2} \right] \underline{E}_{||} = 0$$

The non trivial solution brings us to the dispersion relation

$$\omega^2 - \omega_k^2 - \frac{\omega_p^2 (\omega^2 - c^2 k^2 / \epsilon)}{\epsilon \gamma^3 (\omega - k V_0)^2} = 0$$

- ✓

where $\omega_K^2 \equiv \frac{c^2(k^2 + p^2)}{\epsilon}$ is the solution of the uncoupled equation.

We seek a solution of this coupled dispersion relation. If the perturbation term is small, we find the solution by evaluating the coupled part of the equation directly at synchronism. That is, where

$$k v_0 \approx \omega_K$$

We rewrite the dispersion relation

$$(\omega - \omega_K) \omega'^2 = \frac{\omega_p^2 (\omega^2 - \frac{c^2 k^2}{\epsilon})}{\epsilon \gamma^3 (\omega + \omega_K)}$$

Noting that factors on the left hand side are approximately equal at synchronism, and substituting the "synchronous" frequency into the right hand side, we find that the dispersion relation is cubic in $\omega - \omega_K$:

$$(\omega - \omega_K)^3 = \frac{\omega_p^2}{2\epsilon\gamma^3} (1 - 1/\beta^2\epsilon) c k \beta = \frac{\omega_p^2 \omega_K}{2\epsilon\gamma^3} (1 - 1/\beta^2\epsilon)$$

The roots are then given by

$$|\omega - \omega_K| = \left(\frac{\omega_p^2 \omega_K}{2\epsilon\gamma^3} \right)^{1/3} (1 - 1/\beta^2\epsilon)^{1/3} \left\{ \frac{-1 \pm \sqrt{3}}{2} \right\}$$

And so we find that near synchronism, the root is shifted away from the unperturbed value by a term which may be complex. We conclude that a normal mode of the beam-rf system is a growing

✓

wave of the form

$$\psi \sim e^{\omega_I t} e^{i(k \cdot r - \omega t - \Delta \omega_{\text{real}})}$$

where the growth rate is

$$\omega_I = \frac{\sqrt{3}}{2} \left(\frac{\omega_p^2 \omega_k}{2 \epsilon \gamma^3} \right)^{1/3} \left(1 - \frac{1}{\beta^2 \epsilon} \right)^{1/3}$$

and the real frequency shift is

$$\Delta \omega_{\text{real}} = \frac{1}{\sqrt{3}} \omega_I$$

This wave is Cerenkov unstable.

✓

The factor $1 - \frac{1}{\beta^2 \epsilon}$ in the right hand side of our gain expression is of interest. We see that positive gain will occur only for $\beta^2 \epsilon > 1$, that is, for superluminal beam velocities. This is the Cerenkov threshold once again. It was obtained earlier in a qualitative fashion in connection with our discussion of figure II-2. We now see that the threshold appears directly in the gain expression and is therefore quite rigorous.

✓

To conclude this section, let us consider the case of forward propagating radiation. In this limit, the transverse wave number, p , vanishes. The dispersion relation reduces to

$$1 - \frac{\omega_p^2}{\gamma^3 (\omega - k v_0)^2} = 0$$

which we recognize as a purely longitudinal mode. In fact, the equation describes the fast and slow space charge waves.

✓

These waves are clearly stable and we conclude that there is no Cerenkov instability for a forward propagating wave.

✓

Chapter Three

We have seen that in the limit of strong magnetization, the slow space charge wave can be unstable. Growth occurs only for beam velocities exceeding the Cerenkov threshold. The gain is maximized for propagation at the Cerenkov angle and vanishes entirely in the forward direction.

Let us go on to study the second of the negative energy beam modes: the slow cyclotron mode. As a model, we consider an infinite, isotropic medium characterized by a dielectric constant ϵ . The dielectric is immersed in a constant magnetic field, B_0 , which we take to be along the z -axis. Next, we let an electron beam pass through the medium. The unperturbed beam velocity is V_0 and also lies in the z -direction. We treat the beam as an infinite, cold plasma of electrons and so ignore the effects of boundaries to the system and of thermal spread in the beam. Finally, we introduce an electromagnetic wave propagating through the beam-dielectric medium at some angle θ to the z -axis. The electric and magnetic fields associated with the wave will be treated as perturbations to the beam-dielectric system. We use a linearized, cold fluid theory and so work in the small

26

195

✓

signal limit. The system is shown in figure III-1.

III.1 The Dispersion Function

As above, we treat the perturbed current density as a source term in Maxwell's equations. The self-consistent fields are then governed by

$$\nabla \times \underline{E} = -\frac{1}{c} \frac{\partial \underline{B}}{\partial t}$$

$$\nabla \times \underline{B} = \frac{4\pi}{c} \underline{J} - \frac{1}{c} \frac{\partial \underline{D}}{\partial t}$$

where μ has been set equal to unity. Combining the curl equations in the usual way,

$$\nabla \times \nabla \times \underline{E} = \frac{-4\pi}{c^2} \frac{\partial \underline{J}}{\partial t} - \frac{1}{c^2} \frac{\partial^2 \underline{D}}{\partial t^2}$$

Using the vector identity

$$\nabla \times \nabla \times = \nabla \nabla \cdot - \nabla^2$$

as well as the constitutive relation

$$\underline{D} = \epsilon \underline{E}$$

we see that

$$\left(\nabla \nabla \cdot - \nabla^2 + \frac{\epsilon}{c^2} \frac{\partial^2}{\partial t^2} \right) \underline{E} = \frac{-4\pi}{c^2} \frac{\partial \underline{J}}{\partial t}$$

Finally, we introduce the conductivity tensor $\underline{\sigma}$ which relates perturbations in the current density to the electric field. Substituting $\underline{J} = \underline{\sigma} \cdot \underline{E}$ we find

$$\left[\nabla \nabla \cdot - \nabla^2 + \frac{\epsilon}{c^2} \frac{\partial^2}{\partial t^2} + \frac{4\pi}{c^2} \frac{\partial}{\partial t} (\underline{\sigma} \cdot) \right] \underline{E} = 0$$

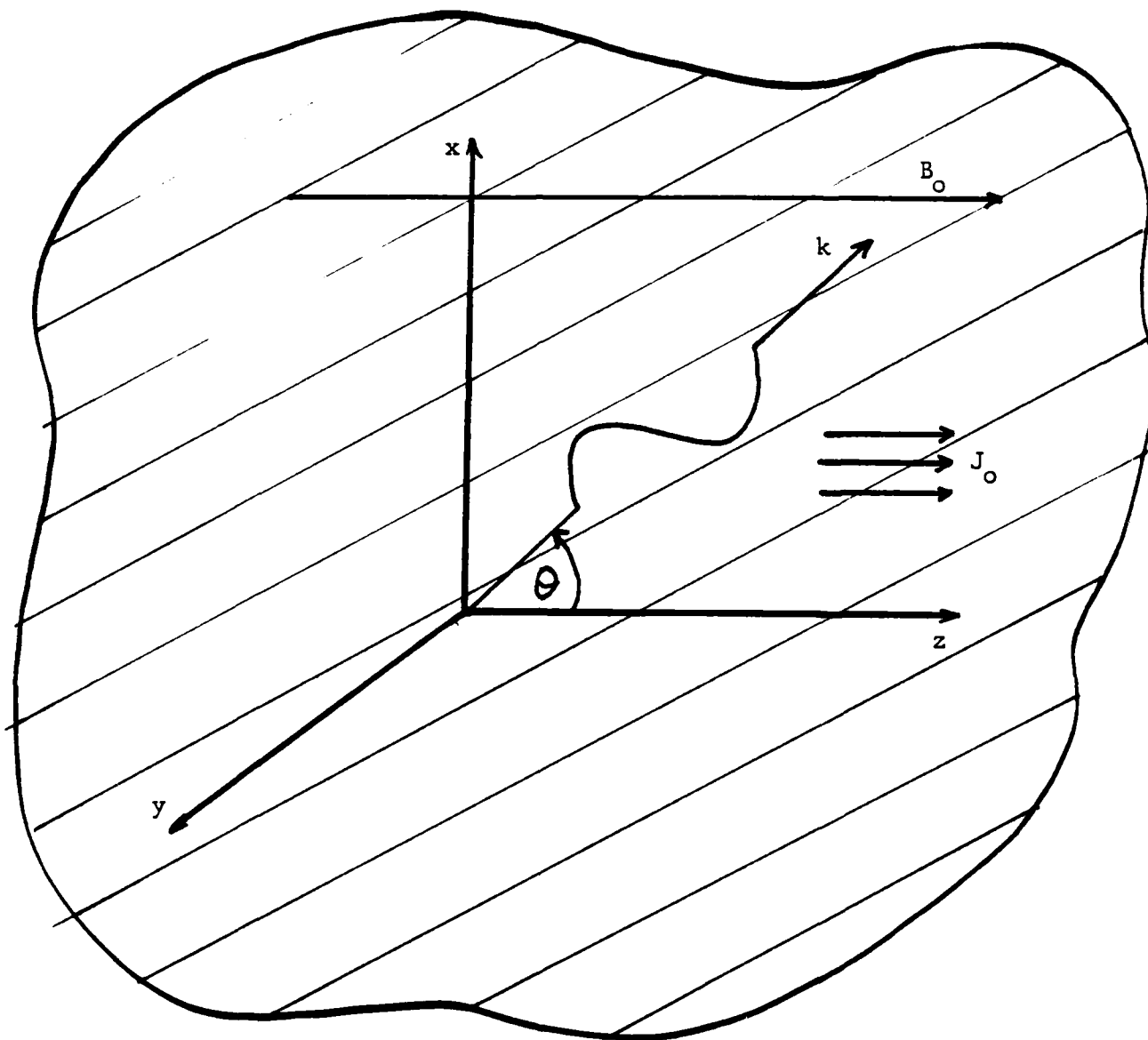


Figure III-1 The model

Next we consider a single Fourier component of the wave by assuming a plane wave dependence of the form

$$\underline{E} \sim e^{i(\underline{k} \cdot \underline{r} - \omega t)}$$

Our wave equation now takes the form

$$\left[-\underline{k} \underline{k} \cdot + \left(k^2 - \frac{\omega^2 \epsilon}{c^2} \right) \underline{1} - \frac{4\pi i \omega}{c^2} \underline{\sigma} \right] \underline{E} = 0$$

Defining the dispersion function

$$D(\omega, \underline{k}) = \text{Det} \left| \left(\frac{\omega^2 \epsilon}{c^2} - k^2 \right) \underline{1} + \frac{4\pi i \omega}{c^2} \underline{\sigma} + \underline{k} \underline{k} \right|$$

where $\underline{1}$ is the unit tensor, we require that $D(\omega, \underline{k})$ vanish for a non trivial solution. Thus we arrive at a determinantal dispersion relation governing small amplitude waves in the system. The physics is still hidden, however, in the conductivity tensor $\underline{\sigma}$. Our next task, then, is to calculate the response of the electron fluid to the electromagnetic wave.

III.2 Derivation of the Conductivity Tensor

We begin by calculating the force on a fluid element due to the perturbation. We will solve the resulting equation of motion to compute the perturbed beam velocity.

$$\underline{F} = \frac{d\underline{p}}{dt} = -e \left(\underline{E} + \frac{\underline{v} \times \underline{B}}{c} \right)$$

We linearize the force law by assuming small perturbations around an equilibrium solution. Explicitly,

$$\underline{V} = \underline{V}_0 + \underline{V}_1 = V_0 \hat{e}_z + \underline{V}_\perp + V_{||} \hat{e}_z$$

$$\underline{B} = \underline{B}_0 + \underline{B}_1 = B_0 \hat{e}_z + \underline{B}_\perp$$

$$\underline{E} = \underline{E}_1 = E_x \hat{e}_x + E_y \hat{e}_y + E_z \hat{e}_z$$

here, B_0 and V_0 are zero-th order quantities. All other terms are first order.

Also, we are free to choose our axes such that the propagation vector lies entirely in the x-z plane. Then

$$\underline{k} = k \hat{e}_x + k \hat{e}_z$$

To start, let us rewrite the left hand side of the force law. We linearize using the assumptions listed above and resolve the left hand side into parallel and perpendicular components.

$$\frac{d\underline{p}}{dt} = \frac{d}{dt} (\gamma m \underline{v}) = m \left[\gamma \frac{d\underline{v}}{dt} + \underline{v} \frac{d\gamma}{dt} \right]$$

$$\begin{aligned} \frac{d\gamma}{dt} &= \frac{d}{dt} \left(1 - \frac{v^2}{c^2} \right)^{-1/2} = \frac{1}{2} \left(1 - \frac{v^2}{c^2} \right)^{-3/2} \left(\frac{2}{c^2} \right) \underline{v} \cdot \frac{d\underline{v}}{dt} \\ &= \gamma^3 \underline{v} \cdot \frac{d\underline{v}}{dt} \end{aligned}$$

We combine these expressions to give

$$\frac{d}{dt} (\gamma m \underline{v}) = m \left[\gamma \frac{d\underline{v}}{dt} + \frac{\gamma^3 \underline{v} \cdot \left(\underline{v} \cdot \frac{d\underline{v}}{dt} \right)}{c^2} \right]$$

For \underline{V} perpendicular to $\frac{d\underline{V}}{dt}$,

$$\underline{F}_\perp = m\gamma \frac{d\underline{V}_\perp}{dt}$$

For \underline{V} in the direction of $\frac{d\underline{V}}{dt}$,

$$\underline{F}_\parallel = m\gamma \frac{d\underline{V}_\parallel}{dt} \left[1 + \frac{V^2}{c^2} \right] = m\gamma^3 \frac{d\underline{V}_\parallel}{dt}$$

where we have used $\beta^2\gamma^2 + 1 = \gamma^2$.

Returning to the full force law, we have

$$\frac{d\underline{V}_\perp}{dt} = \frac{-e}{m\gamma} \left(\underline{E} + \frac{\underline{V} \times \underline{B}}{c} \right)_\perp$$

$$\frac{d\underline{V}_\parallel}{dt} = \frac{-e}{m\gamma^3} \left(\underline{E} + \frac{\underline{V} \times \underline{B}}{c} \right)_\parallel$$

Here, $m\gamma^3$ is an effective longitudinal mass. The fluid element seems heavier in the direction of motion than it does in the transverse sense. As the beam energy is increased, then, the electron beam becomes "stiffer," a relativistic effect.

Next, let us linearize the $\underline{V} \times \underline{B}$ term.

$$\underline{V} \times \underline{B} = \underline{V}_0 \times \underline{B}_0 + \underline{V}_1 \times \underline{B}_0 + \underline{V}_0 \times \underline{B}_1 + \underline{V}_1 \times \underline{B}_1$$

The first term of the right hand side vanishes identically. The last term is ignored to first order giving,

$$\frac{d\underline{V}_\perp}{dt} = \frac{-e}{m\gamma} \left(\underline{E}_\perp + \frac{\underline{V}_0}{c} \times \underline{B}_1 + \frac{\underline{V}_1}{c} \times \underline{B}_0 \right)$$

$$\frac{d\underline{V}_\parallel}{dt} = \frac{-e}{m\gamma^3} E_\parallel$$

Rewriting the transverse part,

$$\frac{d\underline{V}_\perp}{dt} + \left(\underline{V}_1 \times \underline{B}_0 \right) \frac{e}{mc\gamma} = \frac{-e}{m\gamma} \left(\underline{E}_\perp + \frac{\underline{V}_0 \times \underline{B}_1}{c} \right)$$

$$\text{or } \begin{pmatrix} \frac{d}{dt} & \Omega_c \\ -\Omega_c & \frac{d}{dt} \end{pmatrix} \underline{V}_\perp = \frac{-e}{m\gamma} \left(\underline{E}_\perp + \frac{\underline{V}_0 \times \underline{B}_\perp}{c} \right)$$

where $\Omega_c = \frac{eB_0}{\gamma mc}$ is the relativistic cyclotron frequency.

Next, we consider the $\underline{V}_0 \times \underline{B}_\perp$ term. From Maxwell's equations,

$$\nabla \times \underline{E} = -\frac{1}{c} \frac{\partial \underline{B}}{\partial t}$$

giving for a single Fourier component,

$$\underline{k} \times \underline{E} = \frac{\omega}{c} \underline{B}$$

or

$$\underline{B} = \frac{c}{\omega} \underline{k} \times \underline{E}$$

then

$$\frac{\underline{V}_0 \times \underline{B}_\perp}{c} = \frac{1}{\omega} \underline{V}_0 \times (\underline{k} \times \underline{E})$$

writing out the cross products explicitly we have

$$\underline{k} \times \underline{E} = \begin{vmatrix} \hat{e}_x & \hat{e}_y & \hat{e}_z \\ p & 0 & k \\ E_x & E_y & E_z \end{vmatrix} = \hat{e}_x (-E_y k) - \hat{e}_y (p E_z - k E_x) + \hat{e}_z (p E_y)$$

$$\underline{V}_0 \times (\underline{k} \times \underline{E}) = \begin{vmatrix} \hat{e}_x & \hat{e}_y & \hat{e}_z \\ 0 & 0 & V_0 \\ -E_y k & (E_x k - p E_z) & p E_y \end{vmatrix} =$$

$$\hat{e}_x V_0 (p E_z - k E_x) + \hat{e}_y (V_0 E_y k) = \frac{\omega}{c} (\underline{V}_0 \times \underline{B}_\perp)$$

Having specialized the right hand side of our equation of motion to a single Fourier component, we must do the same to the left hand side. $\frac{d}{dt}$ is the convective derivative and so we have

$$\frac{d}{dt} \longrightarrow -i(\omega - \underline{k} \cdot \underline{v}_0)$$

Defining the quantity

$$\omega' = \omega - \underline{k} \cdot \underline{v}_0$$

we have for the transverse part of the force law,

$$\begin{pmatrix} \omega' & i\Omega_c \\ -i\Omega_c & \omega' \end{pmatrix} \underline{v}_\perp = \frac{-ie}{m\gamma} \left[\underline{\hat{e}}_x \underline{\hat{e}}_y + \underline{\hat{e}}_y \underline{\hat{e}}_x + \frac{\underline{\hat{e}}_x v_0 (p \underline{\hat{e}}_z - k E_x)}{\omega} + \frac{\underline{\hat{e}}_y (v_0 E_y k)}{\omega} \right]$$

or

$$\begin{pmatrix} \omega' & i\Omega_c \\ -i\Omega_c & \omega' \end{pmatrix} \underline{v}_\perp = \frac{-ie}{m\gamma} \left\{ \underline{\hat{e}}_x \left[E_x \left(1 - \frac{k v_0}{\omega} \right) + \frac{p v_0 E_{||}}{\omega} \right] + \underline{\hat{e}}_y \left[E_y \left(1 - \frac{k v_0}{\omega} \right) \right] \right\}$$

Writing the right hand side in matrix form,

$$\begin{pmatrix} \omega' & i\Omega_c \\ -i\Omega_c & \omega' \end{pmatrix} \underline{v}_\perp = \frac{-ie}{m\gamma} \begin{pmatrix} \frac{\omega'}{\omega} & 0 & \frac{p v_0}{\omega} \\ 0 & \frac{\omega'}{\omega} & 0 \\ 0 & 0 & 0 \end{pmatrix} \underline{E}$$

We can solve this matrix equation for the transverse component of the perturbed velocity. This is easily accomplished by matrix inversion giving

$$\underline{V}_\perp = \frac{-ie}{m\gamma(\omega'^2 - \Omega_c^2)} \begin{pmatrix} \frac{\omega'^2}{\omega} & \frac{-i\Omega_c\omega'}{\omega} & \frac{pV_0\omega'}{\omega} \\ \frac{i\Omega_c\omega'}{\omega} & \frac{\omega'^2}{\omega} & \frac{i\Omega_c pV_0}{\omega} \\ 0 & 0 & 0 \end{pmatrix} \underline{E}$$

Now let us add information about the longitudinal perturbation. We have

$$\frac{dV_{||}}{dt} = \frac{-e}{m\gamma^3} \frac{E_{||}}{\omega'}$$

Fourier transforming the convective derivative as above,

$$\underline{V}_{||} = \frac{-e}{m\gamma^3} \frac{E_{||}}{\omega'}$$

Finally, we combine our two equations of motion to yield a single matrix equation for the perturbed velocity as a function of the perturbing electric field.

$$\underline{V}_\perp = \frac{-ie}{m\gamma} \frac{1}{(\omega'^2 - \Omega_c^2)} \begin{pmatrix} \frac{\omega'^2}{\omega} & \frac{-i\Omega_c\omega'}{\omega} & \frac{pV_0\omega'}{\omega} \\ \frac{i\Omega_c\omega'}{\omega} & \frac{\omega'^2}{\omega} & \frac{i\Omega_c pV_0}{\omega} \\ 0 & 0 & \frac{(\omega'^2 - \Omega_c^2)}{\gamma^2 \omega'} \end{pmatrix}$$

Examining this equation, we see that the zero-th order motion gives rise to matrix elements which couple the axial and

perpendicular fields. The beam mixes the axial and perpendicular motion.

Also, we notice a factor of $\frac{1}{\omega'^2 - \Omega_c^2}$. This term is divergent for $\omega' = \pm \Omega_c$ and so we anticipate a resonance near this frequency. In fact, $\omega' = \pm \Omega_c$ is just the dispersion relation for cyclotron waves on the electron beam. We anticipate then, that the response will be greatest near a normal mode of the system.

Next, we solve the equation of continuity to give an expression for the perturbed beam density.

$$\frac{\partial n}{\partial t} + \nabla \cdot (n \underline{v}) = 0$$

Linearizing and Fourier transforming,

$$\nabla \cdot (n \underline{v}) \longrightarrow n_1 \cdot \underline{k} \cdot \underline{v}_1$$

$$\frac{\partial n}{\partial t} \longrightarrow -i\omega n_1$$

$$i n_0 (\underline{k} \cdot \underline{v}_1) + i n_1 (\underline{k} \cdot \underline{v}_0) - i \omega n_1 = 0$$

And solving for the perturbed density,

$$n_1 = \frac{n_0 \underline{k} \cdot \underline{v}_1}{\omega'}$$

Now we are ready to construct the perturbed current density,

$$\begin{aligned} \underline{J} &= -ne\underline{v} = -e(n_0 + n_1)(\underline{v}_0 + \underline{v}_1) \\ &= -e(n_0 \underline{v}_0 + n_0 \underline{v}_1 + n_1 \underline{v}_0 + n_1 \underline{v}_1) \end{aligned}$$

Defining the perturbed current density as

$$\underline{J}_1 = -e(n_1 \underline{v}_1 + \underline{v}_1 n_0)$$

and using the result for n_1 , derived above, we find

$$\underline{J}_1 = -e \left[n_0 \underline{v}_1 + \frac{n_0 \underline{v}_1 (\underline{k} \cdot \underline{v}_1)}{\omega'} \right] = \frac{-e n_0}{\omega'} (\omega' \underline{1} + v_0 \underline{k} \cdot) \underline{v}_1$$

where $\underline{1}$ is the unit tensor.

Computing $\omega' \underline{1} + v_0 \underline{k} \cdot$ and using the expression for \underline{v} obtained above, we have

$$\underline{J}_1 = \frac{i n_0 e^2}{m \gamma \omega' (\omega'^2 - \Omega_c^2)} \begin{pmatrix} \omega' & 0 & 0 \\ 0 & \omega' & 0 \\ v_0 p & 0 & \omega \end{pmatrix} \begin{pmatrix} \frac{\omega'^2}{\omega} & \frac{-i \Omega_c \omega'}{\omega} & \frac{p v_0 \omega'}{\omega} \\ \frac{i \Omega_c \omega'}{\omega} & \frac{\omega'^2}{\omega} & \frac{i \Omega_c p v_0}{\omega} \\ 0 & 0 & \frac{(\omega'^2 - \Omega_c^2)}{\gamma^2 \omega'} \end{pmatrix} \underline{E}$$

Carrying out the matrix multiplication, we can express the perturbed current solely in terms of \underline{E}

$$\underline{J}_1 = \underline{\sigma} \cdot \underline{E}$$

where

$$\underline{\sigma} = \frac{i \omega_p^2}{4 \pi \omega \gamma (\omega'^2 - \Omega_c^2)} \begin{pmatrix} \omega'^2 & -i \Omega_c \omega' & p v_0 \omega' \\ i \Omega_c \omega' & \omega'^2 & i p v_0 \Omega_c \\ p v_0 \omega' & -i p v_0 \Omega_c & \frac{p^2 v_0^2 + (\omega'^2 - \Omega_c^2) \omega^2}{\gamma^2 \omega'^2} \end{pmatrix}$$

is the tensor of conductivity describing the response of the beam

to the electromagnetic wave and $\omega_p^2 \equiv \frac{4\pi n e^2}{m}$ is the beam plasma frequency.

III.3 Construction of the Dispersion Relation

We have used the Lorentz force law together with the equation of continuity to derive a conductivity tensor for the electron beam-rf system. We are now ready to return to the dispersion function and calculate a useful dispersion relation. Substituting $\underline{\sigma}$ into the dispersion function D,

$$D = \left| \left(\frac{\omega^2 \epsilon}{c^2} - k^2 \right) \underline{1} + \frac{4\pi i \omega}{c^2} \underline{\sigma} + k k \right|$$

we arrive at a determinantal dispersion relation:

$$D = 0 =$$

$$\text{Det} \begin{vmatrix} \frac{\omega^2 \epsilon}{c^2} - k^2 - \frac{\omega_p^2 \omega'^2}{\gamma c^2 \omega''^2} & \frac{i \omega_p^2 \omega' \Omega_c}{\gamma c^2 \omega''^2} & k p - \frac{\omega_p^2 p v_0 \omega'}{\gamma c^2 \omega''^2} \\ \frac{-i \omega_p^2 \omega' \Omega_c}{\gamma c^2 \omega''^2} & \frac{\omega^2 \epsilon}{c^2} - k_{\text{tot}}^2 - \frac{\omega_p^2 \omega'^2}{\gamma c^2 \omega''^2} & \frac{-i \omega_p^2 p v_0 \Omega_c}{\gamma c^2 \omega''^2} \\ k p - \frac{\omega_p^2 p v_0 \omega'}{\gamma c^2 \omega''^2} & \frac{i \omega_p^2 p v_0 \Omega_c}{\gamma c^2 \omega''^2} & \frac{\omega^2 \epsilon}{c^2} - p^2 - \frac{\omega_p^2 \omega^2}{\gamma^2 c^2 \omega'^2} - \frac{\omega_p^2 p^2 v_0^2}{\gamma c^2 \omega''^2} \end{vmatrix}$$

III-a

$$\omega''^2 \equiv \omega'^2 - \Omega_c^2$$

This equation defines the normal modes of the coupled system. It is exact to within the limits of our cold fluid approach.

The dispersion relation looks quite formidable but is actually tractable. We expand in cofactors and then group terms in powers of $\frac{1}{\omega'^2 - \Omega_c^2}$. $\frac{1}{\omega'^2 - \Omega_c^2}$ is in some sense a measure of the strength of the interaction. We will call terms proportional to $\frac{1}{\omega'^2 - \Omega_c^2}$ resonant since they become large when the electromagnetic wave resonates with a cyclotron wave.

Grouping the resonant terms together, we can express the dispersion function as

$$\begin{aligned}
 D = & \frac{\omega_c^2}{c^2} \left(\frac{\omega_c^2}{c^2} - k_{\text{res}}^2 \right)^2 - \left(\frac{\omega_c^2}{c^2} - k_{\text{res}}^2 \right) \left(\frac{\omega_c^2}{c^2} - k^2 \right) \frac{\omega_p^2 \omega^2}{\epsilon^3 c^2 \omega'^2} \\
 & + \frac{\omega_p^2}{\epsilon c^2 \omega'^2} \left\{ \frac{\omega_c^2}{c^2} \left(\frac{\omega_c^2}{c^2} - k_{\text{res}}^2 \right) \left[-2\omega' + \frac{c^2 p^2}{\epsilon} (1 - \beta^2 \epsilon) + \frac{\omega_p^2}{\epsilon \delta^3} \right] \right. \\
 & \quad \left. + \frac{\omega_c^2}{c^2} \left(\frac{\omega_c^2}{c^2} - k^2 \right) \frac{\omega_p^2}{\epsilon \delta^3} \right\} \\
 & + \left(\frac{\omega_p^2}{\epsilon c^2} \right)^2 \frac{1}{\omega'^2} \frac{\omega_c^2}{c^2} \left[\omega'^2 - \frac{c^2 p^2}{\epsilon} (1 - \beta^2 \epsilon) - \frac{\omega_p^2}{\epsilon \delta^3} \right] = 0
 \end{aligned}$$

This is a complicated function of ω , k , and all the five parameters. It describes the general case of propagation at an unspecified angle through arbitrary magnetic field strength.

Before attempting a solution of the general problem, let us consider two further limiting conditions to the dispersion relation. First, we will let the cyclotron frequency become very large. We will show that the Cerenkov results for a strongly

magnetized electron beam are then recovered. We will define the infinite Ω_0 limit precisely during that discussion. Next, we will let the cyclotron frequency approach zero and show that the resulting dispersion relation describes the Cerenkov interaction on an unmagnetized beam.

III.4 Limit of Strong Magnetization

We let the applied magnetic field increase without bound. In the infinite Ω_0 limit, the quantity $\frac{1}{\omega'^2 - \Omega_c^2}$ becomes very small and the resonant terms vanish. The dispersion relation reduces to

$$\omega^2 - \frac{c^2 k_{\text{tot}}^2}{\epsilon} + \frac{\omega_p^2 (\omega^2 - \frac{c^2 k^2}{\epsilon})}{\epsilon \gamma \omega'^2} = 0$$

We recognize this as the relation derived in chapter two in connection with our discussion of the Cerenkov instability. The "Cerenkov" dispersion relation appears easily as a limit of the present, more general D.

Let us next determine precisely how large the applied field must be to be properly regarded as infinite. Our procedure will be as follows. We will first assume the cyclotron frequency to be large, but finite. We will then compute the shift in the Cerenkov roots owing to the B-field dependent terms. Requiring

that this shift be small, we will define the sense in which a field is infinite.

As a first approximation we assume

$$\Omega_c^2 \gg \omega'^2$$

Recognizing that ω' is proportional to the Cerenkov growth rate, we can restate this inequality as follows. We assume that the frequency of gyromotion of the electrons is much greater than the growth rate of the Cerenkov interaction. Physically, the electrons perform many orbits in one e-folding time. Using this assumption in equation III-a, we have for our large Ω_0 dispersion relation,

$$D = \begin{vmatrix} \frac{\omega^2 \epsilon}{c^2} - k^2 & 0 & kp \\ 0 & \frac{\omega^2 \epsilon}{c^2} - k_{\text{res}}^2 & \frac{i\omega_p^2 p V_0}{rc^2 \Omega_c} \\ kp & \frac{-i\omega_p^2 p V_0}{rc^2 \Omega_c} & \frac{\omega^2 \epsilon}{c^2} - p^2 - \frac{\omega_p^2 \omega^2}{\partial^2 c^2 \omega'^2} + \frac{\omega_p^2 p^2 V_0^2}{\partial c^2 \Omega_c^2} \end{vmatrix} = 0$$

Expanding the determinant,

$$\left(\frac{\omega^2 \epsilon}{c^2} - k^2\right) \left(\frac{\omega^2 \epsilon}{c^2} - k_{\text{res}}^2\right) \left(\frac{\omega^2 \epsilon}{c^2} - p^2 - \frac{\omega_p^2 \omega^2}{\partial^2 c^2 \omega'^2} + \frac{\omega_p^2 p^2 V_0^2}{rc^2 \omega'^2}\right) - kp \left(\frac{\omega^2 \epsilon}{c^2} - k_{\text{res}}^2\right) - \left(\frac{\omega^2 \epsilon}{c^2} - k^2\right) \left(\frac{\omega_p^2}{rc^2}\right)^2 \frac{p^2 V_0^2}{\Omega_c^2} = 0$$

The last term in this expression is much smaller than the others and we may ignore it. We rewrite the remainder to give

$$\frac{\omega^2 \epsilon}{c^2} - k^2 - \frac{P^2}{\left(1 + \frac{\omega_p^2}{\epsilon \gamma \Omega_c^2}\right)} - \frac{\omega_p^2 \left(\frac{\omega^2 \epsilon}{c^2} - k^2\right)}{\epsilon \gamma^3 \left(1 + \frac{\omega_p^2}{\epsilon \gamma \Omega_c^2}\right)} = 0$$

This is just the Cerenkov relation for a strongly magnetized beam modified by the factor $1 + \frac{\omega_p^2}{\epsilon \gamma \Omega_c^2}$ in the last two terms. The precise result derived in chapter one is recovered if we require

$$\frac{\omega_p^2}{\gamma \Omega_c^2} \ll 1$$

Let us express this last in terms of more fundamental quantities. We have, then,

$$\frac{4\pi n e^2 / m}{\gamma \left(\frac{e B_0}{m c \gamma}\right)^2} \ll 1$$

$$\frac{4\pi \gamma n c^2 m}{B_0^2} \ll 1$$

III-b

$$B_0 \gg \sqrt{4\pi \gamma c^2 n m}$$

This relation defines the B_0 equal to infinity condition. To

✓

a first degree of approximation, a field is infinite if it satisfies equation III-b. Only the space charge wave is unstable in this limit; the cyclotron wave is disregarded.

III.5 Limit of Weak Magnetization

As the applied magnetic field falls to zero, the dispersion relation reduces to

$$D = \begin{vmatrix} \frac{\omega^2 \epsilon}{c^2} - k^2 - \frac{\omega_p^2}{\gamma c^2} & 0 & k p - \frac{\omega_p^2 p V_0}{\gamma c^2 \omega'} \\ 0 & \frac{\omega^2 \epsilon}{c^2} - k_{\text{tor}}^2 - \frac{\omega_p^2}{\gamma c^2} & 0 \\ k p - \frac{\omega_p^2 p V_0}{\gamma c^2 \omega'} & 0 & \frac{\omega^2 \epsilon}{c^2} - p^2 - \frac{\omega_p^2 \omega^2}{\gamma^3 c^2 \omega'^2} - \frac{\omega_p^2 p^2 V_0^2}{\gamma c^2 \omega'^2} \end{vmatrix} = 0$$

✓ We note immediately that $\frac{\omega^2 \epsilon}{c^2} - k_{\text{tor}}^2 - \frac{\omega_p^2}{\gamma c^2}$ is a factor of D . Expanding the determinant and grouping terms in powers of $\frac{1}{\omega'}$, we can write the dispersion relation as follows.

$$\omega^2 - \frac{c^2 k_{\text{tor}}^2}{\epsilon} - \frac{\omega_p^2}{\epsilon \gamma} + \frac{1}{\omega'^2} \left(\frac{\omega_p^2 c^2}{\epsilon^2 \gamma^3} \right) \left[k^2 + \gamma^2 p^2 - (\omega^2 + \gamma^2 p^2 V_0^2) \frac{\epsilon}{c^2} + \frac{\omega_p^2}{\gamma c^2} \right] = 0$$

This result reproduces previous calculations⁷.

III.6 Discussion

As in our discussion of the Cerenkov instability, it is useful to plot the dispersion relations for the free wave and slow cyclotron wave on the same axes. See figure III-2. In contrast to the Cerenkov case, the constraint $k v_0 > \frac{c k}{\sqrt{\epsilon}}$ does not insure an intersection. Requiring that $k v_0 - \Omega_c > \frac{c k}{\sqrt{\epsilon}}$ we find

$$\beta > \frac{1}{\sqrt{\epsilon}} + \frac{\Omega_c}{c k}$$

That is, the beam velocity must exceed the speed of light in the medium by an amount equal to the phase velocity of the cyclotron wave in the beam frame. This relation constitutes the Cerenkov-cyclotron threshold.

Let us next use figure III-2 to determine a relationship between k and p . That is, to specify the angle of propagation at synchronism. Setting

$$(k^{\text{tot}} \cos \theta) v_0 - \Omega_c = \frac{c k^{\text{tot}}}{\sqrt{\epsilon}}$$

and solving,

$$\cos \theta = \frac{1}{\beta \sqrt{\epsilon}} + \frac{\Omega_c}{k v_0}$$

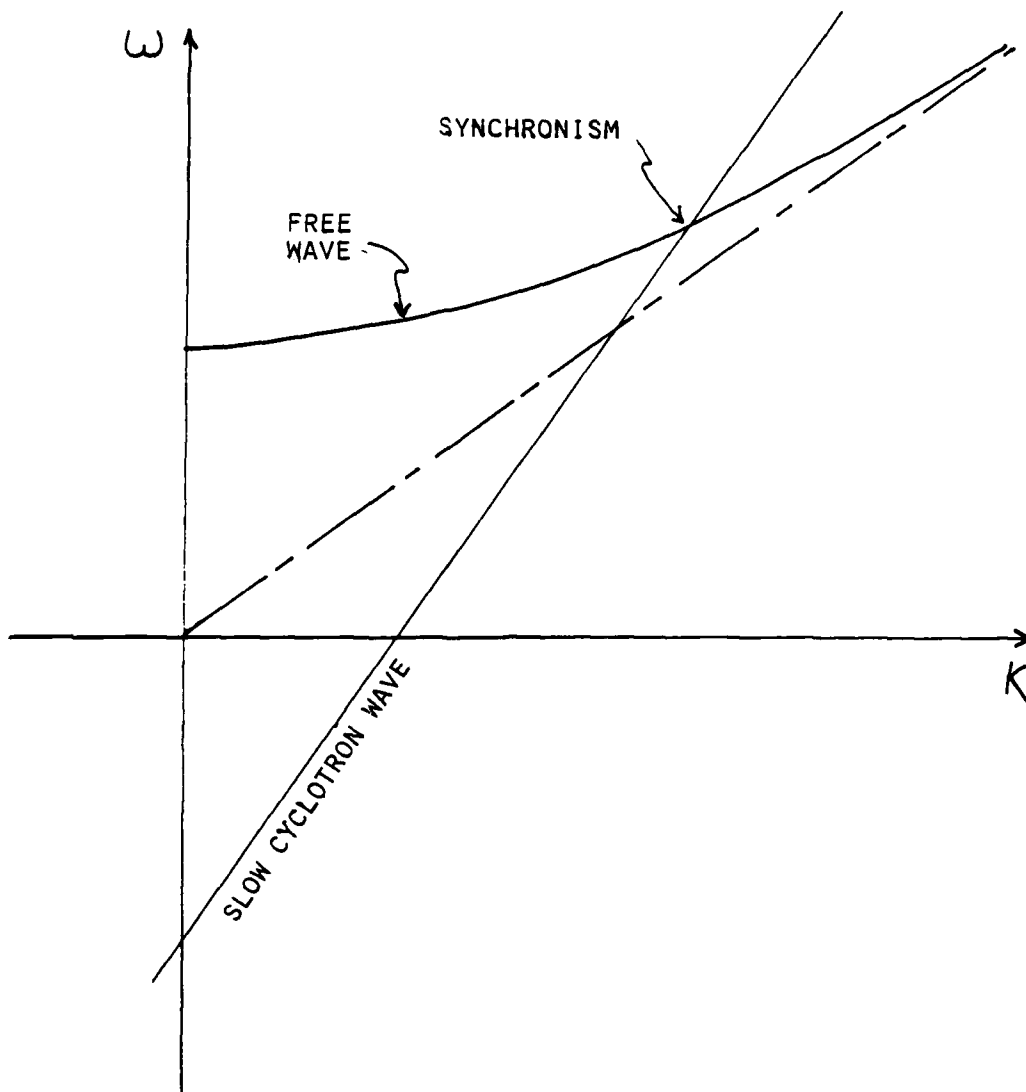


Figure III-2 Synchronism with the slow
cyclotron
Figure III-2 Synchronism with the slow cyclotron wave

This, then, is the angle at which the peak growth occurs. Equivalently, it is the angle at which synchronous radiation of wave number k propagates.

This is understood as follows. We consider radiation of a particular frequency. Fixing the applied field (Ω_c) and the accelerating voltage (γ), we can look out through theta and ask about the growth of the wave. For small angles, some growth will occur. The exchange of energy is inefficient, however. Electrons spend almost as much time having work done on them by the wave as they do doing work on the wave. As we increase theta from zero, the gain increases and is maximized at an angle dictated by synchronism. Effectively, we have varied the detuning of the electromagnetic wave from the beam. Best coupling is achieved for minimum detuning; that is, at synchronism⁸.

Let us now examine the form of the dispersion function. We can write D as the sum of an uncoupled part and two coupled parts.

$$D = D^{(0)} + D^{\text{Cerenkov}} + D^{\text{Cerenkov-cyclotron}}$$

the uncoupled part, given by

$$D^{(0)} = \omega^2 - \omega_K^2$$

is obviously the free wave solution. It depends neither on resonant terms nor on the beam plasma frequency. $D^{(0)}$ is the unperturbed solution of the problem of an electromagnetic wave moving through a dielectric medium.

The first of the coupling terms is given by

$$D^{\text{Cerenkov}} = \frac{-\omega_p^2 \left(\omega^2 - \frac{c^2 k^2}{\epsilon} \right)}{\epsilon \omega^3 \omega'^2}$$

This term is independent of the cyclotron frequency and describes a longitudinal mode, the space charge mode. We have seen that when the applied magnetic field is increased without bound, is the dominant perturbation to $D^{(0)}$. That is

$$D^{\text{Cerenkov}} \gg D^{\text{Cerenkov-Cyclotron}}$$

as B_0 becomes finite, both terms perturb the free wave. There are two separate synchronisms here and two resonant frequencies. How distant the two effects are and which one dominates must be determined from a careful solution of the dispersion relation. As B_0 goes to zero, both coupling terms become resonant with the space charge wave. This suggests the Cerenkov interaction on an unmagnetized beam.

We conclude from this qualitative inspection of the dispersion function that, as the parameter B_0 is varied from zero through the infinite regime, the roots of the dispersion function are smoothly varying. This, together with the fact of recovering the

- ✓

$B_0=0$, $B_0=\infty$ limits, provides evidence that we have correctly derived the general dispersion relation.

We next sketch the roots of the unperturbed dispersion relation in the $\omega - k$ plane. These include two beam cyclotron waves, two beam space charge waves, and the free electromagnetic wave. We neglect the plasma frequency with respect to the cyclotron intercept and show these curves in figure III-3.

There are two points of particular interest. The first is the intersection of the space charge line and the free wave curve; the second is the intersection of the slow cyclotron line with the free wave. The former defines a synchronism of the space charge wave with an electromagnetic wave. The latter defines synchronism with the slow cyclotron wave.

We have seen that the slow space charge wave is unstable near synchronism. For frequencies greater than the synchronous frequency, there are two real roots. Below a critical value, the roots are complex.

Similarly, we expect the slow cyclotron wave to destabilize near synchronism. In this case, however, the instability is bounded both above and below in frequency. Beyond these cutoffs, the solutions are both real; within, a complex conjugate pair. A sketch of the perturbed dispersion relation is shown in figure III-4.

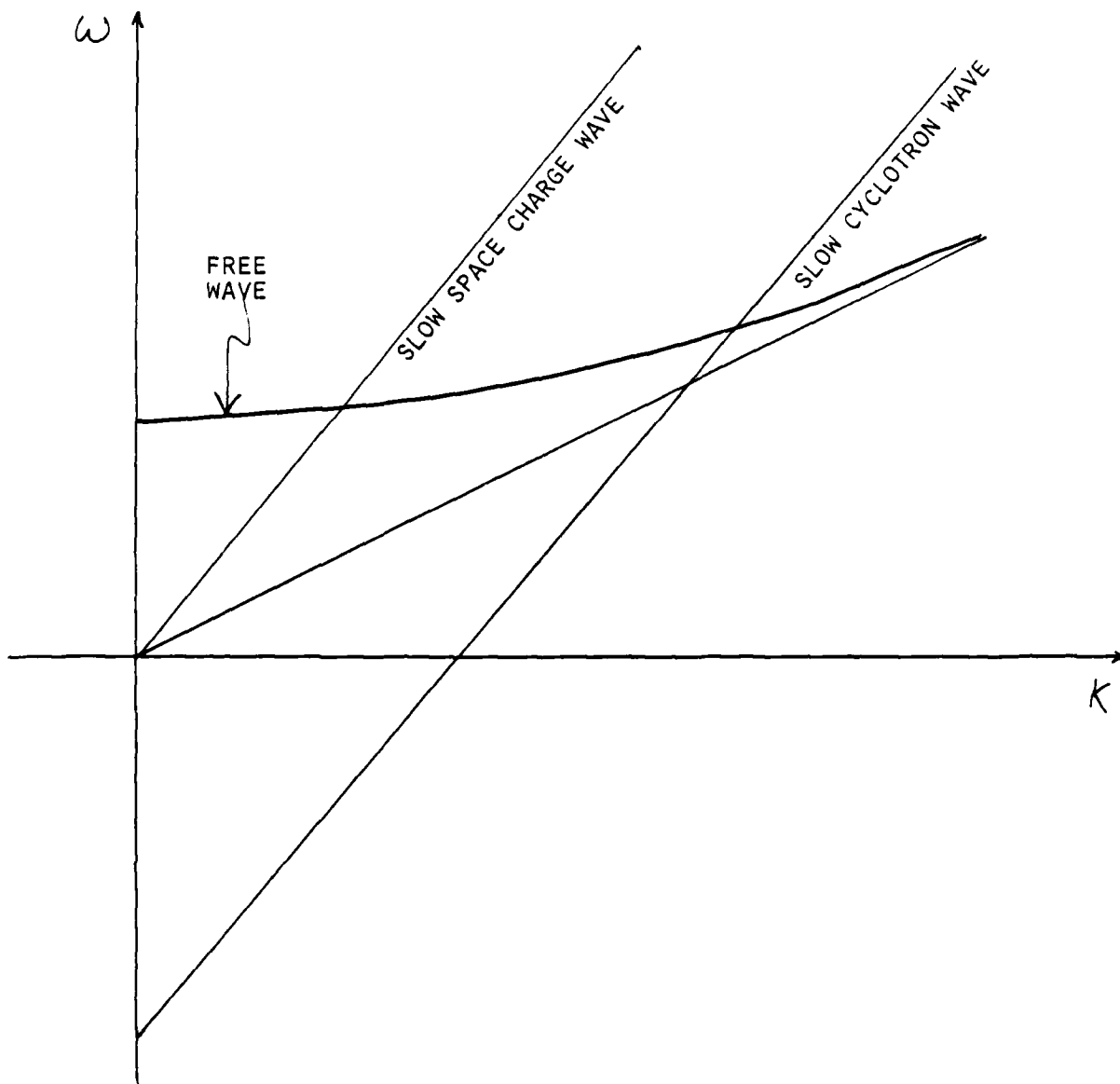


Figure III-3 The unperturbed roots

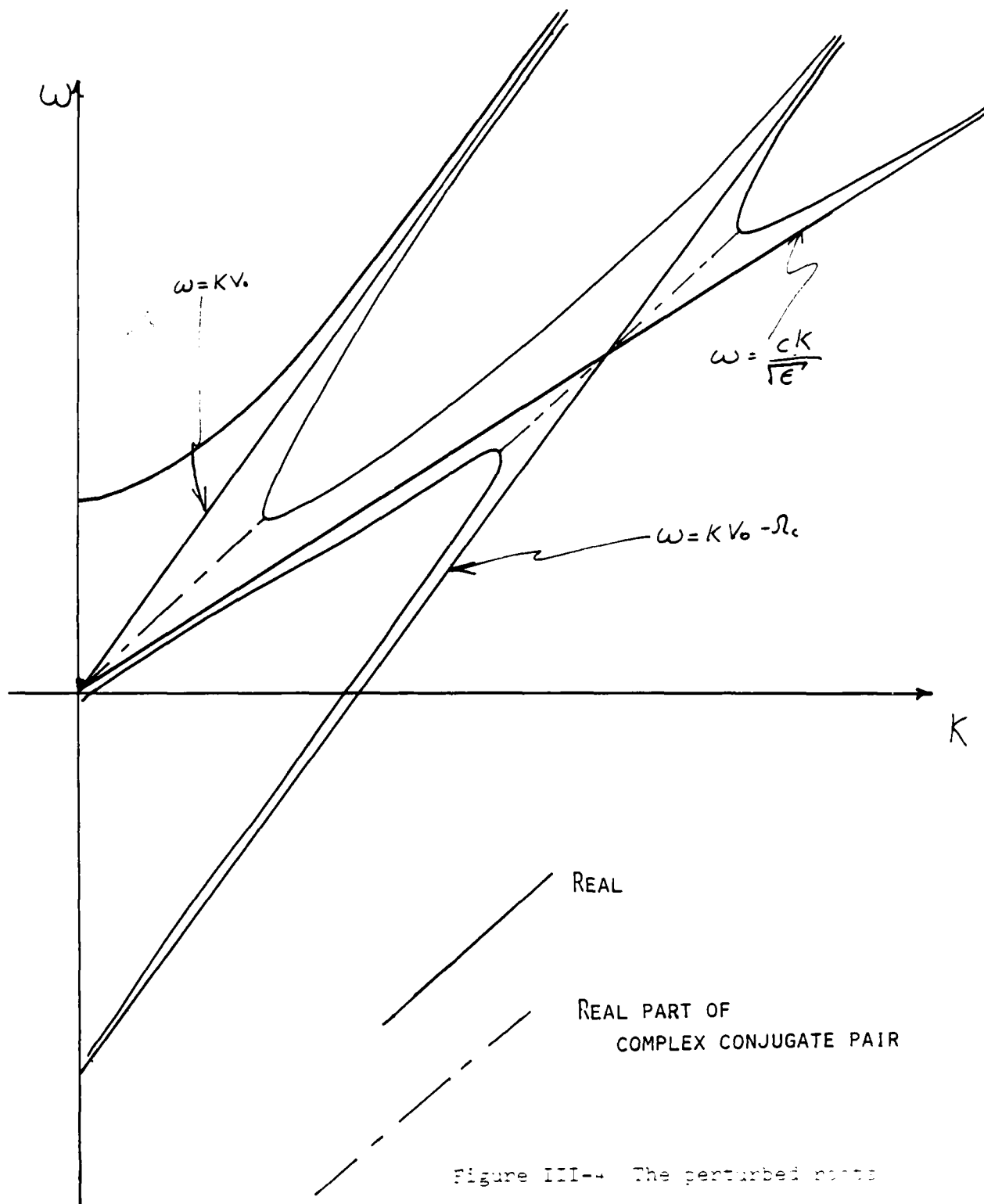


Figure III-4 The perturbed roots

- ✓

In the next two chapters we will investigate the Cerenkov-cyclotron instability in detail by solving the dispersion relation near synchronism with the slow cyclotron wave. For now, however, let us make a few observations relating to the general phenomenology predicted by figure III-4.

To begin, we note that for a given beam energy the cyclotron interaction occurs at a higher frequency than does the Cerenkov interaction. For realistic field strengths, this points to an intrinsically higher frequency device.

Also, the resonant frequency tunes to the magnetic field strength as well as the beam energy. We have seen that tunability is an important feature of a useful radiation source and so this is an attractive feature.

✓ The question of which instability dominates is certainly of interest. In the limit of weak magnetization, the slow cyclotron line coalesces with the space charge line. The roots vary smoothly into the previously obtained solutions of that problem.

In the limit of large β_0 , as defined precisely above, the cyclotron roots are shifted to infinite frequency. We will see in a later chapter that this implies the dominance of the space charge roots.

- ✓

For finite magnetic field, the two effects coexist. The longitudinal and transverse instabilities both occur, their proportions being dictated by the growth rates. While coupling to the space charge wave has been verified experimentally, there has been no report of coupling to the cyclotron mode in a free electron laser system. It is of extreme interest to demonstrate this effect. We will see that it is a very promising source of high frequency waves.

✓

Chapter Four

IV.1 Forward Propagation

The expressions we have derived thus far are still quite general in the sense that they describe radiation propagating at an arbitrary angle to the zero-th order beam motion. The magnetic field strength is also unspecified. Before solving the general problem, however, let us consider the case of a forward propagating electromagnetic wave. That is $\theta = 0$. In this limit, the radiation copropagates with the electron beam, both in the z-direction. Recall also that we are no longer working in the $\beta_0 \rightarrow \infty$ limit and so anticipate solutions which depend on the gyromotion of the electrons. For $\theta = 0$ we have,

$$\underline{T} = \frac{i\omega_p^2}{4\pi\gamma} \frac{\omega'/\omega}{\omega'^2} \begin{pmatrix} \omega' & -i\Omega_c & 0 \\ i\Omega_c & \omega' & 0 \\ 0 & 0 & \frac{\omega^2 \omega'^2}{\gamma^2 \omega'^3} \end{pmatrix}$$

Recall now the dispersion function

$$D(\omega, k) = \left| \left(\frac{\omega^2 \epsilon}{c^2} - k^2 \right) \underline{1} + \frac{4\pi i \omega}{c^2} \underline{T} + k k \right|$$

Constructing $\underline{\underline{\sigma}}$ we see

$$\left(\frac{\omega^2 \epsilon}{c^2} - k^2\right) \underline{\underline{1}} + \underline{\underline{k}} \underline{\underline{k}} = \begin{pmatrix} \frac{\omega^2 \epsilon}{c^2} - k^2 & 0 & 0 \\ 0 & \frac{\omega^2 \epsilon}{c^2} - k^2 & 0 \\ 0 & 0 & \frac{\omega^2 \epsilon}{c^2} \end{pmatrix}$$

a diagonal matrix. The conductivity tensor is only block diagonal but is easily diagonalized. We define $\underline{\underline{\sigma}}_{\perp}$ by

$$\underline{\underline{\sigma}}_{\perp} = \frac{i \omega_p^2 \omega' / \omega}{4 \pi \gamma \omega'^2} \begin{pmatrix} \omega' & -i \Omega_c \\ i \Omega_c & \omega' \end{pmatrix}$$

Solving the characteristic equation, we have for the eigenvalues of $\underline{\underline{\sigma}}_{\perp}$

$$\lambda_{1,2} = \omega' \pm \Omega_c$$

so that

$$\underline{\underline{\sigma}}_{\perp} \rightarrow \frac{i \omega_p^2 \omega'}{4 \pi \gamma \omega} \begin{pmatrix} \frac{1}{\omega' - \Omega_c} & 0 \\ 0 & \frac{1}{\omega' + \Omega_c} \end{pmatrix}$$

Next, we can ask about the eigenvectors of the system. Equivalently, what is the change of basis which decouples the system? Solving the eigenvector problem we find

$$\underline{\underline{e}}^{(1)} = \frac{1}{\sqrt{2}} (\hat{e}_x + i \hat{e}_y)$$

$$\underline{\underline{e}}^{(2)} = \frac{1}{\sqrt{2}} (i \hat{e}_x + \hat{e}_y)$$

and so the normal modes of the system are circularly polarized waves. Performing the change of basis, we have for the dispersion function

$$D = \begin{vmatrix} \frac{\omega^2 \epsilon}{c^2} - k^2 - \frac{\omega_p^2 \omega'}{\gamma c^2 (\omega' - \Omega_c)} & 0 & 0 \\ 0 & \frac{\omega^2 \epsilon}{c^2} - k^2 - \frac{\omega_p^2 \omega'}{\gamma c^2 (\omega' + \Omega_c)} & 0 \\ 0 & 0 & \frac{\omega^2 \epsilon}{c^2} - \frac{\omega_p^2}{c^2 \gamma^{3/2} \omega'^2} \end{vmatrix} = 0$$

The determinant is, of course, trivially evaluated giving four solutions. Defining the quantity

The four solutions are

$$\omega^2 - \omega_K^2 - \frac{\omega_p^2 \omega'}{\epsilon \gamma (\omega' - \Omega_c)} = 0 \quad \text{IV-a}$$

$$\omega^2 - \omega_K^2 - \frac{\omega_p^2 \omega'}{\epsilon \gamma (\omega' + \Omega_c)} = 0 \quad \text{IV-b}$$

$$\omega' = \frac{\omega_p}{\gamma^{3/2}} \quad \text{IV-c}$$

$$\omega' = -\frac{\omega_p}{\gamma^{3/2}}$$

IV-d

Relations IV-c and IV-d describe fast and slow space charge waves. These modes are decoupled from the transverse motion and show no dependence on the cyclotron frequency.

Relations IV-a and IV-b describe the coupling of the fast and slow cyclotron waves to the rf. Dependence of the applied magnetic field as well as on the dielectric constant of the medium is seen.

IV.2 Analysis of the Dispersion Relations

We have derived expressions relating ω and k for the eigenmodes of our coupled beam-rf-dielectric system. We can next ask if any of these normal modes are growing waves. The space charge waves are easily seen to be stable by inspection of equation IV-c,d. The cyclotron modes require more detailed attention.

We will employ a technique known as root locus plotting. A root locus plot shows regions in the complex plane which are roots of the dispersion function for some combination of problem parameters. Only certain ω -vectors satisfy the phase relations dictated by the dispersion relation; those that do not can never be roots of the dispersion function. A real root indicates a stable mode. A non zero imaginary component, however, describes an exponentially growing wave. We rewrite the cyclotron dispersion function as follows:

$$F(\omega, k) = \frac{D(\omega, k)}{\omega^2 - \omega_K^2} = 1 - \frac{\omega_p^2 \omega'}{\epsilon \gamma (\omega + \omega_K)(\omega - \omega_K)(\omega' \pm \Omega_c)}$$

where the plus/minus sign indicates the slow/fast wave, respectively. Roots of the function $F(\omega, k)$ are also roots of D , except possibly along the line $\omega = \pm \omega_K$. We require then that the quantity

$$G(\omega, k) \equiv \frac{\omega'}{(\omega + \omega_K)(\omega - \omega_K)(\omega' \pm \Omega_c)}$$

be real and positive if ω is to satisfy the dispersion relation. Equivalently, a number $\omega = \omega_R + i\omega_I$ must introduce a phase shift of $2n\pi$ (n an integer) if ω is a root.

Also, we can vary the coupling parameter: $\frac{\omega_p^2}{\gamma}$. As we do so, the quantity $\frac{\omega_p^2}{\epsilon \gamma} G(\omega, k)$ must remain equal to unity if $F(\omega, k)$ is to vanish. For weak coupling, a root must approach a pole of $G(\omega, k)$:

$$\omega \rightarrow \pm \omega_k; \quad kv_0 \mp \Omega_c$$

As the coupling strength increases, the roots leave the poles and move toward the zeros of G :

$$\omega \rightarrow kv_0$$

In so doing, the roots describe trajectories along which the beam strength $\frac{\omega_p^2}{\gamma}$ is a parameter.

Let us now draw root locus plots of the fast cyclotron wave. Plots are shown for both subluminal ($v_0 < \frac{c}{\sqrt{\epsilon}}$) and superluminal ($v_0 > \frac{c}{\sqrt{\epsilon}}$) propagation in figures IV-1 and IV-2.

The fast cyclotron roots lie entirely along the real axis. Only real frequencies satisfy the dispersion relation and we conclude that the fast cyclotron wave is stable. This could have been anticipated since we expect only slow waves to be unstable.

We show root locus plots for the slow cyclotron wave in figures IV-3 and IV-4. For beam velocities less than the speed

✓

of light in the dielectric, the roots are real; the system is stable. Above Cerenkov threshold, however, the root trajectory leaves the real axis and takes on a non zero imaginary component. This wave grows exponentially in time and is said to be Cerenkov-cyclotron unstable.

$$F(\omega, k) = 1 - \frac{\omega_p^2 (\omega - k \cdot v_0)}{(\omega - k \cdot v_0 - \Omega_c)(\omega^2 - \omega_K^2)} = 0$$

$$\omega_K^2 \equiv \frac{c^2 k^2}{\epsilon}$$

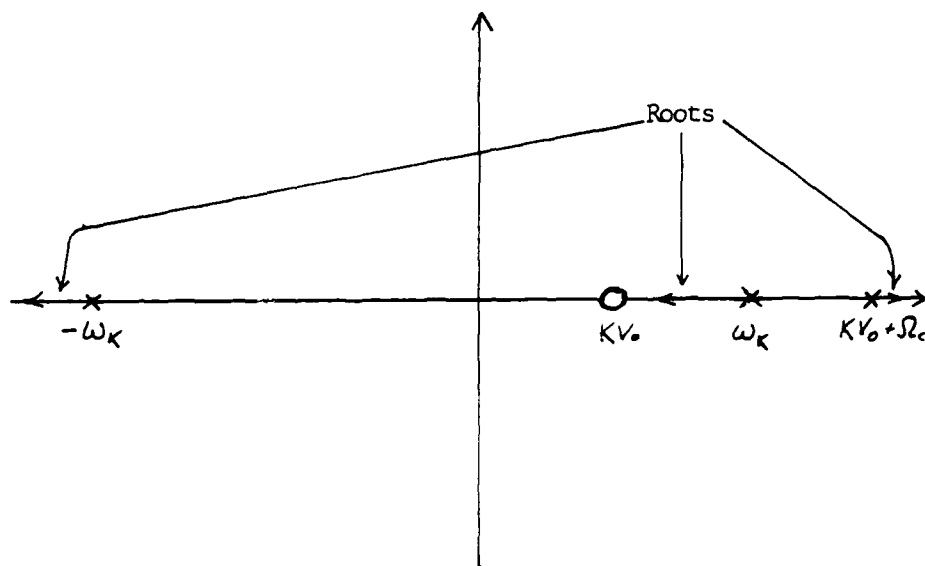


Figure IV-1 Root locus plot of the fast cyclotron mode

Case 1: $K v_0 < \frac{cK}{\sqrt{\epsilon}}$

$$F(\omega, k) = 1 - \frac{\omega_p^2 (\omega - k \cdot v_0)}{(\omega - k \cdot v_0 + \Omega_c)(\omega^2 - \omega_K^2)} = 0$$

$$\omega_K^2 = \frac{c^2 k^2}{\epsilon}$$

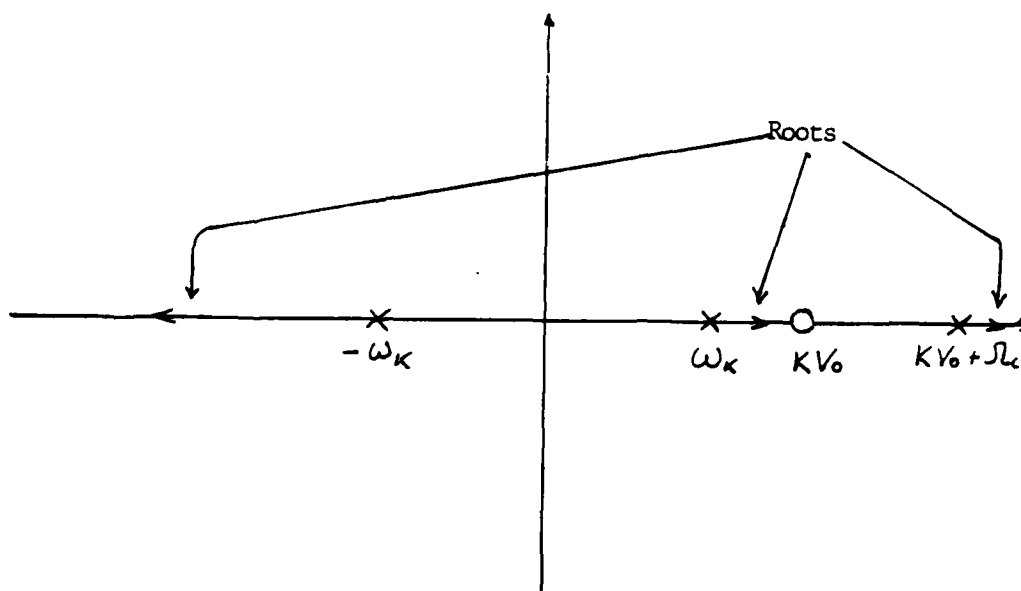


Figure IV-2 Root locus plot of the fast cyclotron mode

Case 2: $KV_0 > \frac{cK}{\sqrt{\epsilon}}$

$$F(\omega, k) = 1 - \frac{\omega_p^2 (\omega - k \cdot v_0)}{(\omega - k \cdot v_0 + \Omega_e)(\omega^2 - \omega_k^2)} = 0$$

$$\omega_k^2 = \frac{c^2 k^2}{\epsilon}$$

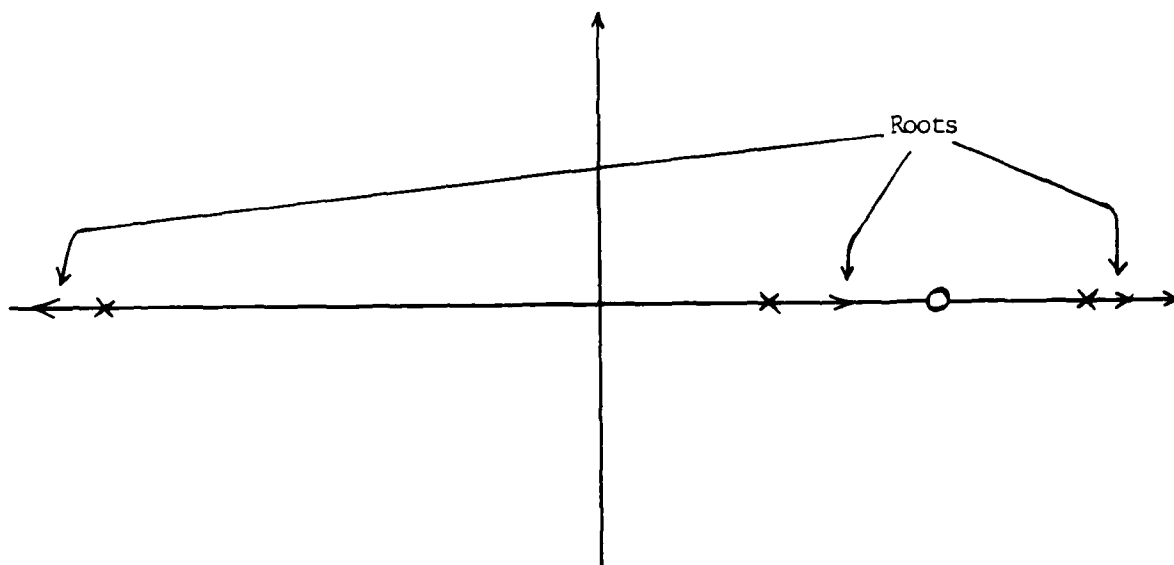


Figure IV-3 Root locus plot of the slow cyclotron mode

Case 1: $KV_0 < \frac{cK}{\sqrt{\epsilon}}$

230

$$F(\omega, k) = 1 - \frac{\omega_p^2 (\omega - k \cdot v_0)}{(\omega - k \cdot v_0 + \Omega_e)(\omega^2 - \omega_k^2)}$$

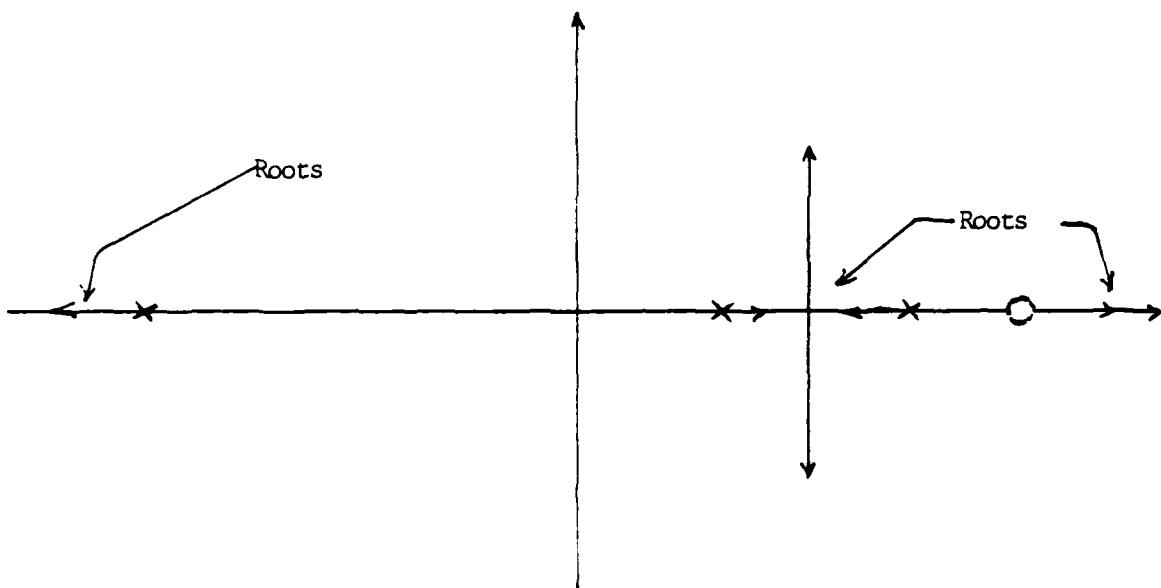


Figure IV-4 Root locus plot of the slow cyclotron mode

Case 2: $KV_0 > \frac{cK}{\sqrt{\epsilon}}$

231

IV.3 Solution of the Dispersion Relation

we can find an analytic expression for the peak gain of the system by solving the dispersion relation near synchronism. Recall

$$\omega^2 - \omega_k^2 - \frac{\omega_p^2 \omega'}{\epsilon \gamma (\omega' + \Omega_c)} = 0$$

If the coupling terms are small compared to the unperturbed root, we expect solutions which are shifted slightly from that root. Of interest is the imaginary part of the shift. We estimate the magnitude of that quantity by evaluating the perturbation term directly at synchronism.

Operationally, we rewrite equation IV-a to give

$$(\omega - \omega_k)(\omega' + \Omega_c) = \frac{\omega_p^2 \omega'}{\epsilon \gamma (\omega + \omega_k)}$$

Setting ω' equal to $-\Omega_c$ in the right hand side, and recognizing that $\omega_k \approx kv_0 - \Omega_c$ at synchronism, we find,

$$(\omega - \omega_k)^2 = \frac{-\omega_p^2 \Omega_c}{\epsilon \gamma (2\omega_k)}$$

Solving, we obtain the following simple expression for the growth rate:

$$\omega_I = \sqrt{\frac{\omega_p^2 \Omega_c}{2\epsilon \gamma \omega_k}}$$

IV-e

✓

The gain is seen to be a function of the wave number, cyclotron frequency, beam energy, dielectric constant, as well as beam strength. At synchronism, however, only four of these parameters vary independently. If any three of the first four parameters just mentioned are fixed, the fourth is uniquely specified according to

$$\omega_k = kv_0 - \Omega_c \quad \text{IV-f}$$

where v_0 is expressible in terms of δ .

Using equation IV-e, we can make explicit the dependence of the gain function on a particular parameter. Plotting the resulting relations, we can investigate the gain characteristics of the system.

Dependence of the Gain on Beam Energy

We treat the dielectric constant of the medium, plasma frequency (beam current), and cyclotron frequency (applied magnetic field) as constants, and eliminate the dependence of the gain of wave number. The growth at synchronism is then

expressible as the following function of the beam energy:

$$\omega_I = \left(\frac{\omega_p^2}{2\sqrt{\epsilon}} \right)^{1/2} \left(\frac{\sqrt{1 - 1/\delta^2} - 1/\sqrt{\epsilon}}{\gamma} \right)^{1/2}$$

Using this relation, we can express the threshold condition in terms of the electron beam energy as

$$\gamma > \sqrt{\frac{\epsilon}{\epsilon - 1}}$$

As the energy rises from unity, the gain "turns on" at this threshold, reaches a maximum, and then falls off as $1/\delta^{1/2}$ in the limit of high energy. A plot is shown in figure IV-5.

Dependence of the Gain on Frequency

Noting that at synchronism, the wavenumber is expressible in terms of the radiation frequency (in Hz) according to

$$|k_{\text{res}}| = \frac{2\pi\epsilon}{c} \nu$$

we rewrite the growth rate as

$$\omega_I = \left(\frac{\omega_p^2 \Omega_c}{4\pi\epsilon \delta \nu} \right)^{1/2}$$

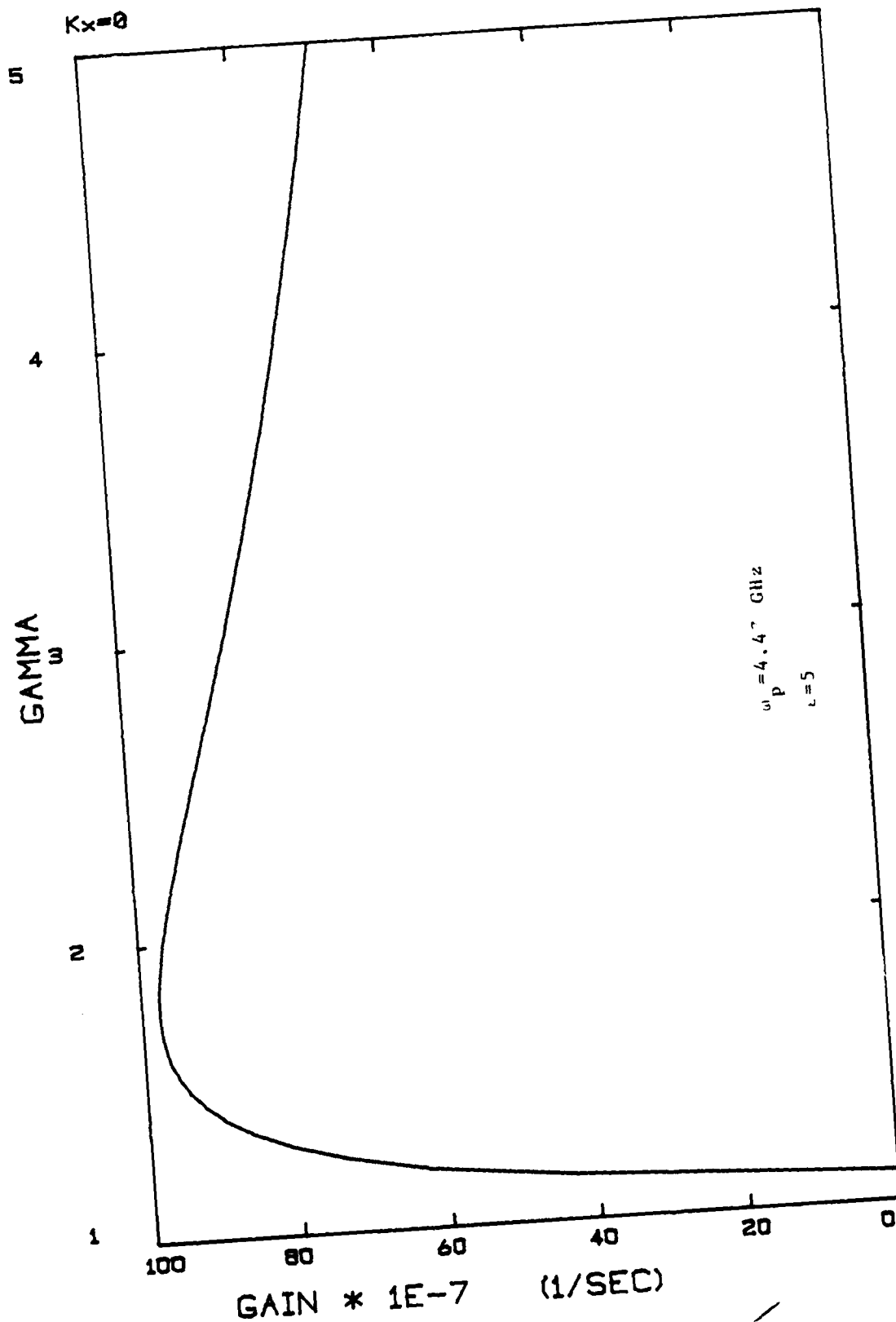


Figure IV-5 Gain vs. beam energy for experimental parameters

235

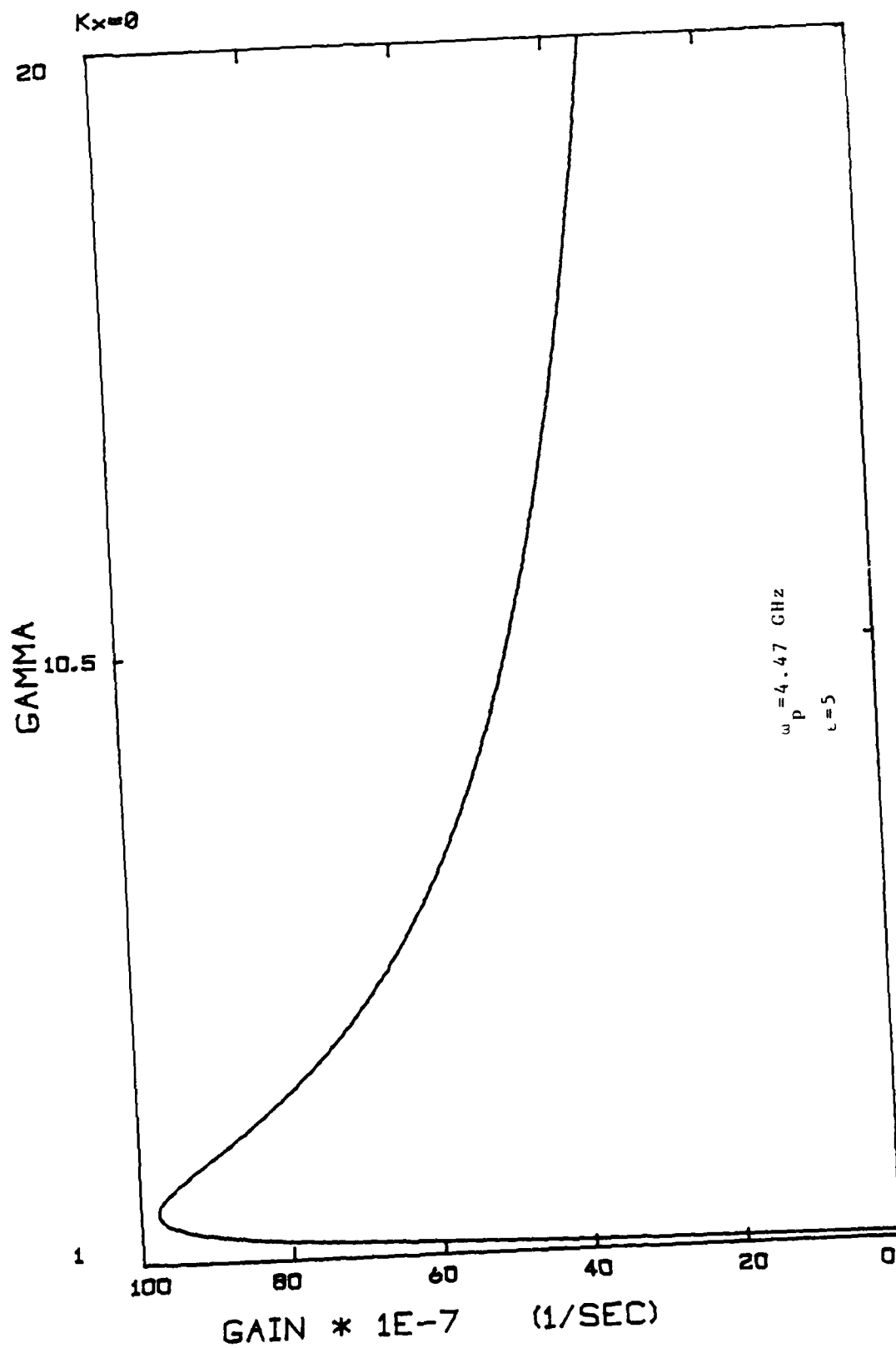


Figure IV-5a Gain vs beam energy for experimental parameters

✓

Fixing the cyclotron frequency, we can tune the radiation to beam energy. A wave of frequency ν is synchronous with a beam of energy

$$\gamma = \left[1 - \frac{1}{\epsilon} \left(1 + \frac{\Omega_c}{2\pi\nu} \right)^2 \right]^{-1/2}$$

Using this expression in equation IV-2, we can express the gain at constant cyclotron frequency and beam current in terms of the radiation frequency to give

$$\omega_I = \left[\frac{\omega_p^2 \Omega_c \sqrt{1 - \frac{1}{\epsilon} \left(1 + \frac{\Omega_c}{2\pi\nu} \right)^2}}{4\pi\epsilon\nu} \right]^{1/2}$$

We see that for $\nu \gg \frac{\Omega_c}{2\pi}$, the numerator approaches a constant. The gain in this high frequency limit falls off as the frequency to the minus one half power. A plot is shown in figure IV-6.

Finally, we note that the gain is independent of the cyclotron frequency for fixed beam energy.

We see, then, that a circularly polarized electromagnetic wave, copropagating with a superluminal electron beam, is Cerenkov-cyclotron unstable. This effect has no analogy in the pure Cerenkov case where the forward propagating wave was seen to be stable. The study of propagation through a finite magnetic field is therefore well motivated. The question is now raised,

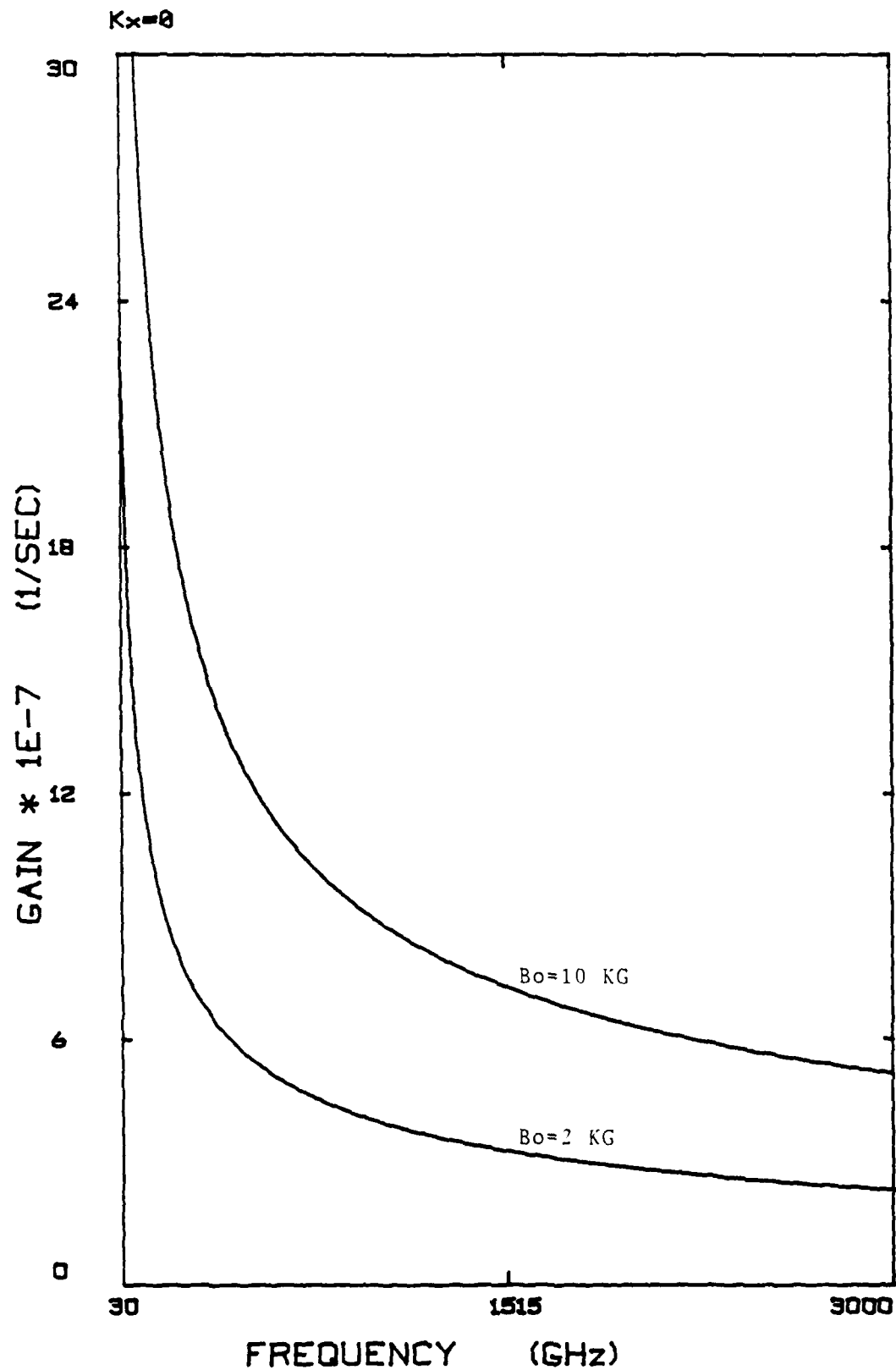


Figure IV-6 Gain vs. frequency for experimental parameters

✓

however, whether one can extract more energy from the electron beam by propagating an electromagnetic wave through it at some angle not equal to zero. In analogy with the Cerenkov case, we expect that the general case will show a larger growth rate and that propagation at a modified Cerenkov angle will maximize the gain.

✓

Chapter Five

We have used Maxwell's equations together with our conductivity tensor to derive a dispersion relation. The dispersion relation governs small amplitude electromagnetic waves propagating at an angle through a magnetized electron beam. In the limits of strong and weak magnetization, this equation reproduces the Cerenkov relations. In the limit of small transverse wave number, it yields the forward propagating cyclotron results.

✓

V.1 Solution of the General Dispersion Relation

It is, in general, difficult to obtain an analytic solution to the dispersion relation. Even near synchronism the equation is sixth degree in the frequency. A solution of the most general problem is only practical using numerical techniques in conjunction with a high speed computer. We can, however, solve the problem analytically in the limit of low beam density. In this limit, the beam plasma frequency is small compared to the

✓

✓

operating frequency. We retain terms of the order of $\frac{\omega_p^2}{\omega_K^2}$ but discard higher order terms. We will see in the next section that this is an excellent approximation.

Our "weak beam" dispersion relation is given by

$$D = \frac{\omega^2 \epsilon}{c^2} \left(\frac{\omega^2 \epsilon}{c^2} - k_{\text{rot}}^2 \right) + \frac{1}{\omega'^2} \frac{\omega_p^2}{8c^2} \left[p^2 \omega^2 (1 - \beta^2 \epsilon) - 2 \frac{\omega^2 \epsilon}{c^2} \omega'^2 \right] = 0$$

We rewrite this expression to give

$$(\omega - \omega_K)(\omega + \omega_K)(\omega' - \Omega_c)(\omega' + \Omega_c) = \frac{-\omega_p^2}{\epsilon \gamma} \left[\frac{c^2 p^2}{\epsilon} (1 - \beta^2 \epsilon) - 2 \omega'^2 \right]$$

solving near synchronism with the slow cyclotron wave we find

$$(\omega - \omega_K)^2 = \frac{\omega_p^2}{4c\gamma\Omega_c\epsilon^{1/2}} \left[\frac{c^2 k_{\text{rot}}^2}{\epsilon} \sin^2 \theta (1 - \beta^2 \epsilon) - 2\Omega_c^2 \right]$$

where we have made use of

$$\omega' - \Omega_c = -2\Omega_c$$

v-a

Finally, we have for our solution,

$$|\omega - \omega_K| = \left(\frac{\omega_p^2}{4c k_{\text{rot}} \gamma \Omega_c \epsilon^{1/2}} \right)^{1/2} \left[\frac{c^2 k_{\text{rot}}^2}{\epsilon} (1 - \beta^2 \epsilon) \sin^2 \theta - 2\Omega_c^2 \right]^{1/2}$$

As in the case of the forward propagating wave, it is important to note that not all the parameters which appear in equation v-b may be specified independently at synchronism.

Setting

$$\omega_K = kv_0 - \Omega_c$$

we find that the angle of propagation must satisfy the following relation:

$$\sin^2 \theta = 1 - \left(\frac{1}{\beta^2 \epsilon} + \frac{\Omega_c}{c k \beta} \right)^2$$

Substituting this expression into equation V-b, we can rewrite the growth rate to give

$$\omega_I = \left(\frac{\omega_p^2}{4\epsilon \omega_K \Omega_c} \right)^{1/2} \left[\frac{\omega_K^2 (1 - \beta^2 \epsilon)}{\beta^2 \epsilon} \left\{ \beta^2 \epsilon - \left(1 + \frac{\Omega_c}{\omega_K} \right)^2 \right\} - 2\Omega_c^2 \right]^{1/2}$$

Here, we have made explicit the dependence on the beam energy, rf frequency, and cyclotron frequency. To the extent that they do not violate equation V-a, these parameters may now be treated as independent variables.

V.2 Threshold

Before analyzing our gain expression, let us obtain a threshold condition for the instability. Requiring that the right hand side of equation V-b be imaginary, we find

$$\left[\frac{\omega_K^2 (1 - \beta^2 \epsilon)}{\beta^2 \epsilon} \right] \left[\beta^2 \epsilon - \left(1 + \frac{\Omega_c}{\omega_K} \right)^2 \right] < 2\Omega_c^2$$

✓

It is clear that the two bracketed factors can never have the same sign. This would imply the contradiction of $\beta^2 \epsilon$ being both greater than and less than unity. Since $\omega_k^2 / \beta^2 \epsilon$ is a positive definite quantity, we may rewrite the inequality as follows:

$$\left[1 - \beta^2 \epsilon \right] \left[\beta^2 \epsilon - \left(1 + \frac{\Omega_c}{\omega_k} \right)^2 \right]$$

Since $\frac{\Omega_c}{\omega_k}$ is also a number greater than zero, we have that

$$\beta^2 \epsilon > 1 + \frac{\Omega_c}{\omega_k}$$

This is identical to the threshold condition obtained in our discussion of figure III-2.

V.3 Validity of the Weak Beam Criterion

✓

Let us next define the limitations imposed by the weak beam approximation. We have discarded second and third degree terms in the quantity ω_p^2 . We require then that

$$\omega_p^2 \ll \omega_k^2$$

We rewrite the plasma frequency as follows.

$$\omega_p^2 = 4 \frac{I}{I_0} \frac{c^2}{\beta a^2}$$

✓

where $I_0 = \frac{r_0}{ec}$ is a characteristic current equal to 17.5 kilampères and r_0 is the classical radius of the electron. "a" is the radius of the electron beam. Finally, we have

$$4 \frac{I}{I_0} \frac{c^2}{a^2 \beta} \ll \omega_k^2$$

or

$$\frac{I}{I_0} \ll \left(\frac{\pi a}{\lambda} \right)^2 \beta$$

For λ of order one centimeter and a beam radius of order 1 centimeter, this relation is well satisfied for beam currents approaching one tenth I_0 . The weak beam regime thus includes currents of one to two kiloampères.

For λ of order one hundred microns, this domain is extended greatly. Beam currents of order 10^5 begin to violate the approximation. These currents are several orders of magnitude greater than typical values in a Cerenkov type device. We conclude that the weak beam approximation is an extremely good one, imposing only mild limitations on the problem.

V.4 Analysis

We plot the growth rate versus beam energy in figure V-1. As

✓

expected, there is no gain below threshold. At threshold the gain rises sharply and peaks near $\gamma = 2$. As in the case of the forward propagating wave the growth falls as γ to the minus one half power in the high energy limit.

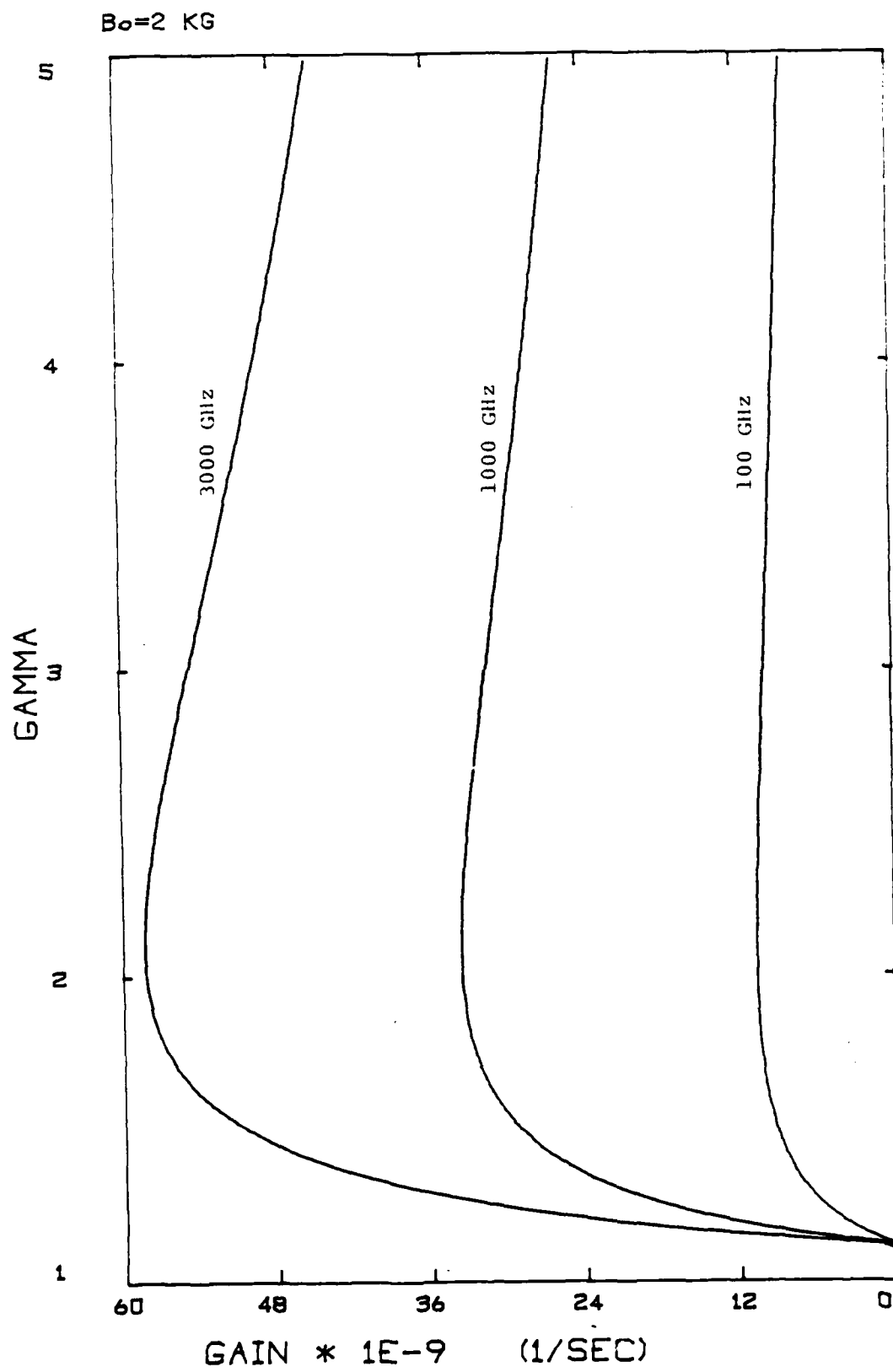


Figure V-1a Gain vs. Beam Energy

246

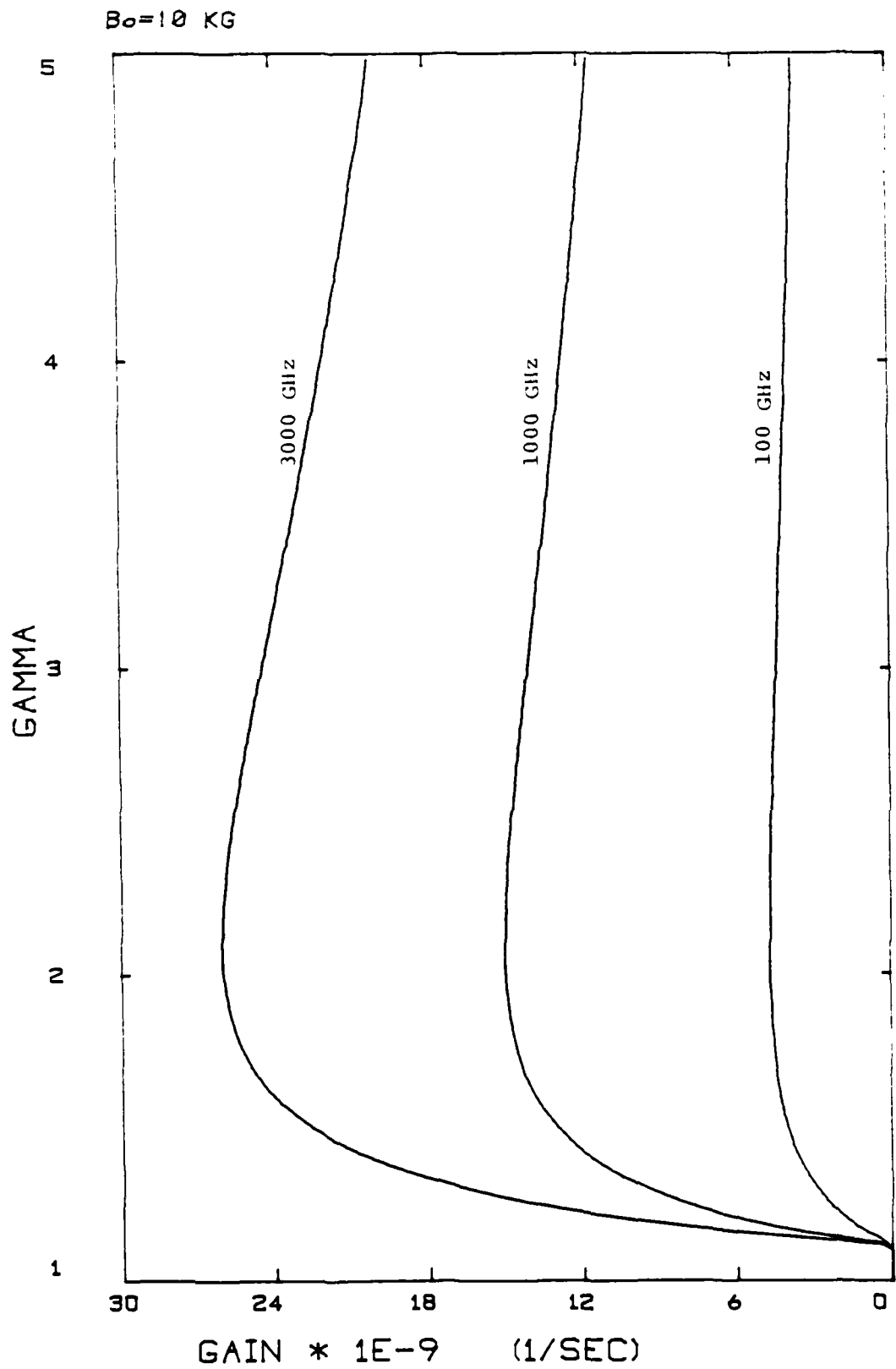


Figure V-1b Gain vs. Beam Energy

✓

Next we show the dependence of the gain on operating frequency. Curves are shown for two values of the applied magnetic field and beam energy in figure V-2. Gain is an increasing function of frequency. Substantial growth is, indeed, possible at high frequencies.

For $\gamma = 1.4$ And magnetic fields in the range from two to ten kilogauss, gains between 10^9 and 10^{10} per second are predicted. These are quite large. At $\gamma = 2$ (500 KeV), these figure are doubled, approximately. We see, then, that substantial growth is possible using modest beam energy and applied field strength.

Let us consider next how the gain function responds to changes in the applied field. The behavior is shown in figure V-3. The gain is a slowly decreasing function of field strength. Gains at low field are very large; these exceed 10^{10} per sec. For higher fields, these figures drop by a factor of two. Recalling that the interaction frequency rises linearly with the magnetic field, we are tempted to conclude that high frequency, high power operation is simply a matter of increasing the magnetic field strength. This is not so. We will see in the next section that problems associated with high frequency operation of a real device complicate the issue. These results do show, however, that substantial gain of a submillimeter wave can be achieved for reasonable experimental parameters.

77

248

✓

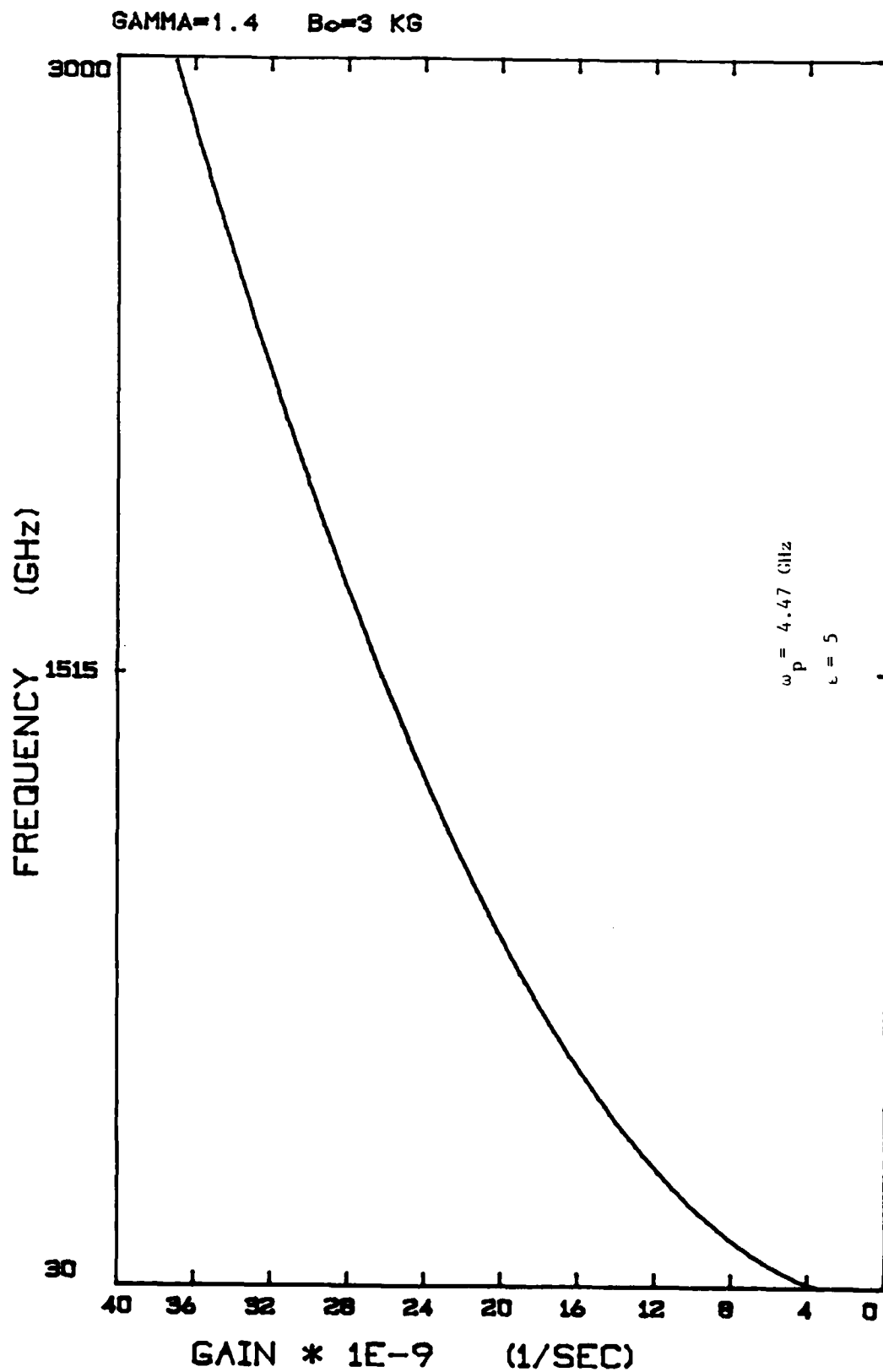


Figure V-2a Gain vs. frequency

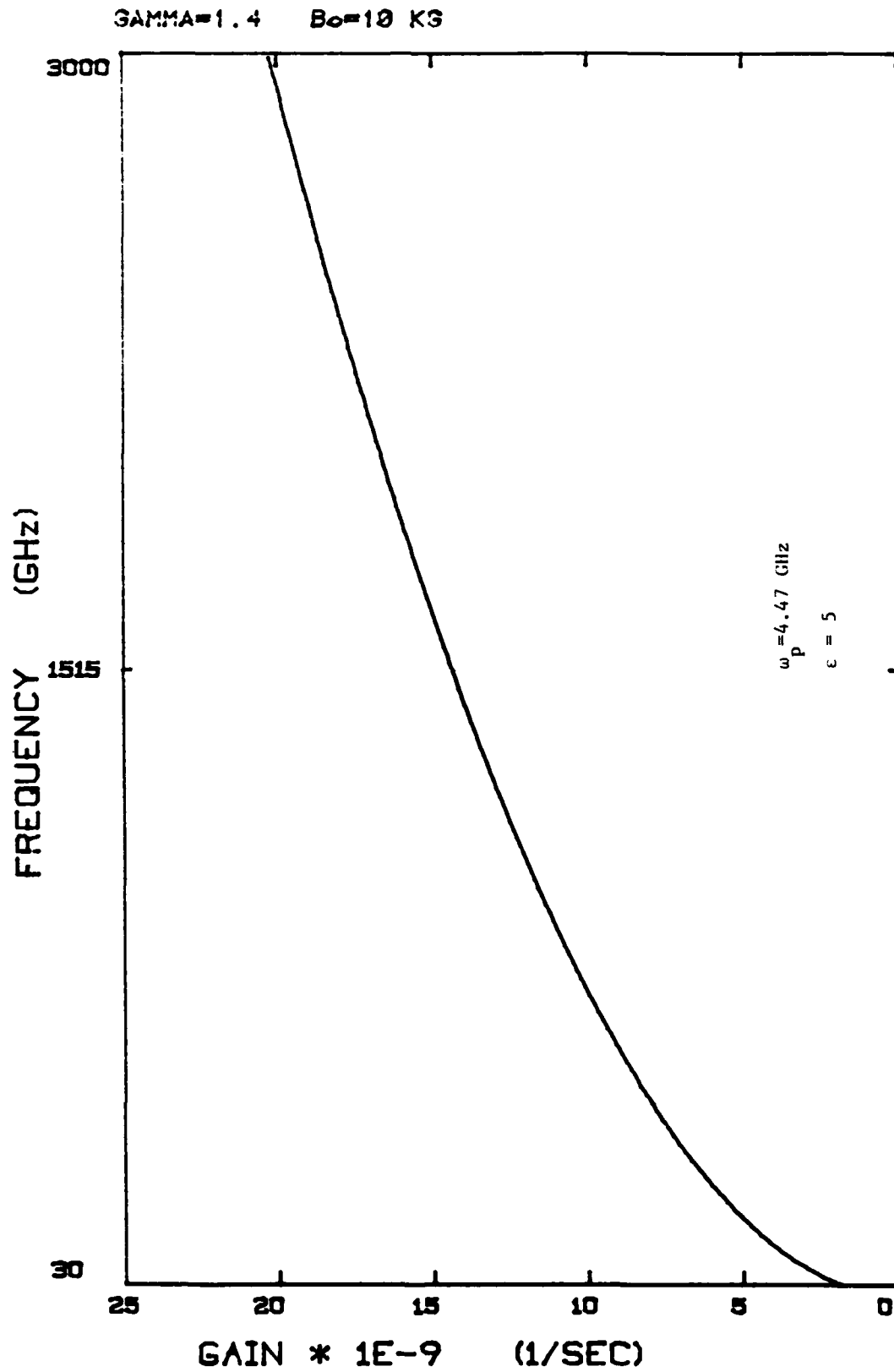


Figure V-2b Gain vs. frequency

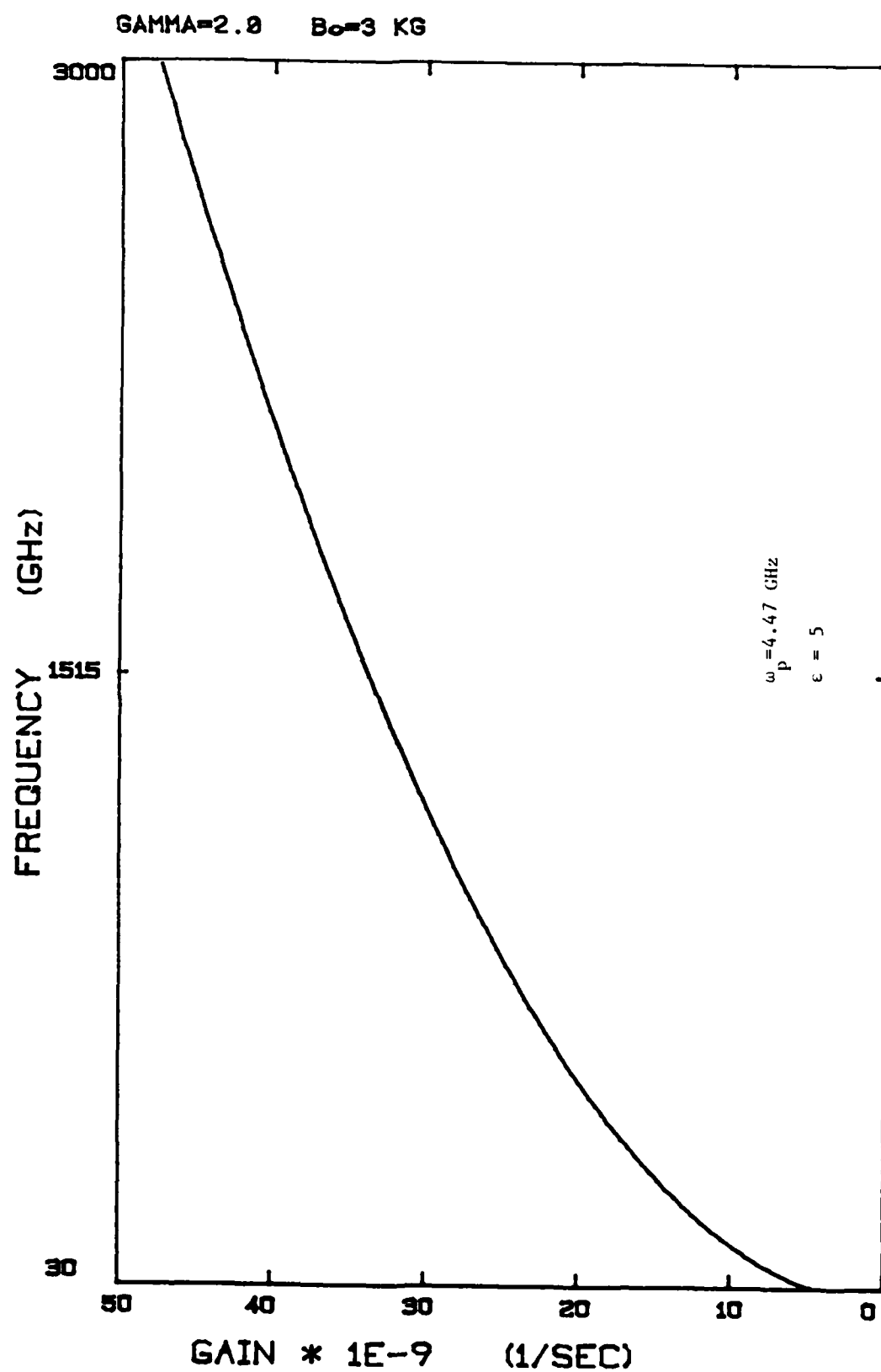


Figure V-2c Gain vs. frequency

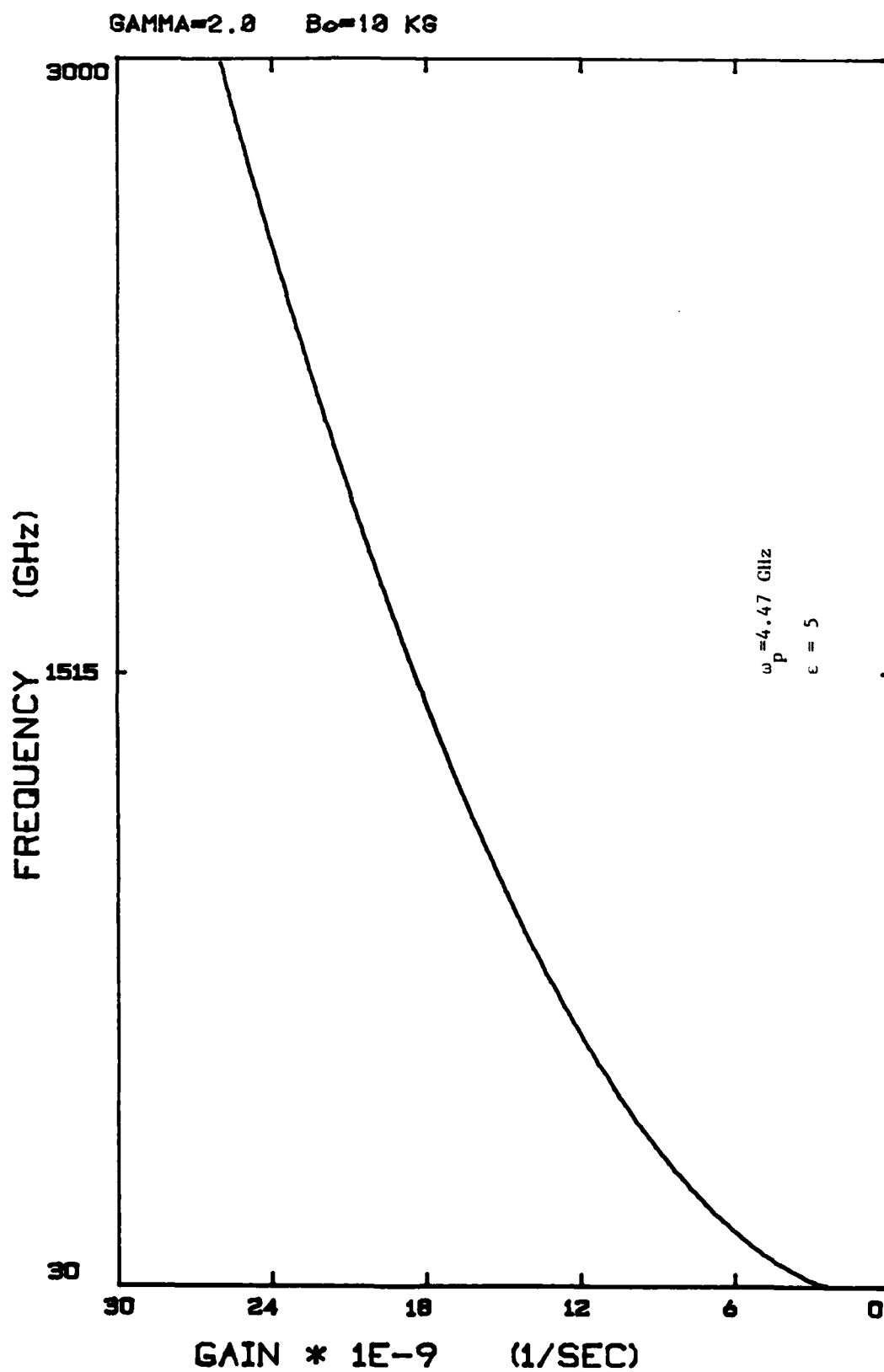


Figure V-2d Gain vs. frequency

252

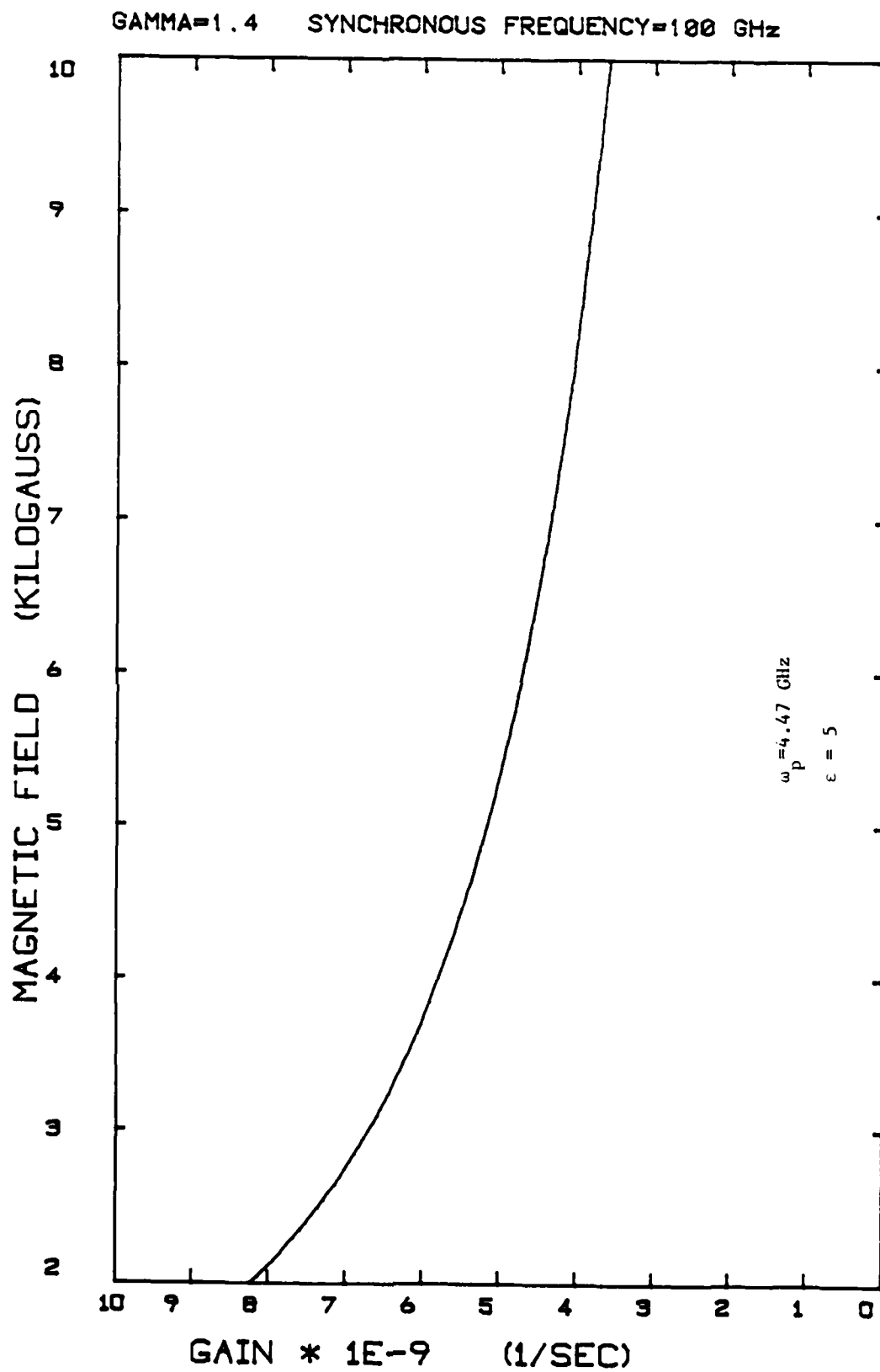


Figure V-3a Gain vs. applied magnetic field

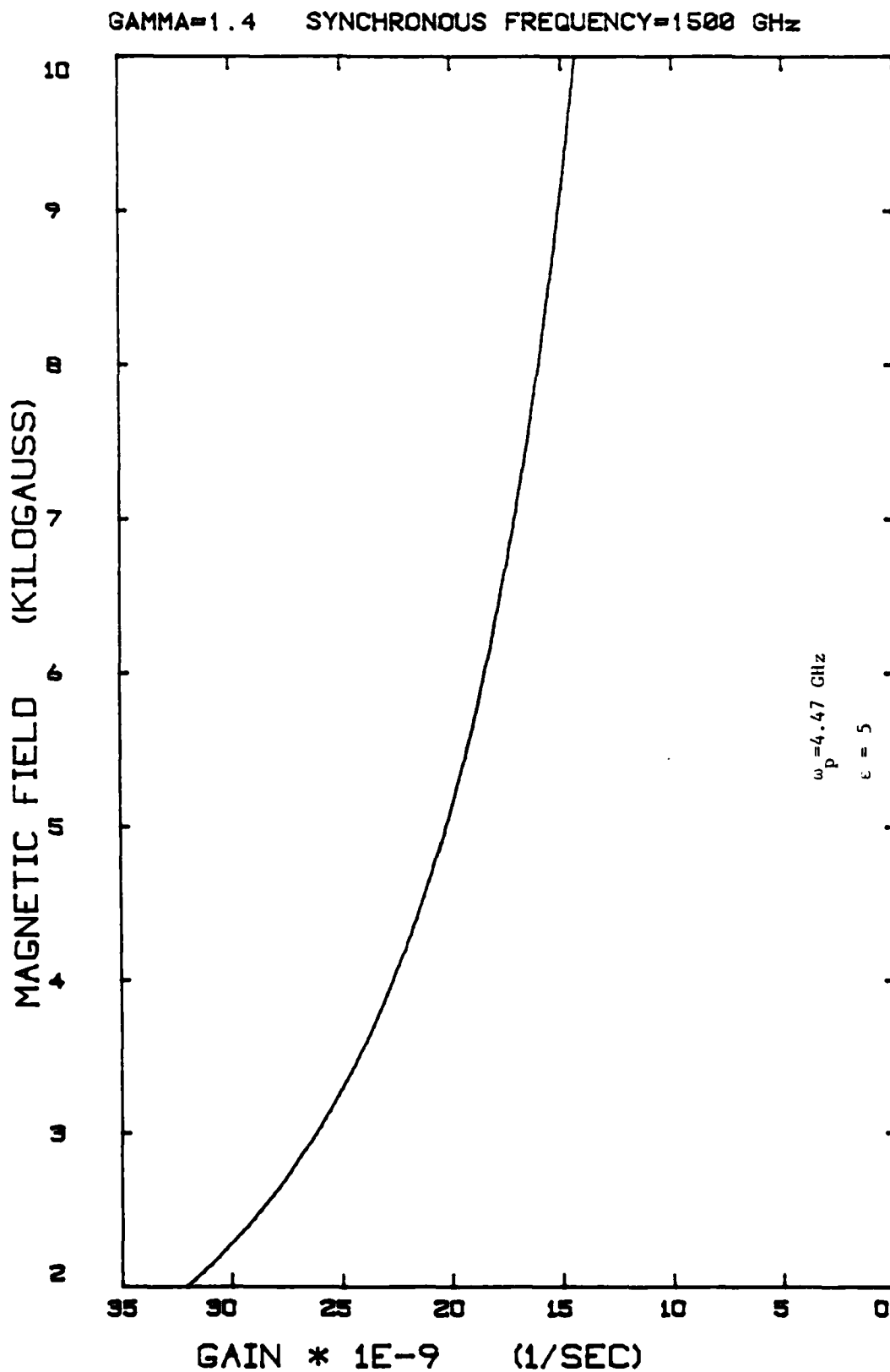


Figure V-3b Gain vs. applied magnetic field

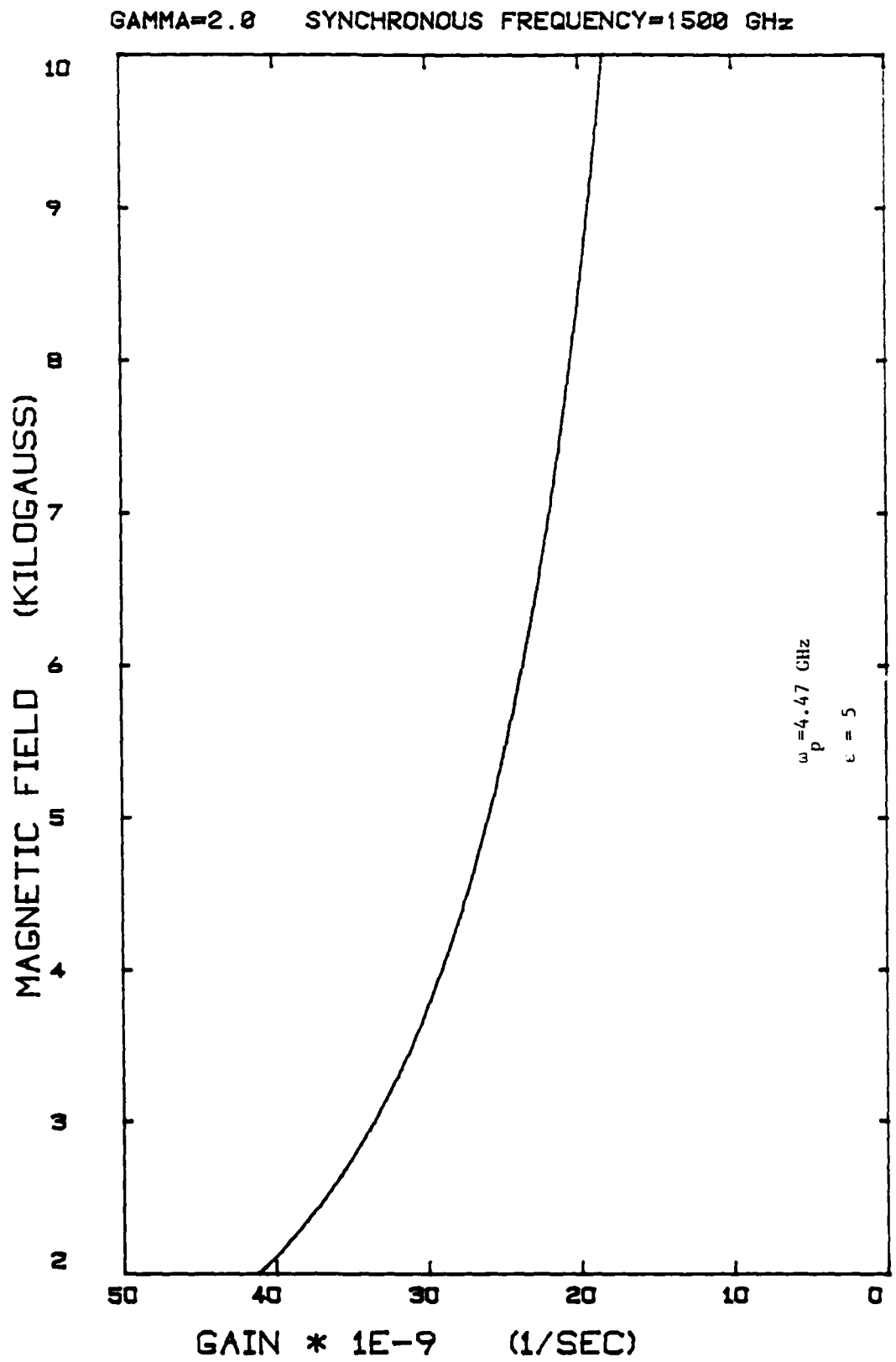


Figure V-3c Gain vs. applied magnetic field

✓

Chapter Six

VI.1 A Cerenkov-Cyclotron Free Electron Laser

Until this point, we have been concerned with understanding the character of the Cerenkov-cyclotron instability in the infinite medium. The focus has been on understanding the behavior of the gain function and on determining the topology of the roots in the ω - k plane. Let us now address the issue of a real Cerenkov-cyclotron device.

✓ Our theory has considered an electron beam passing directly through the dielectric medium. While a system of this design may prove practical using gaseous dielectrics and extremely relativistic beams ($\gamma \sim 20$ -?), it will not be given attention here. Rather, we will imagine the electron beam passing close to, but not through, a finite, dielectric structure. One possible configuration is shown schematically in figure VI-1. It employs a semi-infinite, dielectric slab. An electron beam of circular cross section and diameter "b" passes through the vacuum channel in the guide. Above threshold, Cerenkov radiation is excited in the dielectric lining. Consideration of the transverse boundary value problem shows that such radiation is evanescent in

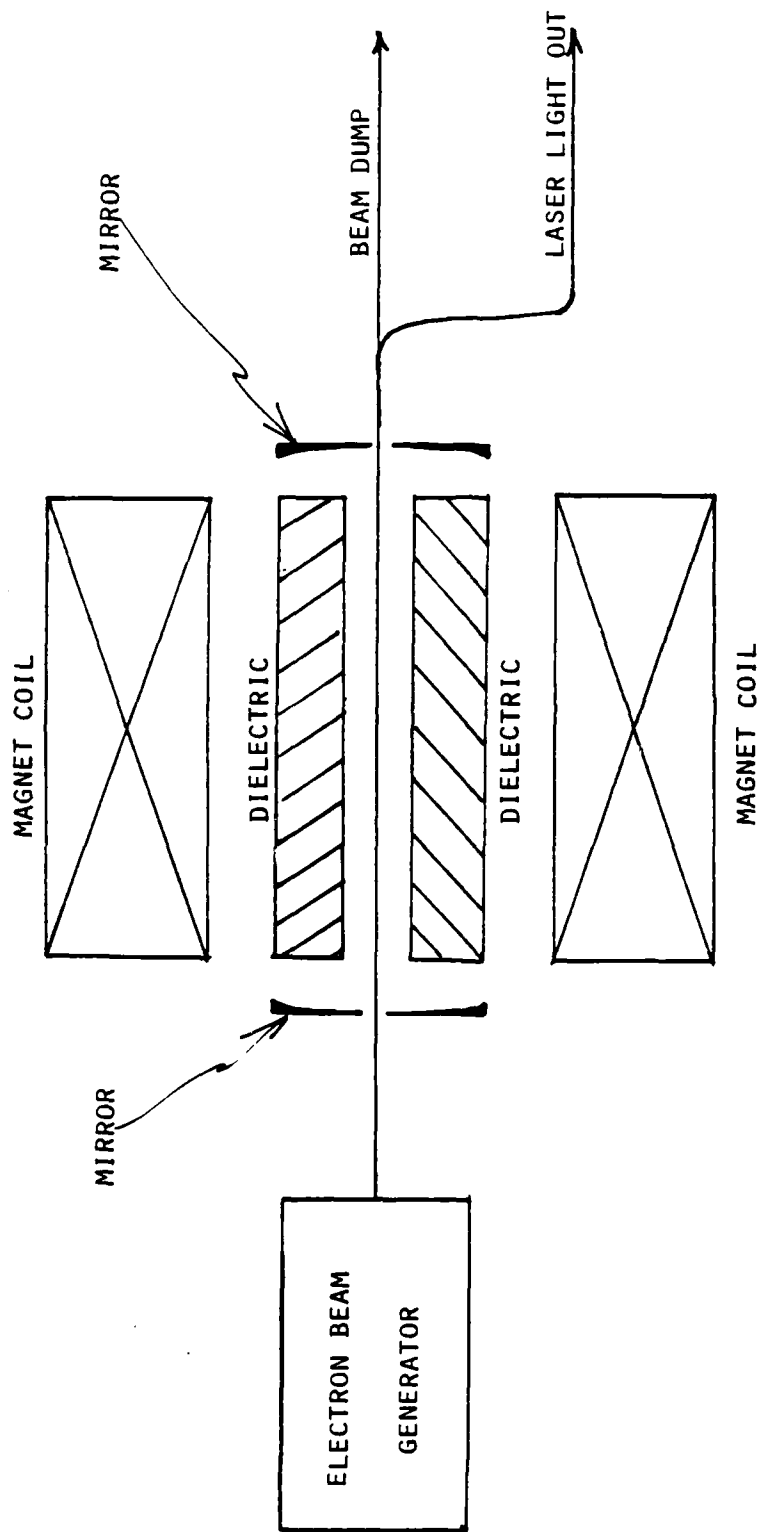


Figure VI-1 Schematic of Cerenkov (-cyclotron) free electron laser

the vacuum region. The exact dependence is given by

$$E \sim e^{-2q d}$$

VI-a

where

$$q = \sqrt{k^2 - \frac{\omega^2}{c^2}}$$

and "d" is the distance to the dielectric wall.

It is to this decaying electromagnetic field that the slow waves couple. The fields are sketched in figure VI-2.

There is one further complication. A real electron beam cannot pass arbitrarily close to the vacuum-dielectric interface. Space charge effects are one reason for this. Early electrons caught on the insulating surface repel later electrons. We must therefore suppose a finite gap between the beam edge and the dielectric wall. This gap is of dimension "d" and has been included in figure VI-1.

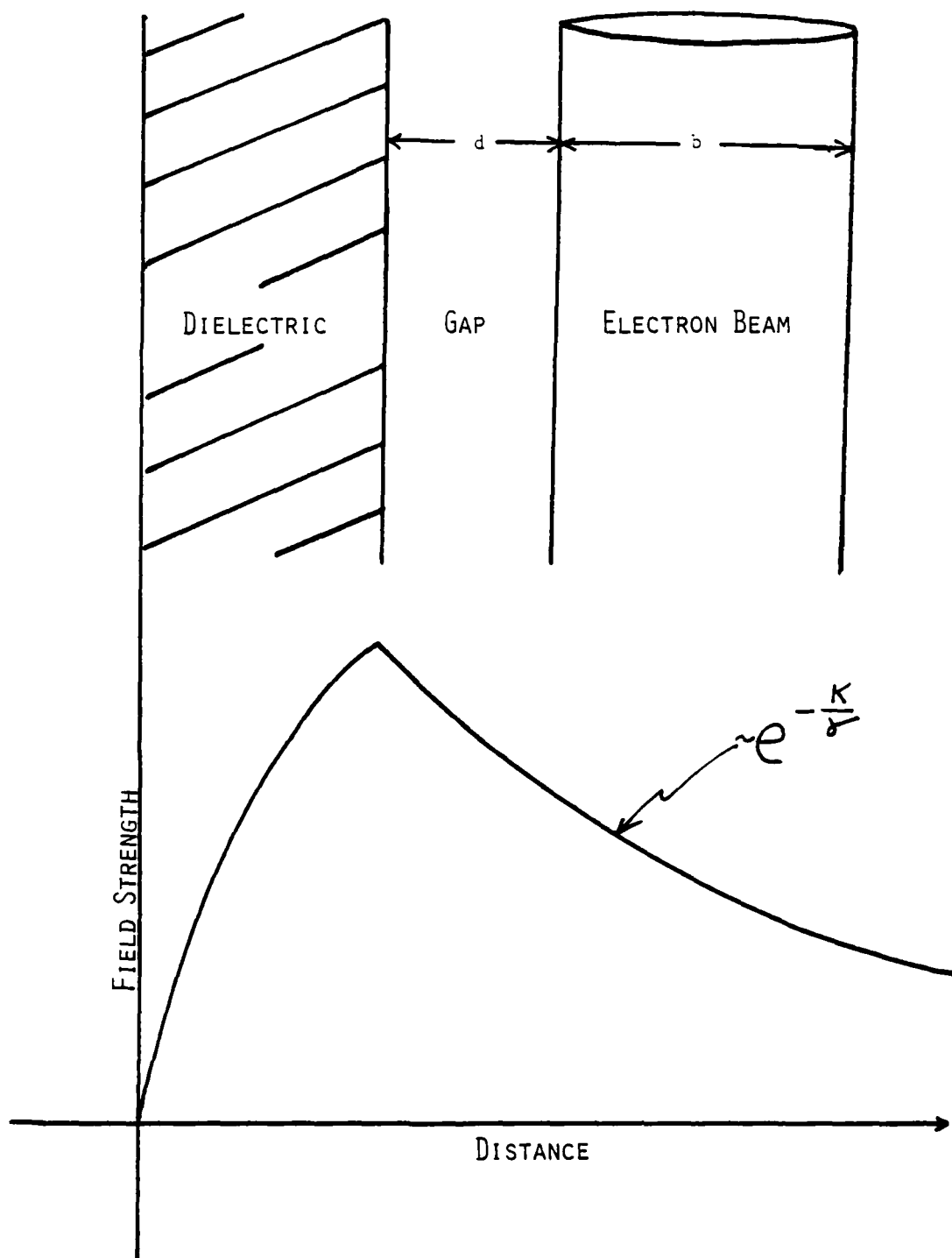
We have said that the beam couples to a degraded electromagnetic field in the vacuum region. Qualitatively, this system retains many of the features of the infinite medium. The strength of the interaction is lessened, however. We can incorporate this effect into our theory by defining an effective coupling parameter, $\omega_p^2\text{-eff.}$

We use equation VI-a to average the fields in the vacuum region over the beam cross section. This gives

$$\omega_p^2\text{-eff} = \frac{\omega_p^2 e^{-2q d} (1 - e^{-2q b})}{2q b}$$

or

258



VI-2 Field strength vs. distance (arbitrary units)

here, the strength of the interaction depends on the fields which the beam actually "sees" in the hole.

Obviously, beam optics plays an important role in this device. Tight, well focused beams and narrow gaps lead to better coupling according to equation VI-a. Wide beams and large gaps yield less gain.

The best electron beam generator and focusing available today would permit us $b=50$ microns and $d=10$ microns for the beam diameter and gap size, respectively. These figures could be as large as 1 centimeter and 1 millimeter, however. We will use these values to define a "best case" and a "worst case." Both cases will be examined.

Let us next use our effective coupling strength to determine the gain characteristics of the system. Substituting into equation V-b we find

$$\Gamma = \text{gain} = \sqrt{\frac{e^{-2gd}(1 - e^{-2gb})}{2gb}} \times \omega_r$$

At synchronism, g can be rewritten to give

$$g = \frac{k}{r} = \frac{2\pi}{\lambda \beta r}$$

Examination of this expression reveals one of the most serious limitations to short wavelength operation. Coupling strength

✓

falls off at the shorter wavelengths until the instability is quenched. Growth at the very shortest wavelengths vanishes simply because there is not enough field in the beam region to drive the interaction.

Let us try to understand more precisely the limitations imposed by this coupling problem. We define the reciprocal quality of the system by

$$\frac{1}{Q_{\text{Theory}}} = \frac{\text{Power lost}}{\text{Energy Stored}} = \frac{\Gamma}{\omega_K}$$

It is this number which carries information about the feasibility of a real laser. Assigning a phenomenological Q-laser to the cavity shown in figure VI-1, we require that

$$Q_{\text{Laser}} > Q_{\text{Theory}}$$

for break-even gain or better. That is, we require that the growth of the wave be great enough to offset frequency-dependent losses in a real, optical system.

For typical microwave cavities, a Q of 1k is considered small. 10k is reasonable and 1m is quite large. For submillimeter and far infrared operation, the figures may be a factor of ten greater. We will take the range 10k to 100k as characteristic of a realistic laser cavity.

Our next step, then, is to examine the reciprocal Q of our bounded system. We plot 1/Q versus 1/gamma in figure VI-3 for two

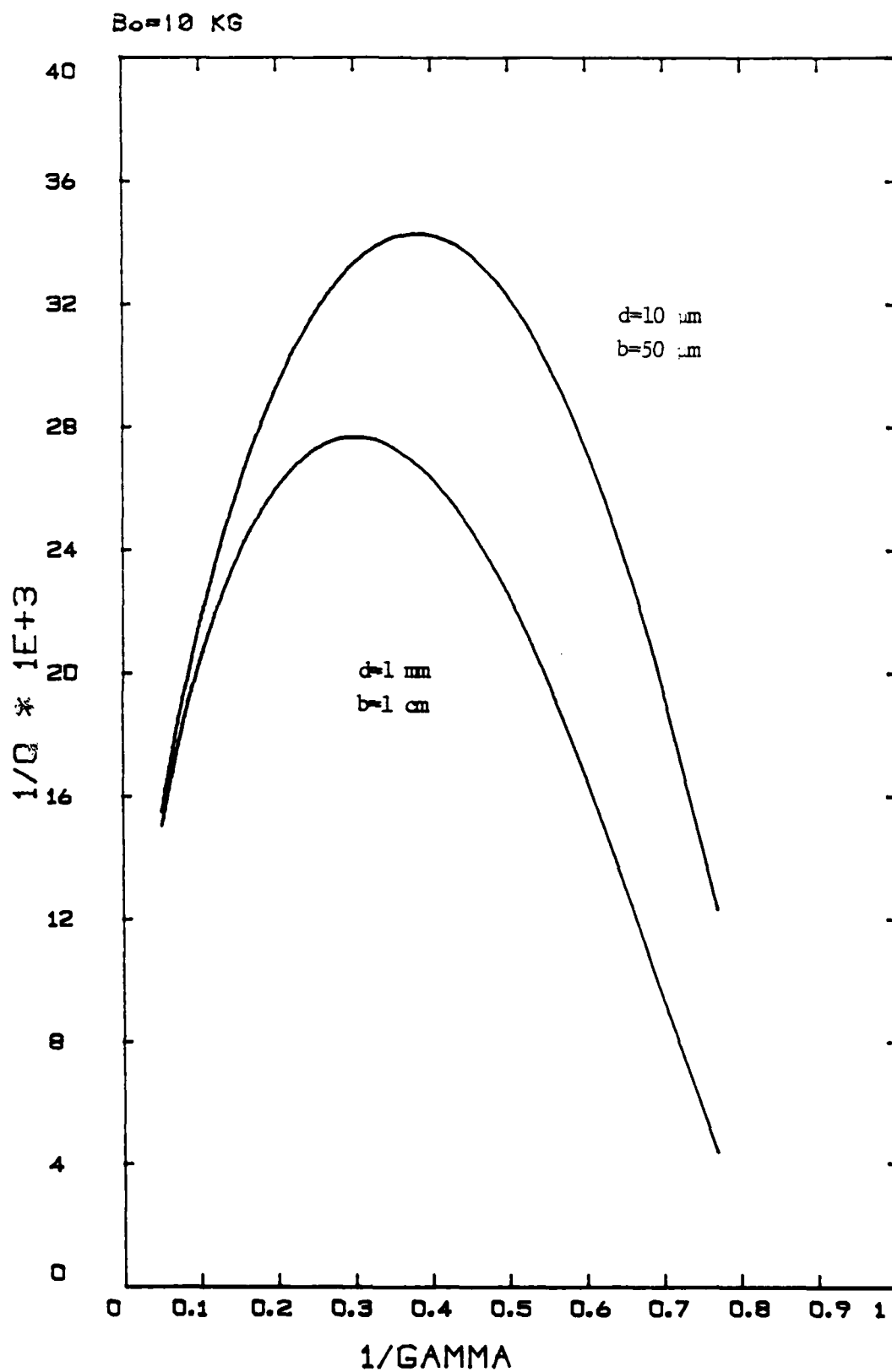


Figure VI-3 Reciprocal Q vs. reciprocal beam energy

262

✓

✓

values of applied field. The frequency is governed by the requirement of synchronism and so varies along the curve.

At the extremes, the reciprocal Q falls to zero. With it goes the possibility of extracting energy from the beam in these limits. For small $1/\gamma$, this drop reflects the $1/(\gamma)^{1.5}$ dependence of the gain in the high energy limit. As $1/\gamma$ approaches unity, the drop is more abrupt. This is a threshold effect.

The function reaches a broad maximum in the neighborhood of $\gamma=0.7$. This suggests that beams in the range 300-600 KeV couple most effectively to the radiation field. These are modest beam energies. A device capable of producing such beams could be quite compact. And since synchronous frequency decreases with increasing beam energy, there seems to be no compelling reason to pursue very high energy operation⁹. Certainly this is important for fusion applications where space and device accessibility are at a premium. It is also a clear economic advantage.

✓

At the maximum, figure VI-3 predicts a Q -theory of about 500. We have said that laser Q 's of many times this figure are quite reasonable. We see, then, that the Cerenkov-cyclotron instability is powerful. The effect can drive even modest resonators to yield substantial growth.

Another configuration of current interest is the dielectric-lined circular waveguide. All the arguments of decaying field

✓

and effective coupling still hold here. In addition, there is the problem that the plane wave dependence assumed throughout the theory may no longer be valid. In general, this discrepancy introduces a factor E_z^2/P into the gain where P is the power and the axial electric field is governed by the boundary value problem. We mention this problem but will not treat it in any way here. The problem of finding form factors which extend calculations in the infinite medium to specific geometries is being investigated. It may be possible to develop a general, theoretical machinery based simply on the dispersion relation or its derivatives. This would, of course, be of great use in the study of different resonator structures.

83/8

264

✓

✓

Chapter Seven

VII.1 Summary

We have defined and understood a fundamental plasma instability: the Cerenkov-cyclotron instability. The effect arises when the negative energy cyclotron wave on a superluminal electron beam resonates with an electromagnetic wave in the medium.

Our model was a simple one. We considered plane electromagnetic waves propagating through an infinite, cold sea of electrons. A cold fluid theory described the interaction and the dispersion relation derived in chapter three governs the phenomenon.

Although forward propagating radiation cannot couple to the slow space charge wave, we saw in chapter four that it does couple to the slow cyclotron wave. The gain of this system is modest, however. Growth rates of 10^8 to 10^9 (1/sec) were calculated. We argued in analogy with the pure Cerenkov results that propagation at an angle other than zero might improve the situation.

✓

This suspicion was confirmed in chapter five. There we calculated peak gains which are one to two orders of magnitude greater than those of the forward propagating case. Gain is an increasing function of frequency for general propagation. The gain rises approximately as the frequency to the one half power. This is less restrictive than the space charge results. There, the gain rose as the one third power of the frequency. It is also an improvement over the case of the forward propagating wave where the gain fell with frequency.

We derived an explicit relation defining the infinite magnetic field limit. We found the simple result that the square of the cyclotron frequency must be much greater than the square of the beam plasma frequency. In this limit Cerenkov-cyclotron growth becomes negligible. The slow space charge interaction dominates.

✓ Finally, we considered the possibility of a real Cerenkov-cyclotron device. We saw that one of the major problems with these devices is the coupling problem. Electron beam modes must couple to radiation fields which evanesce in the beam region. Defining an effective coupling parameter, we were able to incorporate this problem into the theory. The reciprocal Q of the interaction was introduced. We required that the Q of our laser cavity exceed the theoretical Q associated with the instability. Laser Q 's of about five hundred were indicated and these are quite reasonable.

VII.2 The Transition Wavelength

Perhaps the most serious approximation made in this paper has been the neglect of thermal spread in the electron beam. The use of a cold fluid description limits the applicability of the theory. We must now define that limitation precisely.

Our cold beam description implies a delta function distribution in velocity space at $\frac{\omega}{ck_{\text{rer}}} = \beta_0$. Cyclotron waves on the beam add to this picture by placing spikes at

$$\beta_0 = \frac{v_0}{c} = \frac{k_{\parallel} v_0 \pm \Omega_c}{ck_{\text{rer}}}$$

This is an idealization. A distribution function characterizing any real electron beam has finite width. We denote that spread in velocity space by $\Delta\beta$ and show cold and warm beam distributions in figure VII-1.

We now have a criterion by which to evaluate the coldness of the beam. We require that the spread in velocity owing to thermal motion of the electrons be small compared to the spread associated with the normal mode of oscillation. Symbolically,

$$\Delta\beta < \frac{\Omega_c}{ck_{\text{rer}}} \quad \text{VII-a}$$

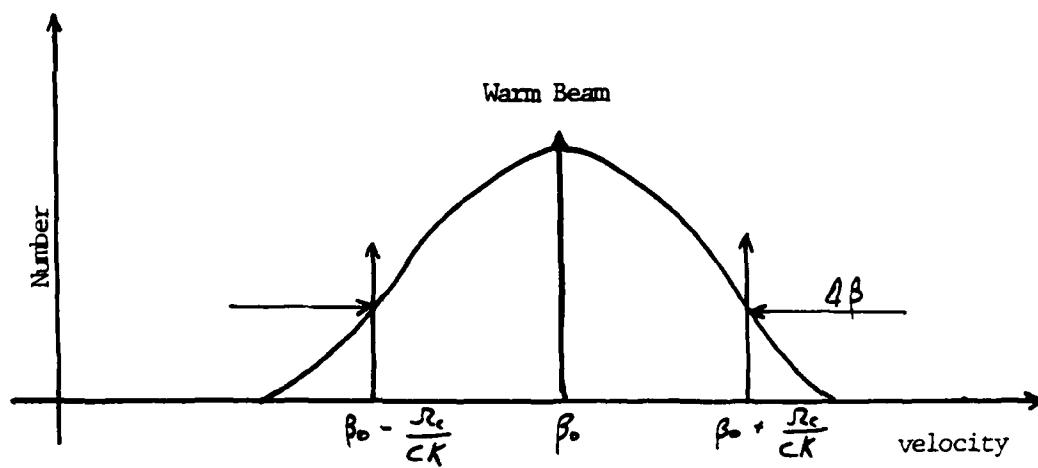
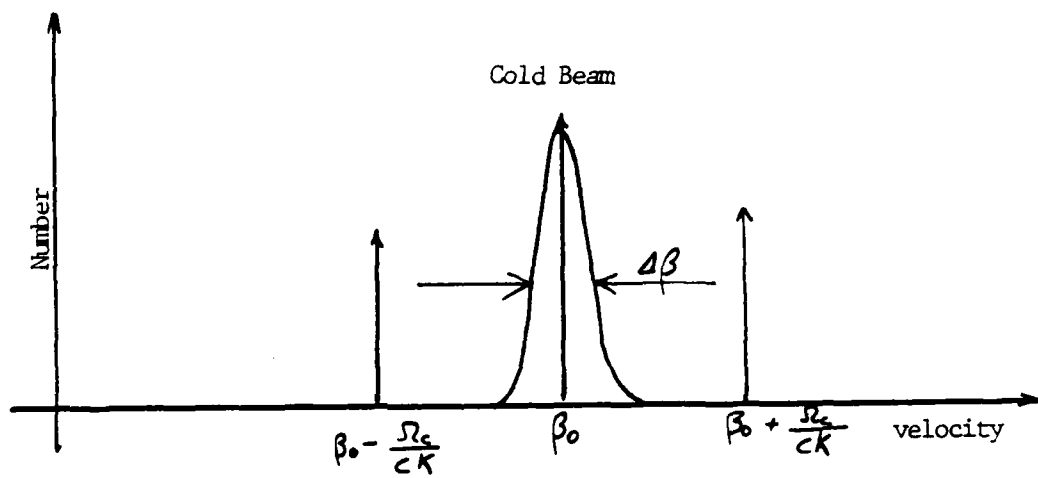


Figure VII-1 Cold and warm beam distribution functions

By definition we also have

$$\Delta\beta = \frac{\Delta\sigma}{\beta\sigma^3}$$

and

$$K_{nr} = \frac{2\pi}{\lambda_{desired}}$$

Substituting these into equation VII-a, we require

$$\frac{2\pi\Delta\sigma}{\beta\sigma^3} < \frac{eB_0\lambda_{desired}}{r mc^2}$$

$$\lambda_{desired} > \frac{2\pi mc^2}{eB_0} \frac{\Delta\sigma}{\beta\sigma^2} = \lambda_{cyclotron} \frac{\Delta\sigma}{(\beta\sigma)^2} \equiv \lambda_{transition}$$

where $\lambda_{cyclotron} = \frac{2\pi mc^2}{eB_0}$ is the Larmor radius.

Wavelengths far in excess of the transition wavelength are well described by the present theory. Wavelengths slightly greater than λ -transition are qualitatively well described by our cold fluid theory although the actual gain may be reduced. Numerical analysis has shown this reduction to be on the order of fifty percent. Wavelengths below the transition are badly described by the present theory.

Since the gain extracted from a cold beam always exceed warm beam growth, it is of interest to specify the transition wavelength. This, in turn, will define the limit of applicability of the theory presented in this paper. Reasonable experimental parameters give a λ -cyclotron of one centimeter. Now $\beta\sigma$ is a number of order unity and so our transition wavelength depends

✓

crucially on the energy spread--48. A crude electron gun gives an energy spread of about one percent. Less than one percent is certainly attainable. We use this "worst case" value in our expression for λ -transition to give

$$\lambda_T \approx 100 \mu m$$

And so wavelengths far into the submillimeter are well described by our cold beam analysis. This is extremely promising. We have seen that substantial gains are predicted. The discovery that these predictions hold for wavelengths as short as one hundred microns bodes very well for the device.

VII.3 Conclusions

Finally, we point out that a Cerenkov-cyclotron free electron laser is an intrinsically high frequency device. For a given beam energy, the intersection of the slow cyclotron line with the free wave dispersion relation occurs at a greater frequency than the intersection with the slow space charge line.

Also, an electron beam seems "colder" to cyclotron wave than it does to the space charge wave. We can see this by recalling the derivation of the transition wavelength presented above. Had we required that the distribution function lie between delta functions positioned not at $\beta_0 \pm \frac{\Omega_c}{c\hbar}$, but at $\beta_0 \pm \frac{\omega_p}{\gamma^{3/2} c \hbar}$,

- ✓

we would have found a transition wavelength of about 500 microns. Since gain from a cold beam is always greater than gain from a warm beam, this is a great advantage.

we know that substantial gain is possible at high frequencies. We also know that problems associated with a real device can limit that gain. Having briefly examined one such problem, the coupling problem and found it to be tolerable, we conclude that the Cerenkov-cyclotron instability could be exploited to great advantage in a free electron laser system.

✓

REFERENCES

1. Cerenkov and Cerenkov-Raman Radiation Sources, John E. Walsh, in Physics of Quantum Electronics, eds. S. Jacobs and M. Scully, Vol. 7, p. 255, (Addison-Wesley 1980).
2. Cerenkov Radiation in Dielectric-Lined Waveguides, K.L. Felch, K.O. Busby, R.W. Layman, D. Kapilow, and J.E. Walsh, Appl. Phys. Lett. 38(8), 601 (1981).
3. I am grateful to Professor Christine Celata for the following.
4. Cerenkov Radiation in Dielectric-Loaded Waveguides, K.L. Felch, (Ph.D. Thesis), Dept. of Physics and Astronomy, Dartmouth College, Hanover, N.H.

Cerenkov Instability in a Relativistic Beam-Driven Waveguide, J.A. Bagger, (Honors Thesis), Dept. of Physics and Astronomy, Dartmouth College, Hanover, N.H.

Novel Sources of Coherent Radiation, Jacobs, Scully, eds., P.Q.E. 5 (1978).
5. Cerenkov-Cyclotron Instability, D. Kapilow and J.E. Walsh, Bull. Am. Phys. Soc. 25, 6 (1980).

- ✓
6. J.A. Bagger, Honors Thesis.
 7. Stimulated Cerenkov Radiation, John E. Walsh,
in Advances in Electronics and Electron Physics, ed.
C. Marton (Academic Press, to be published).
 8. This is not strictly true. The gain is proportional to
the detuning from synchronism.
 9. This, for a cold beam in the collective regime. Consi-
deration of the single-particle problem or of the warm
beam problem may prove this conclusion false.
- ✓
- ✓

✓

Submitted to Applied Physics Letters
for summer 1982 publication.

A High Power Cerenkov Maser Oscillator

S. Von Laven, J. Branscum, J. Golub, R.
Layman, J. Walsh, Dartmouth College, Hanover,
New Hampshire 03755

An electron beam driven,
dielectric-lined waveguide has produced
30-100 kW of coherent radiation over an
octave band on the TM_{01} mode of the
waveguide. Operation on the TM_{02} mode has
been realized as well. Impedance mismatches
at the ends of the liner section provide a
reflected signal, which undergoes
amplification during successive passes.

✓

Recent experimental work in the production of stimulated
Cerenkov radiation has upheld predictions with regard to output
frequency and determined rough threshold beam parameters.¹ New
data demonstrate the high power and wide tunability obtainable
through the Cerenkov interaction.

The Cerenkov radiation that is generated when a beam of
charged particles passes at superluminal velocity through or near
a dielectric can, in turn, modulate the beam. Some of the
radiation must be constrained to propagate in the volume occupied

✓

by the beam. The nature of the beam modulation is an axial bunching, which enhances the intensity of subsequent radiation. Beams of sufficient current density, which are strongly coupled to the radiation field, will achieve a growth rate for this Cerenkov instability sufficient to overcome the various loss mechanisms. Discussion of the theoretical background pertaining to this device has been presented earlier.²

The work described here employs a pulsed, 1-40 ampere beam of 100-250 keV electrons directed along the axis of a dielectric lined circular waveguide. The pulse duration is about four microseconds. Design details of the electron beam generator are described in an earlier article.¹

✓ The waveguide geometry is such that lowest order, azimuthally symmetric, transverse magnetic modes will have a large axial electric field amplitude in the beam volume, even when the phase velocity of the mode is less than c . The strength of the Cerenkov interaction is greatest for phase velocities slightly less than the beam velocity. Since the phase velocity of any of the waveguide modes decreases with increasing frequency, a favorable scaling law is obtained for output frequency with respect to beam energy for a given dielectric liner.

Quartz ($\epsilon=3.78$), stycaat ($\epsilon=5$), and boron nitride ($\epsilon=4.2$) liners of several thicknesses have been employed. Frequency measurements are made with a mechanically driven, free space, Fabry-Perot interferometer.³ Power measurements are made with

✓

calibrated lengths of a lossy material and either square-law detector diodes or a pyro-electric energy meter.

For almost every dielectric liner used, the fundamental output frequency is near the frequency at which the TM₀₁ mode is synchronous with the beam. Figures 1a, 1b, and 1c show the frequencies obtained in 12.5 mm diameter waveguide. A large systematic offset is noted for the case of the 3 mm quartz liner. A surface charge build-up on the quartz is suspected of decelerating the beam to velocities synchronous with the observed output. The problem nearly disappears for 2 mm quartz. The longitudinal electric field associated with the 1 mm liner geometry is too weak to give good coupling for the beam energy employed. At the higher voltages and currents which are necessary, the beam generator's performance is less consistent. Thus the probability of recording a noise-free interferogram, requiring approximately 1000 shots, is low.

✓ The general behavior of the power as a function of beam current for the 2 mm quartz liner is shown in Figure 2. In a separate, absolute measurement with the same liner geometry, a 12 A, 115 keV beam generated 30 kW of radiation at 50 GHz. The power is consistent with the power which would be produced by a strongly bunched beam ($n=n_0 \exp\{-i(\omega t - kz)\}$).⁴ Powers up to 100 kW were obtained at lower frequencies for 3 mm thick boron nitride in the 12.5 mm diameter waveguide. Power is often sufficient to cause atmospheric breakdown in X-band waveguide.

✓

The range of frequencies obtainable on a single mode has reached nearly an octave. In some of the 12.5 mm diameter waveguide experiments and in a 9.5 mm waveguide experiment, it has been possible to suppress the TM01 mode and observe coupling to the TM02 mode. (Fig. 1c,d) Frequencies between 100 and 120 GHz have been attained. The power appears to be less than that obtainable on the TM01 mode, but still significant. Output of still lower apparent power has been observed through a 200 GHz filter with the 2 mm quartz liner 12.5 mm waveguide. All the shorter wavelength power measurements are made with 1N53 diodes in a Ka band mount. This system is difficult to calibrate when it is far out of band. The voltage response generated at these short wavelengths would have corresponded to one-tenth to one-quarter of the power measured in the 8 mm region, if the wavelengths had been in the design band of the mount. Hence, at the shorter wavelengths the output power would, at a minimum, be in the one kW range.

✓

The Cerenkov interaction is not continuously tunable within a given band in the present experiment. Signals which undergo longitudinal reflections and make many passes through the liner section of the waveguide without suffering destructive interference reach large amplitude, as in a conventional laser. Thus discrete cavity modes are observed rather than a continuous waveguide spectrum.

Assume that output is generated when the beam is at its peak energy, as in Figure 3a. A small increase in the peak energy

✓

which is insufficient to reach synchronism with the adjacent longitudinal mode, often leads to output on the original mode. However the output is now generated when the beam energy is at its original peak value, earlier or later in the pulse than the new peak, or both earlier and later. (Figures 3b, 3c, and 3d)

If the effective reflectivity at either end of the liner section is reduced, a higher beam voltage threshold is observed. As shown in Fig. 4a a copper liner with transverse dimensions identical to the dielectric liner is positioned to act as an upstream mirror. A lower reflectivity downstream is provided by a normal dielectric-vacuum interface. The net reflectivity is reduced by removing the copper liner or by tapering the downstream inner diameter of the dielectric liner outward. The data in Fig. 4b indicate the increased threshold due to tapering. A very large current increase could probably substitute for the voltage increase. However, such a current is not available from our present device.

In summary, Cerenkov devices are a potentially useful member of the family of millimeter wave sources. Peak output power at longer wavelengths is comparable to that of other sources, such as gyrotrons,⁵⁻⁷ and the peak efficiency (1-10%) is what would be expected for a non-optimized traveling wave device. It also performs well in the regime where the wavelength is less than the transverse dimension of the guide. Thus, it also shows promise as a lower mm and sub-mm source.

Support by AFOSR contract 77-3410D is acknowledged.

✓
¹K.L.Felch, K.O.Busby, R.W.Layman, D.Kapilow, and J.E.Walsh,
Appl. Phys. Lett. 38,601 (1981).

²J. Walsh, "Stimulated Cerenkov Radiation," in "Advances in
Electronics and Electron Physics," vol. 58 (Academic Press, New
York, 1982).

³D.Wise, Master's Thesis (1981) - Available from Dartmouth
College Thayer School of Engineering.

⁴S. Von Laven, Ph.D. Thesis (1982) - Available from
Dartmouth College Physics Department.

⁵R. S. Symons and H. R. Jory, "Cyclotron Resonance Devices,"
in "Advances in Electronics and Electron Physics," vol. 55
(Academic Press, New York, 1980).

⁶J. L. Hirshfield, "Gyrotrons," in "Infrared and Millimeter
Waves," vol. 1 (Academic Press, New York, 1979).

⁷A. A. Andronov, V. A. Flyagin, A. V. Gapanov, A. L.
Gol'denberg, M. I. Petelin, V. G. Usov and V. K. Yulpatov,
Infrared Phys., 18, 385 (1978). ✓

✓

Figure Captions

Fig. 1. (a) The frequency of a coupling mode is plotted vs. the synchronous beam voltage to give a "tuning curve". The frequency measurements made with quartz liners of one, two, and three mm thicknesses are displayed along with the TM_{01} tuning curves for those liners. The guide diameter, $2b$, is 12.5 mm. (b) Data and TM_{01} tuning curves for two and three mm thick boron nitride liners in 12.5 mm guide. (c) TM_{01} and TM_{02} tuning curves and data for a three mm styrcast liner in 12.5 mm guide. (d) TM_{01} and TM_{02} tuning curves and data for a 1.5 mm boron nitride liner in 9.5 mm guide.

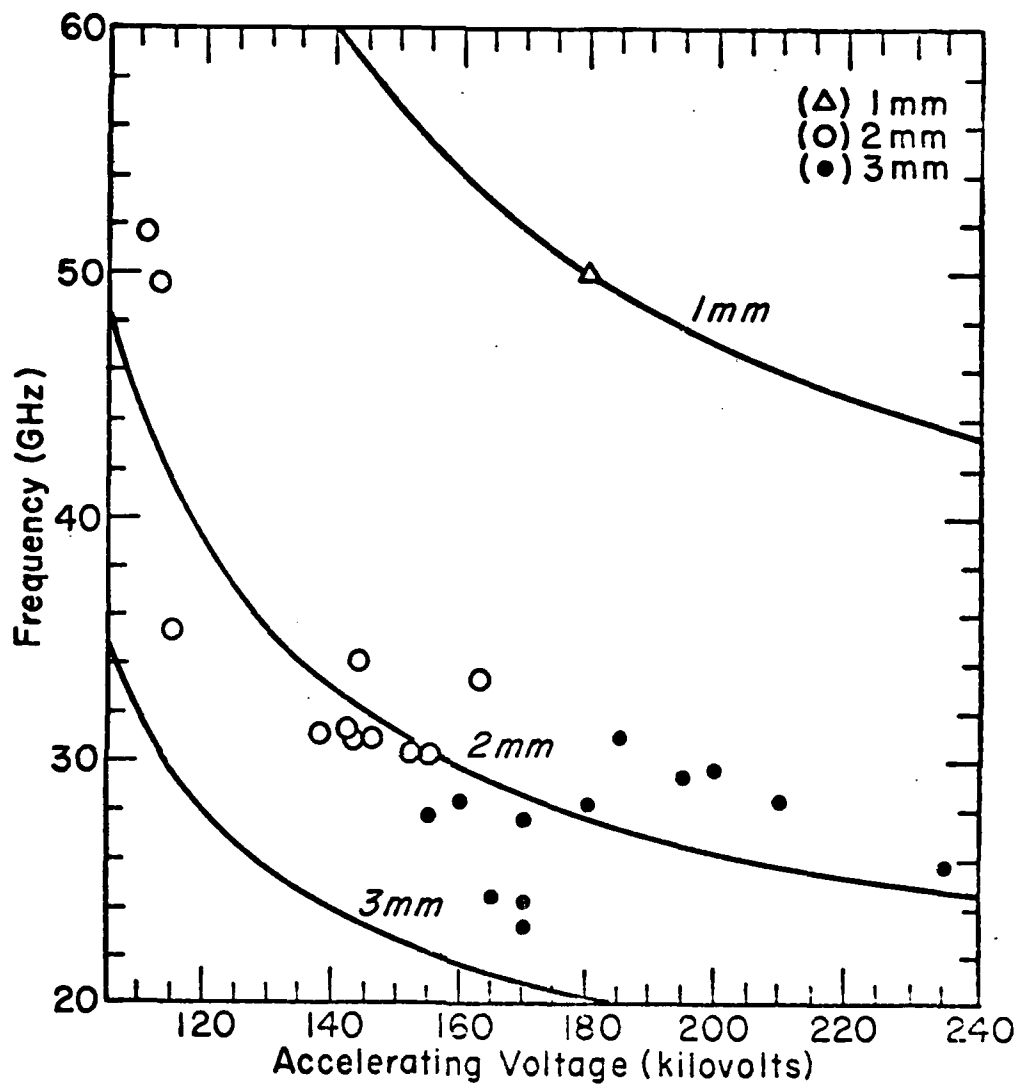
✓
Fig. 2. Saturating power and measurements (+) for two mm boron nitride with a 150 keV beam. The saturating power is evaluated assuming a six mm beam diameter.

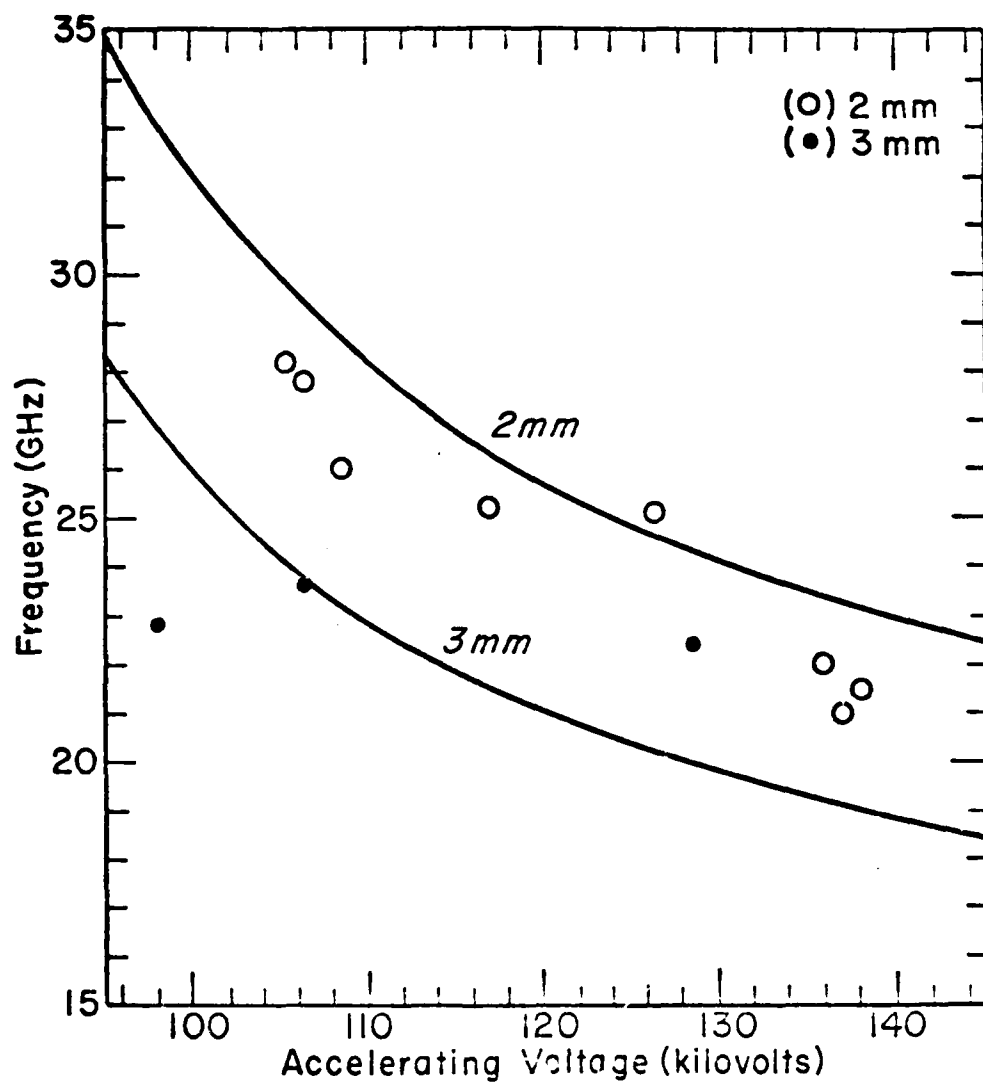
Fig. 3. The microwave output (bottom trace) occurs when the beam velocity (top trace indicates voltage) is synchronous with one of the axial modes of the resonating cavity, not necessarily at the peak beam voltage. (One microsecond per division.)

Fig. 4. (a) The cavity formed by the metal-dielectric and vacuum-dielectric interfaces at the ends of the liner section has a

✓

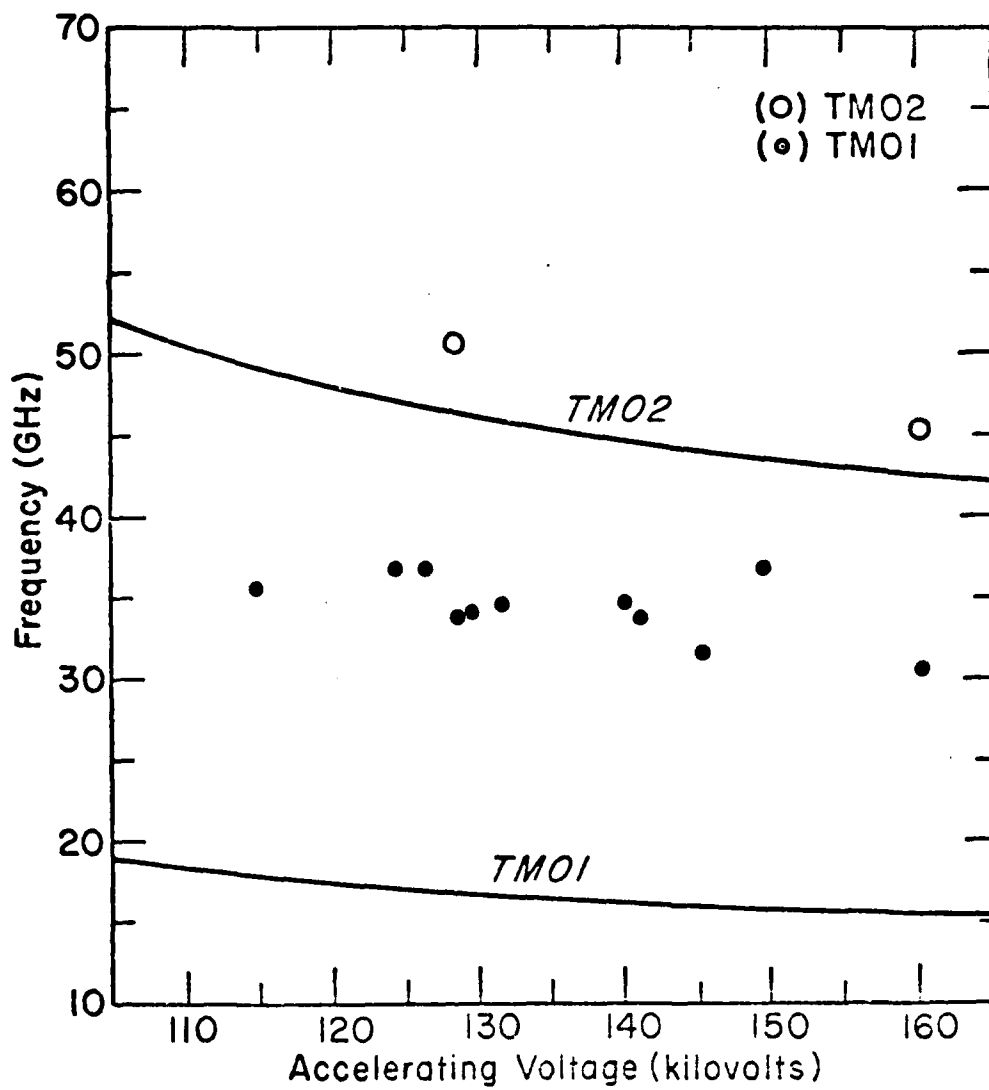
sufficient Q for oscillation, given the high gain of the Cerenkov maser. (b) The threshold for oscillation rises for a cavity with lower Q . The lower Q is obtained with a short taper at the downstream end of the liner to reduce the reflected signal.





283

✓



AD-A126 990

LARGE AMPLITUDE ION WAVES(U) DARTMOUTH COLL HANOVER N H
DEPT OF PHYSICS AND ASTRONOMY J E WALSH 19 NOV 82
AFOSR-TR-83-0266 AFOSR-77-3410

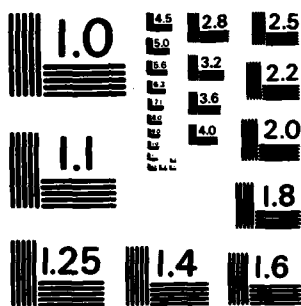
44

UNCLASSIFIED

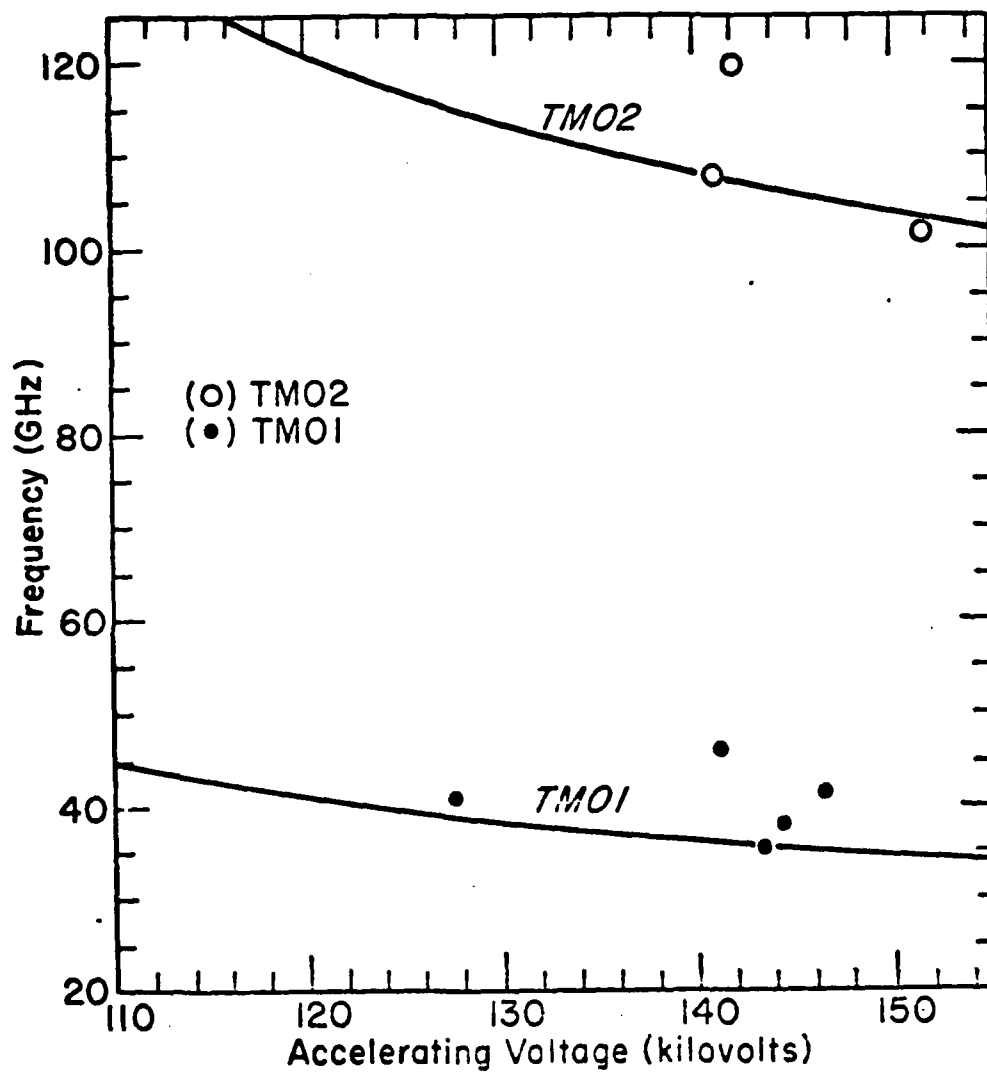
F/G 20/7

NL

						END DATE FILMED 5 83 DT
--	--	--	--	--	--	-------------------------------------

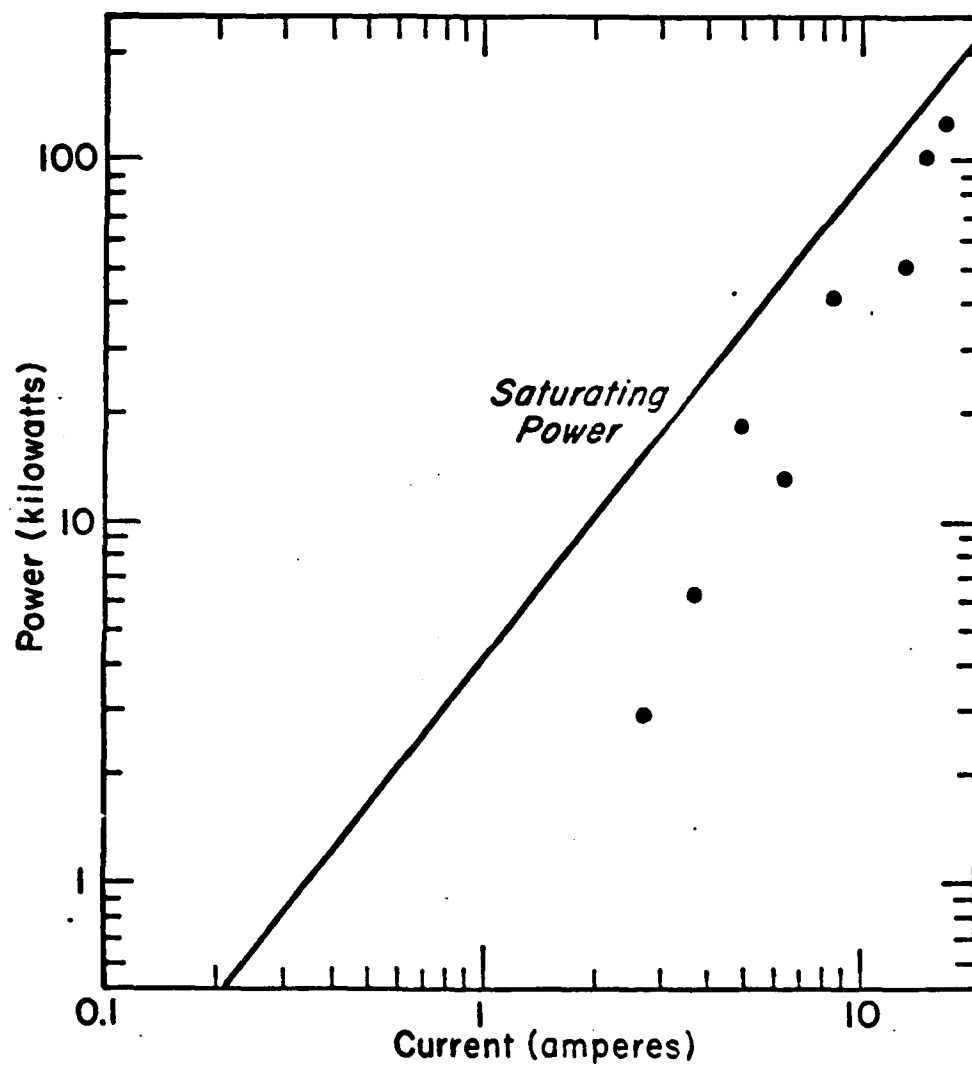


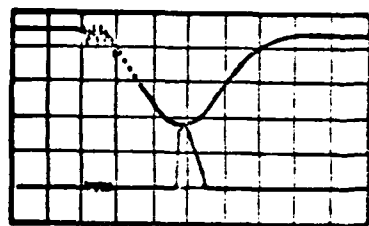
MICROCOPY RESOLUTION TEST CHART
NATIONAL BUREAU OF STANDARDS-1963-A



285

✓





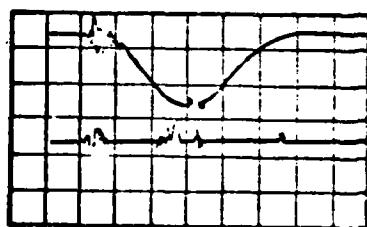
50 kV/div, 20 mV/div

(a)



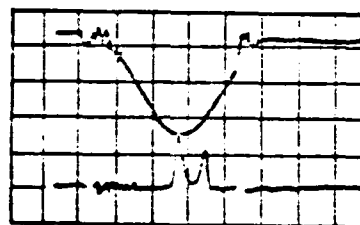
50 kV/div, 100 mV/div

(b)



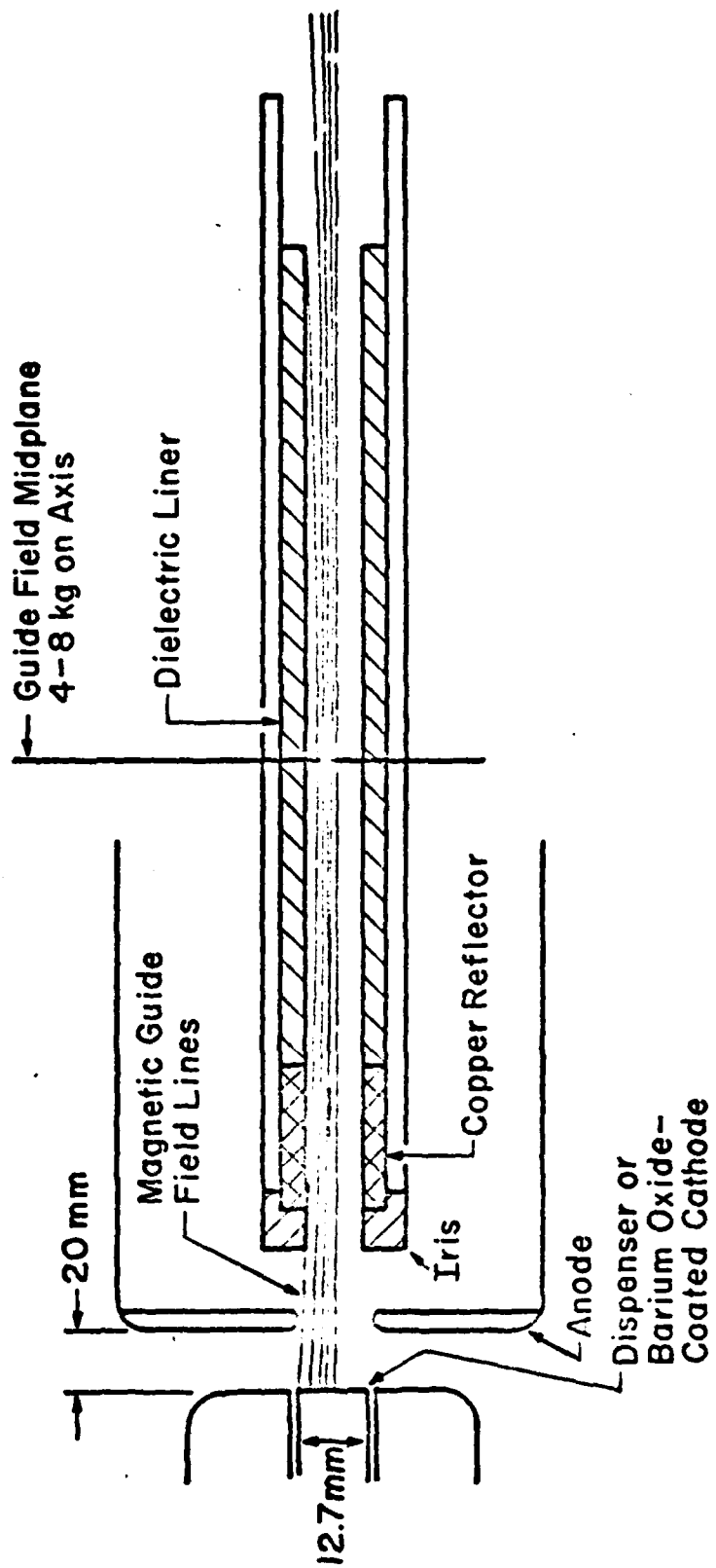
100 kV/div, 50 mV/div

(c)

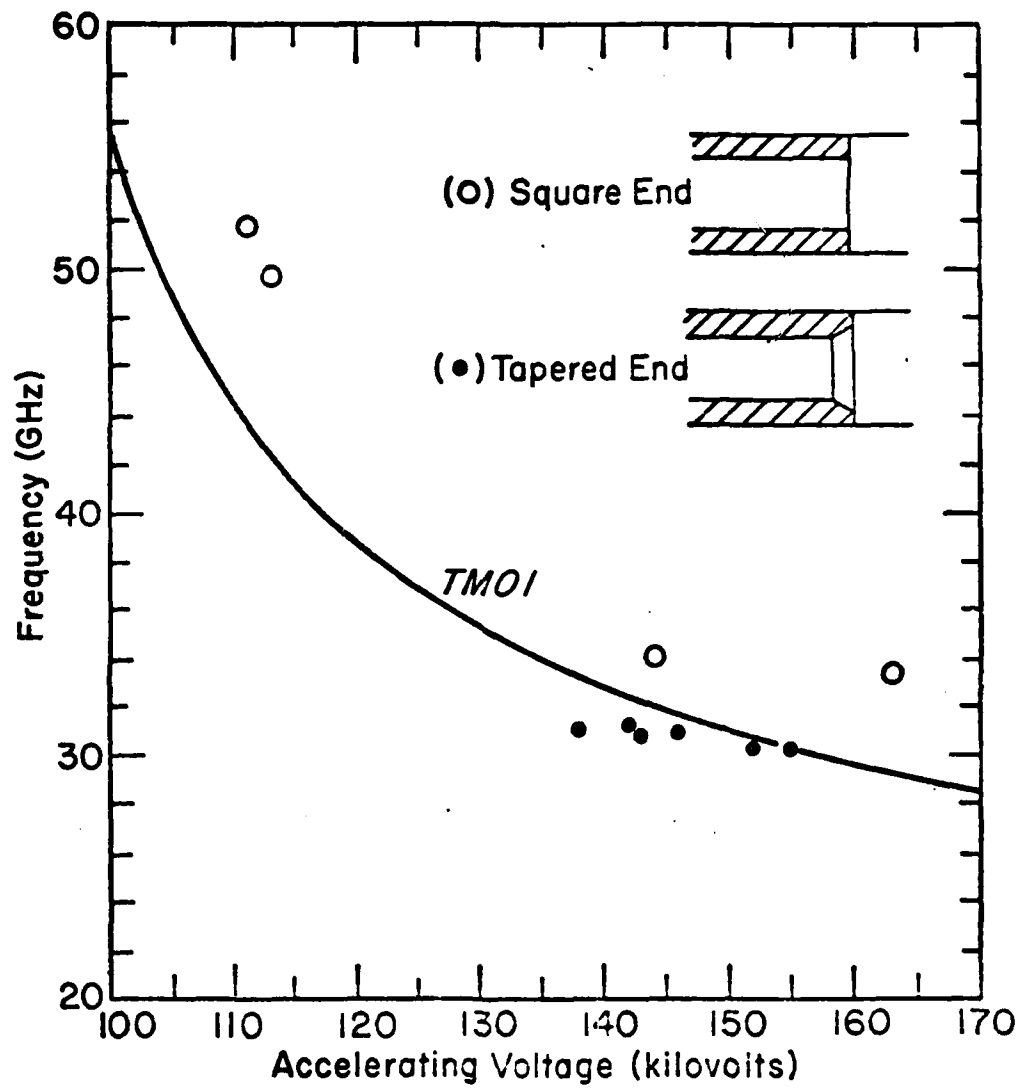


50 kV/div, 50 mV/div

(d)



882



DATE
ILMED
8